The Impact of Slag Composition on the Microstructure of Composite Slag Cements Exposed to Sulfate Attack

Mark James Whittaker

Submitted in accordance with the requirements for the degree of
Doctor of Philosophy

The University of Leeds
School of Civil Engineering

November 2014

The candidate confirms that the work submitted is his/her own, except where work which has formed part of jointly-authored publications has been included. The contribution of the candidate and the other authors to this work has been explicitly indicated below. The candidate confirms that appropriate credit has been given within the thesis where reference has been made to the work of others.

The work in Chapter 5 of the thesis has appeared in the following publication:

WHITTAKER, M., ZAJAC, M., BEN HAHA, M., BULLERJAHN, F., BLACK, L., The role of Alumina Content of Slag, Plus the Presence of Additional Sulfate on the Hydration and Microstructure of Portland Cement-Slag Blends, Cement and Concrete Research, 66, 2014, pp. 91-101

Any thermodynamic data within the publication and chapter 5 was supplied by Dr. Maciej Zajac from Heidelberg Cement Technology. Mark James Whittaker was responsible for the remainder of the work.

Acknowledgements

This work was funded by a University Research Scholarship from the University of Leeds for Mark James Whittaker, with additional funding and materials provided by HeidelbergCement Technology Centre GmbH.

I would like to thank first of all Dr. Leon Black for making any of this a possibility. His guidance, support, and knowledge was always greatly appreciated and of great value.

My thanks and appreciation also go out to the Heidelberg Cement Technology research team, primarily Dr. Maciej Zajac and Dr. Mohsen Ben Haha, for their hard work and involvement towards the project, and in keeping me motivated.

I am further indebted to the younger research members, past and present, here at the University of Leeds, including Julia, Robin, James, Josh, and Rae who shared their expertise in the labs and provided further moral support. I am also thankful to Sam, Tom and Anton, for the numerous discussions and, more importantly, the numerous games of golf putting in the office

Abstract

The work presented here focuses on the impact of slag composition on the resistance of slag composite cements exposed to sulfates. Such composite systems can be an effective way to provide better sulfate resistance of the binder. However, the differing composition and hydration kinetics between slag and cement results in a change in the phases present and their quantities, the effect of which is often overlooked when assessing their sulfate resistance. Rather, the composition of the slag is typically considered.

Compared to cement, slags are richer in Si, Al and Mg, but poorer in Ca. Blended with cement, they hydrate much more slowly to produce comparable hydrates including a C-S-H phase deficient in calcium plus a hydrotalcite-like phase. Furthermore, aluminium from slag can promote the formation of other aluminate hydrates. The changes in microstructure and ultimately performance is then dependent on the composition of the slag.

The aim of the work was to determine how slag composition affected the performance of slag cements in sulfate rich environments by means of the developed microstructure. A first hydration study was carried out to follow how slag composition affected microstructural developments by comparing a neat (control) cement with several slag blends curing in idealised lab conditions. Subsequently, the same samples were exposed to a $3g.L^{-1}$ Na_2SO_4 solution. By comparing hydration in controlled conditions and in aggressive media in parallel, analysing only the degraded zone in the latter case, the role of slag composition on phase assemblage and composition and, ultimately, on sulfate resistance was highlighted

All the slag blended systems showed great resistance to sulfate attack during the testing period. This can be attributed to several changes in the microstructure in slag blended systems including (i) a lowering of the calcium content of the C-S-H phase which led to (ii) an increase in the amount of alumina bound to a possibly water rich silicate hydrate, (iii) a greater amount of a hydrotalcite phase varying in alumina content and (iv) a diluted calcium hydroxide content. Furthermore, monosulfate had formed in the slag blended systems during attack whereas ettringite had only formed in a neat system. This implies an availability of alumina from the slag keeping the $/Al of the pore solution low favouring monosulfate formation. Lastly, the role of calcium and ettringite stability was tentatively probed at.

Table of Contents

List of Figures

List of Tables

List of Abbreviations

Cement Nomenclature:

C = CaO	S = SiO_2	A = Al_2O_3
\$ = SO_3	M = MgO	F = Fe_2O3
C = CO_3	N = Na_2O	K = K_2O
H = H_2O		

Clinker Phases and Hydrates

Alite		$3CaO.SiO_2$
Belite		$2CaO.SiO_2$
Tricalcium Aluminate		$3CaO.Al_2O_3$
Tetracalcium aluminoferrite		$4CaO.Al_2O_3.Fe_2O_3$
Gypsum		$CaSO_4.2H_2O$
Portlandite		$Ca(OH)_2$ / CH
Calcium Silicate Hydrate		$CaO\text{-}SiO_2\text{-}H_2O$
Calcium Aluminate Silicate Hydrate		$CaO\text{-}Al_2O_3\text{-}SiO_2\text{-}H_2O$
Ettringite / AFt		$3CaO.Al_2O_3.3CaSO_4.32H_2O$
Monosulfate / Ms	AFm	$3CaO.Al_2O_3.CaSO_4.12H_2O$
Hemicarboaluminate / Hc	AFm	$3CaO.Al_2O_3.0.5Ca(OH)_2.0.5CaCO_3.11.5H_2O$
Monocarboaluminate / Mc	AFm	$3CaO.Al_2O_3.CaCO_3.11H_2O$
Stratlingite		$2CaO.Al_2O_3.SiO_2.8H_2O$
Hydrotalcite / Ht		$Mg_6Al_2(OH)_{16}.CO_3.{}_4H_2O$[1]

[1] The formula above describes that of pure hydrotalcite. In cement, it is much more common to encounter a phase whose Mg/Al is closer to 2.

Techniques

BSE	Back Scattered Electron
DTA	Differential Thermal Analysis
EDX	Energy Dispersive X-Ray Spectroscopy
ICC	Isothermal Conduction Calorimetry
SEM	Scanning Electron Microscopy
STA	Simultaneous Thermal Analysis
TEM	Transmission Electron Microscope
TGA	Thermogravimetric Analysis
W/C	Water to Cement Ratio
W/B	Water to Binder Ratio
XRD	X-Ray Diffraction

Chapter 1

Introduction

Increasingly, more and more pressure is put on the cement industry to reduce its environmental burden; the industry alone is responsible for 5-8 % of the anthropogenic CO_2 [1, 2]. In developing a more sustainable future, it is imperative that greener alternatives be sought. One such method is using composite systems, where part of the cement has been substituted with a greener alternative.

Cement can be partially replaced with supplementary cementitious materials (SCMs) like ground granulated blast furnace slag (GGBS). Slag is a by-product from the iron industry which, when quenched rapidly, takes the form of a glassy phase. In composite slag cements, the high alkalinity of the pore solution allows for its dissolution, and its constituents can partake in hydrate formation. The use of the composite is well known to be beneficial; slags hydrate to produce phases analogous to cement, including a C-S-H phase, hydrotalcite and possibly stratlingite. Slag hydration in parallel to the cements allow for composite systems to outperform the mechanical properties of neat systems, and provide greater resistance against chemical attacks. As much as cement hydration is an increasingly understood mechanism, less can be said about blended systems [3]. Typical studies on durability or mechanical aspects of such systems, and more often than not, omit the lead role of the microstructure. This is starting to get recognition, and more recent studies have been focusing on the microstructure of blended systems, for both slag or PFA blended systems [4, 5, 6].

Slag blended systems are however much harder to characterise. Firstly, because rather than just one hydrating system, both have to be considered which may very well influence one another. In the presence of slag, cement hydration is accelerated because of a filler effect, and the individual clinker phases are all affected differently; C_3S, C_3A and C_4AF dissolution is accelerated, whereas that of belite's is delayed.

Secondly, slag is a by-product and as such differ in composition, depending on their source and method of treatment [7, 8]. Subsequently, not all slags perform adequately. Basicity ratios have been developed in an attempt to isolate ‘good performing’ slags based on composition alone. Such ratios however are inaccurate and sometimes contradictory. Mantel [9] tested these ratios and found that they failed to recognise which slags lead to the stronger matrix. Still, some composition requirements must be met for their use in cement [10]. Evidently, the composition of a slag will affect the final microstructure of a system.

Thirdly, because of their hydration kinetics, slags dissolve much more slowly than cement. No more than 50 % would be expected to have hydrated after 28 days of curing, compared to 80 %, or more, for cement. The potential benefits of slag rely on prolonged curing.

Several key changes in the microstructure in composite systems are expected. In neat cement systems, C-S-H is expected to have for composition 1.8C-S-H_n. In blended systems, the Ca/Si is lowered, the impact of which is greater at high slag loads. In response, more aluminium is bound to the C-S-H phase, replacing the bridging silica tetrahedra. The changes in composition are then reflected on the microstructure of the phase, which convert from a fibrillar morphology at high Ca/Si ratio to a foil-like morphology at a low Ca/Si ratio. Slags are also richer in magnesium and produce a hydrotalcite like phase, however deficient in magnesium. Partial substitution of the cement dilutes the clinker phases and in response less aluminate hydrates will form. The balance between AFm and ettringite phases depend on the $/Al of the pore solution and, unless the sulfate content is corrected for, the former will dominate and slag may also contribute to their formation. This is however limited to the slow dissolution of the slag. The use of slag with cement will also typically lead to a refined porosity.

Sulfates present in water sources can percolate through the cement matrix potentially causing damage. The sulfates react with available aluminium and calcium to

convert monosulfate to ettringite $C_6A\bar{S}_3H_{32}$, and under extreme circumstances portlandite to gypsum. Furthermore, the reaction to yield ettringite from monosulfate requires an extra 2 moles of calcium ($Ca/Al_{AFt}=6$). This extra calcium may be sourced from calcium hydroxide. The formation of ettringite is associated with an overall loss of volume when including the water in calculations, but the overall solids volume is increased. Although the increase in volume is a pleasing explanation for damage associated with sulfate attack, it is simplistic. On the basis that there is typically enough capillary porosity to accommodate ettringite growth, no expansion should occur. Ettringite must therefore grow in confined spaces, most likely from a supersatured solution (crystallisation pressure). Further exchanges of ions, e.g. calcium leaching, cannot be ignored either.

Blends prepared with SCMs are known to improve sulfate resistance of the parent cement [11, 12, 13, 14, 15, 16]. The accepted mechanisms behind improved resistance are two folds. On one hand, the blending results in a dilution of the clinker species, reducing the overall AFm content (assuming the calcium sulfate content is kept constant). On the other hand, blended systems typically exhibit a refined pore structure opposing sulfate ingress.

With respect to slag composite cements, the literature offers conflicting results on their performance exposed to sulfates, though some trends are usually observed [11, 12, 13, 14, 15, 16]. Composite systems prepared with slags whose alumina content is low will outperform blends prepared with a high alumina slag. This already implies that slags play a role in sulfate attack. Blends prepared with a low slag content (<40% by weight) may in fact perform worse than a neat system. At low levels of replacement, AFm phases are still prominent, and because slags can promote even partake in their formation resistance may be worsened. Blends rich in slag greatly reduce the AFm content, potentially improving resistance. This may appear contradictory at first as a blend with a greater slag fraction will have a greater overall alumina content. This implies a change in the microstructure and phase composition such that aluminium is not readily

available to react with sulfates. It has been previously suggested that at low levels of replacement, resistance is dependent on the amount of AFm initially present, whereas at higher slag loading, resistance is dependent on the overall Al_2O_3 content. However this explanation relies on the composition of the slag cement, and less so on the microstructure.

Mehta [17] already recognised the importance of the microstructure when assessing sulfate resistance of PFA systems. He discussed that the R-factor approach, devised to assess whether or not the blending of a fly ash with cement will provide protection based on PFA composition, was insufficient. Rather the microstructure developed with respect to the aluminate hydrates was more important.

The impact of the differing composition of slags compared to cement on the microstructure of composite systems have not yet been fully developed. After all, the nature and amount of the phases that has formed, plus the porosity, is dependent mostly on the composition of the raw materials. In the same train of thought, the impact of the microstructure developed in blended systems on sulfate resistance is not fully understood.

Prior to assessing the role of slag composition on sulfate resistance its impact on microstructure first needed developing by carrying out an extensive hydration study, detailed in chapter 5. Subsequently, slag cements, using both pastes and mortars, plus a control neat cement, were exposed to a sodium sulfate rich environment and the impact of the changes in microstructure, which depended on the composition of the raw materials, in slag rich blends on sulfate resistance were assessed (chapter 6). The study is split into the following chapters:

Chapter 2 concerns itself with a survey of the current knowledge on hydration mechanisms of cement and slag, plus sulfate attack.

Chapter 3 describes the techniques used

Chapter 4 details the preliminary work carried out to determine which 5 mixes ought to be carried forward.

Chapter 5 follows the hydration mechanisms and developed microstructure of the investigated systems

Chapter 6 follows the resistance of slag blended systems, in relation to the developed microstructure in blended systems.

Chapter 7 Conclusions and further work

Chapter 2

Literature Review

2.1 Properties of CEM I cement

Portland Cement, designated as CEM I or type I cement in EN 197-1:2011 [10] and ASTM C150/C150M-12 [18] respectively according to European or American standards, is a hydraulic binder composed mostly of calcium silicate phases. Aluminium and ferrite containing phases are also present. Cement is produced by calcining together a calcium source (limestone) with an aluminosilicate (clay) to temperatures approaching 1500°C. This forms a clinker composed of 4 principal phases. These include C_3S, C_2S, C_3A and C_4AF. This clinker is then ground to a fine powder with additives (calcium sulfate and calcium carbonate), the end product of which falls under the classification given above.

2.1.1 Composition of CEM I Cement

2.1.1.1 Tricalcium Silicate

Tricalcium aluminate, C_3S, is the most abundant phase, typically making up 60% of the clinker by weight. Upon heating the phase shows polymorphism with respect to temperature, as shown [19]:

$$T_1 \overset{620°C}{\longleftrightarrow} T_2 \overset{920°C}{\longleftrightarrow} T_3 \overset{980°C}{\longleftrightarrow} M_1 \overset{990°C}{\longleftrightarrow} M_2 \overset{1060°C}{\longleftrightarrow} M_3 \overset{1070°C}{\longleftrightarrow} R$$

C_3S is stable at higher temperatures, with respect to (C_2S+CaO). However, the incorporation of impurities in the crystal matrix stabilizes higher temperature forms at ambient conditions. Impure C_3S, denoted as alite, typically includes Mg^{2+}, Al^{3+}, Fe^{3+}, SO_3, and alkalis [20]. Their inclusion in C_3S stabilizes it in either of the monoclinic forms M_1 or M_3. Maki and Goto [21] found that greater incorporations of SO_3 and MgO favoured the

formation of M_1 and M_3 alite respectively. At intermediate levels, both may very well coexist. Regardless of the adopted structure, the reactivity of C_3S remains the same.

C_3S reacts rapidly with water to form a calcium silicate hydrate C_xSH_y and portlandite CH according to:

$$C_3S + (3 - x + y)H \rightarrow C_xSH_y + (3 - x)CH$$

C-S-H takes the form of an amorphous gel whose composition varies (as indicated by the dashes in C-S-H). 'x' denotes the Ca/Si ratio of the C-S-H phase. In mature C_3S and cement pastes, the Ca/Si ratio has an average value of 1.7-1.8 [22]. 'y' is the water content of the C-S-H. It is difficult to determine the water content of the C-S-H phase as any drying will cause dehydration of the phase, but in saturated conditions y = 4. Odler and Dorr [23] measured y values ranging from 1.3-1.7 for C-S-H found on d-dried C_3S pastes.

Despite the amorphous nature of the C-S-H phase, naturally occurring crystalline analogues have been used as a proxy to understand the nature of the phase in cement. Two such crystalline phases are tobermorite and jennite (Figure 2-1) [19, 24, 25, 26, 27].

1.4nm Tobemorite has the chemical formula $[Ca_4(Si_3O_9O_2H)_2]Ca.8H_2O$. Structurally tobermorite is built upon a central layer of CaO_2, to which a chain of silica tetrahedra is linked, via oxygen bonding. The bonding of the tetrahedra follows a pattern. Typically, two paired SiO_4 units directly share an oxygen with Ca, and a third 'bridging' tetrahedron then shares an oxygen with 2 paired tetrahedra; a fundamental component known as 'dreierkette'. Tobermorite, however, only has a Ca/Si ratio of 0.83, much lower than that seen in neat cement or C_3S pastes. Jennite has the formula $[Ca_8(Si_3O_9H)_2(OH)_8].Ca.6H_2O$, and a Ca/Si of 1.5, higher than that of tobermorite. The central Ca layer is corrugated, and one of the silicate chains is substituted with an OH group. The interlayer space separating 2 'sheets' consists of water and charge balancing ions (Ca^{2+}, H^+ and alkalis).

C-S-H can also host foreign elements. Aluminium is often incorporated into the structure, replacing the bridging tetrahedra [28]. The amount of which, however, is dependent on the Ca/Si ratio, with more aluminium incorporated in a calcium-poor C-S-H [29]. Charge balancing alkalis can also be bound by the C-S-H phase [30, 31]. TEM observations of hydrated cements pastes reveal that C-S-H adopts a fine fibrillar morphology in C_3S and neat cement. C-S-H formed in the water filled space appears coarser compared to C-S-H formed within the grain boundary, where space restraints are minimal [32].

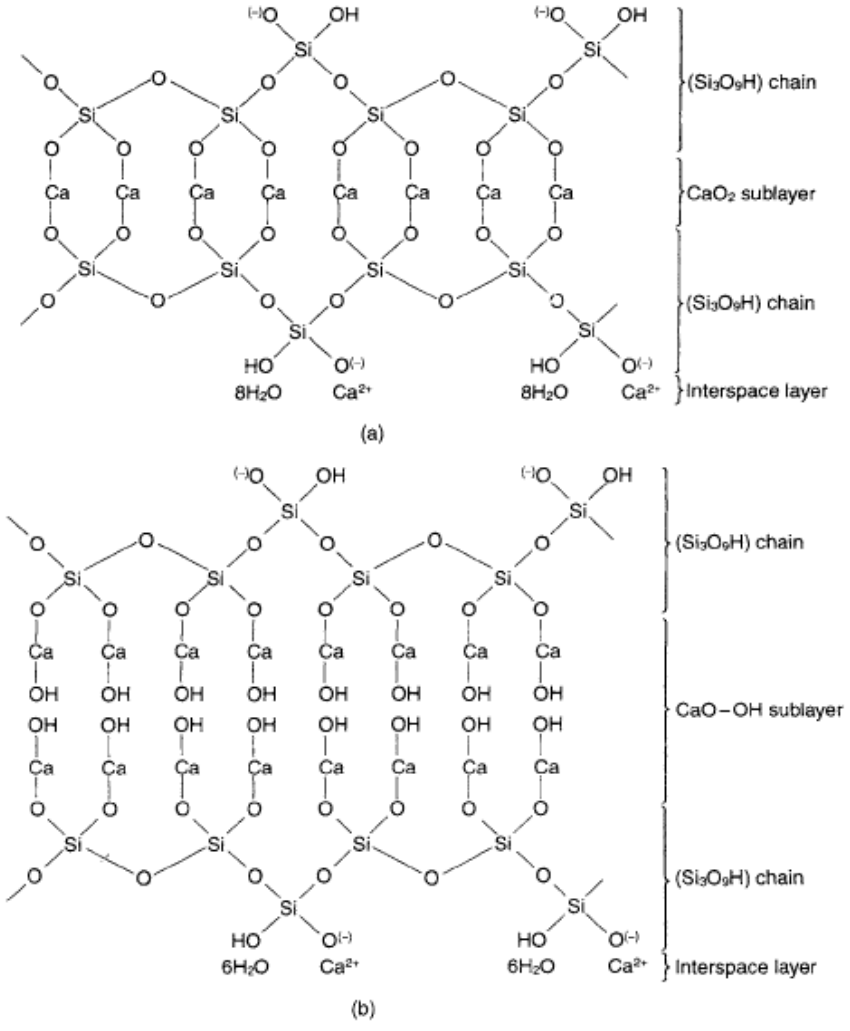

Figure 2-1 –Tobermorite and Jennite Models (taken from [33])

2.1.1.2 **Dicalcium Silicate**

Much like alite, pure dicalcium silicate C_2S, exhibits polymorphism with temperature, as shown below [19]. The more common form of C_2S found in cement is stabilized as β-C_2S, with the incorporation of foreign elements. The impure form is termed belite. Compared to alite, belite can take up more foreign ions (Al^{3+}, Fe^{3+}, Mg^{2+}, K^+, SO_4^{2-} and PO_4^{3-}).

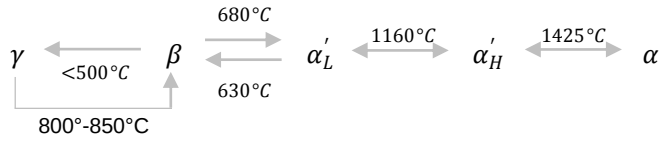

However, the reactivity of belite is greatly dependent on the adopted crystal structure. For instance γ-C_2S is almost unreactive, although it does hydrate slowly [34]. Most commonly, β-C_2S is found in cement, largely stabilized by the presence of K^+. α'-C_2S can also be found and is more hydraulic than β-C_2S. The reaction with water produces the same hydrates as C_3S, although the reaction is more gradual [35]:

$$C_2S + (2 - x + y)H \rightarrow C_xSH_y + (2 - x)CH$$

2.1.1.3 **Tricalcium Aluminate**

Pure tricalcium aluminate has a cubic structure and does not exhibit polymorphism [19, 36]. The cubic structure can still incorporate impurities (Fe^{3+}, Mg^{2+}, Na^+, K^+, Si^{4+}). The incorporation of sodium can, however, alter the structure of the phase. The original cubic structure converts to orthorombic and monoclinic as the sodium content increases in the structure [37]. C_3A is very reactive and reacts with water to produce C_4AH_{13} and C_2AH_8. These phases are metastable with regard to C_3AH_6 at room temperature. In the presence of lime, e.g. in a hydrating cement paste, C_3A will hydrate to produce C_4AH_{13} and the conversion to C_3AH_6 is inhibited (Table 2-1).

Table 2-1 – Hydration Products of C_3A [38]

Reaction	Comments
$2C_3A + 21H \rightarrow C_4AH_{13} + C_2AH_8$	Metastable to C_3AH_6
$C_3A + CH + 12H \rightarrow C_4AH_{13}$	Conversion to C_3AH_6 is inhibited Slower hydration
$C_4AH_{13} + C_2AH_8 \rightarrow 2C_3AH_6$	
$C_3A + 3C\bar{S}H_2 + 26H \rightarrow C_3A.3C\bar{S}H_{32}$	Sulfates added to prevent flash set C_3A hydration is delayed
$C_3A.3C\bar{S}H_{32} + 2C_3A + 4H \rightarrow 3C_3A.C\bar{S}H_{12}$	Forms upon sulfate depletion

However, the simple reaction of C_3A in water leads to flash set. This phenomenon is undesirable removing the dormant period needed to place and compact concrete. The hydration of C_3A in the presence of calcium sulfate prevents flash set, temporarily delaying hydration. This delay is greater when the sulfate content increases [39, 40]. The hydrate produced is now ettringite $C_3A.3C\bar{S}H_{32}$. Also referred to as AFt, the phase is highly crystalline taking the form of acicular crystals with a hexagonal cross-section. Once the sulfate source is depleted, ettringite can react with any remaining unreacted C_3A to form monosulfate $3C_3A.C\bar{S}H_{12}$. Monosulfate is an AFm phase, whose structure is related to hydrocalumite. A representative formula for AFm phases is $[Ca_2(Al,Fe)(OH)_6].X.xH_2O$ where X denotes an exchangeable singly charged (Cl^-) or doubly charged anion (SO_4^{2-}, CO_3^{2-}) [41].

Typically calcium carbonate is added to clinker to produce cement. Although traditionally considered inert, its presence can lead to the substitution of sulfates by carbonates in the AFm phase [42, 43]; hemicarboaluminate $Ca_4Al_2(CO_3)_{0.5}(OH)_{13}.5.5H_2O$ and monocarboaluminate $Ca_4Al_2(CO_3)(OH)_{12}.5H_2O$ are two such carbonate AFm phases. The expelled sulfates then help stabilize ettringite.

2.1.1.4 **Calcium Aluminoferrite**

Calcium aluminoferrite has the formula $C_2(A_xF_{1-x})_2O_5$ and is a solid solution between C_2F and C_2A. The structure is built upon layers of tetrahedral FeO_4 and octahedral FeO_6 linked together by Ca^{2+}. Aluminium can substitute for iron, the amount of which can vary in one single sample. For values of 'x' up to 0.33, Al^{3+} substitutes for Fe^{3+} in tetrahedral sites. For higher values, substitution on the octahedral sites can also occur. Commonly, calcium aluminoferrite is written down as C_4AF (and x=0.5), while it too contains impurities (Mg^{2+}, Si^{4+} and Ti^{4+}). The reactivity of C_4AF increases with A/F to produce hydration products analogous to that of C_3A [44], although its rate of hydration is much slower.

2.1.2 **Hydration of CEM I Cement**

2.1.2.1 **Early Stage Hydration**

The hydration of CEM I cement is an exothermic reaction which involves the aforementioned reactions of the clinker phases; C-S-H is the main hydrate, and ettringite and AFm phases are finely intermixed with it. The CH crystals precipitated are, however , more sizeable, although microcrystalline CH does occur too. Hydration leads to stiffening and hardening of cement. Figure 2-2 illustrates the rate of heat output during the hydration of typical cement [45, 46].

The reactions start as soon as cement is in contact with water, marked by the high heat output in the first few minutes of hydration. During that time, C_3A, C_3S and calcium sulfate start to dissolve, leading to the formation of an alumina rich gel on the surface of the particle. Short ettringite rods also nucleate at the edge of the gel and in solution [19]. Reaction is almost immediately halted and heat output is minimal.

This period of low heat is the induction, or dormant, stage. It is the existence of such a stage that allows for transportation and compaction of the concrete. Hydration accelerates once more to a maximum, and the heat released is associated with the hydration of C_3S, leading to the nucleation and growth of 'outer product' C-S-H and

portlandite in the space originally filled by water. After the maxima (~10h of hydration), C_3S hydration becomes diffusion controlled and continually decelerates [45]. The lack of space or water can also contribute to deceleration.

It is sometimes noticeable to see a little hump soon after the maximum of alite hydration. This is the result of renewed C_3A hydration upon sulfate depletion, leading for the formation of secondary ettringite. Hesse et al. [47] followed the hydration of synthetic clinker composed of C_3S, C_3A and calcium sulfates by both calorimetry and in-situ quantitative XRD. They found that C_3A hydration was halted during which time the calcium sulfate continually dissolved. Once the sulfate source depleted, C_3A hydration would resume to form secondary ettringite soon after the rate of C_3S hydration was at its greatest. The precipitation of secondary ettringite is greatly dependent on the sulfate and C_3A content of the cement. A cement can be considered to be properly sulfated when the formation of secondary ettringite occurs soon after the maximum rate of C_3S hydration [48]. At later ages, beyond 24 hours of hydration, the conversion of ettringite to monosulfate can lead to renewed heat evolution. As hydration continues, inner product C-S-H gradually forms, as the original space occupied by cement grains is filled with hydration product. Inner products consist predominantly of C-S-H, with AFt, AFm, CH and a hydrotalcite like phase [22].

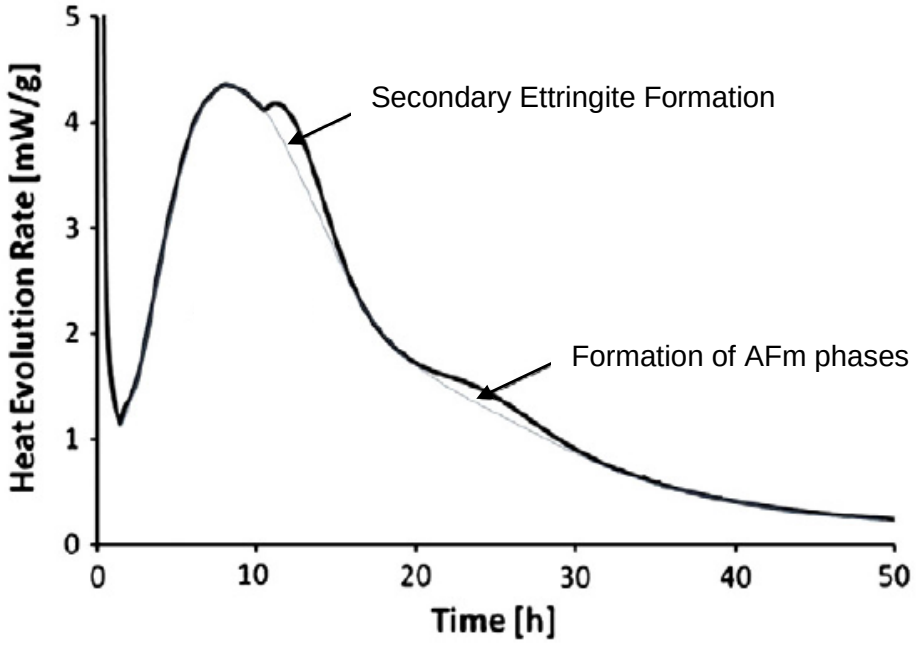

Figure 2-2 – Typical Heat Evolution Curve of hydrating CEM I Cement (taken from [45])

2.1.2.2 **Microstructural Development**

Figure 2-3 shows a typical SEM image of a neat Portland cement paste cured for 180 days. The microstructure comprises unreacted materials, pores and hydrates. Hydrates are formed in the space originally filled with water (outer products) or within the space originally occupied by the cement grains (inner product). Both outer and inner products include C-S-H, CH, AFt and AFm. The composition of the C-S-H is also comparable between inner product and outer product [22]. Any space that has not been filled with hydrates in the outer region results in the formation of pores. These are an inherent part of the microstructure. However, the resolution of a scanning electron microscope limits the observation to larger pores only. Calcium hydroxide is also easily distinguishable appearing as light grey deposits.

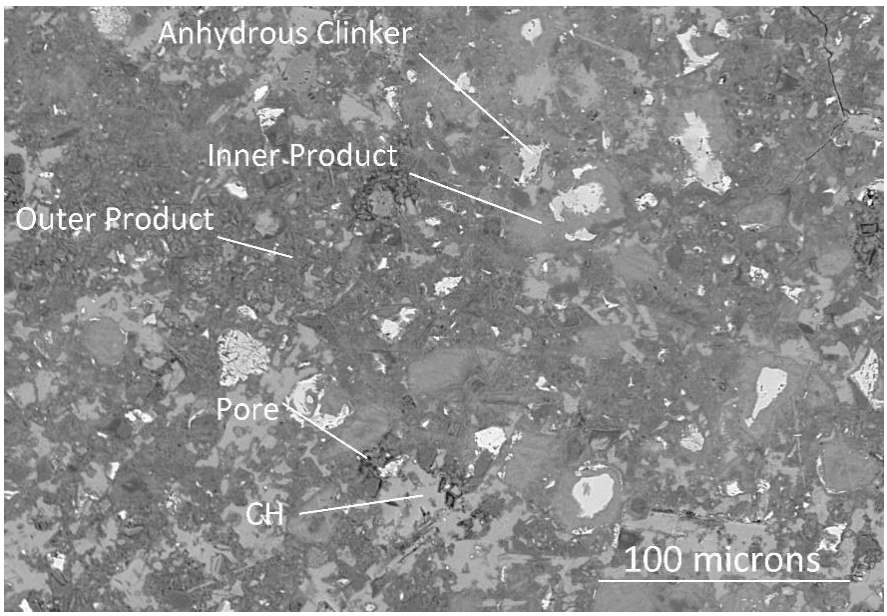

Figure 2-3 – Typical SEM-BSE Micrograph of a Neat Cement Cured for 180 Days (20C, W/C = 0.5)

2.1.2.3 **Porosity**

Pores vary in size and may be typically classified into 2 categories (Table 2-2). Firstly are the smaller gel pores, which are an intrinsic feature of the C-S-H phase, and compromise the interlayer space between C-S-H sheets and micropores [38, 49]. These sized pores have no effect on strength, and rather govern any shrinkage and creep effect to which the cement may be exposed to.

Secondly are the capillary pores, which are the originally water filled spaces that have not been filled by hydration products. These are considerably larger than gel pores, and it is these that determine the strength and the permeability of a specimen. Increasing the water/cement ratio increases the distance between particles and results in a more porous system, thus weakening a cementitious system [50].

Table 2-2 – Pore Classification

	Diameter	Description	Properties Influenced
Capillary Pores	10-0.05 μm	Large capillary	Strength/permeability
	50-10 nm	Medium capillary	Strength/permeability
			Shrinkage (RH> 80 %)
Gel Pores	10-2.5 nm	Small (gel) capillaries	Shrinkage (50>RH<80%)
	2.5-0.5 nm	Micropores	Shrinkage/creep
	<0.5 nm	Micropores	Shrinkage/creep
		interlayer water	

2.1.2.4 **Water Phase**

Water is essential for cement hydration and is present in all hydrates. Water is found in several states. Powers and Brownyard [51] recognized 3 classes of water in a saturated cement paste. These include capillary water, gel water and non-evaporable water. As the name suggests, capillary water fills the capillary pores in saturated conditions. In the larger capillary pores, greater than 50 nm in diameter, water can be considered to be free water where it is not affected by attractive forces from the solid surface. Gel water is water that is associated with water in the C-S-H structure. Gel water can be further distinguished; between physically adsorbed water and interlayer water (Figure 2-4) [38]. These two types of water can be removed, for which several approaches may be adopted [52, 53].

The last type of water is non evaporable water and can be considered as water that is inherently part of a hydrate, e.g. chemically bound water. The determination of such water usually requires a thermal treatment. The distinction between chemically bound water from capillary or gel water can be difficult as all drying techniques can partially dehydrate C-S-H and ettringite [53], leading to errors.

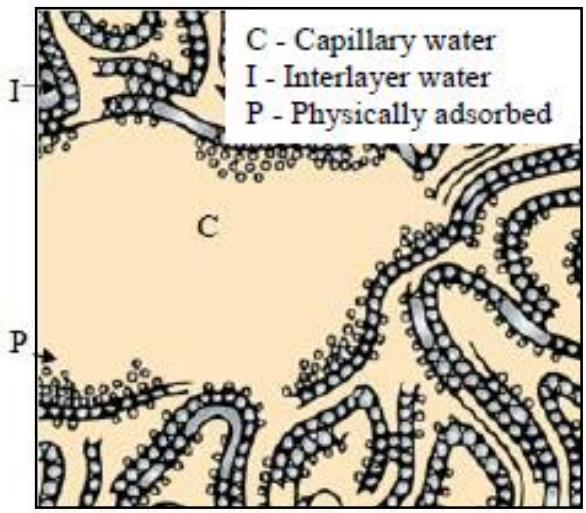

Figure 2-4 – Schematic Model of the Water Associated with C-S-H (Taken from [38] [54])

2.2 Properties of Ground Granulated Blast-Furnace Slag

2.2.1 Production of Ground Granulated Blast-Furnace Slag

Ground granulated blast-furnace slag (GGBS) is a by-product from the iron industry [55]. Iron ores are rich in iron oxides with some impurities, including Al_2O_3 and SiO_2. To extract the iron, the iron oxides have to be reduced which requires a flux stone, usually limestone ($CaCO_3$ or dolomite $CaMg(CO_3)_2$). The iron and the flux are melted together by heating the raw ingredients up to temperatures near 1500°C. The iron ore is reduced to iron and the impurities combine with the flux stone to produce slag, rich in CaO, SiO_2 and Al_2O_3. The quality of the slag will depend on the purity of the iron ore, the flux stone stone, and the coke (fuel) and compositions vary upon the origin of production [7].

When slags are cooled rapidly, formation of crystalline phases is suppressed and a glassy material is formed, typically above 90% glass [56]. This is done by forming the molten slag into granules and cooling with water jets. The resulting material is ground to a similar fineness as cement to yield ground granulated blast furnace slag (GGBS). The material has latent hydraulic properties. In water GGBS hydration is very slow and limited and needs to be activated. Chemical activation is achieved by having slag reacting in a highly alkaline environment [57, 58, 59, 60], dissolving the glass. High alkalinity in slag

cement blends is ensured by the presence of calcium hydroxide produced during hydration of the silicate phases, plus alkalis of Portland cement.

2.2.2 Structure of Ground Granulated Blast Furnace Slag

Rapidly cooled slags mainly compromise a high amorphous glassy phase, with possible inclusions of crystalline phases. Any crystalline phases are inert and it is the glassy phase that is reactive. The reactivity of the slag depends on many factors, including its chemical composition, the glass content, the particle size distribution (fineness) and surface morphology [61]. As such it is very difficult to determine how reactive a slag is based on just one of the aforementioned aspects. For their use in cement, the chemical composition has to satisfy criteria set in BS EN 197-1:2011 [10] such that:

1. At least 2/3 of the slag by mass must be glassy and must possess sufficient hydraulic properties when activated.
2. At least 2/3 of the slag by mass be made up of CaO, SiO_2 and MgO.
3. The ratio (CaO+MgO)/SiO_2), by mass, should exceed 1.

2.2.2.1 Chemical Composition of Slag Glass

The main chemical components of slags are CaO, SiO_2, Al_2O_3, and MgO; Minor phases include TiO_2, MnO, FeO, S^{2-}, Na_2O, and K_2O [7, 36, 55]. Compared to cement, slags are richer in all the major phases, except CaO, as highlighted in Figure 2-5.

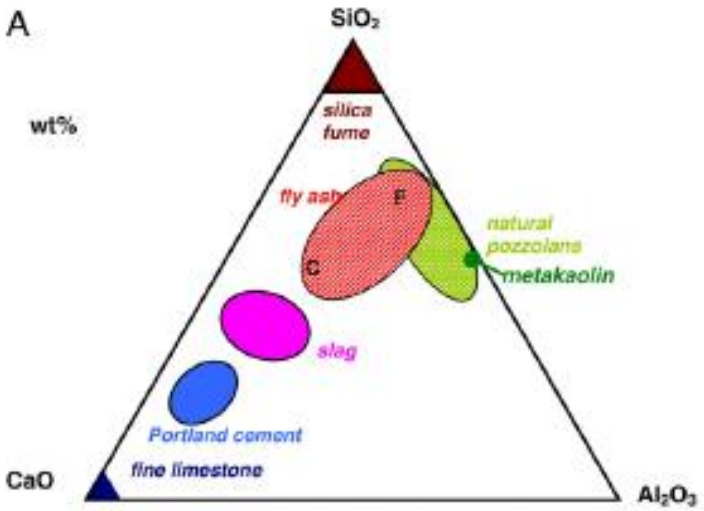

Figure 2-5 – CaO-Al2O3-SiO3 Ternary Diagram of Cementitious Materials (taken from [3, 62])

The glass fraction makes up for more than 90% of the slag by mass. The glass structure consists of Si-O-Si covalent bonds which are the network formers, although four-coordinated aluminium $Al_2O_4^{5-}$ and magnesium MgO_4^{6-} can also act as network formers. Network formers have a smaller ionic radii and high possible ionic valencies [7]. Silicates are tetrahedrally coordinated to oxygen atoms which may be shared between tetrahedra leading to a residual negative charge which must be balanced by structure modifiers. These have larger ionic radii and higher co-ordination numbers compared to network formers and are situated in the cavities of the structure [63]. Typical modifiers include six-coordinated Ca^{2+}, Al^{3+} and Mg^{2+}. The more the network modifiers are present the smaller the polymerisation degree will be, resulting in a less stable glass structure, thus increasing reactivity [7]. It has been suggested that the reactivity of a slag glass then perhaps is attributed to the ratio of octahedral to tetrahedral aluminium and magnesium. According to Uchikawa and Uchida [64], the silicates within the structure are mostly present as monomers and dimers.

Attempts have been made to relate glass composition to reactivity and ultimately performance, and comprehensive lists can be found in literature, summarized here [7, 9, 65]:

Table 2-3 – Composition Ratios Proposed to Determine the Reactivity of Slags

Ratio	Requirement for Good Performance
$P_1 = \frac{CaO}{SiO_2}$	>1.0
$P_2 = \frac{CaO + MgO}{SiO_2}$	>1.0
$P_3 = \frac{CaO + MgO}{SiO_2 + Al_2O_3}$	1.0-1.3
$P_4 = \frac{CaO + 0.56Al_2O_3 + 1.4MgO}{SiO_2}$	>1.65
$P_5 = \frac{CaO + MgO + Al_2O_3}{SiO_2}$	>1.0

P_1 and P_2 are the most recognized ratios and good reactivity is expected if these are greater than one, where the slag is said to be basic. However, the two ratios fail to recognise the role of aluminium. This is corrected in P_3, in which alumina is assumed to have a negative influence. However, in the ratios P_4 and P_5 aluminium has a positive influence. These ratios only allow for an approximation as other factors are not taken into account. Slag reactivity is dependent on the activator used, the clinker and the presence of additives (accelerators, retarders, plasticisers, etc…) as well as on the physical properties of the slag (glass content, fineness) and conditions of hydration.

Smolczyk [7] stated that an increase of CaO and MgO contents also has a positive effect on slag reactivity. In every case, however, MnO had a negative effect. The effects of P_2O_5 vary depending on the clinker used and the age of testing, but are typically positive beyond 28 days of curing. TiO_2, FeO and sulphur seem to have no real influence. An increase in the SiO_2 content is associated with decreased reactivity. An increase in the Al_2O_3 content above 13% only increases the early age strength, with higher values having an undesirable effect at later ages. Wang et.al [66] found that there is a strong link between the Al_2O_3 and CaO content, where slags richer in aluminium had greater reactivity provided that the CaO content was above 37%.

Studies have followed the impact of slag composition on strength development. Itoh [67] found that increasing the CaO content in slag increased strength, whereas SiO_2 and Al_2O_3 had negative effects. Mantel [9] has tested these formulae on a series of blends; using in total five different slags and eight cements to determine a correlation between performance of the slag blends and their hydraulicity. All the slags but one tested had a glass content greater than 94%. Depending on the slag's composition, their hydraulicity was determined according to Table 2-3. It was found that the formulae developed have no real correlation with the performance of a slag although P_1 and P_2 could serve as a rough estimation.

Ben Haha et al. [68, 69] more recently compared the impact of Al_2O_3 and MgO content of slags on alkali activated systems. They found that increasing the Al_2O_3 content of the slag reduced the reactivity of the slags at lower ages, but led to similar degrees of hydration beyond 28 days of curing. Thermodynamic modelling further revealed that the total volume of the hydrate to be constant regardless of the aluminium content, such that any changes should not be reflected on performance as such. Increasing the MgO content favoured the formation of the more voluminous hydrotalcite phase, resulting in greater strengths.

2.2.2.2 **Crystalline Fraction**

Typical GGBS has a minor crystalline fraction, usually below 10%, which is typically inert [70]. The most common crystal structure in GGBS is melilite [7], a solid solution of gehlenite (C_2AS) and akermanite (C_2MS). Merwinite (C_3MS_2) and calcite may also be found [71]. Despite their inert nature, the presence of some crystalline phases can improve reactivity, as they provide nucleation sites [19]. Results obtained by Demoulian et al. [65] suggested an increase in strength for slags with a crystalline content up to 5%, above which the strength decreased.

2.2.3 **Hydration of Slag Cements**

As stated at the start of this section, slag hydration needs to be activated . Successful activation of slags requires an alkaline medium. As such, slags can hydrate in the presence of alkalis (e.g KOH, NaOH, $NaSiO_3$, Na_2CO_3, $Na_2SO_{4...}$) [72, 73] or when blended with cement. Slag hydration can also be activated by sulfates [71], although hydration is slow, but hydration may be accelerated by addition of small dosages of an alkaline activator [60]. Mechanical activation is possible, but requires excessive grinding to greatly reduce the particle size [74]. Like cement, slag hydration increases with particle size fineness and temperature.

2.2.3.1 **Hydration of Alkali Activated Slag**

Activation of the slag typically produce a C-S-H phase and a hydrotalcite phase, though other hydrates have been reported. Regourd [75] identified C_4AH_{13} and C_2ASH_8 in NaOH activated slags. Strätlingite C_2ASH_8 can also form, the likelihood of which increases with the aluminium content of the slag [3, 68]. If sulfates are present in the activating solution, ettringite may also form [60].

Richardson et al. studied closely the C-S-H phase in alkali activated slags [57]. TEM observations showed that the outer product C-S-H was totally foil-like and partially crystalline (C-S-H(I)). The C-S-H present within the slag hydration rims of the slag was characterized by having a finer morphology compared to that observed in the originally water filled space. The C-S-H that had formed in such system was also characterized by having a lower Ca/Si ratio (close to 1) and higher Al/Si [32, 68]. The magnesium released by the slag during hydration does not integrate within the C-S-H phase [76]. Rather a hydrotalcite like phase is formed. Unlike pure hydrotalcite $Mg_6Al_2(OH)_{16}(CO_3)\cdot 4H_2O$, that produced from slag hydration has a Mg/Al ratio closer to 2 [59, 77]. The ratio again depends on the composition of the raw material and can vary with age [78].

With respect to the activating medium only, the performance of slags depends on the activator used, in both type and dosage. Alkali activated systems can effectively be

as strong, if not stronger, than typical cement systems, even after short periods of curing [79]. Ben Haha et al. [59] compared the activation capacity of two different activators on slags, finding startling differences. Slags were initially more reactive when activated by sodium hydroxide producing a much stronger binder at early stages of hydration compared to waterglass activated slags. However, the reverse was true beyond 7 days of hydration. The fast reactivity of the slags activated by NaOH produced a dense, water deficient C-S-H with poorly distributed hydrates resulting in a more porous system compared to waterglass activated slags. In the latter system, the slower hydration allowed for a better distribution of the hydrates filling the pore space; the waterglass system produced a stronger binder for the same degree of hydration.

2.2.3.2 **Hydration of Slag Cement Blends**

When blended with cement, the dissolution of the slag glass is possible because of the validated by the high pH of the solution, sustained by calcium hydroxide and alkalis. Both the clinker and the slag react alongside one another producing C-S-H, which can prove beneficial improving the overall performance of such systems [80].

In such systems, the slag fraction typically hydrates much more slowly than its counterpart [81]. It can be accelerated much like cement, increasing the water/cement (W/C), the curing temperature and slag fineness can all improve reactivity [77]. A higher slag load however can dampen reactivity [82]. Lumley et al. [77] measured that up to 30 to 55 % of the slag had reacted in slag cement blends cured at 20°C, whose water/binder ratio ranged from 0.4 to 0.6 after 28 days of curing, and 45 to 75 % of the slag had reacted after 2 years of curing. These values of slag hydration are typical in blended systems [83, 84]. Note that the data from references [77] and [83] rely on measuring the slag hydration from selective dissolution using EDTA. The technique relies of full dissolution of clinker and hydrates, leaving behind only unreacted slags. However residues of portlandite, belite and a hydrotalcite like phase have been reported [84], underestimating the overall degree of hydration. Unlike alkali activated systems, the use of different cements has little impact on the hydration of the slag [62, 77, 85].

2.2.3.2.1 Nature of the Hydrates

Just as in alkali activated systems, slags hydrate to produce C-S-H and a hydrotalcite phase, and possibly strätlingite [3]. The hydration of slag in blended systems is visible in a backscattered electron image by the formation of a darkened hydration rim growing centripetally, rich in hydration products (Figure 2-6).

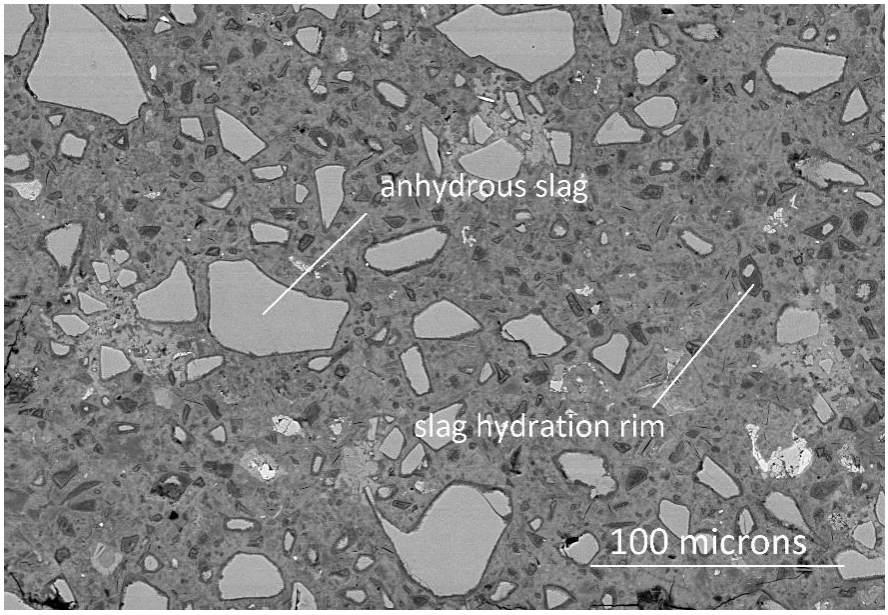

Figure 2-6 – SEM-BSE Micrograph of a Slag Cement Paste, with 70% Slag, Cured for 180 Days

With the dilution of cement, less AFt, AFm and CH are expected to be formed. This does not exclude the possibility that aluminium from slags may contribute to AFm phases [4]. Furthermore, there remains debate concerning the fate of calcium hydroxide. Slag hydration can consume it, although the literature offers conflicting results. Kocaba [85] observed that CH consumption was only modest, agreeing with the findings obtained by Luke and Glasser [83]. Other studies however have seen the consumption of CH, even at an early age [4, 86]. Escalante et al. [82] and Kolani et al. [87] noticed that CH content increased to a maximum during hydration before decreasing soon after. Taylor et al. [78] analysed slag blended systems that had hydrated for 20 years. Compared to the same samples that had cured for 2 years, the older samples were deficient in calcium hydroxide, consumed by the hydrating slag.

The C-S-H formed within slag blended systems differs from that found in neat systems in its composition. An incremental increase in slag content will produce a C-S-H increasingly depleted in calcium. In response, more aluminium will be bound within the C-S-H [29, 78, 88]. The Ca/Si appears to be comparable across the outer product (Op) C-S-H, inner product (Ip) C-S-H and C-S-H in hydrated slags, whereas the Al/Si of C-S-H in slag hydration rims is higher [29]. Mg- and Al-rich laths, indicating the presence of a hydrotalcite like phase, can also be found finely intermixed in Ip and slag hydration rim C-S-H [32], with magnesium not migrating from its source. Richardson [88] studied the microstructural development of slag cement blends. The change in composition of the C-S-H led to a change in its morphology. Ca rich C-S-H is fibrillar in nature which progressively changes to a foil-like morphology as the slag content in blends increases, much like the C-S-H seen in alkali activated systems [32].

2.2.3.2.2 Impact of Slag on Clinker Hydration

The early-stage hydration of clinker can be accelerated in the presence of an inert filler material and this effect is equally true with slags [3, 89, 90], promoting the nucleation and growth of C-S-H. This is the result of the filler effect [3, 4, 62, 91, 92]. This is illustrated in Figure 2-7. Two blends were prepared where the clinker was replaced with either 40 % slag or quartz. The difference in heat evolved between the neat cement and the cement quartz blend is due to the filler effect. Naturally the difference in heat evolved between the slag cement paste and the quartz cement paste is then due to the slag hydration itself [85].

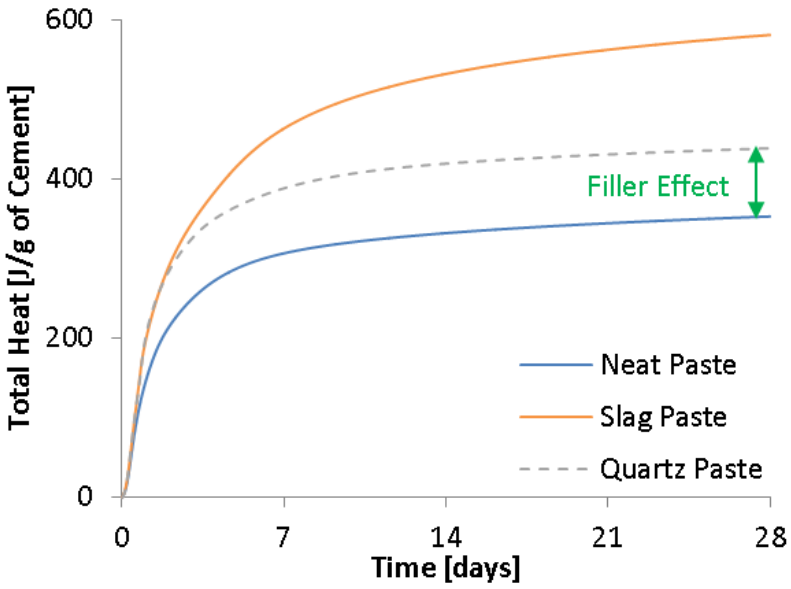

Figure 2-7 – Total Heat of a Neat Cement Paste and a Slag Cement Paste with 40% Slag, W/B = 0.5

The filler effect promotes clinker hydration by increasing the effective water/cement ratio and providing nucleation sites [3]. Berodier and Scrivener [93] further stated that the provision of nucleation sites alone was insufficient to explain the effect. They further recognized the importance of interparticle distance, which can vary with particle size and shearing of a mix.

The kinetics of the individual clinker phases have been followed in slag [4, 85] and PFA-blended systems [5]. Their presence of such additions led to an increase in reactivity of C_3S, C_3A and C_4AF. The filler effect on aluminate hydration is seen again in Figure 2-8, with it forming a peak soon after the main hydration peak, attributed to C_3S hydration [46, 47]. However, hydration of C_2S was greatly delayed in the presence of slag or PFA.

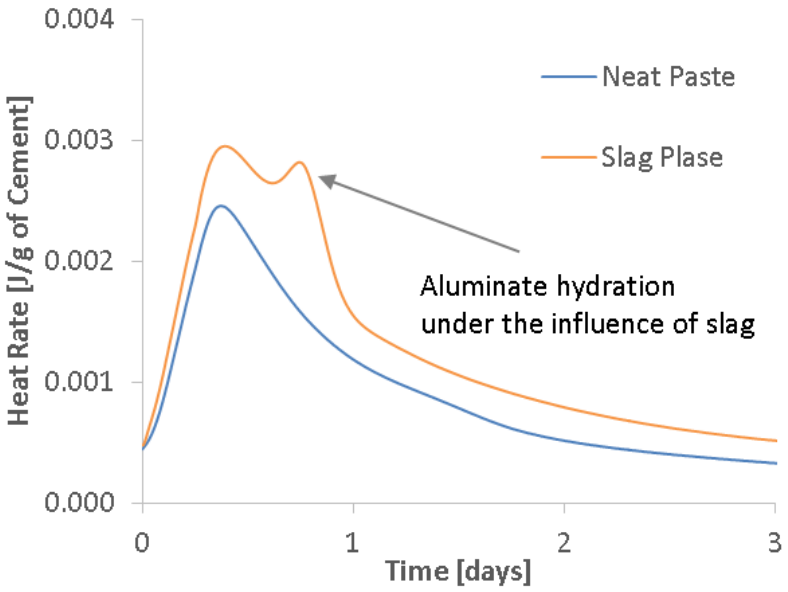

Figure 2-8 – Heat Rate of a Neat Cement Paste and a Slag Cement Paste with 40 % Slag, W/B = 0.5

2.2.3.3 **Benefit of Slags**

It is well known that the use of slag composite systems offers an array of benefits compared to neat cementitious systems. Richardson and Groves [29] recognized the potential benefits of slag, where the foil like C-S-H potentially improves space filling, where the porosity of a system can be refined [54]. A slag blended system can outperform pure cement systems on a strength development basis [8, 94, 95]. This is well accepted and the improvement in strength can be seen as early as 28 days, depending on the level of replacement and temperature. Oner and Akuyz [95] tested an array of mix designs, varying the slag content. They found that concretes with a slag content in the range of 55 % to 60 % gave optimum strength. If the slag content increased past that point, much of the slag would remain unreacted providing no real benefit to strength. Slag blended systems have also been seen to improve resistance to Alkali-Silica Reaction [96] and sulfate attack [13, 97].

2.3 **Sulfate Attack Mechanisms**

Simply put, sulfate attack encompasses a series of chemical and physical interactions that occur between hardened cement paste and sulfates. While sulfates already present in cement, often as gypsum to prevent flash set may, depending on

curing conditions, cause damage in the form of expansion and cracking in the form of delayed ettringite formation [98, 99], this is not the focus of this review. Rather, the review covers the deleterious impact of external sources of sulfate on cement paste and, therefore, concrete.

Ground water is a natural sulfate source to which buried concrete can be exposed. These waters typically have a low sulfate content; a fact recognized in standard BS EN 206:2013 [100]. The more severe class with respect to sulfate attack (class XA3) fixes the concentration of SO_4^{2-} between 3000 and 6000 $mg.L^{-1}$ (Table 2-4). These sulfate ions can penetrate through the cement matrix leading to damage. In fully buried structures, the ingressing sulfates react with aluminate hydrates to produce ettringite and gypsum, the antagonists of chemical sulfate attack. Failure is typically marked by expansion, cracking and spalling of a concrete specimen [101, 102]. Softening and loss of strength are also possible failure methods [103, 104]. Thankfully, the process is slow and can take years to manifest itself [105].

Table 2-4 – Limiting Value for Exposure Classes for Chemical Attack from Groundwater [100]

Chemical		XA1	XA2	XA3
SO_4^{2-}	mg/L	≥ 200and ≤ 600	> 600 and ≤ 3000	> 3000 and ≤ 6000
CO_2 agg	mg/L	≥ 15 and ≤ 40	> 40 and ≤ 100	> 100
NH^{4+}	mg/L	≥ 15 and ≤ 30	> 30 and ≤ 60	> 60 and ≤ 100
Mg^{2+}	mg/L	≥ 300 and ≤ 1000	> 1000 and ≤ 3000	> 3000
pH		≤ 6.5 and ≥ 5.5	< 5.5 and ≥ 4.5	< 4.5 and ≥ 4.0

Damage can also be caused by the precipitation of sulfate salts in porous structures such as concrete. This physical form of damage however requires some form of drying of the solution for the sulfates to crystallize in pores. Such a mechanism can be encountered in tidal zones, where a cyclic wetting and drying phenomenon can occur, and in half buried structures for example. Naturally both chemical and physical attack can occur in one single specimen [106].

2.3.1 Chemical Sulfate Attack

2.3.1.1 Sulfate Ingress

Sulfate attack requires intimate contact between sulfate anions and the cement paste of the concrete. Therefore, if sulfate attack is to be anything more than superficial, ions must be transported from the surface into the concrete bulk. Sulfate ingress is driven by a concentration gradient (diffusion), and impeded by the low permeability of the sample. Consequently, it has been shown that the use of a lower W/C will result in better resistance to external sulfate attack [105]. Yu et al. [107] measured the sulfate profile of Portland cement mortars immersed in a sodium sulfate solution and were able to identify 3 distinct zones:

1. An outer surface lacking in sulfate, due to the absence of calcium to bind the element
2. An increasing sulfate concentration to a maximum at a depth of 0.5-1 mm
3. A gradual decrease in sulfate concentration to background levels over a depth of several millimeters.

Yu et al. observed that the sulfate penetration depth remained unvaried with the sulfate content of the aggressive media.

2.3.1.2 Precipitation of Ettringite

The most common image of sulfate attack is associated with the precipitation of ettringite, leading to expansion and cracking. Ettringite is a calcium sulphoaluminate hydrate with a composition of $C_6A\bar{S}_3H_{32}$. As such, the penetrating sulfates need to find a source of aluminium and calcium with which to react. Aluminium is distributed among unreacted material and several hydrates, including C-S-H, hydrotalcite and, most commonly, AFm phases. The conversion of AFm to ettringite requires provision of an extra 2 calcium atoms (Ca/Al_{AFt}=6). This may be sourced from the calcium hydroxide.

The actual conversion from monosulfate to ettringite is in fact not expansive [108, 109]. Instead, the reaction is associated with an overall loss of volume. However, the

precipitation of ettringite, at the expense of monosulfate, results in a doubling in solids volume, increasing from 312.7 $mL.mol^{-1}$ to 714.9 $mL.mol^{-1}$. The same situation applies to the precipitation of gypsum from portlandite (increasing from 33.2 $mL.mol^{-1}$to 74.2 $mL.mol^{-1}$) [110]. It is this increase, in solid volume, which is the origin of the expansion and cracking seen upon sulfate attack.

Although it would be convenient to explain concrete failure as being due to an increase in solids volume, it is not enough to explain degradation upon ettringite precipitation. There is no link between the amount of ettringite and/or gypsum precipitation and the extent of expansion [14, 111]. Lothenbach et al. [112] showed that the increase in solids volume upon sulfate attack did not exceed the total capillary porosity, when modelling for changes in phase assemblage for a neat mortar exposed to either 4 $g.L^{-1}$ or 44 $g.L^{-1}$ of Na_2SO_4 (Figure 2-9). Therefore, if the expansive agents formed only in the capillary pores, then no expansion should occur. As such, ettringite must precipitate in confined spaces to cause damage.

With such attention attributed to ettringite formation, it follows that preventing its formation can assist in attempting to improve sulfate resistance. Decreasing the overall C_3A content, which reacts with water and sulfate to form ettringite, can result in improved resistance to sulfate attack. Several studies have shown that a lower C_3A content can lead to improved resistance [105, 113, 114]. The impact of reducing the C_3A content is wildly recognized and sulfate resisting cements have been subsequently devised (Type V from ASTM C150/C150M-12 [18] and the CEM I-SR series from BS EN 197-1:2011 [10]).

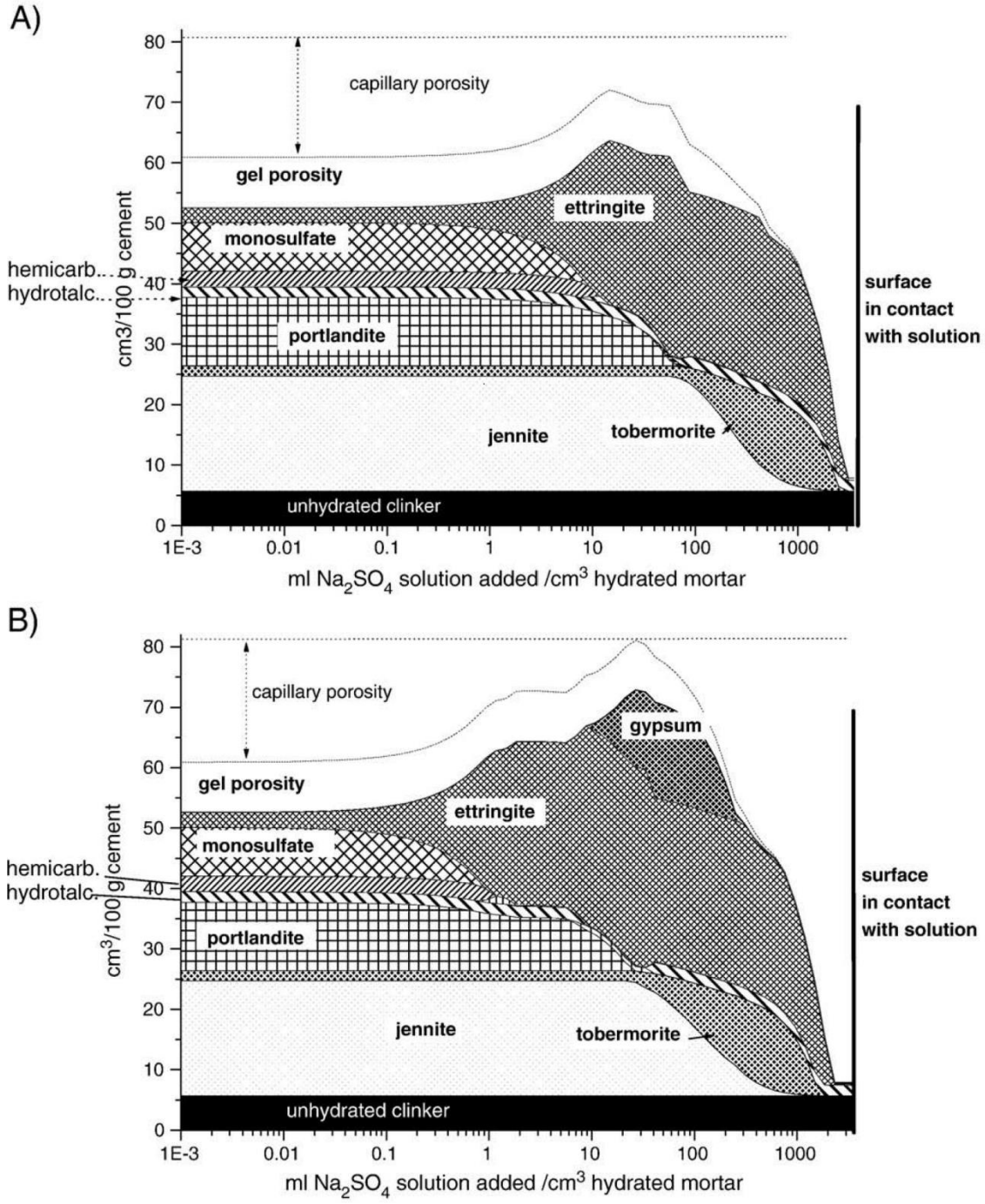

Figure 2-9 – Phase Assemblage of Mortar Samples Immersed in A) 4 g/L Na_2SO_4 and B) 44 g/L Na_2SO_4 (Taken from [112])

2.3.1.3 **Precipitation of Gypsum**

In addition to work on ettringite precipitation, previous work has probed the role of gypsum formation and found that its precipitation also leads to expansion [115, 116, 117]. Wang [118] even stated that gypsum formation is more damaging than that of ettringite.

However, the aforementioned studies rely on the use of strongly concentrated, circa 5% Na_2SO_4, solutions.

Gypsum precipitation is dependent on the sulfate concentration and the pH of the solution. As the pH increases, so must the sulfate content [119]. This agrees with thermodynamic investigations [112, 120], with gypsum predicted to precipitate at higher sulfate concentrations. Some studies have seen the formation of gypsum in already formed cracks [121, 122] and as such its impact on expansion can be debated. Schmidt et al. [122] stated that the role of gypsum precipitation in cement exposed to a strongly sulfate solution was to open up cracks which were already present. Planel et al. [123] however noticed the presence of gypsum in cement pastes exposed to a much lower concentration, i.e. 0.015 $mol.L^{-1}$ (2.1 $g.L^{-1}$) of Na_2SO_4. This is supported by other studies [124, 125]

2.3.1.4 **Leaching**

As sulfates ingress inward, calcium hydroxide leaches out of the cement paste, releasing Ca^{2+} and OH^-, plus alkalis [123, 126, 127, 128, 129, 130]. This is plotted in Figure 2-10; the extent of leaching shows a linear relationship with the square root of time, typical of diffusion-based reactions. With the leaching of these species, the pH of the pore solution is reduced causing C-S-H to decalcify; this is marked by a gradual reduction in the Ca/Si of the phase [126]. The lower pH also causes ettringite to decompose to gypsum at a pH<10.7 [131].

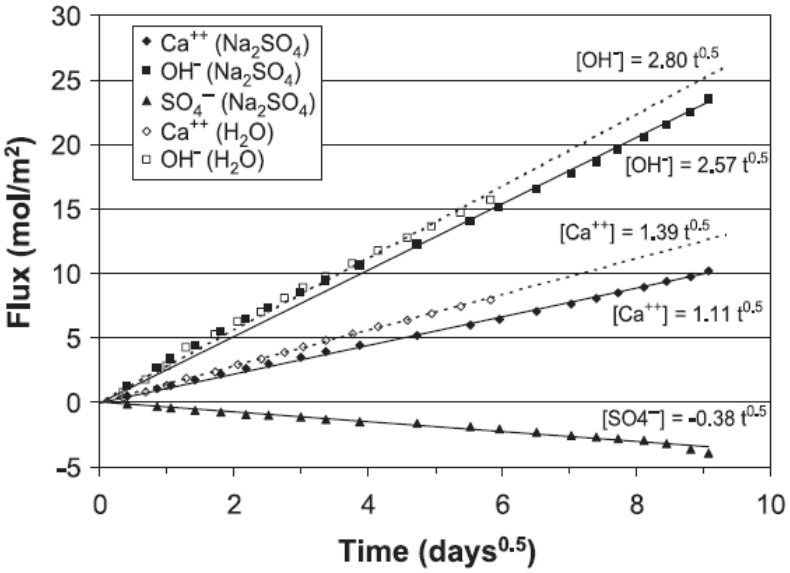

Figure 2-10 – Kinetics of Leaching of Ca^{2+} and OH^- (tested in Deionized Water) and Ingress of SO_4^- (Tested in Na_2SO_4 solution) (Taken from [123])

Leaching results in the softening and loss of strength of the cement paste as the porosity increases [132]. The leaching kinetics are dependent of the nature of the surrounding solution. The extent of leaching is also dependent on the pH [133] and temperature of the solution, the sulfate source, the W/C of the sample, and the use of SCMs [128, 129]. A more concentrated solution can also promote leaching. As such, leaching effects should be taken into account when evaluating sulfate attack [125].

Figure 2-11 summarizes the physiochemical changes usually observed in cement when exposed to sulfates. The model assumes a sodium sulfate solution, with only the sulfate-bearing fraction reacting.

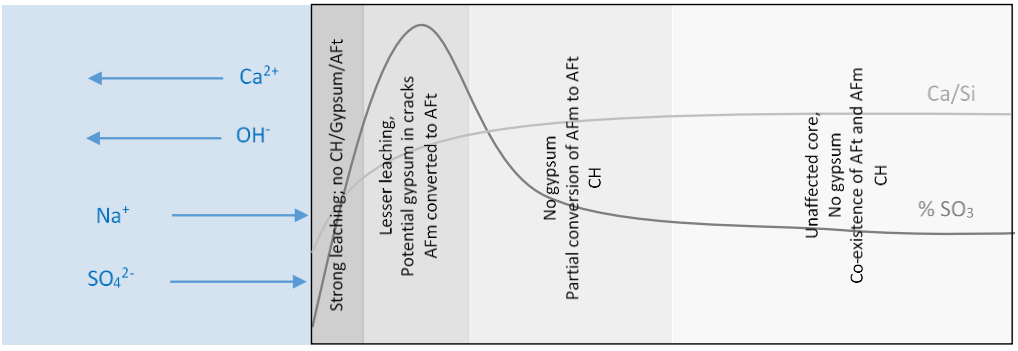

Figure 2-11 – Schematic Physiochemical Changes Typically Observed During Sulfate Attack, Assuming a Na_2SO_4 solution with only Sulfates Reacting

2.3.1.5 **Expansion Mechanism**

Over the years, several theories have been put forward as to explain why expansion occurs upon ettringite precipitation [134]. The more common ones are briefly explained below.

2.3.1.5.1 Swelling Pressure

Mehta [135] suggested that ettringite imbibing water could cause expansive swelling pressure, when working with sulfoaluminate cements mixed with lime and gypsum. It should be noted that in the presence of lime, ettringite takes the form of a colloidal solid, with its high specific surface area adsorbing water molecules [136]. Brown and Taylor [134] stated that swelling is a typical property of gel like materials, being flexible to withstand swelling. However, ettringite is not usually observed to form as a gel and its internal structure cannot take more than 36 moles of water, making this theory unlikely to be the underlying cause of expansion due to ettringite formation.

2.3.1.5.2 Topochemical Growth

Another, early, theory stated that ettringite grows topochemically [137, 138]. This theory, however, appears unlikely owing to the different crystal structures of C_3A, AFm and ettringite. Instead, ettringite appears more likely to precipitate by a through-solution mechanism.

2.3.1.5.3 Crystallisation Pressure

The more recent theory of crystallisation pressure [139, 140, 141, 142, 143] appears to be a more plausible mechanism behind expansion. The theory states that a crystal (ettringite) can precipitate from solution, supersatured with respect to the phase. The maximum pressure exerted is then given by [14]:

$$\Delta P = \frac{RT}{V_m} \ln \frac{IAP}{K_{s0}}$$

Where:

ΔP= pressure needed to halt crystal grown in a pore
R = Molar Gas Constant
T = Temperature (K)
V_m = Molar Volume
IAP = Ion Activity Product
K_{s0} = equilibrium solubility product

The ratio (IAP/K_{s0}) is the supersaturation ratio. The system is stable if the ratio equals 1. If greater ettringite will precipitate; and if lower ettringite will dissolve. It is also necessary for a crystal to grow in a confined space, opposing growth, in order to cause pressure. The stress generated in a single pore is insufficient to cause damage and growth must occur on a larger scale. Crystallisation pressure is also dependent on pore size, humidity, pH and the existence of solid solutions [140, 141, 143]. The application of crystallisation pressure has recently been applied to external sulfate attack [107, 144]. Yu et al. [107] measured a crystallisation pressure as high as 21 MPa from a solution supersatured with respect to ettringite, exposing samples to a 30 $g.L^{-1}$ sodium sulfate solution.

2.3.1.6 **Thaumasite Sulfate Attack**

Thaumasite Sulfate Attack, or TSA, is a form of sulfate attack differing from conventional attack in that it involves the interaction of an external source of sulfate with C-S-H. Thaumasite has no binding capacity, resembling a 'white, incohesive mush' [108]. As a result, in the UK, the Thaumasite Expert Group was formed and identified numerous occurrences of thaumasite sulfate attack [145, 146]. During TSA, the calcium and the silica react together with sulfates and carbonates, primarily at low temperatures, as shown below:

$$3Ca^{2+} + SiO_3^{2-} + CO_3^{2-} + SO_4^{2-} + 15H_2O \rightarrow 3CaO.SiO_2.CO_2.SO_3.15H_2O$$

The phase usually precipitates at lower temperatures (<15°C) [147, 148, 149]. Although some studies have seen the formation at higher temperatures [150, 151, 152]. Limestone cements have been shown to be less resistant to TSA [153, 154]. Nobst and Stark [155] meanwhile showed that more thaumasite formed in C_3A and Al_2O_3 rich cements. They also pointed out that even low C_3A cements were susceptible to thaumasite attack. This was confirmed by Blanco-Valera et al. [148] and even concluded that more thaumasite was formed in C_3A-poor cements compared to C_3A-rich cements, albeit with slower kinetics. In cement devoid of C_3A, however, no thaumasite was noticed [156]. Bellman and Stark [157] demonstrated the role of portlandite, which worsened resistance when present. Perhaps consequently, the use of blended systems appeared to improve resistance to TSA [11, 157, 158, 159].

Thaumasite resembles ettringite from a structural point of view [160, 161, 162], where the alumina has been substituted by 6-fold coordinated silicate ions. In fact, the presence of ettringite is considered a precursor for thaumasite formation. Thaumasite, however, is more easily stabilized at higher SO_3/Al_2O_3 ratios, greater than that required for ettringite ($SO_3/Al_2O_3 = 3$) [122, 163] and a solid solution, woodfordite, exists between the two phases [163, 164, 165]. A study by Kohler et al. [166] found a link between ettringite and thaumasite such that ettringite controls the rate of thaumasite formation.

The mechanism of thaumasite formation has been discussed widely [167, 168]. Bensted [167] proposed two different mechanisms. Firstly, a direct route whereby carbonates reacted with sulfates, silicates (from C-S-H) and calcium in excess water. Secondly, by the woodfordite route, where ettringite, silicates and carbonates react together. According to Crammond [168], thaumasite could either form topochemically from ettringite, substituting [Si] and [SO_4^{-2} + H_2O] for [Al] and [CO_3+SO_4^{2-}] respectively, or through solution, where thaumasite will precipitate if sulfate and carbonates are present, and all the aluminium has been consumed to form ettringite.

2.3.1.7 **Impact of the Sulfate Source**

Sulfates within groundwater do not exist in isolation, but co-exist with other anions and cations. The nature of the cation has been found to play an important role in sulfate attack, and has been the subject of considerable investigation.

2.3.1.7.1 Calcium Sulfate

$CaSO_4$ is perhaps the least aggressive salt, primarily because of its lower solubility (1.46 $g.L^{-1}$ of SO_4^{2-}) [108]. This makes it an unsuitable salt for use in laboratory simulations to assess sulfate resistance. Still, continued exposure to the salt in field conditions can, over time, lead to some damage [169].

2.3.1.7.2 Alkali Sulfates

Alkali sulfates include both potassium and sodium sulfates. Sodium sulfate is perhaps the most widely used salt for assessing sulfate attack. This may be attributed to its high solubility.

Conversely, little work is available on the use of potassium sulfate. Both Hooton et al. [13] and Kunther et al. [14] immersed mortar samples to potassium sulfate solutions both finding rapid expansion. A thermodynamic [14] study predicted that ettringite would be precipitated, plus possibly syngenite $K_2Ca(SO_4)_2.H_2O$.

An early study looked at the role of alkali sulfates in sulfate attack and drew parallels with the conditions required for ASR attack [170] finding both sulfate attack and ASR in several structures.

2.3.1.7.3 Magnesium Sulfate

Magnesium sulfate will initially react with calcium hydroxide, to produce magnesium hydroxide (brucite), and gypsum, according to the reaction shown below:

$$Mg^{2+} + SO_4^{2-} + Ca(OH)_2 + 2H_2O \rightarrow Mg(OH)_2 + CaSO_4.2H_2O$$

Brucite will take the form of a layer close to the surface of the sample, with a sub layer of gypsum [121, 171] lying just beneath this. The layer of brucite can, however, offer some level of protection, reducing permeability [172], but sulfate can still diffuse through the brucite layer to form ettringite deeper into the sample where the pH is higher. The barrier does eventually break, accelerating the degradation mechanism.

The aggressive nature of the salt is a consequence of brucite's very low solubility. A solution saturated in brucite will have a pH of 10.5, too low to stabilise C-S-H and ettringite. As a result, greater decalcification can occur. The combined action of magnesium with sulfate makes this salt particularly aggressive, especially in the absence of calcium hydroxide.

Magnesium sulfate can lead to the formation of magnesium-silicate hydrate (M-S-H) [121, 173]. Gollop and Taylor [174] measured a Mg/Si of 1.5 for the phase suggesting a phase similar in composition to crystalline serpentine, having a composition $M_3S_2H_2$. Bonen and Cohen [175] meanwhile suggested a composition closer to M_2SH_x.

2.3.1.7.4 Mixed Solutions

Most laboratory tests make use of ideal solutions, where only one cation is associated with the sulfate. In reality, several different cations may be present in sulfate-laden water sources. Kunther et al. [14, 176] compared the performance of mortar prisms exposed to various sulfate solutions, including a mixture of different sulfate salts. One of the two studies compared the expansion of at a CEM I mortar prism exposed to a mixed-cation solution and a dilute $MgSO_4$ solution [176]; the overall sulfate content was much greater in the mixed-cation solution. Nonetheless the extents of expansion of the two samples were comparable. The authors only speculated that the different ions somehow affected the degree of supersaturation with respect to ettringite. However, the mechanism of magnesium sulfate attack differs from that of sodium sulfate, making any comparison difficult.

2.3.1.8 Impact of Supplementary Cementitious Materials and Additives on Chemical Sulfate Attack

The use of supplementary cementitious (PFA, GGBS, and silica fume) materials have often been used to suppress sulfate attack; helping to minimize both ettringite and gypsum formation, plus helping to resist thaumasite attack [12, 177, 178]. BS EN 197-1:2011 [10] allows the use of slags or pozzolans, with a minimum content of 66% and 21% by weight respectively. According to Al-AMoudi [173], the use of composite systems aid sulfate resistance by the following processes:

1. Diluting the clinker species. Reducing C_3A and C_3S contents result in less aluminate hydrates and portlandite to react with sulfates. SCMs are usually calcium deficient compared to cement [36].
2. Pozzolans further reduce the portlandite content as they hydrate. Slags may also consume CH, but to a lesser extent. As such, less portlandite is available to form gypsum or to provide calcium to form ettringite.
3. Blended systems usually exhibit a finer pore structure reducing permeability [80], thereby improving resistance.

2.3.1.8.1 Fly Ash

A minimum fly ash content of 20% can effectively lead to improved resistance against sulfate attack [158, 179, 180, 181] . As explained above, this is mostly due to the pozzolanic reaction of the fly ash consuming an already diluted portlandite content. However, the composition of the fly ash must not be ignored, and calcium-rich fly ash can prove to be poorly performing. Consequently, an R-factor was devised and defined as [182]:

$$R = \frac{\%CaO - 5}{\%Fe_2O_3}$$

If R is less than 1.5, then a fly ash can be assumed to perform satisfactorily. Mehta [17] argued that this was insufficient, and suggested rather that it is the nature of the aluminate hydrates present prior to sulfate exposure (ratio of ettringite to monosulfate,

depending on the sulfate content and reactive alumina) which determines the suitability of a fly ash.

2.3.1.8.2 Silica Fume

A blend of up to 15% silica fume with cement has previously been shown to provide good resistance upon exposure to Na_2SO_4 solutions [183]. This is a result of a denser microstructure provided by the hydration of the finer silica fume particles [184]. However, such blends perform poorly when exposed to magnesium sulfate [173, 175, 183]. Such blended systems are depleted with respect to portlandite, and any ingressing magnesium will subsequently react initially with C-S-H to form brucite and gypsum, and ultimately M-S-H.

2.3.1.8.3 Ground Granulated Blast Furnace Slag

Composite systems containing slag can also help prevent sulfate attack [11, 13, 15, 16, 97, 185]. The behaviour of such systems is dependent on the level of replacement and the composition of the slag. Slag cement blends typically behave adequately when slag levels are high (70%). This effect is amplified when using slags with lower Al_2O_3 contents.

The use of high levels of slags to improve resistance may appear to be counterintuitive with their higher aluminium content. Aluminium released during hydration is distributed between C-S-H, aluminate hydrates (AFt and AFm), and hydrotalcite, plus any remaining in unreacted slag. Only aluminium bound by the AFm is readily available to react with sulfates. Gollop and Taylor [16, 97] discussed the impact of how aluminium is distributed in such systems. Slag cements produce a C-S-H phase with a lower Ca/Si ratio, which allows it to bind more aluminium in its structure. The hydrotalcite phase also binds aluminium; how much depends on the composition of the slag (both the Mg content of slag, plus its Mg/Al ratio). Combined, C-S-H and hydrotalcite can actually bind much of the aluminium released, hiding it from sulfates, the impact of which is greatest in blends with high levels of slags potentially improving resistance.

The role of a lack of aluminium availability can be seen in alkali activated systems. Komljenović et al. [186] found that an alkali activated slag system outperformed a CEM II/A-S system. The better resistance of the former resulted from the fact that aluminium was bound to the C-S-H and hydrotalcite and, therefore, unavailable to react with sulfates.

Still, Fernandez-Altable [187] also showed that during sulfate attack, aluminium reacts with sulfates to form secondary monosulfate prior to forming secondary ettringite, where ingressing sulfates react with aluminium from slags. This effect would explain why slag blended systems show improved resistance. He further stated that resistance of a blend is dependent on the initial amount of AFm present at low levels (40%) of slag replacement and the overall Al_2O_3 content at higher levels (70%).

2.3.1.8.4 Impact of Gypsum

A few studies have been concerned with the impact of additional gypsum, that is when adding more than that already present to regulate setting, on sulfate resistance [11, 16, 185, 188]. Gollop and Taylor [16] studied a series of slag-containing blends, one of which contained 65% slag with added gypsum. This last mix showed a much better resistance when compared to blends with 69% slag without gypsum; the sulfate slag blend performed as well as a slag blend containing 92% slag without added sulfates. Similarly, better resistance of fly ash blends containing added gypsum has been seen when samples were exposed to a 10% Na_2SO_4 solution [188]. The work found an optimum sulfate content, beyond which sample resistance worsened due to increased susceptibly to volume instability. The use of additional gypsum favours ettringite precipitation over AFm phases at early ages, before the occurrence of sulfate attack [4]. With more of the original aluminium now bound, less is available to subsequently react with sulfates.

2.3.1.8.5 Impact of Limestone Addition

While often considered to be an inert filler, limestone is actually partially reactive. Its effect is seen in the distribution of the aluminate hydrates and carbonate-AFm phases are preferentially formed over monosulfate; the expelled sulfate then allow for the stabilization of AFt [41]. Ogawa et al. [185] and Higgins [12] reported improved sulfate resistance upon low levels of limestone addition, although the former cautioned that the resistance is limited as the carbonate AFm, which initially formed with the added carbonated, may very well convert to ettringite.

BS EN 197-1:2011 allows for the replacement of cement with limestone, up to 35% by weight. Irassar [150] recently reviewed the use of limestone cements in the presence of sulfates. He concluded that low levels of replacement (<10 %) would have no detrimental effects, but resistance would worsen at higher levels. This was attributed to the increase of the effective W/C of the system, increasing porosity and favoring penetration of the sulfates [122]. Limestone can also promote the thaumasite form of sulfate attack [150].

2.3.2 Physical Sulfate Attack

2.3.2.1 Mechanism

Sulfate attack may manifest itself physically when dissolved salts diffuse through the concrete and precipitate in pores, causing damage [140, 189, 190, 191]. A particularly pernicious salt is sodium sulfate [142, 191, 192]. Two crystalline sodium sulfate salts exist; thenardite ($NaSO_4$) and mirabilite ($NaSO_4.10H_2O$). A solution of thenardite is supersaturated with respect to mirabilite at temperatures below 32°C and humidities above 75 %; the precipitation of mirabilite can then cause damage [142, 193, 194]. Rodriguez-Navarro et.al. [191] noted that at relative humidities above 40%, mirabilite would form first from a supersatured solution of Na_2SO_4, which would subsequently convert to thenardite. Below 40% RH, thenardite would be precipitated directly. Several damage mechanisms have been proposed and have been summarized previously [190], putting forward the idea of crystallisation pressure [139, 140].

Cyclic wetting and drying can favour such damage [124, 189, 195]. The salt precipitates in the drying cycle, where the humidity is allowed to drop. It is usually during the wetting cycle that damage is observed [142], where in the case of sodium sulfate, existing thenardite dissolves and the solution is supersatured again with respect to mirabilite.

Scherer [140] partially submerged porous stone in a sodium sulfate solution which penetrated the sample by capillary action. As the solution percolated upwards, efflorescence took place on the side of the sample and subflorescence occurred within the samples, where the rate of evaporation matched that of the water rise (Figure 2-12). Parallels may be drawn between this study and similar situations arising in concrete. Concrete samples subjected to semi immersion have been tested in the past, in both field and laboratory conditions [106, 124, 196]. The immersed portions will be subjected to chemical sulfate attack, whereas the exposed regions will expect to fail due to salt crystallisation. As such, both actions may have to be considered.

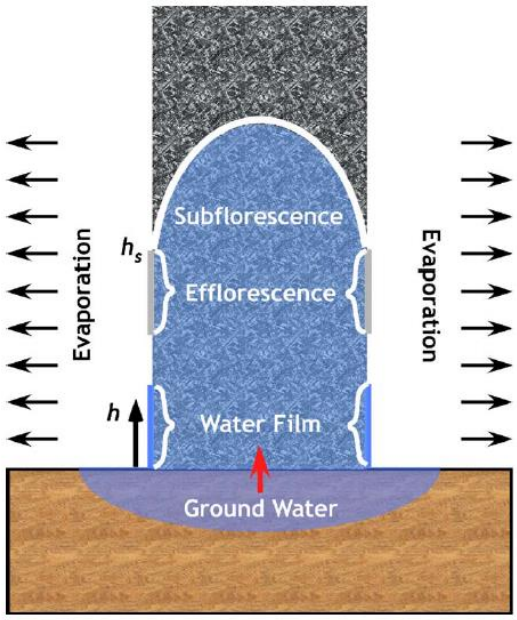

Figure 2-12 – Schematic of Capillary Rise Through a Porous Material In Contact with Groundwater (taken from [140])

2.3.2.2 Supplementary Cementitious Materials on Physical Sulfate Attack

Although the use of SCMs may aid, delay or prevent sulfate attack, the same cannot be said in the event of physical sulfate attack [106, 124, 196]. Nehdi et al. [106] studied partially immersed concrete samples. While the immersed parts suffered from conventional chemical sulfate attack, mirabilite crystallised above the water level, causing further damage. In concretes containing pozzolans (fly ash, metakaolin and silica fume), damage from physical attack was greater in comparison to samples free from pozzolans, due to an increased pores of smaller diameter. This increased capillary suction and the surface area for drying. This agrees with a similar study carried out by Irassar et al. [196].

2.3.3 Sulfate Attack in Field Conditions

Several studies have been concerned with the performance of concrete exposed to sulfates in field conditions [103, 124, 169, 196, 197, 198, 199, 200]. In such conditions, sulfates present in water sources (groundwater, river water, etc) or from the oxidation of sulphide minerals (pyrite, marcasite, pyrrhotite), can penetrate the cement matrix. Key issues with field studies are that concentrations are typically lower than in laboratory simulations and there is a mix of different sulfate species.

It is also important to know how cement based structures interact with the sulfate source. This is seen when comparing two separate studies carried out on samples either partially immersed [196] or fully immersed [200] in sulfate-laden soils for 5 and 19 years respectively. The same material was used for both studies, exposed in the same, sulfate-rich soil (approx. 1% SO_4^{2-}). The impact of admixtures (slags, fly ash and a natural pozzolan) was also studied in these two studies. In fully buried samples, the blended systems were reported to perform the best. However, in half buried samples, the half exposed to the atmosphere showed greater damage in the blended system.

Bellmann [169] assessed the performance of 20 structures across Thuringia, Germany. Some of the structures contained supplementary cementitious materials and

assessing the impact of cement type was made difficult because of the wide range of exposure conditions. The structures were grouped depending on the exposure conditions, reflecting the variability in which concrete structures can be exposed to sulfates. Most of the structures behaved adequately, with only six of the structures being seriously damaged. Often structures showed the formation of thaumasite and the more damaged structures were in contact with sulphide rich rock or soil where low pH can worsen resistance due to an acid attack of the concrete. Structures, however, showed limited damage when exposed to rivers and groundwater, where the sulfate concentrations were the lowest.

Mehta [103] carried out a review of sulfate attack on concrete structures in field conditions. He concluded that cracking and failure is rarely ever attributed to sulfate attack alone, and that weathering and increased permeability of the concrete through micro cracking must also occur. He further stated that structures fail by decohesion and loss of strength due to the decomposition of cement hydrates.

2.3.4 **Experimental Considerations**

2.3.4.1 **Standards**

Due to the multitude of factors influencing sulfate attack in the field, laboratory tests must be simplifications of such real-life scenarios. The most common standard used to assess sulfate resistance is the American standard ASTM C1012-13M [159], testing the resistance of samples exposed to chemical sulfate attack. The standard relies on using mortar prisms of a specified mix design and of a given minimum compressive strength. These prisms are fully immersed in a 5% Na_2SO_4 solution, although the solution can be substituted for another salt ($MgSO_4$). The solution, which by volume is four times that of the sample, is renewed at specified intervals. The extent of sulfate attack is then determined by measuring only linear expansion of the prisms. There is no equivalent European Standard, although BS EN 206:2013 [100] does recognize several exposure classes and specifies several attributes of the concrete to be used accordingly.

The American standard, however, does have its limitations. Soon after immersion, the samples will start leaching Ca^{2+} and OH^-, resulting in the decomposition of CH and C-S-H, quickly raising the pH of the surrounding solution to approximately 12.5.

Secondly, the concentration of the solution greatly exceeds what is expected to be found in natural conditions. The implications of this were previously debated by Bellmann [119]. A highly concentrated solution would favour the formation of gypsum, typically not observed in field conditions, along with ettringite precipitation. Furthermore, the solution used is only associated with one cation when more may be present in field water sources.

A further limitation is that performance is assessed solely on the extent of expansion. Ion exchange with the bathing solution results in leaching of cement hydrates, resulting in softening, decohesion and ultimately degradation of the sample. The loss of strength, elastic modulus and mass change are also indicative of damage, but not probed by the standard.

The RILEM report TC 25-PEM [201] made recommendations on how to assess the performance of stones exposed to sulfate resistance subjecting to wetting/drying cycles and partial immersion. The experimental procedures described in these studies may very well be adapted to concrete samples to test for other field setups, although some issues remain without adaption. For instance, the drying cycle (section V.1a and V.1b) [201] relies on drying samples at 105°C, which could result in dehydration of C-S-H and ettringite.

2.3.4.2 **Effect of Sample Preparation**

When wanting to assess the chemical impact of sulfate attack cementitious binders, several factors must be considered. Careful planning may help to better simulate field conditions. Some of these are detailed below. Fewer studies have been carried out on physical sulfate attack, for which no standard is readily available.

2.3.4.2.1 Size

Larger samples show better resistance [107, 123, 125, 202] to expansion. El-Hachem et al. [125] showed that the onset of expansion was delayed when increasing mortar prisms from 10x10x100 mm to 70x70x280 mm in size. Yu et al. [107] discussed that expansive forces occur near the surface when sulfate penetrate which is restrained by the core. Larger samples will require a greater section subject to expansion to overcome the restraining effect of the core.

2.3.4.2.2 Curing Conditions

Since sulfate attack relies on the transport of aggressive ions into the cement matrix, resistance is dependent on how the sample is prepared. Mangat and El-Katib [203] compared the resistance of air-cured and water-cured samples and found the former to be the more resistant, attributed to the formation of a carbonation layer opposing sulfate ingress. Fernandez-Altable [187] further showed that expansion of core samples, cut from larger samples, expanded faster that non cut samples; the act of cutting removed the carbonation layer, plus surface laitance.

2.3.4.2.3 Water/Cement Ratio

The water/cement ratio also plays a vital role in sulfate resistance, with its reduction increasing sulfate resistance [105, 204, 205, 206]. Specimens made with higher W/C results in an increase in porosity and permeability [207], favouring sulfate ingress and worsening resistance. Monteiro and Kurtis [105] suggested a ‘safe domain’, setting the W/C as low as 0.45, below which structures will perform adequately.

2.3.4.2.4 Interfacial Transition Zone

The presence of the interfacial transition zone (ITZ) can also affect sulfate resistance. This zone is characterized by having a higher porosity [208] than the bulk paste. The zone is also usually richer in portlandite [209]. Bonakdar et al. [210] varied the sand/calcium ratio of specimens (by using pastes and mortars), an increase which led to greater expansion of prisms. This was attributed to the higher diffusivity around

the ITZ. El-Hachem [125] found that the ITZ was rich in calcium and sulfate but poor in aluminium after exposing samples to a sulfate solution, indicating the presence of gypsum. This was previously observed by Bonen and Sarkar [211].

2.3.4.3 Effect of the Sulfate Solution

2.3.4.3.1 Sulfate Concentration

The use of a highly concentrated solution has already been debated by Bellman [119]. The use of highly concentrated solutions [107, 122, 125, 144] usually accelerate attack, although Yu et al. [107] noticed that the penetration depth of sulfate in mortar samples is independent of the sulfate concentration. Highly concentrated sulfate solutions, however, will favour the formation of gypsum [112, 119].

2.3.4.3.2 Renewal of the Solution

Fernandez-Altable [187] compared the effect of solution renewal on expansion exposing samples to renewed and non-renewed sodium sulfate solutions. Expansion was delayed in the former case. He attributed this effect to a reduction of the pH hindering ettringite growth. Lothenbach [112] modelled the effect of leaching, which was greatest if the solution was continuously replenished (for example, when in contact with a water flow).

2.3.4.3.3 Effect of the pH

To simulate field conditions better, some experimental setups allow for pH control [118, 123, 124, 130, 204, 212] Cao et al. [212] found a reduction in expansion when reducing the pH of the bathing solution in a neat system, which he attributed to greater C-S-H decalcification. Brown [213] on the other hand found a faster onset of expansion when reducing the pH of the solution. Chabrelie [124] carried out testing at constant pH and found that the leaching of the solution was prohibited as the solution was not renewed. Still, expansion was accelerated. Slag blended systems [212] appeared to be greatly affected by the pH, which worsened resistance as the pH decreased in blends

whose slag content was lower than 60%. Contrarily, PFA and silica fume blended systems performed admirably regardless of the pH.

Chapter 3

Materials and Method

3.1 Materials

Two cements, a CEM I 42.5R (C_1) and a CEM I 52.5N (C_2), conforming to BS EN 197-1:2011 [10] were chosen with this project along with three slags (A, B, and C) which differed mostly in their composition. In the choice of the slags, aluminium was the chief element considered, due to its implication in sulfate attack, and the overall Al_2O_3 content varied from 7.36% for Slag B to 12.33% for Slag C. The chemical composition and the clinker phases identified in the cements are reported in Table 3-1 and Table 3-2 respectively. The particle size distributions of all the raw materials are plotted in Figure 3-1.

Table 3-1 – Oxide Composition and Physical Properties of the As-Received Cements

		C_1	C_2	Slag A	Slag B	Slag C
Loss of Ignition 950 °C	%	2.62	1.8	1.67*	0.85*	1.57*
SiO_2	%	19.21	22.93	36.65	39.75	34.35
Al_2O_3	%	5.5	3.95	11.6	7.36	12.33
TiO2	%	0.27	0.18	0.9	0.25	0.93
MnO	%	0.04	0.03	0.37	2.54	0.4
Fe_2O_3	%	2.77	1.39	0.46	1.33	0.52
CaO	%	62.28	64.67	38.89	38.18	38.49
MgO	%	2.19	0.72	7.83	7.65	9.58
K_2O	%	0.93	0.7	0.66	0.65	0.48
Na_2O	%	0.08	0.15	0.17	0.13	0.24
SO_3	%	3.1	2.48	2.79	1.83	2.61
P_2O_5	%	0.17	0.15	0	0.01	0.01
Total	%	99.16	99.15	100.31	99.69	99.93
Na_2O-Equivalent	%	0.69	0.61			
Soluble K_2O	%	0.04	0.05	<0,01	<0,01	<0,01
Soluble Na_2O	%	0.62	0.36	0.01	<0,01	0.03
Soluble sulfate	%	1.02	1.12	0.06	0.05	0.02
Density [g/cm^{-3}]		3.37	3.21	2.84	2.93	2.81

Table 3-2 – Clinker Phases Identified in C_1 and C_2 (%Weight) by XRD

	C1	C2
C_3S [%]	61.0	58.7
C_2S [%]	11.9	21.6
C_3A [%]	7.5	8
C_4AF [%]	8.3	2.9
Calcite [%]	3.7	3
Anhydrite [%]	2.9	2.4
Hemihydrate [%]	1.5	0.6
Gypsum [%]	0	0.4
Other [%]	3.2	2.4

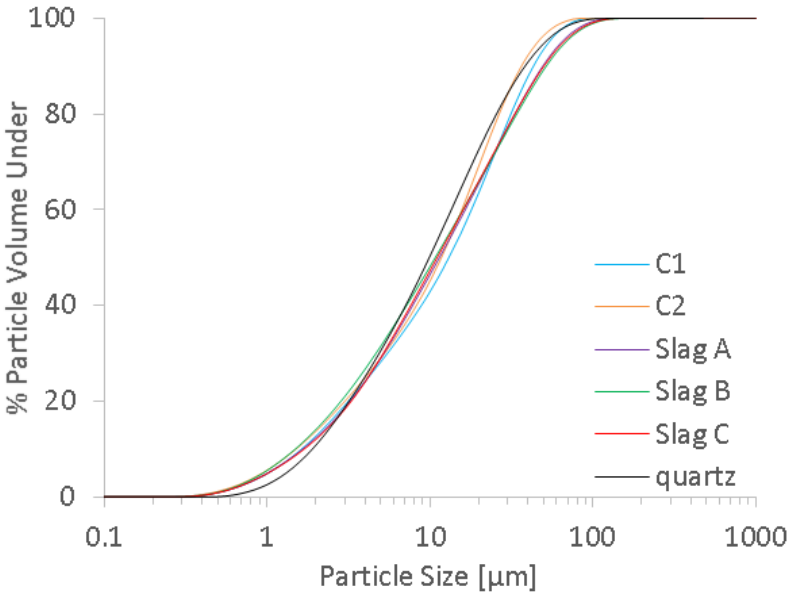

Figure 3-1 – Particle Size Distribution of the As-Received Materials, plus Quartz

Figure 3-2 highlights the high glass content of the slag, marked by the amorphous hump ranging from 20 to 40 2θ; all slags used had a glass content greater than 98%. There was some evidence of crystalline phases present, shown in Figure 3-2 and Table 3-3.

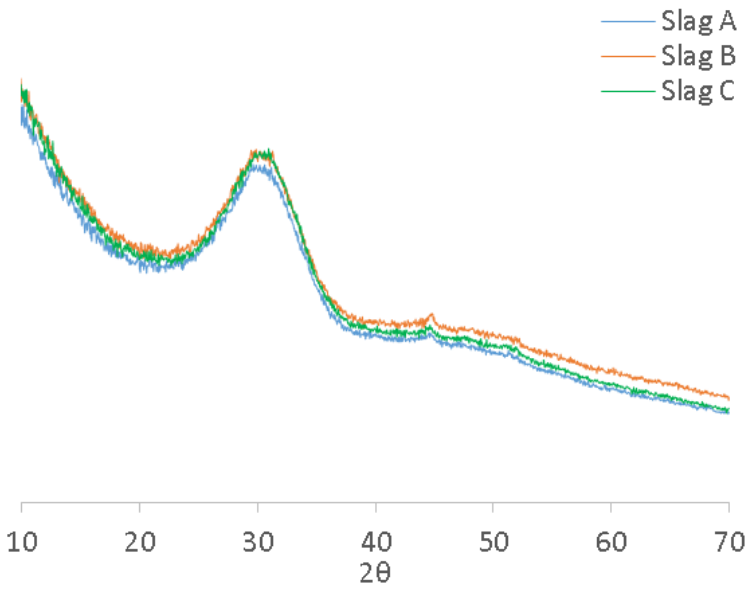

Figure 3-2 – X-Ray Diffractions of the as-Received Slags

Table 3-3 – Crystalline Phases Identified in the Slags

	Slag A	Slag B	Slag C
Calcite	1	0.4	0.7
Quartz	0.4	0.2	
Gehlenite	0.4	0.4	1
Glass content	98.2	99	98.3

Other material used in this study included quartz which was used as a replacement for slags when assessing their physical and chemical impact. Quartz was ground to a similar fineness to that of the slags and cements (Figure 3-1).

The quartz was assumed to be inert. Its reactivity was nonetheless measured by mixing together 50g of quartz with 35g of CH and 5g of calcite in 90mL of a 0.3m KOH solution [6]. Part of the mix was dried after 5 minutes of mixing by solvent replacement, while the rest was left to cure for 28 days. TG analysis revealed that the quartz was minimally reactive, with an increase in the water loss up to 350°C (Figure 3-3). Traces of KOH, however, remained after solvent exchange.

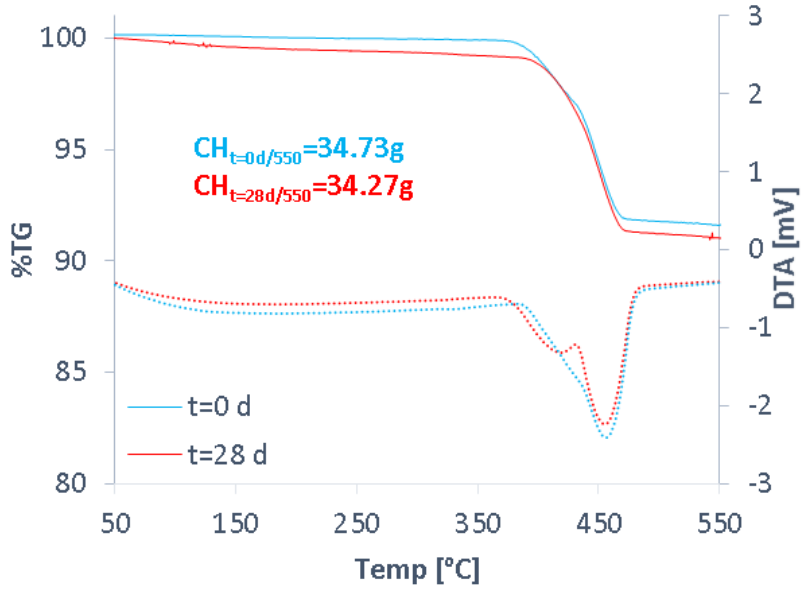

Figure 3-3 – Reactivity of the Quartz

3.2 Mix design

Studies were performed on either pastes or mortars, depending on the test in question. Generically any characterisation was carried out on pastes, including XRD, STA and SEM analysis as well as chemical shrinkage and isothermal conduction calorimetry. The engineering performance, however, was assessed on mortars (strength, expansion).

All samples were made with a water/binder (W/B) of 0.5. The term binder constitutes both the slag and the cement in a blend. Slag cement blends were then prepared replacing either 40% or 70% of the cement by weight. Additional slag blends contained additional anhydrite, replacing 3% of the binder by weight. This resulted in a total of 28 mixes. Although some tests were carried out on all 28 mixes (Table 3-4), including strength evolution, calorimetry and expansion, only 5 mixes were fully analysed in this study, shown in Table 3-5. The W/B and water/cement (W/C) are also shown. Mortars were mixed with 1 part binder to 3 parts sand and 0.5 parts water.

Table 3-4 – Design Matrix of all 28 Mixes

Slag type		**S_a**		**S_b**		**S_c**	
Slag content	0%	40%	70%	40%	70%	40%	70%
w/o $*	**C_1**	C_140S_a	C_170S_a	**C_140S_b**	C_170S_b	**C_140S_c**	**C_170S_c**
	C_2	C_240S_a	C_270S_a	C_240S_b	C_270S_b	C_240S_c	C_270S_c
w/ $	$C_1$$	$C_140S_a$$	$C_170S_a$$	$C_140S_b$$	$C_170S_b$$	**$C_140S_c$$**	$C_170S_c$$
	$C_2$$	$C_240S_a$$	$C_270S_a$$	$C_240S_b$$	$C_270S_b$$	$C_240S_c$$	$C_270S_c$$

***$ = anhydrite**

Table 3-5 – Mix Design of the 5 Selected Mixes Chosen for full Characterisation

	C_1	C_140S_b	C_140S_c	C_170S_c	$C_140S_c$$
Cement	100	60	60	30	58.2
Slag	-	40	40	70	38.8
anhydrite	-	-	-	-	3
water	50	50	50	50	50
total	150	150	150	150	150
W/B	0.5	0.5	0.5	0.5	0.5
W/C	0.5	0.83	0.83	1.67	0.86

3.3 **Drying**

Several drying techniques can be used for stopping hydration all of which have advantages and disadvantages [53, 214, 215]. Freeze drying was chosen as it was initially deemed suitable for the initial characterisation work planned, as stated by both Collier et al. [215] and Zhang and Scherer [214]. Samples were immersed in nitrogen at - 196°C at which point boiled. Samples were kept immersed until equilibrium (when the nitrogen no longer boiled) and placed in a vacuum until constant weight. The water is removed by sublimation with no capillary pressure generated. However, the freezing process may cause some stresses in the microstructure [214]. It was, however, later acknowledged that freeze drying may be severe enough as to damage ettringite [216]. Severe dehydration of this phase can render it undetectable by X-ray diffraction, marking the formation of meta-ettringite [217], having at most 11 to 13 moles of water.

Konecny and Naqvi [218] found that solvent replacement preserved the finer pores best, i.e. those less than 5 nm in size, but concluded that freeze drying was still a suitable

technique for measuring permeability, stating that the latter property depend on a greater extent on the coarser porosity. Galle [219] also suggested that freeze drying was a suitable hydration stopping method for MIP measurement. Korpa and Trettin [220] mentioned that freeze drying better preserved the microstructure due to the softening of capillary stresses generated and measured the highest surface of the pores compared to other hydration stopping methods.

Solvent replacement is known to preserve the microstructure well, but may interact with the sample [221], sorbing on the surface of C_3S and damaging hydrates [222]. Furthermore, solvent replacement is more suitable for small samples with higher diffusivity, otherwise the exposure time needs to be extended, with a high solution to sample ratio [223, 224]. Direct vacuum drying can damage the microstructure due to the higher surface tension of water (71.99 $Nm.m^{-1}$ at 25°C) [214], as well as dehydrating ettringite and monosulfate. Oven drying at 105°C can be severely damaging to the microstructure and can dehydrate C-S-H and ettringite [52, 219, 220] . In summary, no perfect hydration stopping method exists and the method chosen should be tailored for the experimental work carried out.

3.4 Isothermal Conduction Calorimetry

3.4.1 Principle of Isothermal Conduction Calorimetry

With cement hydration being exothermic, it is possible to measure the heat given off by the sample. This can be done using an Isothermal Conduction Calorimetry (ICC) [225]. Usually, the heat evolution rate and the total heat released from a system is measured. Modern calorimeters make use of a twin channel, where the heat given of a sample is compared to that of a reference sample. The use of a reference minimises noise and drift. It is important to ensure that the sample and the reference have same thermal properties [226, 227], with cement and quartz having a specific heat capacity of 0.75 $J.g^{-1}.K^{-1}$ and 0.8 $J.g^{-1}.K^{-1}$ respectively.

3.4.2 **Experimental Setup**

The heat evolved during hydration was measured using a TAM-air 8 twin channel calorimeter on 9 grams of paste. 100g of anhydrous binder was prepared and shaken vigorously from which 6g was then taken and placed in a 20mL plastic ampoule. 3g of water was added and the paste was shaken using an orbital shaker on slow to medium speed for 2 minutes. The ampoules were then placed and the sample channel, with an analogue quartz paste in the reference channel, set at 20°C (Figure 3-4).

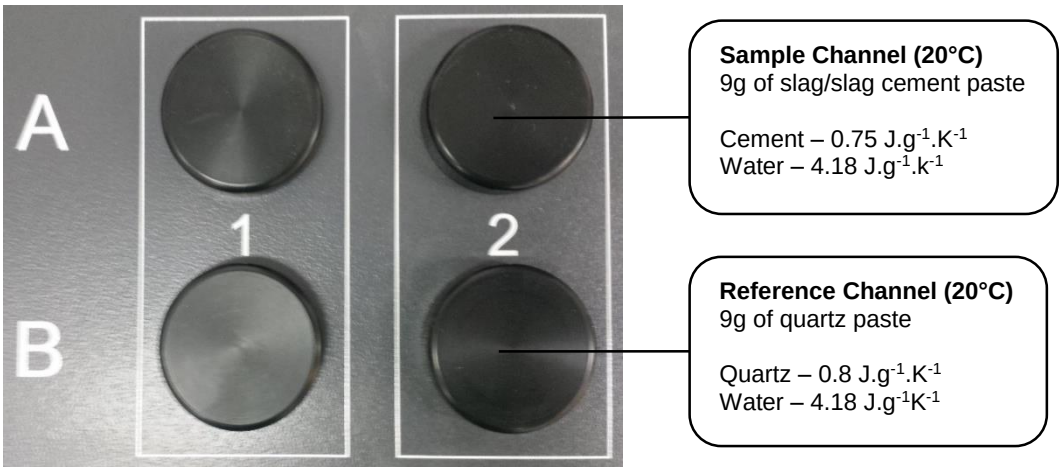

Figure 3-4 – Overview of the Calorimeter Setup. Channel a Contained 9g of Sample Paste, Whereas Channel B Contained 9g of a Quartz Analogue Serving as a Reference

3.4.3 **Slag Hydration Followed by Calorimetry**

By substituting the slag fraction in slag blends with unreactive quartz, it is possible to tentatively separate the heat contribution of the slag from that of the cement. This is detailed in Figure 3-5. The difference in heat between a neat and quartz paste is attributed to the filler effect, and the difference in heat between a quartz and slag paste is due to the hydration of the slag itself (Figure 3-5a). The heat from the slag can then be found by subtracting the heat evolved by a quartz paste from the heat evolved by a slag paste (Figure 3-5b). In doing so, the resultant curve showed apparent negative values. This is most likely due to differences in the hydrates formed between the quartz paste and the slag paste. Consequently, the minimum point on that same resultant curve was taken as the start of slag hydration, and was normalised to the slag content (Figure 3-5c).

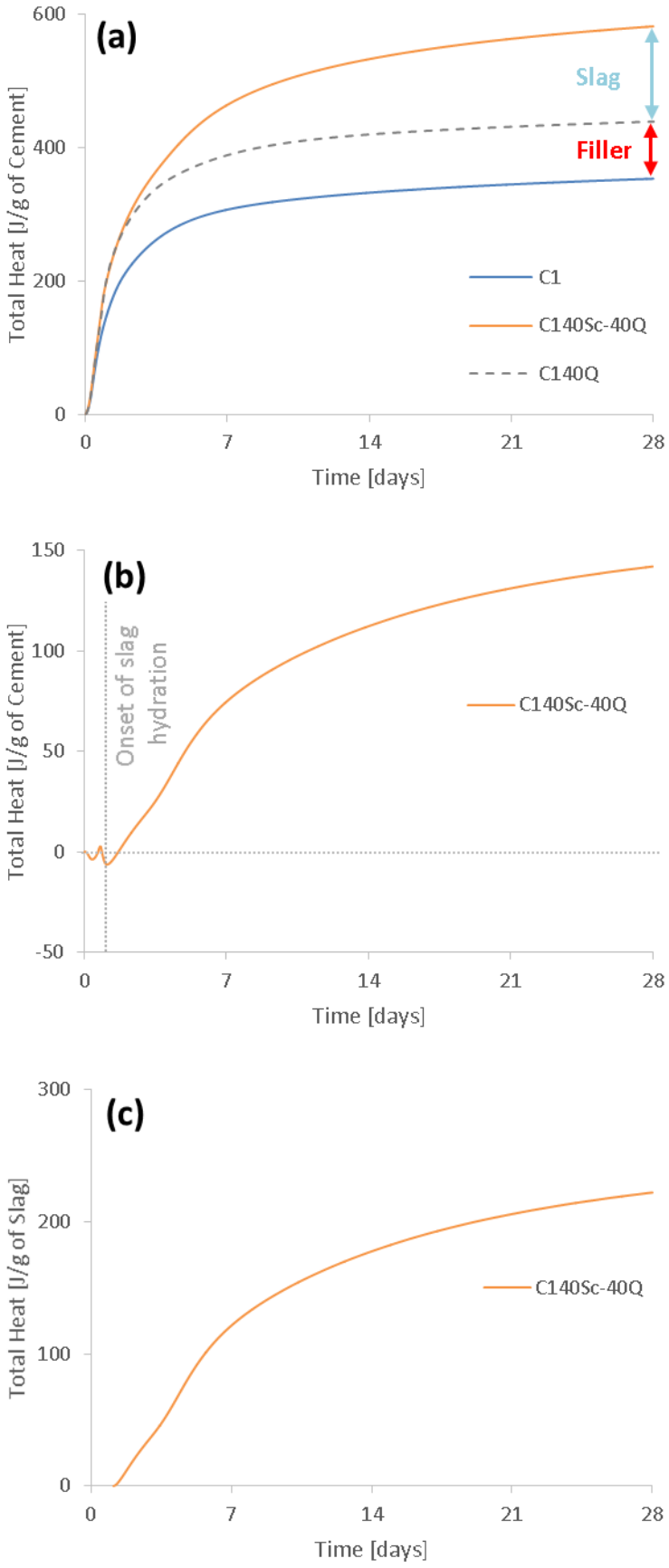

Figure 3-5 – Separating the Heat Evolved from the Slag from that of the Cement

3.5 Chemical Shrinkage

3.5.1 Principle of Chemical Shrinkage

Chemical shrinkage is the phenomenon in which the absolute volume of hydration products is less than the total volume of unhydrated cement and water before hydration. Chemical shrinkage occurs because water has a lower specific volume when bound to a solid than when water is free in a liquid [85, 228]. The shrinkage of a cement paste during hydration was first measured by Le Chatelier [229] in 1905. Chemical shrinkage differs from autogenous shrinkage, which is the macroscopic volume reduction of cementitious materials when cement hydrates after initial setting. Autogenous shrinkage does not take into account the volume change due to loss or ingress of substances, temperature variation and the application of an external force [230]. The difference between chemical and autogenous shrinkage is illustrated in Figure 3-6.

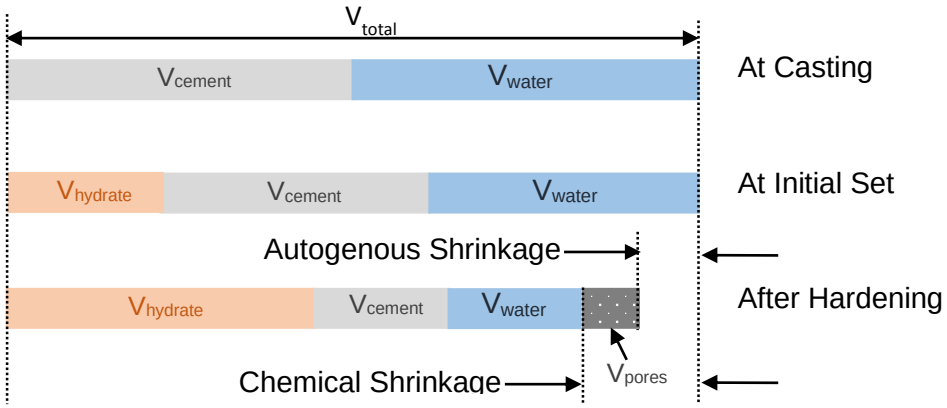

Figure 3-6 – Difference between Autogenous and Chemical Shrinkage [230]

3.5.2 Experimental Setup

Chemical shrinkage was measured by dilatometry [231]. 100 g of anhydrous binder was prepared, as described in section 3.4.2, from which 40 g was taken to prepare 60 g of paste (W/B = 0.5). The paste was mixed by hand for 2 minutes and 15 g was poured into each of 3 individual plastic beakers, 34 mm in diameter and 68 mm high. The beakers were tapped to level the paste and remove any entrapped air. The rest of the beaker was filled with water, using a plastic syringe to minimize disturbance. The beaker was then sealed shut with a rubber stopper through which a 1mL pipette was passed;

with water filling the pipette in the process. A few drops of paraffin oil dyed with 1-(methylamino)anthraquinone, was added on top of the water, acting as a tracer, to follow the total shrinkage. Chemical shrinkage was continuously measured with a 10 MP camera, capturing an image every 5 minutes for 28 days, monitoring the height of the tracer in the pipette. The setup is shown in Figure 3-7.

Maintaining a constant sample size is important, since sample size can affect the amount of shrinkage measured. Sant et al. [232] have shown that increasing the paste size results in a reduction in chemical shrinkage, measured by the buoyancy method, where the pores are less accessible to water. This was previously observed by Geiker [231] and Costoya [228].

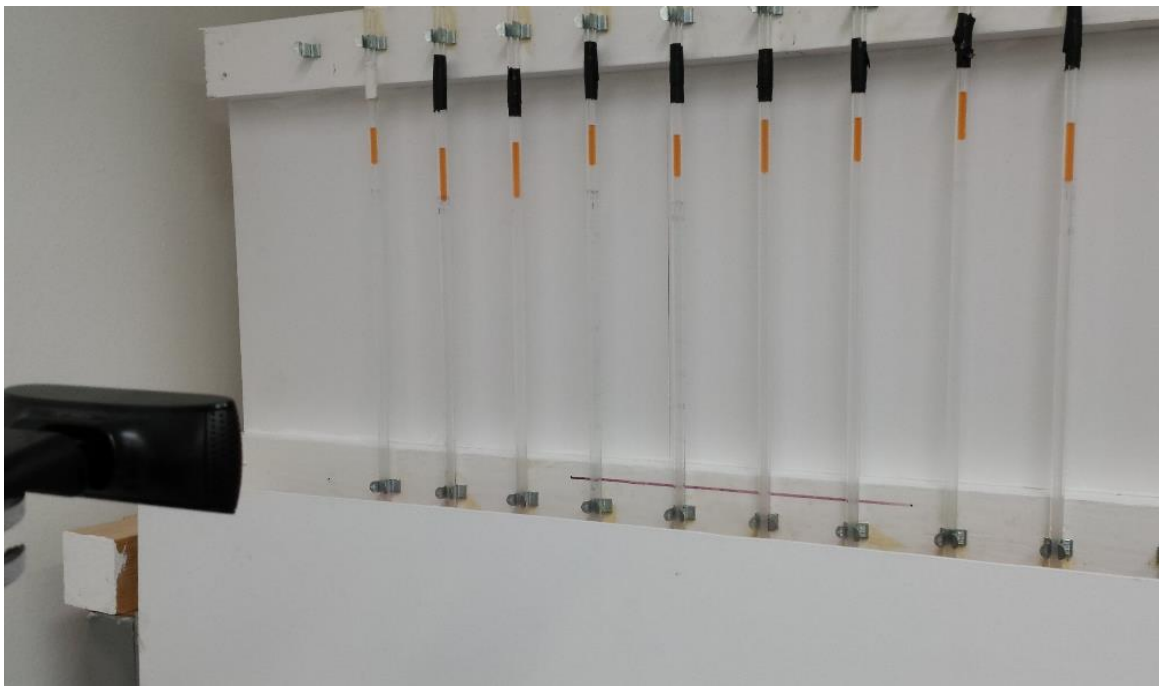

Figure 3-7 – Chemical Shrinkage Setup

3.6 Simultaneous Thermal Analysis (STA)

3.6.1 Principle of Thermal Analysis

Thermogravimetry analysis involved heating up a small amount of sample at a constant rate and measuring the change in mass. During the heating process of hydrated cements, phases decompose releasing water (from hydrates) or CO_2 (from calcite) [233].

The physical mass loss associated is referred to as thermogravimetry analysis. Differential thermal analysis is measured simultaneously, and is defined as the difference in temperature between the measured sample with a reference sample (here, another empty crucible).

The data is affected by sample size and heating rate [234]. A bigger sample mass result in an increase in the time needed to fully decompose a phase. This is seen in both the TGA and the DTA; in the latter, the endothermic peaks are shifted to higher temperatures. Increasing the heating rate increases the decomposition temperature too. Too fast a heating rate may not reveal phases present in too low concentrations on TGA tracings. On DTA tracings, peak amplitude increases with heat rate, and peak maxima shift to higher temperatures.

Figure 3-8 shows a typical thermogravimetry curve (TGA) for a cement sample with its corresponding differential curve (DTA). As the sample is heated, water bearing phases decompose first; starting with C-S-H phase, ettringite, and AFm. Ettringite decomposes around 100 to 150°C [233], while Taylor [19] suggested a narrow window ranging from 135°C to 140°C for ettringite in hydrated cement. The different AFm phases decompose at various temperatures [233]. Between 400 and 500°C calcium hydroxide (CH) decomposes suddenly to CaO, resulting in a sharp mass loss. At higher temperatures, from 600 to 800°C, calcium carbonate decomposes releasing CO_2.

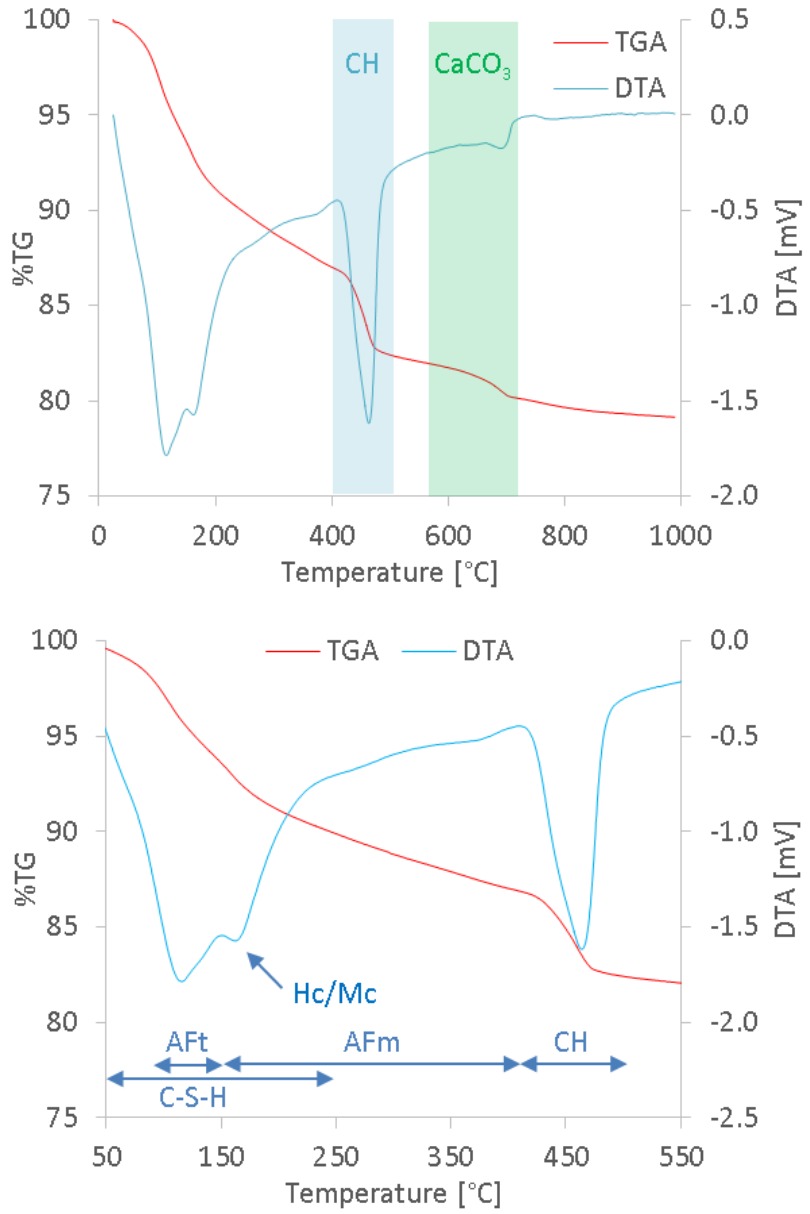

Figure 3-8 – TGA and DTA Plots of C1 Cured for 7 Days (Top) Heated Up to 1000°C, and the Same Tracing Heated up to 550°C Highlighting the Decomposition of Water Bearing Phases Only (Bottom).

3.6.2 Experimental Setup

The portlandite (CH) content and the amount of bound water was measured on freeze-dried paste samples by thermal gravimetric analysis (TGA) analysis using a Stanton Redcroft 780 series under a nitrogen atmosphere. 15 to 18mg was weighed into a platinum crucible and heated from 20 to 1000°C at a constant rate of 20°C/min heating rate from 20 to 1000°C. The CH content was determined using the tangent method. The data was normalised to the total mass loss at 550°C, effectively reporting the data to 100g of anhydrous binder. The bound water content W_n was taken as the mass loss from

50 to 550°C degrees, by which point all the water bearing phases were considered to be fully dehydrated. Care must be taken when evaluating the bound water content as it is dependent on the hydration stopping method [53]. The CH content and W_n were calculated by:

$$\%CH = \left(\frac{CH_w \times \left(\frac{M_{CH}}{M_{H_2O}} \right)}{W_{550}} \right) \times 100$$

$$W_n = \left(\frac{W_{50} - W_{550}}{W_{550}} \right) \times 100$$

where:

CH_w – mass loss of water bound to CH
M_{CH} – molar mass of CH, M_{CH}=74 g.mol^{-1}
M_{H_2O}– Molar mass of water, M_{H2O}=18 g.mol^{-1}

where:

W_{50} – mass loss at 50°C
W_{550} – mass loss at 550°C

The calcium hydroxide content was measured using the tangent method (Figure 3-9). This consists of plotting the derivative of the TGA curve which present peaks where sudden weight loss are seen. The tangents are drawn on the TGA curve where the inflections points occur on the derivative. The water content corresponding to CH is taken at the midpoint between the inflection points, as the mass difference between the tangent lines.

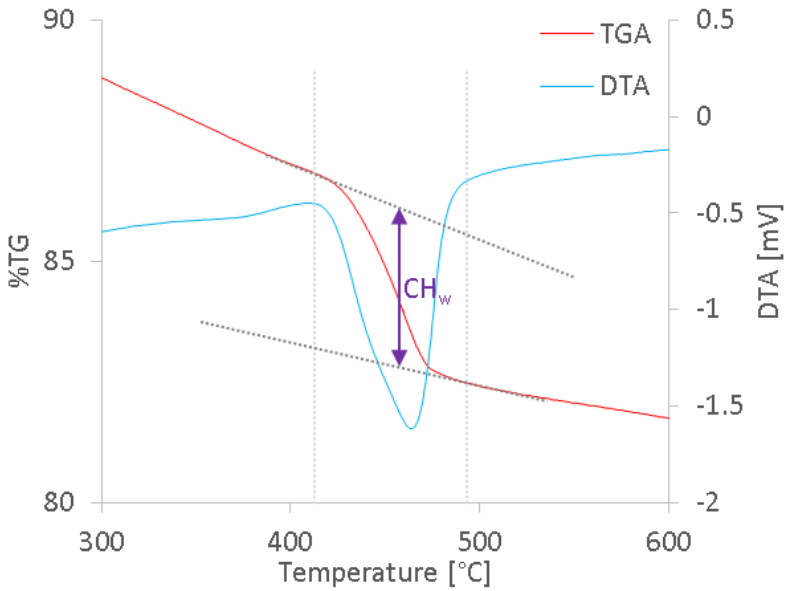

Figure 3-9 – Measuring the CH content using the Tangent Method

3.7 Quantitative X-Ray Diffraction (QXRD)

3.7.1 Principle of X-Ray Diffraction

X-Ray Diffraction (XRD) is a characterisation technique allowing the determination of crystalline phases in a sample. XRD can be defined as the elastic scattering of X-ray photons by atoms in a periodic lattice or plane, e.g. a crystalline material [235]. This is done by bombarding a sample with X-rays, and varying the angle of the incident X-ray beam, interfering with the sample. Constructive interference occurs only when X-rays reflected at different lattices are in phase, as defined by Bragg's Law:

$$n\lambda = 2d \sin\theta$$

Where:
n = integer, called the order of reflection
λ = wavelengths of x-rays
d = characteristic spacing between crystal planes
θ = angle of incidence

The combination of various distances d between lattices is unique for each crystal and can be seen as a unique identifier. Because amorphous phases, such as C-S-H or slags, have no defined crystal structures, no well-defined peaks will mark its presence. Amorphous content appear as humps across a range of angles instead.

3.7.2 Principle of the Rietveld Method

The Rietveld refinement [236] is a method of analysing XRD data enabling phase quantification. It is achieved by comparing the observed diffraction pattern obtained experimentally with a pattern calculated based on refined models of the crystal structure. Parameters are refined until a best fit is found by least-squares. As such it is critical to use the correct crystal structure for each phase. These may be found from the ICSD, the Inorganic Crystal Structure Database. A powder diffraction pattern of a crystalline material may be taken as a collection of individual reflection profiles. Each reflection

profile presents a peak height, a peak position, a breadth, a tail and an integrated area which is proportional to the Bragg intensity I_k.

Many Bragg intensities y_{ci} are observed at any arbitrary chosen point *i*. The calculated intensities are determined from $|F_k|^2$ calculated from the structural model by summing the calculated intensities from the neighbouring Bragg reflections and the background. The model takes into account various factors, including the structure factor, the profile function and preferred orientation.

$$y_{ci} = s\sum_{k} L_k|F_k|^2\varphi\,(2\theta_i - 2\theta_K)P_kA - y_{bi}$$

Where:
s – scale factor
K – Miller indices for a Bragg reflection
Lk – Lorentz, polarization, and multiplicity factors,
φ – profile function
Pk – preferred orientation function
A – absorption factor
Fk – structure factor
Ybi – background intensity

Users are able to vary global parameters (wavelength, specimen displacement) and phase specific parameters. Usually, structural parameters are not refined, and only the overall parameters are considered [237]. These include the scale factor, the unit cell parameter, the profile parameter, and the preferred orientation.

3.7.2.1 **Profile Function**

The profile function models of peak shape of the crystalline phases, taking into account both instrumental and sample effects [236]. Several profile functions exist to best fit the experimental data, and the work here relies on the pseudo-voigt function, defined as a linear function combining the Lorentzian and Gaussian functions:

$$pV = \eta L + (1 - \eta)G$$

Where:

η = mixing parameter, kept constant at 0.6 [238]

L = Lorentzian contribution

G = Gaussian contribution

The breadth, H, of the peaks can also be refined, at full width at half maximum (FWHM), using Caglioti's [239] model by:

$$H^2 = Utan^2\theta + Vtan\theta + W$$

Where U, V and W can be refined. In this study U and V were kept constant, where U=V=0, and only W was refined for selected phases.

3.7.2.2 **Preferred Orientation**

In practice, certain phases can exhibit preferred orientation where some planes are naturally inclined to align themselves parallel to the surface. This leads to a change in intensity of peaks along given Miller indices, e.g. the orientation of crystallographic planes. Sample preparation can affect preferred orientation, and applying strong pressure on the sample should be avoided [237]. McCusker et al. [240] mentioned that preferred orientation can be difficult to eliminate for flat-plate specimen, even when backloading.

Several phases are susceptible to preferred orientation. These typically include alite, calcium sulfate phases, and portlandite $Ca(OH)_2$. It is best to minimise preferred orientation in the first place, but can be partially corrected using the March-Dollase Model [241] during the refinement:

$$P_k = (P_1^2 cos^2\alpha_k + P_1^2 sin^2\alpha_k)^{-\frac{3}{2}}$$

Where:

P_1= Refinable parameter (where a value of 1, indicates no preferred orientation)

α_k =Angle between PO direction and the normal to crystallite

3.7.2.3 **Choice of Background**

Backgrounds may be either manually fitted, either by selecting points or applying the Sonneveld algorithm [242], or modelled. Modelled backgrounds (polynomial, Chebyshev) are desirable when working with highly crystalline material but fail to take into account the presence of amorphous phases; these are marked by the presence of a hump. Cement hydration produces C-S-H, which is amorphous and is therefore poorly modelled. This effect is worsened when working with blended systems containing ground granulated blast furnace slag or pulverized fuel ash which are both highly amorphous materials.

The choice of background is illustrated in Figure 3-10 below. The use of a 5th order polynomial completely ignored the amorphous hump. This is improved when fitting an automatic background using the Sonneveld algorithm. Still, it fails to fit the background fully and only the use of a manual background can fully draw the correct background. As a result, the use of a manual background was preferred in this study for all refinements on blended and hydrated systems.

It is recognized that using a manual background as such is subject to errors induced by the user introducing artefacts. The manual fit was done as to minimise residue. Advances in XRD suggests the use of a ‘partial or no known crystal structure’ (PONKCS) approach to model the amorphous phases [243, 244, 245]

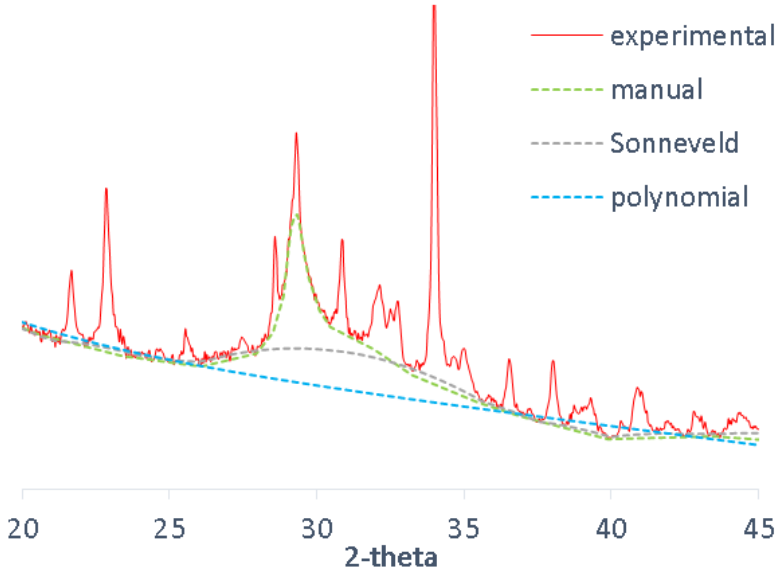

Figure 3-10 – Choice of Background on a Neat System C1 Cured for 180 Days

3.7.3 Selective Dissolution

Selective dissolution was used to enrich, in turn, the silicate phases of the clinker or the interstitial phases. By enriching certain phases, their refinement can be subsequently improved. Several solutions have been suggested to dissolved selected phases [246, 247], and the work here uses a salicylic acid/methanol solution and a potassium hydroxide/sugar solution to dissolve the silicate phases (C_3S and C_2S) and the interstitial phases (C_3A and C_4AF) respectively.

The salicylic acid/methanol (SAM) solution was prepared by mixing 20g of salicylic acid in 300mL of methanol. 5g of cement was stirred in the solution for 2 hours. The solution was then filtered using a Buchner funnel, and the residue washed with methanol prior to drying at 90°C.

The potassium hydroxide/sugar solution (KOH/S) was prepared by mixing 30g of KOH and 30g of sucrose in 300mL of deionized water, and the solution was heated to 95°C. 9g of cement was stirred into the solution for one minute before being filtering the solution with a Buchner funnel. The residue was washed with 50mL of water followed by

100mL of methanol and dried at 60°C. The XRD patterns of the cement before and after both dissolutions are plotted below in Figure 3-11.

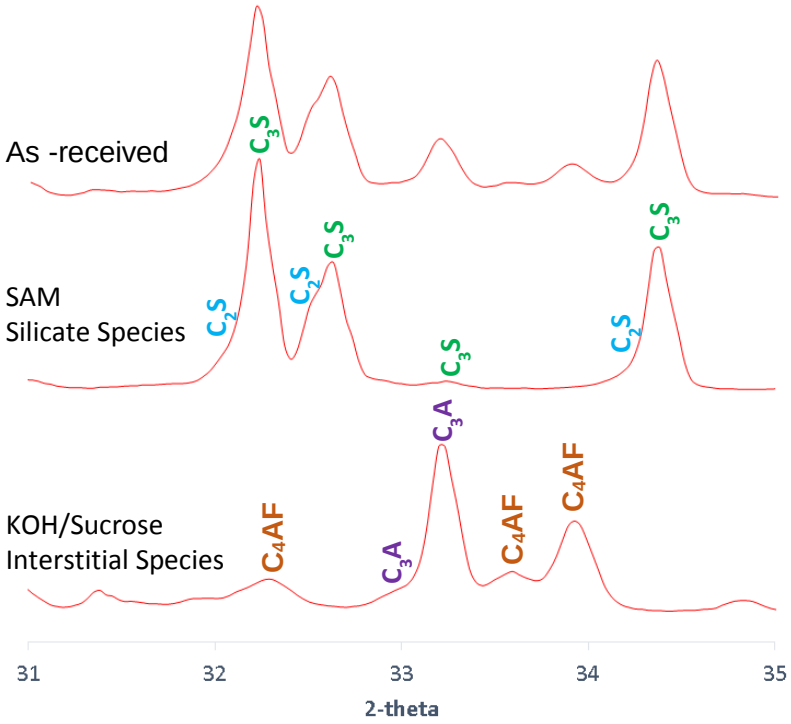

Figure 3-11 – XRD Patterns of the As-Received Cement C_1, Dissolved in SAM and in KOH/S

From the dissolved species, the polymorphs of the clinker phases can be better determined. From Figure 3-11, an intermixing of M_1 and M_3 polymorph of the C_3S phase is present in the clinker [19]. Le Saout et al. [238] stated that the quantification of the silicate phase is not too affected by the choice of the polymorph, and that only one should be chosen to avoid redundant parameters. As such only the M_3 polymorph was used in the refinement. Only β-C_2S was determined, while both a cubic and orthorhombic form of C_3A were found to co-exist. With the correct phases determined, the correct crystal structures can be selected

3.7.4 Development of a Control File

To ease the refinement procedure, a control file can be set up. The file stores all the crystal data and the refined parameters predefined by the user; and need only be turned on in order to carry out the refinement.

The clinker species were refined separately, and the values for the selected parameters were saved. Restraints were set on the unit cell, stabilizing the refinement while making sure the geometry of the structure remained sensible [222, 240]. The refined clinker phases were then combined with the other crystalline phases present in the as-received cement (sulfates, calcite,….), and subsequently refined. The experimental and modelled tracings are plotted in Figure 3-12.

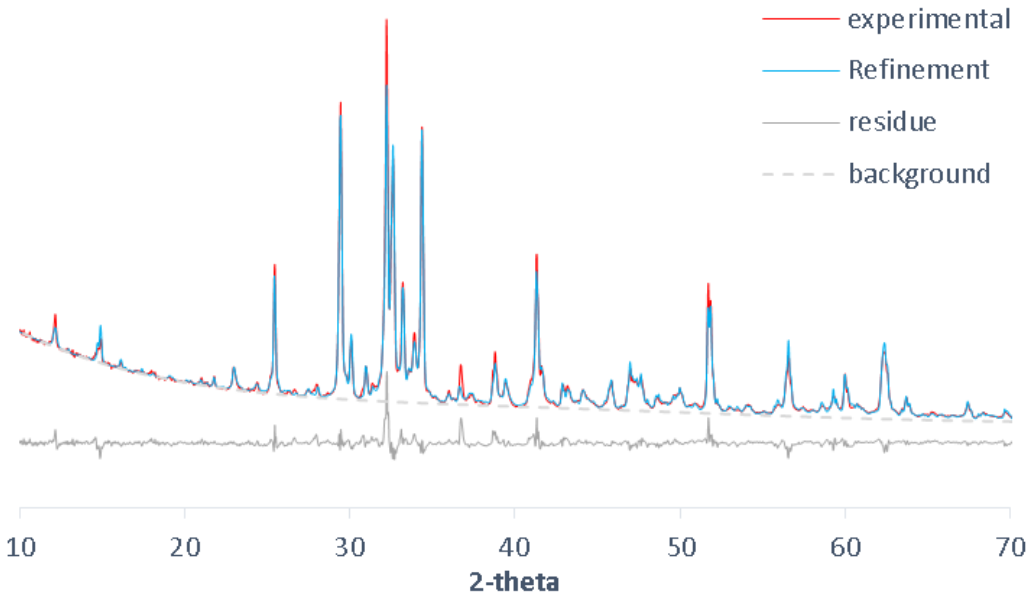

Figure 3-12 – XRD Pattern from 10-70 2-theta of the as-received Clinker

In the hydrated systems, the identified crystalline hydration products were ettringite, hemi- and mono-carbonate, a hydrotalcite-like phase and calcium hydroxide. Ettringite and calcium hydroxide produced strong Bragg reflections and therefore their refinement was straightforward. The other mentioned phases are often poorly resolved by XRD making their refinement difficult (Figure 3-13). Some attempts were made in refining the phase fully but this often resulted in divergence of the refinement. As a result, the refinement of these phases were only limited, such that the best visual fit was achieved.

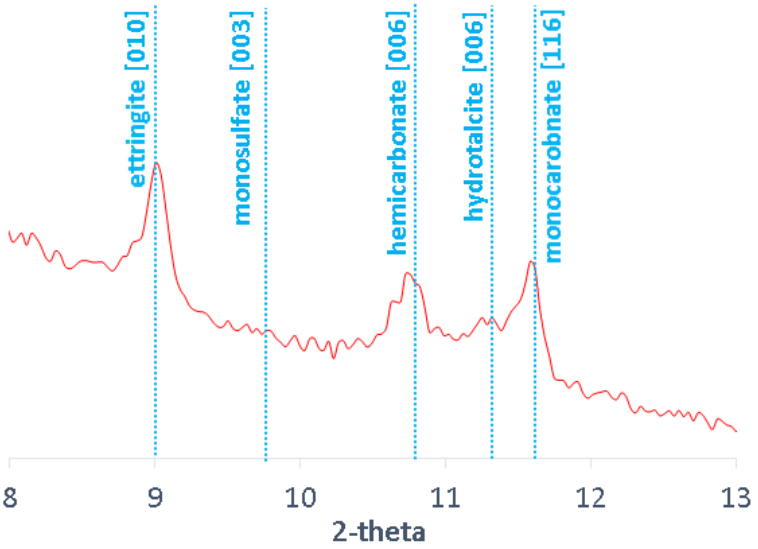

Figure 3-13 – AFt and AFm Phases Identified in a 40 % slag Blend, Cured for 180 Days

Table 3-6 summarises the phases determined in the anhydrous clinker and the chosen crystal files taken from the ICSD database.

Table 3-6 – Summary of the Refined Parameters of the Identified Phases

Phase	crystal structure	ICSD code	SF	Unit Cell							P.O	W
				a	b	c	α	β	γ			
C_3S M_3	monoclinic	64759 [248]	✓	✓	✓	✓		✓			✓	✓
β-C_2S	monoclinic	79552 [249]	✓	✓	✓	✓		✓				
cubic C_3A	cubic	1841 [250]	✓	✓	✓	✓						
Ortho C_3A	orthorombic	1880 [251]	✓	✓	✓	✓						
C_4AF	Orthorombic	245646 [252]	✓	✓	✓	✓		✓				✓
anhydrite	orthorombic	16382 [253]	✓	✓	✓	✓		✓			✓	✓
bassanite	monoclinic	380286 [254]	✓	✓	✓	✓		✓			✓	✓
arcanite	orthorombic	79777 [255]	✓	✓	✓	✓		✓			✓	
MgO	cubic	161059 [256]	✓	✓	✓	✓						
Calcite	hexagonal	166364 [257]	✓	✓	✓	✓					✓	
CaO	cubic	75785 [258]	✓	✓	✓	✓						
$Ca(OH)_2$	monoclinic	15471 [259]	✓	✓	✓	✓		✓			✓	
ettringite	hexagonal	155395 [260]	✓	✓	✓	✓						✓
hemicarboaluminate	hexagonal	263124 [261]	✓	✓	✓	✓						
monocarboaluminate	triclinic	59327 [262]	✓	✓	✓	✓	✓	✓	✓			
monosulfate	hexagonal	100138 [263]	✓	✓	✓	✓						
hydrotalcite	monoclinic	81963 [264]	✓	✓	✓	✓						

3.7.4.1 **Quantification**

The output of a Rietveld refinement is always expressed to 100% of crystalline phases by weight, not taking into account any amorphous phases. The numbers therefore need to be standardized to take into account the X-ray silent phases. This was done using an external standard method; the G factor method [265, 266]' , with corundum serving as the standard. The G-factor method was first mentioned by O'Connor et.al. [265] and was applied to cement chemistry only recently [267, 268, 269]. The sample and the standard are run separately, taking care that the experimental conditions are exactly the same. The use of the external conditions eliminates the need of blending a standard with the sample, and good correlations were found between the two methods [222]. The true content of a crystalline phase, by weight, is given by:

$$C_j = S_j \frac{\rho_j v_j^2 \mu}{G} = \frac{S_j \rho_j v_j^2 \mu}{S_c \frac{\rho_c v_c^2 \mu_c}{C_c}}$$

Where:
Sj=scale factor of phase j
ρj=density of phase j
vj=volume of phase j
μ=mass attenuation coefficient of sample
G=calibration factor determined from the standard
S_c=scale factor of corundum
ρ_c=density of corundum
v_c=volume of corundum
μ_c=mass attenuation coefficient of corundum
C_c=mass fraction of corundum

In order to quantify, it is necessary to work out also the mass attenuation coefficient (MAC) of the sample. This is easily calculated from the oxide composition of the raw materials and is simply the sum of the weighted MAC of the individual oxides. The values can be found in the International Tables for Crystallography (volume C), edited by Prince [270]. For wet pastes, it is also important to factor in the water content [271].

3.7.5 **Measuring the degree of hydration of Clinker**

The clinker phases that make up cement are crystalline, and their dissolution can be followed by X-ray diffraction. The degree of hydration of the individual clinker phase may be determined by [85]:

$$\mathrm{DoH_{clinker}} = \left(\frac{\mathrm{M_{clinker,t=0}} - \mathrm{M_{clinker,t=t}}}{\mathrm{M_{clinker,t=0}}}\right) \times 100$$

Where:

$DoH_{clinker}$= degree of hydration of the clinker
$M_{clinker,\ t=0}$ = Mass fraction of clinker at the start of the reaction
$M_{clinker,\ t=t}$ = Mass fraction of clinker phase after time t

Because clinker is made of four principal phases (C_3S, C_2S, C_3A and C_4AF), the hydration of the individual phases can be followed. The overall degree of hydration is simply given as the change in total mass of all four clinker phases.

3.7.5.1 **Experimental Setup**

For quantitative XRD analysis, hydrated paste samples were crushed to a fine powder by manual grinding in a pestle and mortar without any prior hydration stopping, so as to minimise any damage to phases present [214, 215]. The powders were backloaded into 16mm diameter sample holders and diffraction patterns collected with a Philips Panalytical X'Pert MPD diffractometer equipped with a Cu Kα X-ray source, an X'Celerator detector and operated at 40kV and 40mA. Patterns were measured from 5 to 80° 2θ with a step size of 0.0334°, with a full run lasting 50 minutes. Rietveld refinement of the patterns was conducted using the Philip's X'pert HighScore Plus programme version 2.2a (2.2.1). The quantification of the X-ray amorphous phase content was conducted using the external standard method (G-method) [267] with corundum (Al_2O_3) serving as the standard. Reference files were taken from the ICSD library.

3.8 Scanning Electron Microscopy (SEM)

3.8.1 Principle of Scanning Electron Microscopy

In an SEM, an electron beam is rastered over the sample surface and scattered electrons are collected and used to construct an image. There are many ways in which the electron beam can interact with the sample; to produce secondary electrons, backscattered electrons or X-rays. This study involved the use of backscattered electron imaging. Backscattered electrons are electrons from the incident beam that have been reflected by the sample and their intensity depends on the atomic number of the local area hit resulting in different grey levels visible across a sample. As the atomic number of a feature increases, more electrons are reflected and appears brighter. Low atomic numbers appear dark grey or black. As a result, different phases can be determined according to greyscale; the higher the atomic number of the area hit, the brighter it will appear.

BSE is ideal when analysing flat polished surfaces, were it is possible to work at a wide range of magnifications producing micrographs with reproducible contrast allowing quantification. BSE imagery can also be combined with chemical analysis (by EDS) [272]. Working on flat polished samples reduce edge effects, which are marked by local changes in greyscale [273]. However, there are some limitations. These include that the particle size distribution are skewed towards smaller particles and the connectivity of a 3-D structure cannot be deduced from a 2-D cross-section.

In the anhydrous material, ferrite solid solution appears the brightest followed by alite (C_3S), aluminate (C_3A) and belite (C_2S). The last 2 have very similar grey level. The hydrated materials have a lower atomic number and appear darker. Portlandite is the brightest of the hydrated phases (typically light grey). C-S-H appears dark grey and can present different grey levels depending on the C/S ratio, the temperature upon forming, the micropososity and the water content [272, 274, 275]. It is however difficult to determine the other phases (Ht, AFt, AFm) as they are finely intermixed with the C-S-H phase. A typical micrograph of a slag blend is shown in Figure 3-14 with its associated

histogram. At later ages, there is no distinction between porosity and C-S-H according to the greyscale owing to lower porosity and pore size. In such cases, the porosity was measured following a protocol used previously by Scrivener et al. [276]; the porosity is taken as the intersection of the tangents of the first leg and that of the rising, left hand edge of the C-S-H peak. It was stated that it is impossible to fix an unambiguous pore threshold and, as such, an arbitrary value must be set [272].

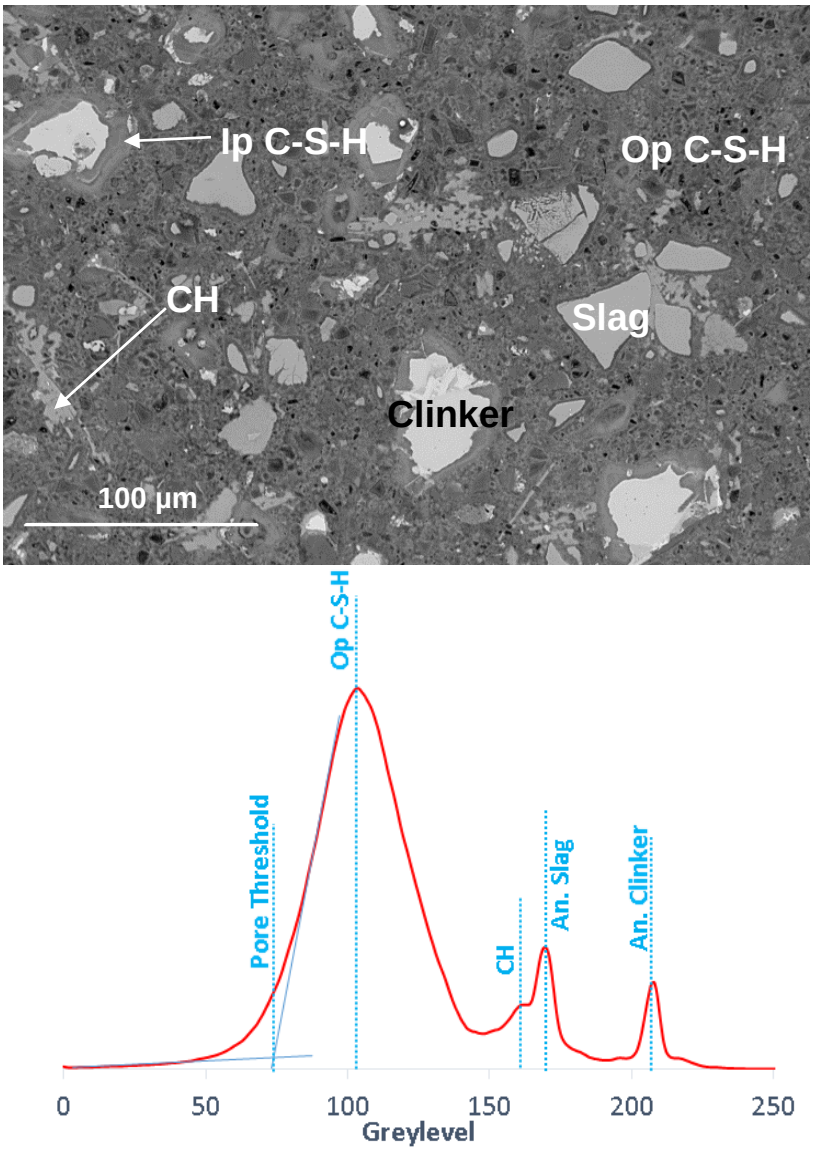

Figure 3-14 – SEM Micrograph of Slag Blend $C_1 40S_c$ Cured for 180 days, and its Associated Greylevel Histogram

3.8.2 **Measuring the Degree of Hydration of Slag**

To determine the degree of hydration of the slag component in a blended system, chemical mapping with respect to the magnesium content is needed to segregate fully the anhydrous slag fraction. This is because the grey levels of anhydrous slag and CH overlap (Figure 3-14). As such, when applying a threshold to only select the anhydrous slag fraction there will be some interference from the hydrate, which can be eliminated with the use of a magnesium map. Slags are rich in magnesium and, because of the element's low solubility, it has a very low mobility, staying within the original slag grain boundaries. Hence, magnesium maps highlight the original position of the anhydrous slag. As slags hydrate, they produce a hydration rim around the original unhydrated slag grain. The rim is of a darker shade and is, therefore, omitted when segregating the anhydrous slag particles. Applying the threshold produces a binary image which is effectively used as a stencil over the map, marking the shape, size and position of the slag fraction only, as illustrated in Figure 3-15. The degree of hydration of the slag can be found by [85]:

$$DH_{slag} = \frac{Vf_{anhydrous\ slag}(t=0) - Vf_{anhydrous\ slag}(t)}{Vf_{anhydrous\ slag}(t=0)}$$

Where:

$Vf_{anhydrous\ slag}(t=0)$ - Volume of initial anhydrous slag

$Vf_{anhydrous\ slag}(t)$- Volume of anhydrous slag at time t

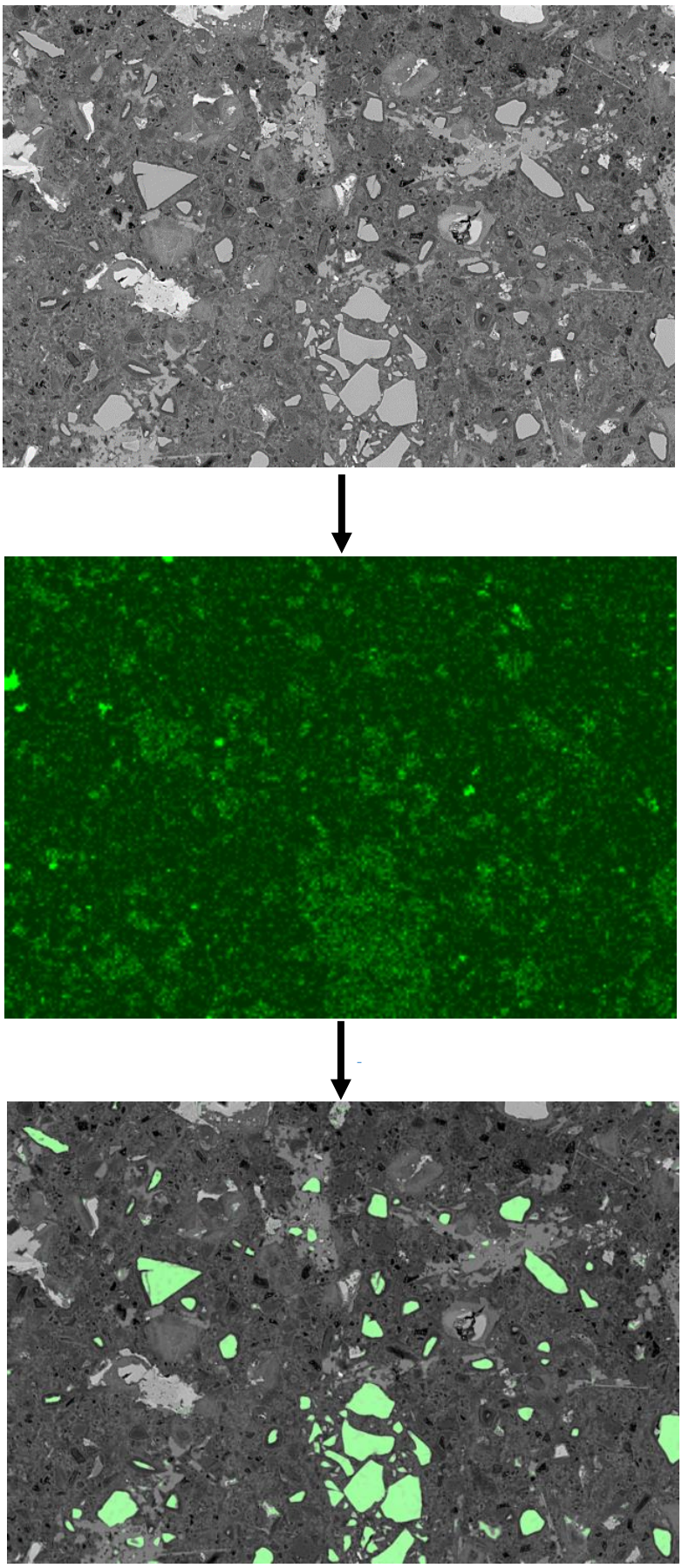

Figure 3-15 – A micrograph of Blend C140Sc Cured for 180 days Combined with its Respective Mg Map, Highlighting only the Anhydrous Slag Area Fraction

Figure 3-16 shows the errors associated in assessing the area fraction of unreacted slags based on 50 images. The errors remain high due to the heterogeneous nature of the microstructure.

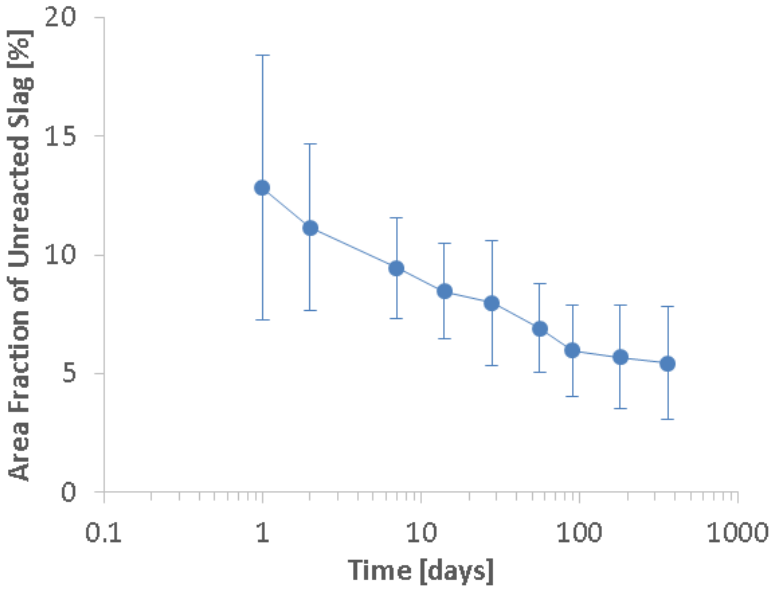

Figure 3-16 – Error Associated in Measuring the Area Fraction of Unreacted Slag

Although the approach is reproducible it is not perfect. The quality of the data relies on the microscope set up and the number of images taken (evidently, the more the better). The data would be better if the images were taken at a higher magnification where the smallest features would be more easily detected. However, mores images would be needed for a given area of analysis; the number of micrographs would be quadrupled if the magnification was doubled greatly increasing the time needed for collection and treatment of the data. As such, it is advantageous to work at a resolution where the work load is kept low all the while maximising quality.

3.8.3 Experimental Method

Pastes were used for any SEM analysis. 2 mm disks were cut and freeze-dried to constant weight. Samples were then impregnated in epoxy resin under vacuum and allowed to harden under ambient conditions. Prior to observation, samples were polished

using silicon carbide paper and any scratches were removed with diamond paste to a final grade of 0.25 µm. Samples were then carbon coated.

The degree of hydration of the slag fraction was measured on 50 images acquired at 800x magnification with a working distance of 8 mm and an acceleration voltage of 15 KeV using a Carl Zeiss evoMA15.

Mg maps were collected with an Oxford Instrument Xmax SDD detector with a 80 mm^2 detector with a minimum acquisition time of 90 seconds. The analysis was done using ImageJ.

3.9 Compressive Strength

Compressive strength was measured on mortars prisms, 40x40x160 mm in size. 450 g of binder was mechanically mixed with 1350 g of sand and 225 g of water, enough to make three prisms. Samples were kept in water until testing. Samples were chiseled in half and tested in compression only. Strength was measured on 6 samples, testing at 1, 2, 7, 14, 28 and 180 days. If one of the measurements deviated by more than 10% of the mean, then this was discarded and only the average of 5 was taken.

3.10 Sulfate Attack

Two sets of samples were cast to assess external sulfate attack. Firstly mortar prims were cast to measure linear expansion. Pastes were cast in parallel to assess any changes in microstructure within the first few millimetres.

3.10.1 Linear Expansion of Mortar Prisms

Often, sample preparation and the used solution are chosen such to accelerate the test. Smaller samples fail faster [277] and the time of failure can be accelerated by increasing solution concentration. Using specimens, cut from larger ones, also increases the failure rate [187].The higher concentration of the solution, however, does not reflect field conditions.

Currently there are no European standards and only the ASTM C1012 [159] specifies a consistent exposure method. Among the specifications, the standard makes the use of a highly concentrated Na_2SO_4 solution, 50 $g.L^{-1}$, renewed at specific intervals, with more frequent renewals at the early stages of testing. The liquid to solid ratio should also be maintained at 4. The pH of the solution increases due to leaching of portlandite [133] and as such should be renewed periodically.

25x25x200 mm mortar prisms in size were cast in triplicate according to the mix design set in section 3.2. The prisms were left to cure in water for 14 days after which the samples were transferred to a 3 $g.L^{-1}$ Na_2SO_4 solution. The lower concentration was chosen to better reflect field conditions [119, 124]. Prior to the transfer, the samples were polished down with sand paper until the coarser sand aggregates were visible by eye. The sulfate solution was replaced every 2 weeks, with a liquid to solids ratio of 4, to renew sulfates and reset the pH to neutral. Expansion was measured at the same time. Reference samples were cast and kept in a lime solution.

3.10.2 **Characterisation of Damage (XRD, SEM, STA)**

For characterisation, pastes with a W/B of 0.5 (Figure 3-17) were cast and cured in polyethylene vials for 14 days prior to exposure to a sulfate solution of same concentration, renewed every fortnight. Another reason for a lower sulfate solution was due for smaller samples prepared for characterisation. At specific time intervals, for a period of up to 1 year, 2 mm thick transverse disks were cut to measure the sulfate ingress under the SEM. At the same time the outer most 1 mm of the sample was cut off and analysed by STA and XRD analysis, as described previously in sections 3.6 and 3.7. The sulfate penetration depth was assessed by EDS analysis. 12x12 point grids were taken on 130x97 µm micrograph, at 1000x magnification, at 0.5 mm intervals from the outer surface of the sample down to a maximum depth of 5 mm, progressing orthogonally from the surface inwards. Points were filtered such that only the hydrated mass was considered, ignoring anhydrous phases, CH, and pores. This approach allowed

simultaneous measurement of the total sulfate content and changes in the composition of the hydrates.

It should be noted that in the present document, the samples prepared for characterisation are referred to their total curing time, and not their time exposed to sulfates. For example, a sample that has cured for 56 days in the presence of sulfates has only been exposed to sulfates for 56-14 = 42 days.

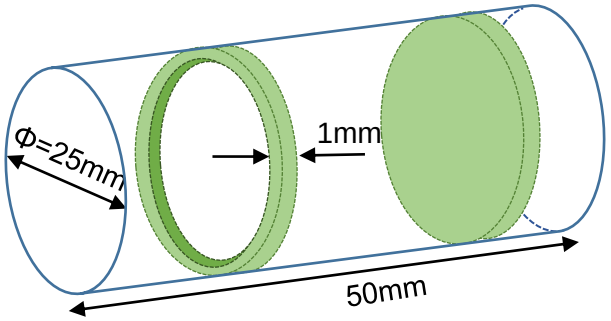

Figure 3-17 – Schematic Illustration Showing the Sample Size of the Paste Exposed to a Sulfate Solution, prepared for Characterisation, and the Relevant Cuts Taken for Analysis

Chapter 4

Scoping Study

Time restraints meant that it would have been unreasonable to perform a detailed characterisation on all 28 of the originally planned mixes. Therefore, a preliminary scoping study was performed to enable further work to focus on 5 key mixes. The most urgent information needed was the reactivity of the slags, their performance, measured by means of mechanical strength and their composition. The reactivity of the slags was assessed by calorimetry measurements, up to 28 days, as detailed in chapter 3. The sections below present the data collected (calorimetry and strength) that led to the selection of the 5 mixes.

4.1 Reactivity of all 28 Mixes

4.1.1 Reactivity of the Cements

Figure 4-1 follows the heat evolved in the neat cement systems. C_2 evolved more heat than C_1. The addition of sulfate had no noticeable effect on the hydration of C_2, but differences could be seen between C_1 and C_1\$. In the latter, the heat evolution presented a step after 7 days of hydration. This was the result of the delay in C_3A hydration in the presence of sulfates. This is observed in Figure 4-2; the abundant amount of sulfates in C_1\$ was depleted long after sulfates were consumed in C_1, as evidenced by the occurrence of the broad peak labelled as 'A'. Furthermore, sulfate addition in C_1\$ led to more heat evolution. This is explained simply by the fact the C_3A hydration in the presence of sulfates, producing ettringite, has a greater enthalpy than when C_3A dissolves to form either monosulfate or other calcium aluminate hydrates [19]. This effect was greater in the systems using C_1 because of the greater C_3A and C_4AF content of the cement.

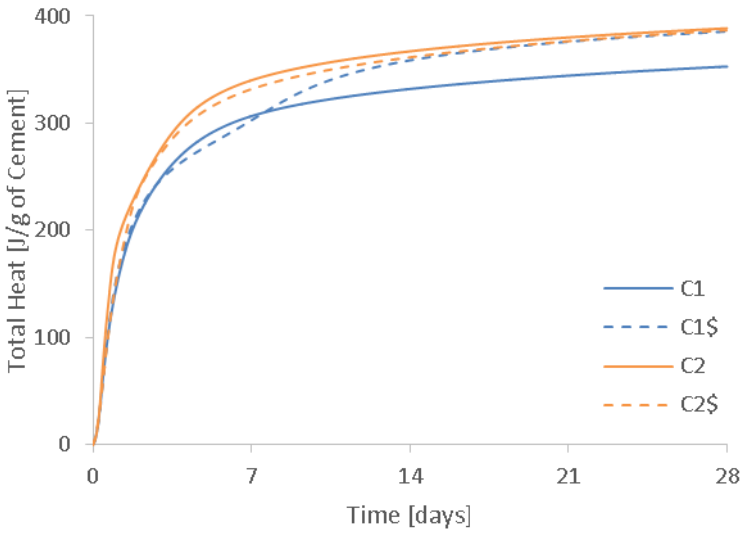

Figure 4-1 – Total Heat Evolved During the Hydration of the Cements, With and Without Sulfates

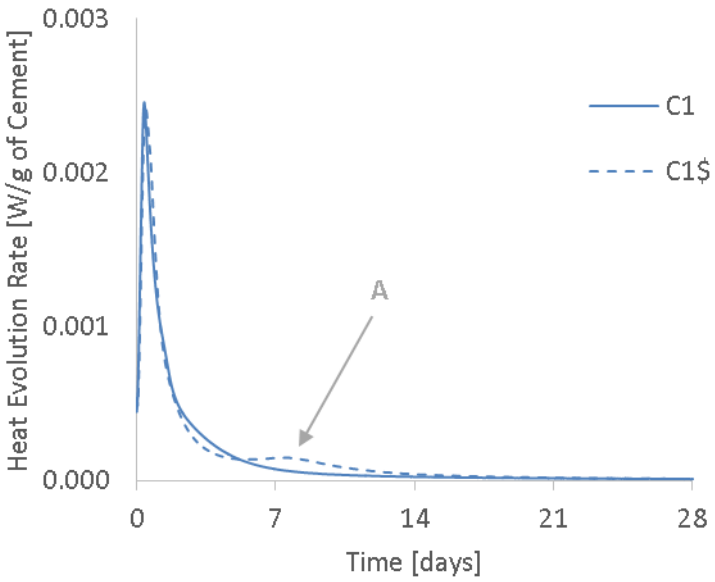

Figure 4-2 – Heat Evolution Rate of C_1 and C_1\$

4.1.2 Effect of Cement and Slag Composition

The impact of cement type on heat evolution in blends containing either 40% and 70% slag is plotted in Figure 4-3 and Figure 4-4, normalized to the cement content. When normalized, the composite systems had evolved more heat compared to the neat systems because of the filler effect; clinker dissolution was accelerated because of the provision of nucleation sites in a medium where the effective water/cement ratio was higher [3, 91, 92]. The effect can be illustrated by substituting the slag fraction in a blend with unreactive quartz, the difference in heat between a neat system and a quartz paste was due to the filler effect. The difference in heat between the quartz paste and the slag paste is due to the hydration of the slag.

At either levels of replacement, the total heat evolved by the end of the testing period was greatest in blends using slag C; blends prepared with slag B had evolved the least. This suggests already that slag C is more reactive owing to its higher CaO/SiO2 ratio (0.96 and 1.12 for slag B and C respectively). Clinker composition had no apparent effect on the hydration kinetics of the slag, i.e. the solid and dotted lines in Figure 4-3 and 4-4 were, for the most part, coincident.

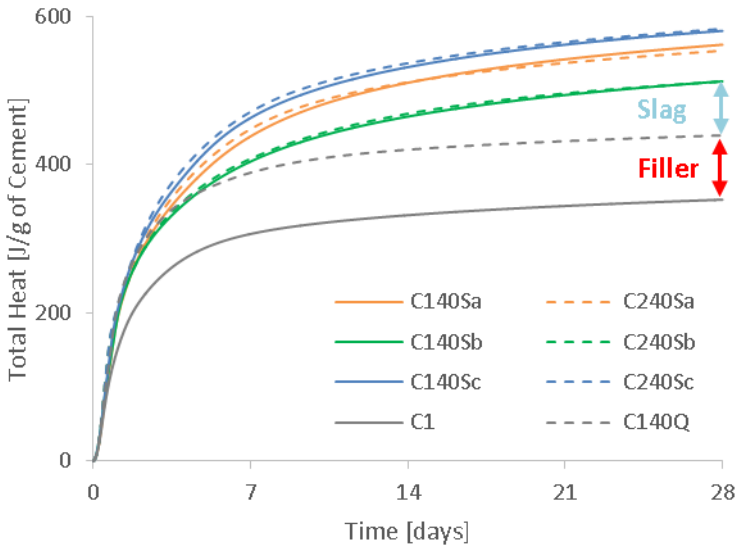

Figure 4-3 – Effect of the Cement Type on the Total Heat Evolved in Blends Prepared with 40 % Slag

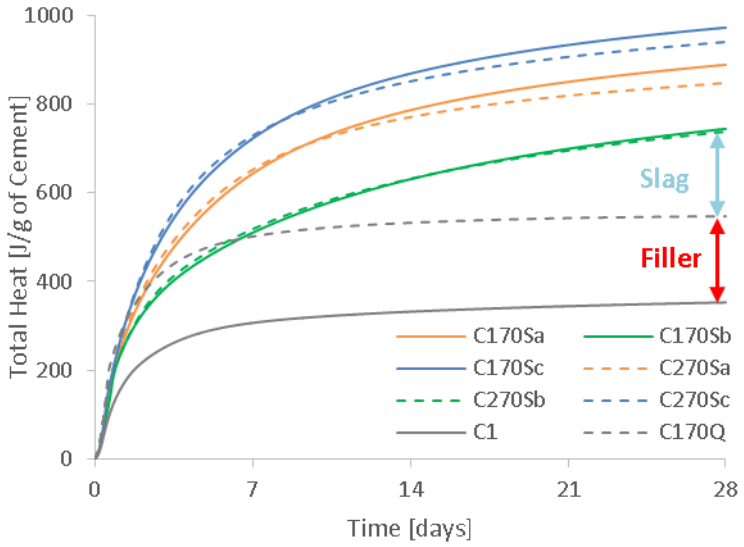

Figure 4-4 – Effect of the Cement Type on the Total Heat Evolved in Blends Prepared with 70 % Slag

4.1.3 Effect of Slag Loading

Figure 4-5 and Figure 4-6 show that by increasing the slag loading, the filler effect was greater. With respect to slag composition, the same trend in total heat evolved was observed. Slag C had evolved the most heat by 28 days of curing, and changing the slag composition resulted in reduced heat, in the same order as seen just above.

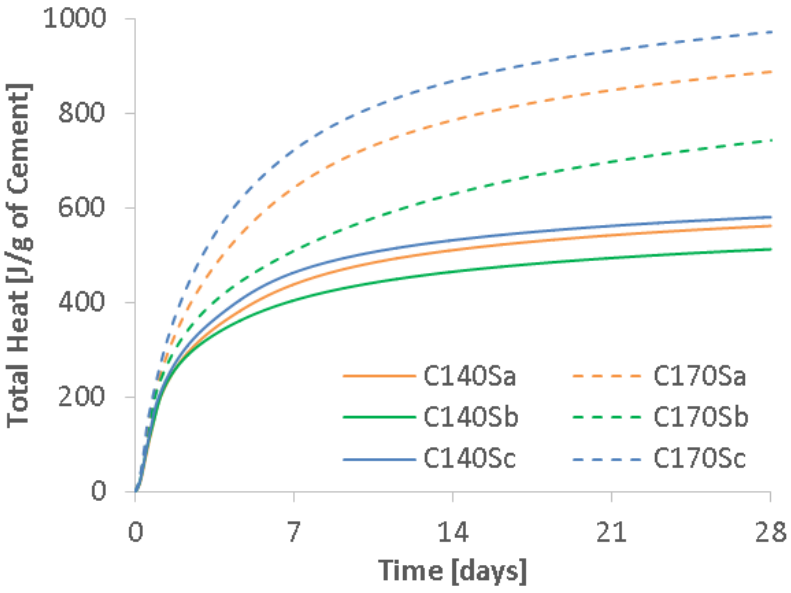

Figure 4-5 – Effect of Slag Loading on the Total Heat Evolved in Blends Prepared with C_1

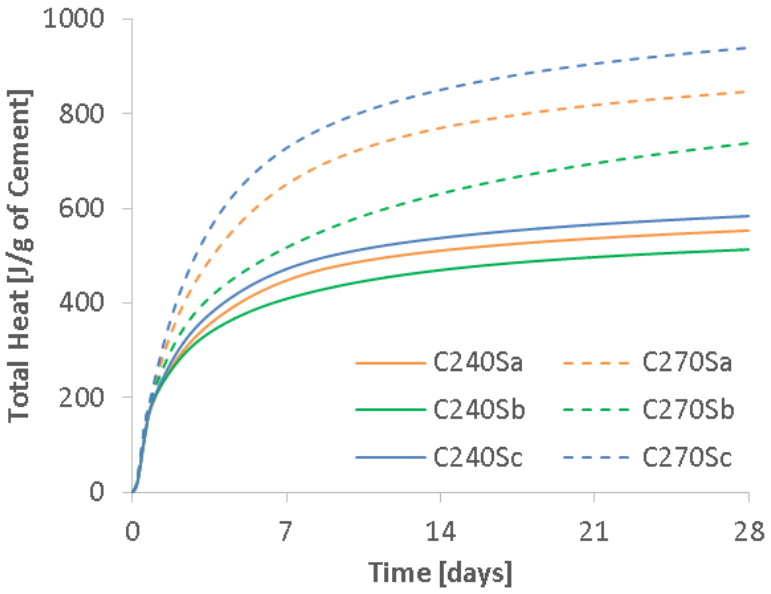

Figure 4-6 – Effect of Slag Loading on the Total Heat Evolved in Blends Prepared with C_2

4.1.4 Effect of Sulfates on Slag Hydration

Figure 4-7 through Figure 4-10 highlight the impact of additional sulfates on the hydration of slag cement blends. In systems using C_1, the addition of sulfates increased the amount of heat released during the earlier stages of hydration, i.e. up to 7 days. Beyond that, the heat evolution rates between non sulfated and sulfated slags blends were similar; the greater heat release in the latter blends was more likely the result of changes in hydration of the clinker in the presence of added sulfates. Sulfates had no impact on the hydration of the slag when blended with C_1.

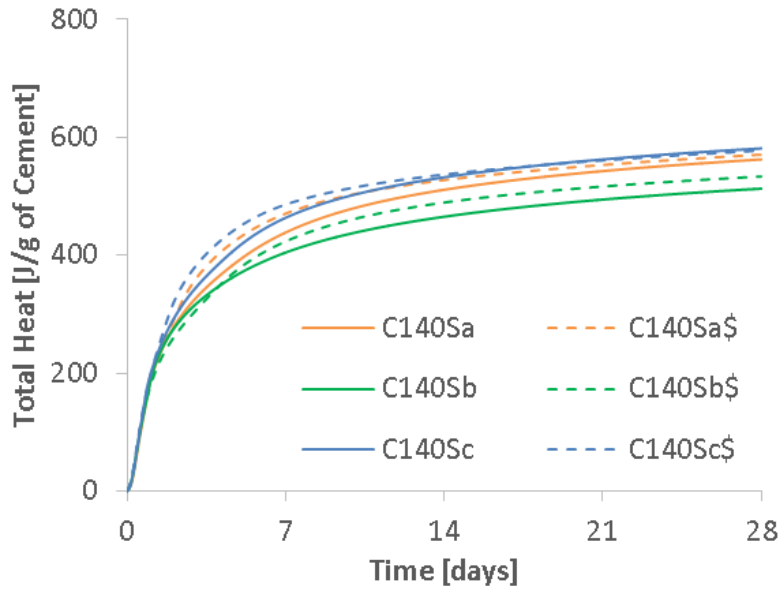

Figure 4-7 – Effect of Sulfates on the Total Heat Evolved in Blends Prepared with C_1 Containing 40 % Slag

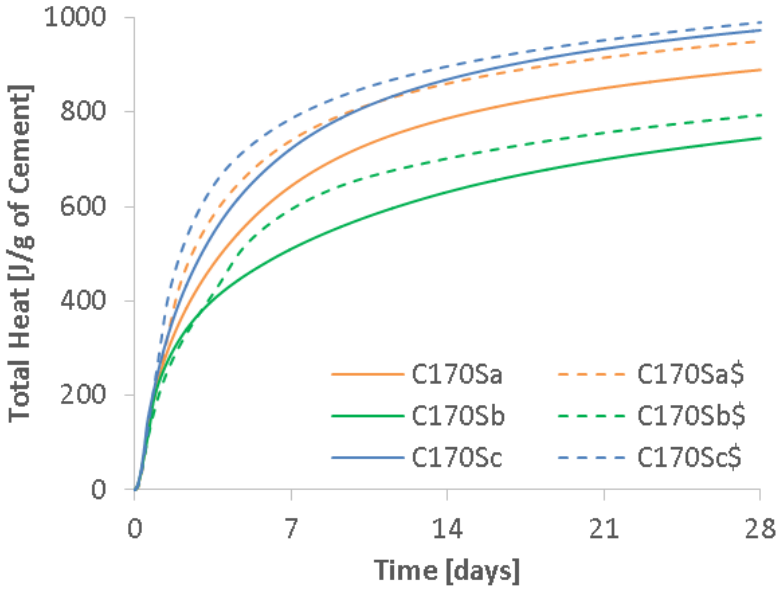

Figure 4-8 – Effect of Sulfates on the Total Heat Evolved in Blends Prepared with C_1 Containing 70 % Slag

In the systems prepared with C_2, the early heat released was once again greater in the sulfate slags blends, irrespective of slag content. However, the observed slope after 7 days of hydration in the sulfated slag blends was greater compared to their sulfate-free analogues. This remained true for both blends prepared with 40% and 70% slag contents.

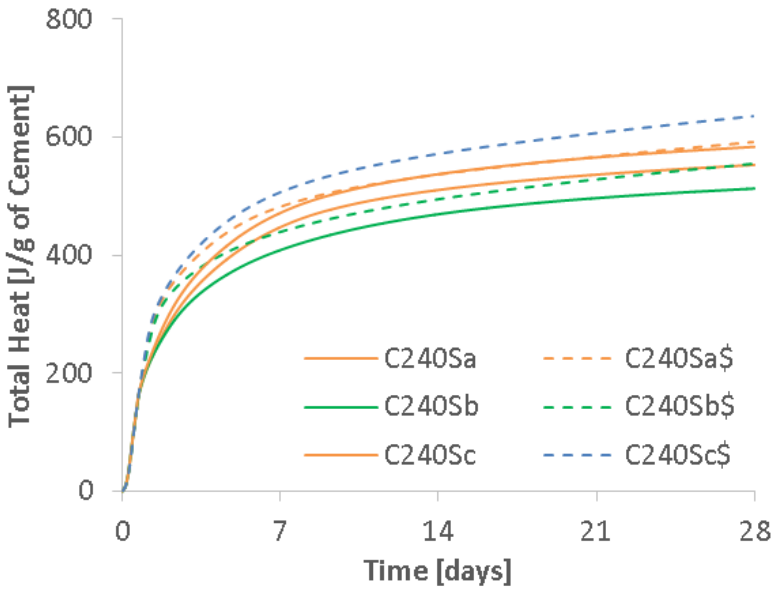

Figure 4-9 – Effect of Sulfates on the Total Heat Evolved in Blends Prepared with C_2 Containing 40 % Slag

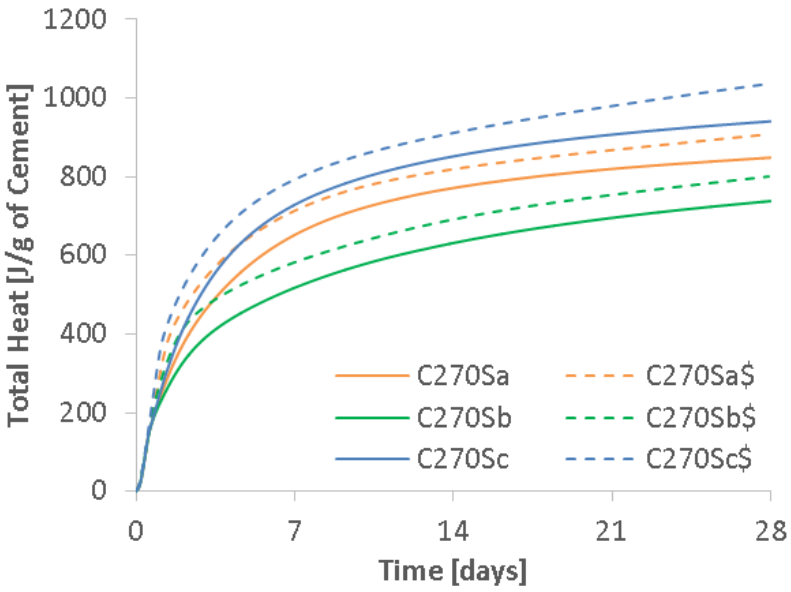

Figure 4-10 – Effect of Sulfates on the Total Heat Evolved in Blends Prepared with C_2 Containing 70 % Slag

Sulfates can act as an activator for slag hydration [60, 75]. Sulfates appeared to have promoted the hydration of the slags, irrespective of the slag content, in all composites systems prepared with C_2 only. The changes in composition of the cement is most likely the cause of this effect. C_1 had a greater alumina content, and was richest in aluminates when considering both C_3A and C_4AF (Table 3-2); their hydration would have consumed sulfates quicker, preventing any reaction with slags. These changes in

composition of the cement would have therefore allowed for sulfates to react with slags such that their hydration be promoted at later ages in C_2 systems. Regardless, Slag C had evolved again the most heat followed by Slag A, and finally Slag B.

4.2 Strength Evolution

4.2.1 Strength Evolution of the Cements

Figure 4-11 follows the strength evolution of the neat cements, prepared with and without additional sulfates. Of the 2 cements, C_2 produced a stronger matrix. Despite some variation in the data, the impact of sulfates on strength addition was minimal in neat systems, despite the changes in heat evolution (Figure 4-2)

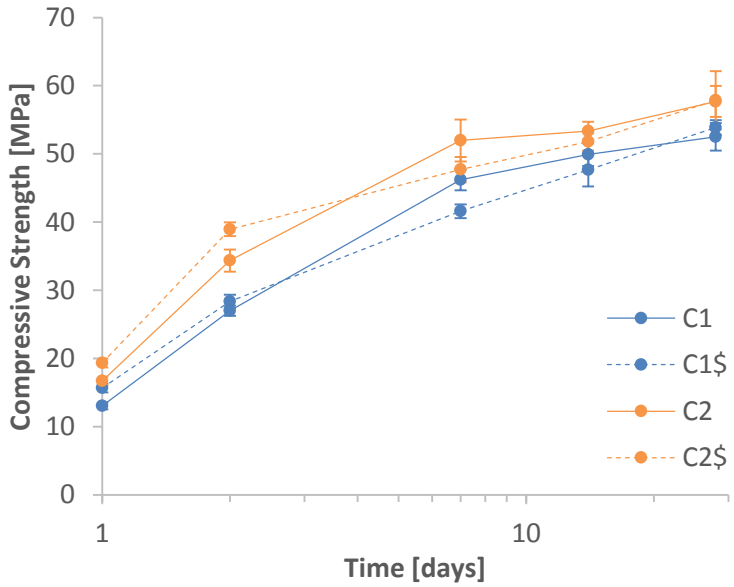

Figure 4-11 – Strength Evolution of the Cements, With and Without Sulfates

4.2.2 Effect of Cement and Slag Composition

The impact of cement and slag composition on strength evolution is plotted in Figure 4-12 and Figure 4-13 for blends prepared with 40% and 70% slag blend respectively. Compared to the neat systems, all the composite systems were generally weaker, particularly at early ages. This is because of the slow hydrating nature of the slag [77]. The difference in strength after 28 days was, however, minimal.

In blends containing 40%, the strength evolution was very much comparable in all systems and blends prepared with C_2 showed a greater strength only after 28 days of curing.

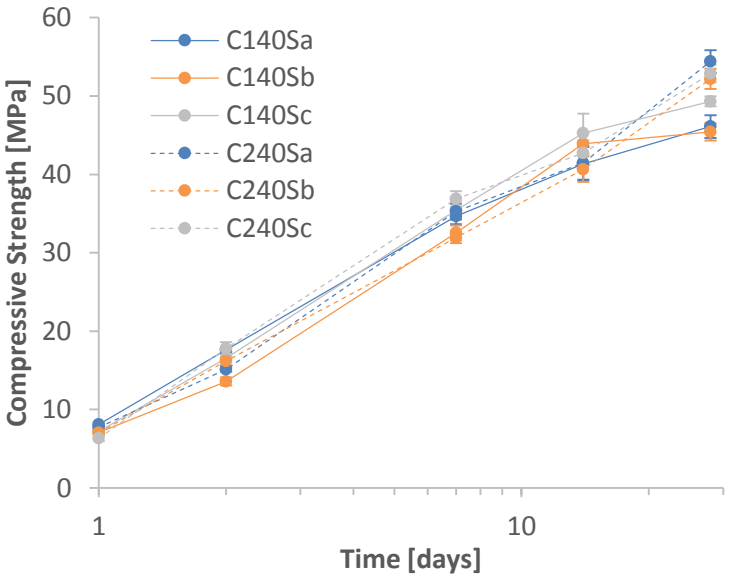

Figure 4-12 – Effect of the Cement Type on the Strength Evolution of Blends Prepared with 40 % Slag

In blends prepared with 70% slag, the impact of slag composition on strength was much more evident. Slag cements prepared with slag C had the greatest strength, particularly at intermediated ages (7 and 14 days); blends made with slag A were slightly weaker, and those made with slag B were the weakest. After 28 days of curing, the differences in strength between the systems were much less evident. The impact of cement composition appeared to have no great effect on strength evolution.

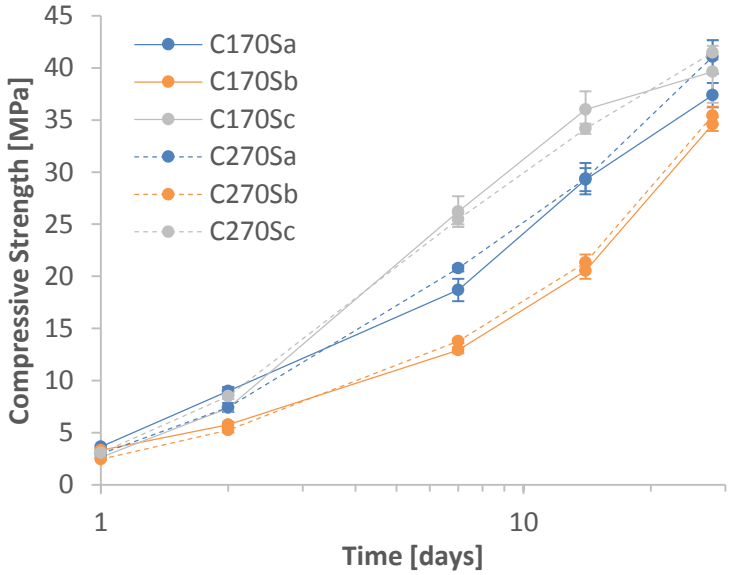

Figure 4-13 – Effect of the Cement Type on the Strength Evolution of Blends Prepared with 70 % Slag

4.2.3 Effect of Slag Loading

Figure 4-14 and Figure 4-15 compare the strength evolution of blends with differing slag loads. Blends prepared with 70 % replacement were generally weaker than those made with 40% replacement. This may be attributed to the lower clinker content of the blends, with the reduced reactivity of the slags with loading [82].

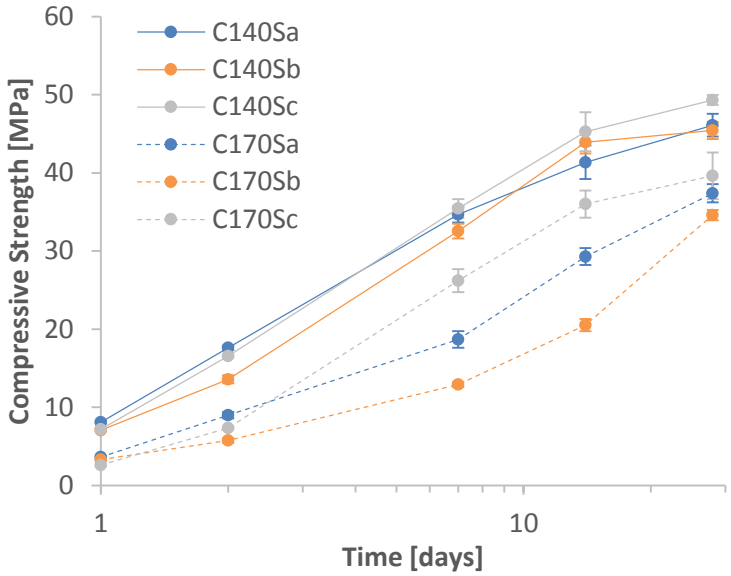

Figure 4-14 – Effect of Slag Loading on the Strength Evolution in Blends Prepared with C_1

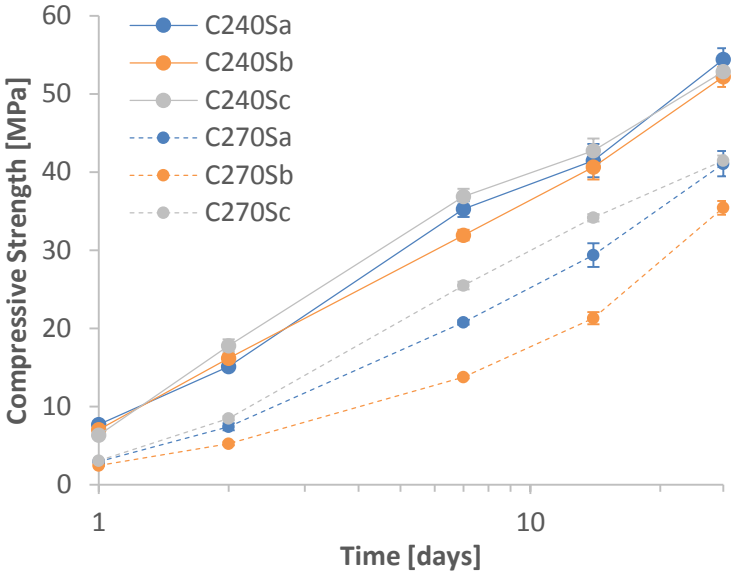

Figure 4-15 – Effect of Slag Loading on the Strength Evolution in Blends Prepared with C_2

4.2.4 Effect of Sulfates

The role of sulfates on strength is plotted in Figure 4-16 to Figure 4-19. In all cases, there was no clear trend on the impact of sulfates on strength development. The impact of sulfate can prove beneficial or detrimental with respect to strength development depending on the sulfate content [278, 279], but this was not clearly observed in the data presented here.

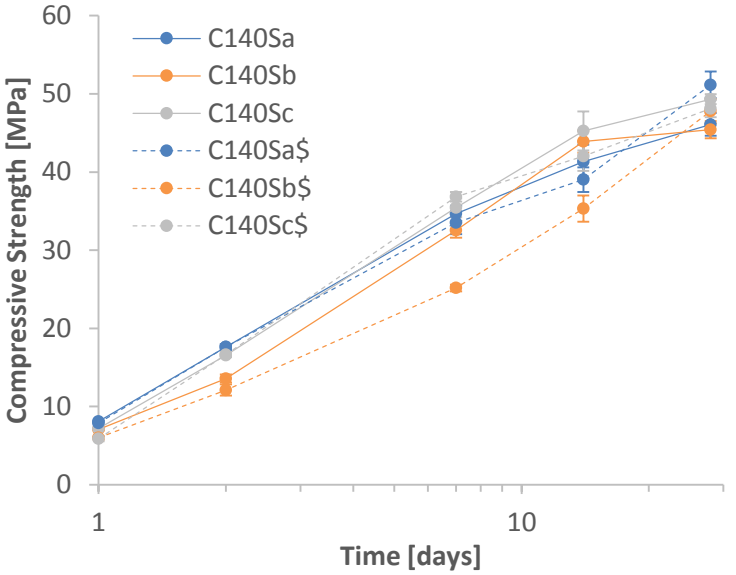

Figure 4-16 – Effect of Sulfates on the Strength Evolution in Blends Prepared with C_1 Containing 40 % Slag

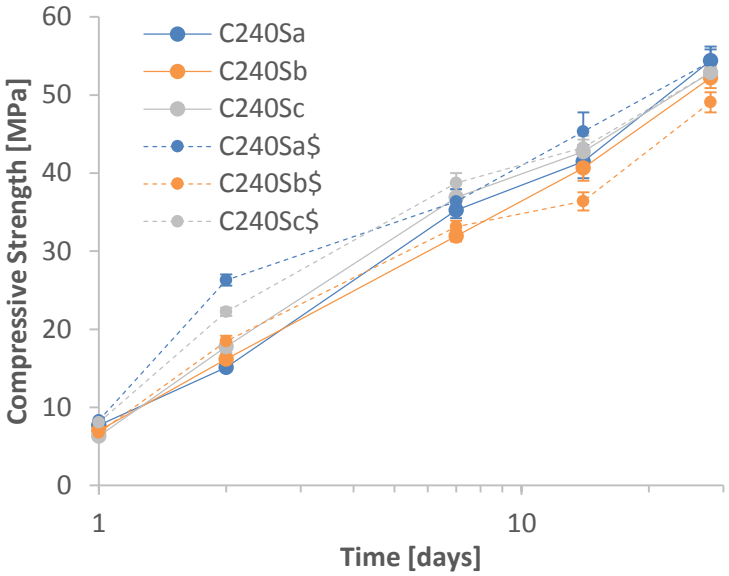

Figure 4-17 – Effect of Sulfates on the Strength Evolution in Blends Prepared with C_2 Containing 40 % Slag

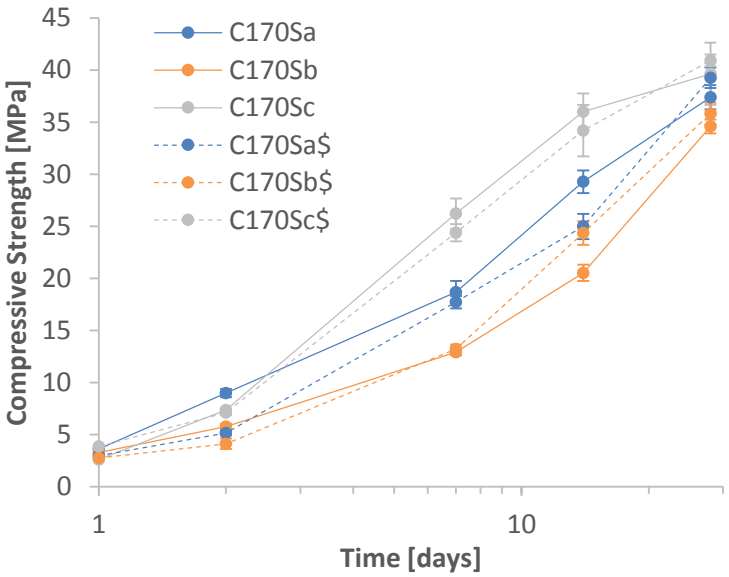

Figure 4-18 – Effect of Sulfates on the Strength Evolution in Blends Prepared with C_1 Containing 70 % Slag

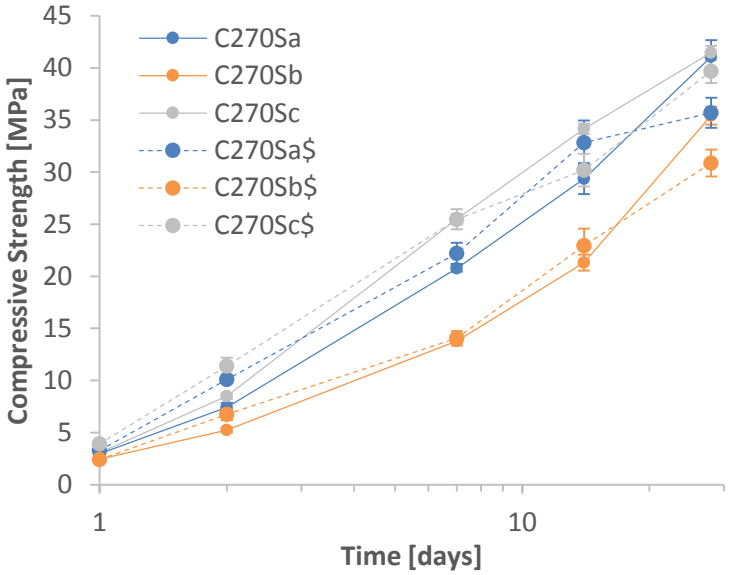

Figure 4-19 – Effect of Sulfates on the Strength Evolution in Blends Prepared with C_2 Containing 70 % Slag

4.3 Selection of the Final 5 Mixes

From the data presented in this chapter, it can be concluded that blends prepared with slag C led to the greatest heat evolution. The same blends prepared with slag B evolved the lowest amount of heat. That is to say that slag C was the more reactive slag, while slag B was the least reactive. Strength evolution agreed with calorimetric evolutions such that blends prepared with slag C were generally stronger and those prepared with slag B weaker. This is particularly evident in blends prepared with 70% slag. Furthermore, the cement type had no appreciable effect on heat and strength evolution, nor did the addition of sulfates. Generally, strength evolution agreed with calorimetric observations.

The cement was chosen based on its composition only. C_1 was the richest in alumina and in aluminate clinker phases (C_3A and C_4AF). As such, it was deemed to be more prone to attack by sulfates, making it a suitable candidate. Slag B and slag C were chosen for their higher and lower reactivity respectively, plus, slag C was the richest in alumina and slag B the poorest. Composite systems prepared with low slag contents may not prove to be sulfate resistance, while slag rich blends typically are [16]. As such slag blends prepared with either slag containing 40% were prepared (C_140S_b and

$C_1 40 S_c$), with an additional prepared with 70% slag C ($C_1 70 S_c$). Although sulfates had no discernible effect, they do impact the microstructure, consuming more aluminium and calcium to form ettringite. The addition of sulfates are known to improve resistance of a system exposed to sulfate attack [11, 185], and this effect wanted to be tested. As such, sulfates were added to the blend prepared with 40% slag C ($C_1 40 S_c$\$).

Chapter 5

Impact of Slag Composition and Loading, Plus Additional Sulfate, on the Microstructure of Slag Composite Cements

5.1 General Overview of Hydration

The bound water content gives an indication of the progress of hydration (Figure 5-1) but cannot be directly related to the overall degree of hydration [86, 280]. All the blended systems showed a lower total bound water content, with the blend richest in slag showing the lowest. The addition of anhydrite in blend $C_140S_c\$$ had no noticeable impact upon the total bound water content. Similar results were found by Zajac et al. at longer hydration times for limestone composite cements [281].

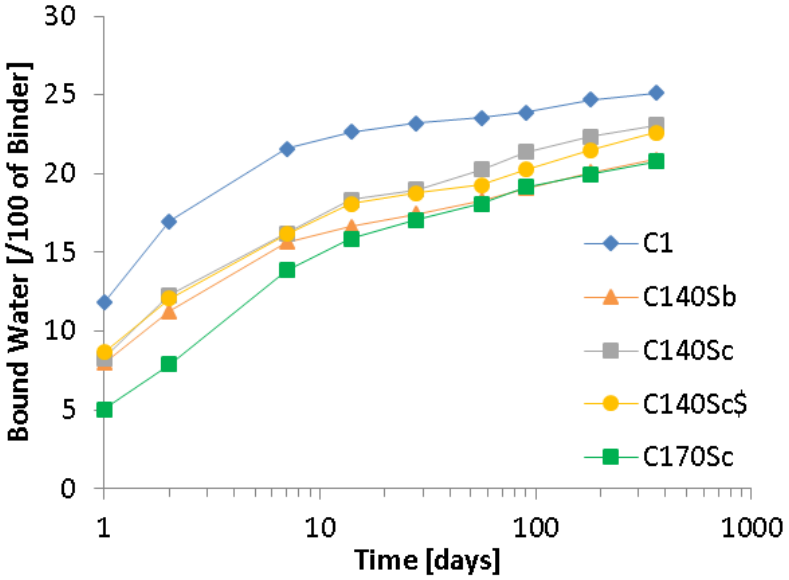

Figure 5-1 – Bound Water Content in Investigated Blends

The influence of binder composition could also be observed via development of the portlandite content (Figure 5-2). Replacement of cement clinker resulted in production of significantly lower levels of portlandite, since portlandite is produced only by the hydrating cement clinker. However, when normalised back to the cement content, the portlandite content in all slag blends was still lower than that of the neat system. Since

slag hydration can be accompanied by portlandite consumption, to form C-S-H [87], the reduction in portlandite content was due to slag hydration [78].

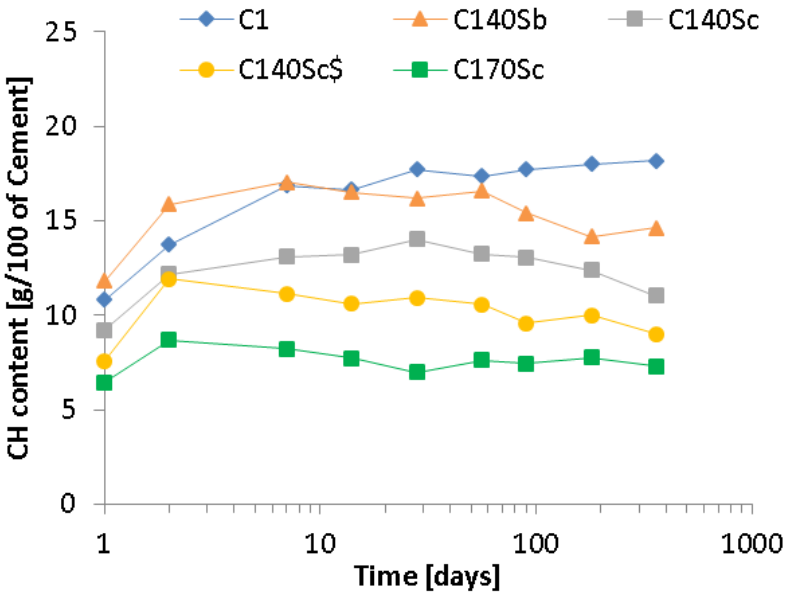

Figure 5-2 – Calcium Hydroxide Content of the Investigated Samples

There were also slight differences between the slag blends made with 40% slag. Blend C140S_b showed comparable or greater levels of portlandite to C_1 for the first 7 days of hydration, after which there was a slight deviation as the portlandite content declined in the blend. However, for blend C_140S_c the portlandite content was much lower from a very early stage, paired too with further, modest consumption as slag hydration progressed. This was possibly due to a change in composition of the slag, where slag C has a higher CaO/SiO_2 ratio, or reactivity. The addition of anhydrite in blend C_140S_c\$ encouraged AFt formation requiring a source of calcium, provided by the added anhydrite. It is unlikely that calcium has been sourced from calcium hydroxide and its lower content in blend C_140S_c\$ may be explained by an increase in the Ca/Si of the C-S-H phase as calcium sulfate are sorbed unto its surface [282]. Naturally blend C_170S_c showed the lowest portlandite content.

Blend composition did impact on compressive strength evolution (Figure 5-3). Replacement of the cement by 40% slag led to lower early-age strengths, but continued gradual strength development at later ages, such that all of the blends containing slag had comparable strengths to the neat system after 180 days, in line with previous research which has shown that slag cement blends can evolve equivalent or even greater strengths than neat cement systems at later ages [8, 94, 95]. Blends prepared with 40 % slag had comparable strength, though it can be hinted that the use of slag C led to a stronger composite system. Blend $C_1 70 S_c$ was the weakest after just one day of curing. However, its strength evolution was possibly the greatest beyond 28 days of hydration in this blend, where slags continued to hydrate. Oner and Akyuz [95] estimated an optimum cement replacement level by slag of 55 % to reach a maximum strength at later ages of curing.

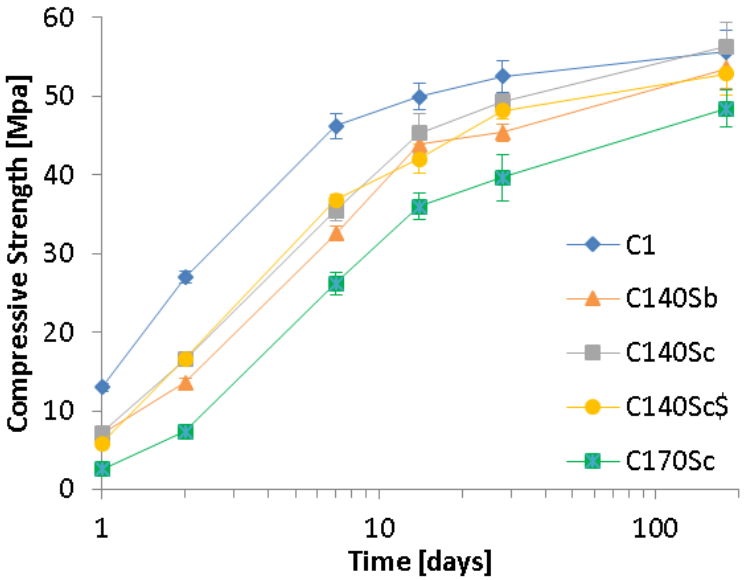

Figure 5-3 – Unconfined Compressive Strength (MPa)

The preliminary results clearly showed on-going hydration in all slag systems. This was seen firstly in the evolution of the bound water. The neat system C_1 showed little change in bound water beyond 7 days of hydration, by which time most of the clinker phases would have hydrated. However, all the slag blends showed a continual increase. Furthermore, the portlandite content continually decreased over time in all the slag blends, most likely consumed by the slags. This indicates that hydration continued in the

slag blend, such that all the investigated systems had comparable strengths after 180 days of hydration. A deeper investigation was therefore performed to better understand the interplay of hydration kinetics, phase assemblage and microstructure on the evolution of slag cement performance.

5.2 Hydration Kinetics

5.2.1 Hydration of the Cement Clinker

Hydration of the individual cement clinker phases was followed by XRD (Figure 5-4 through Figure 5-7, plus Table 5-1). Alite dissolution in the neat system was fast with over 90 % having reacted within 28 days in C_1, and 61 % within just one day. Belite hydration was inhibited upon slag addition, but did eventually approach the degree of hydration of the neat system at the end of the test period.

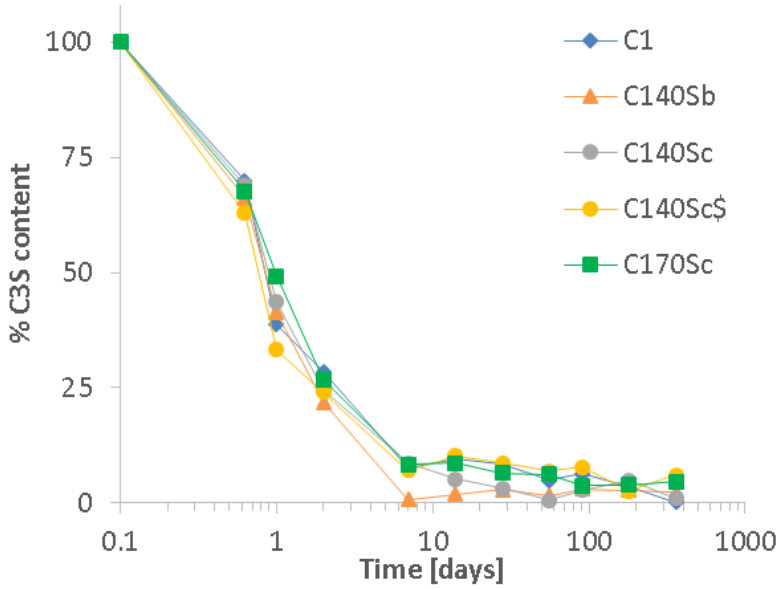

Figure 5-4 – Evolution of C_3S Measured by XRD-Rietveld in the Investigated Systems

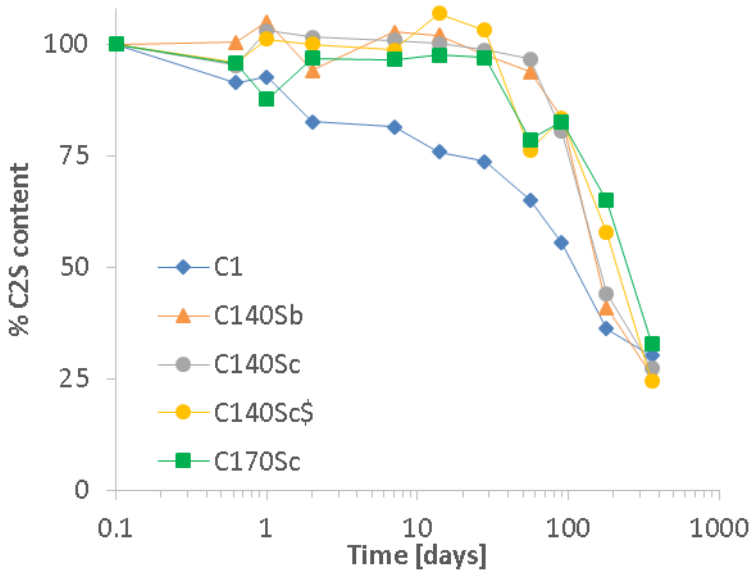

Figure 5-5 – Evolution of C_2S Measured by XRD-Rietveld in the Investigated Systems

C_3A was very reactive, with only traces being detected beyond 28 days of hydration in the neat system C_1. Its reactivity has increased in the presence of slag with only traces remaining after just 2 days of hydration in blend C_170S_c. The addition of sulfate, however, caused a delay in its reactivity but only marginally; C_3A consumption was initially delayed to a greater extent than C_1, but had fully reacted within 7 days.

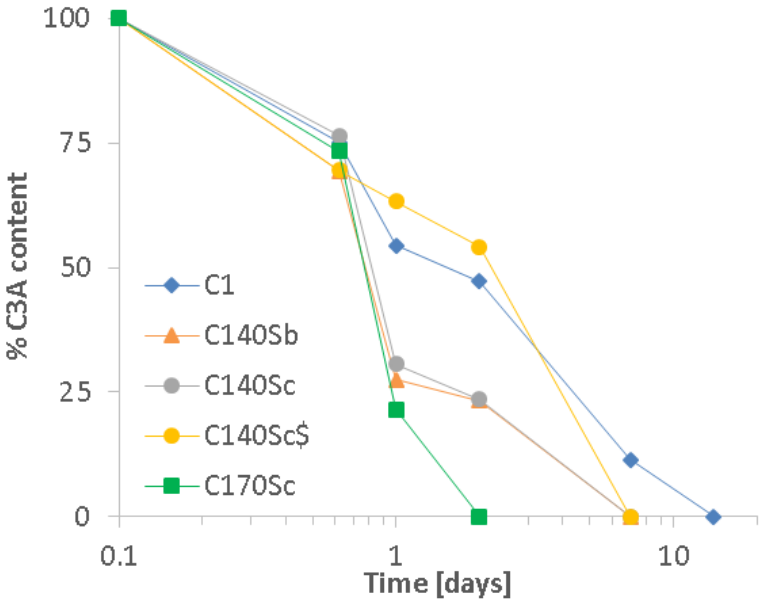

Figure 5-6 – Evolution of C_3A Measured by XRD-Rietveld in the Investigated Systems

Ferrite hydration was modest and only 59 % of the phase reacted within 28 days in C_1. Slag addition accelerated ferrite hydration, such that after 28 days of hydration, 60 to 80 % had reacted in all blended systems. The presence of additional sulfate had no discernible effect. This effect of slag on the individual clinker phases is in agreement with the literature [62, 85], and a similar effect has been seen with ternary cement systems containing limestone powder and fly ash [5].

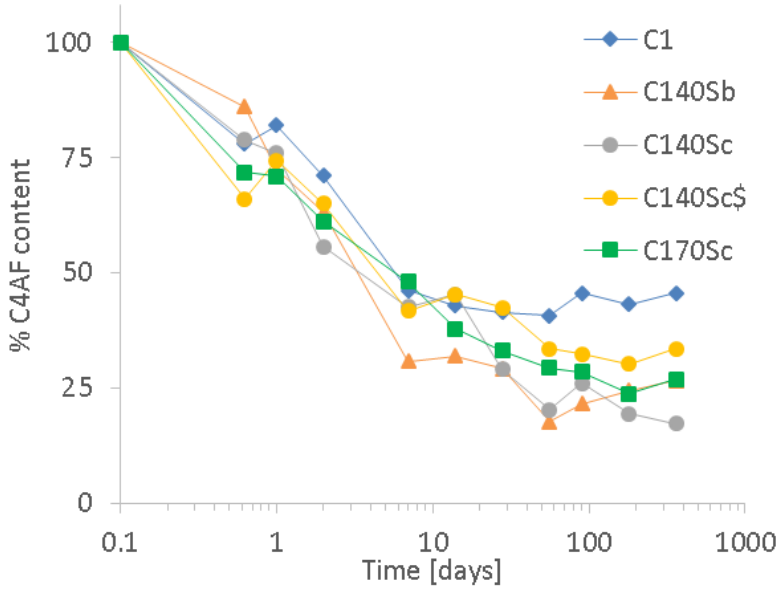

Figure 5-7 – Evolution of C_4AF Measured by XRD-Rietveld in the Investigated Systems

Table 5-1 – Evolution of the Clinker Phases in all Investigated Systems

	C1				C140Sb				C140Sc				C140Sc$				C170Sc			
Time [days]	C_3S	C_2S	C_3A	C_4AF	C_3S	C_2S	C_3A	C_4AF	C_3S	C_2S	C_3A	C_4AF	C_3S	C_2S	C_3A	C_4AF	C_3S	C_2S	C_3A	C_4AF
0	61.0	11.9	7.5	8.3	61.3	10.7	7.5	7.5	62.9	10.1	7.2	7.9	61.9	9.9	6.8	7.3	59.7	11.1	7.2	7.7
1	23.6	11.0	4.1	6.8	25.4	11.2	2.1	5.4	27.4	10.4	2.2	6.0	20.5	10.0	4.3	5.4	29.4	9.7	1.6	5.5
2	17.3	9.8	3.5	5.9	13.5	10.0	1.8	4.7	15.4	10.2	1.7	4.4	14.9	9.9	3.7	4.7	16.0	10.7	0.0	4.7
7	4.6	9.7	0.0	3.8	0.5	11.0	0.0	2.3	5.5	10.2	0.0	3.4	4.4	9.7	0.0	3.0	5.0	10.7		3.7
14	5.8	9.0		3.6	1.2	10.9		2.4	3.3	10.1		3.6	6.3	10.5		3.3	5.1	10.8		2.9
28	5.2	8.8		3.4	1.8	10.4		2.2	2.0	9.9		2.3	5.3	10.2		3.1	3.9	10.7		2.6
56	3.0	7.7		3.4	1.0	10.0		1.3	0.4	9.7		1.6	4.3	7.5		2.4	3.7	8.7		2.3
90	3.8	6.6		3.8	1.9	8.9		1.6	1.7	8.1		2.1	4.8	8.2		2.4	2.3	9.1		2.2
180	2.2	4.3		3.6	1.7	4.4		1.8	3.1	4.4		1.6	1.6	5.7		2.2	2.3	7.2		1.8
360	0.1	3.6		3.8	1.4	2.8		2.0	0.6	2.8		1.4	3.8	2.4		2.4	2.8	3.7		2.1

All numbers expressed as g/100g of cement

As a verification of the quality of the refinements carried out on the samples, the CH content measured by XRD and TGA were plotted against one another in Figure 5-8. The data typically agreed within ±1.5 %.

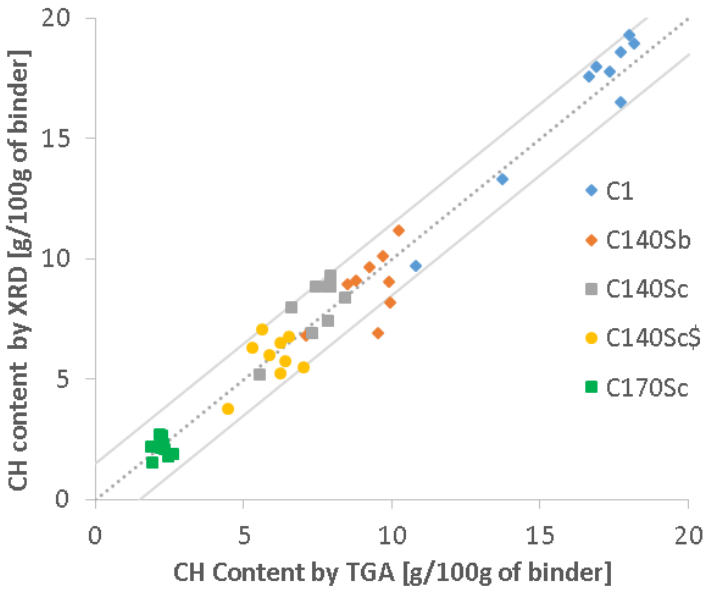

Figure 5-8 – CH content measured by XRD and TGA. Data typically agreed ±1.5 %

Despite the changes in kinetics of the individual phases, the overall degree of hydration of the clinker was comparable between all systems, as seen in Figure 5-9, with 75 % of the clinker having reacted by 7 days of curing.

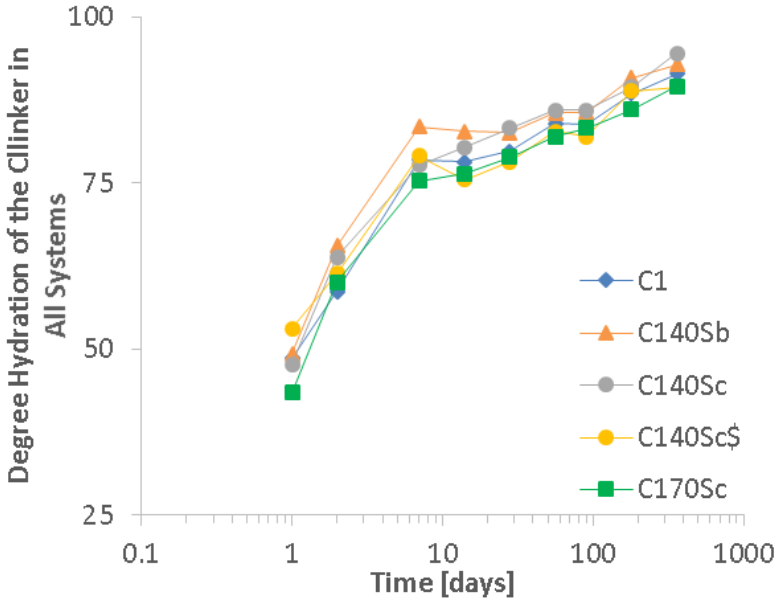

Figure 5-9 – Influence of the Slag on the Overall Degree of Hydration of the Clinker

5.2.2 **Hydration of the Ground Granulated Blast-Furnace Slag**

The degree of slag hydration (DoH) was followed by BSE-IA, the results of which are plotted in Figure 5-10. After 1 day 20 % of slag in blend C_140S_b had hydrated, while the figure for slag C was 26 %, whether or not additional sulfate was added, or if the slag content was higher. After 1 year of hydration there was a clear difference in slag reactivity between the 40% slag blends, with 57 % and 68 % of slag B (Al poor) and slag C (Al rich) having reacted respectively. However, the hydration kinetics of slag C in blend C_170S_c were slower, with 60% of the slag having reacted by the end of the testing period. Interestingly, the hydration of slag C in blend C_170S_c showed similar hydration kinetics to the blend prepared with 40% of the slag up to 28 days of hydration. Beyond 28 days, slag C hydrated more slowly in C_170S_c. This also coincides with the moment when calcium hydroxide was no longer consumed by the slag in C_170S_c rich blend(Figure 5-2). The slowing of slag hydration may be related with the overall calcium hydroxide content, such that slag hydration is limited if the CH content, and consequently pH, is too low.

Slag reactivity is dependent on several factors; including w/b ratio, slag fineness, and slag loading [82]. Because the slags' physical properties and the water/binder ratios in this study are constant, this suggests that slag chemistry defines the degree of hydration provided that there is sufficient activator, in this instance cement. The reactivity of slags has been previously investigated based on their composition alone and several ratios have been proposed [7]. The most common is the basicity ratio CaO/SiO_2 where good reactivity is expected for values greater than 1; Slag B and slag C have a CaO/SiO_2 of 0.96 and 1.12 respectively.

The measured degrees of hydration agree with previous findings. Luke and Glasser [83] found that 41 % of the slag had reacted after 1 month of curing and 65% had reacted after a full year in blends containing 30 % slag. Similarly, Lumley et al. [77] measured a degree of hydration varying from 30-55 % after 28 days of curing, and 45-75 % after 1 to 2 years of curing for blends with varying w/b and slag content. The difference measured

here between slag B and slag C for a same slag loading may very well be due to the change in composition and glass structure [7, 64, 75]. It must, however, be acknowledged that the measured degree of hydration after 1 day of curing may be slightly overestimated, where the smaller slag particles may not have been segregated successfully from the hydrated mass as explain in chapter 3. This may possibly be gleaned at in Figure 3-16 where the standard deviation was greatest at early stages of hydration.

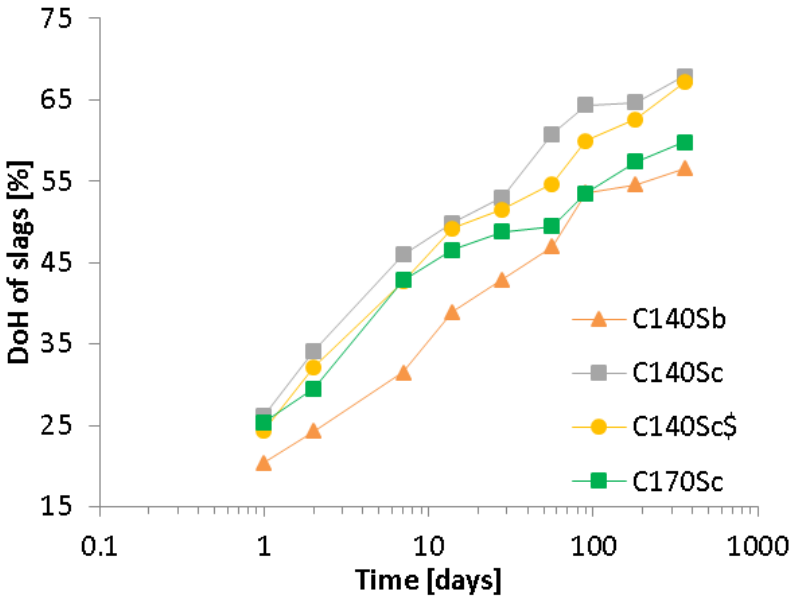

Figure 5-10 – Quantitative Degree of Hydration of Slags

5.2.3 Hydration of the Composite Systems

Figure 5-11 shows the hydration of all the systems investigated by the means of chemical shrinkage and calorimetry, normalised to the cement content. Figure 5-12 shows the high degree of linearity between the two techniques. Slag addition was accompanied by an increase in the total heat and shrinkage, when normalised to the cement content. This effect was dependent on the slag type and loading. In blends having the same slag content, the more basic, alumina-rich slag C blend evolved more heat and showed greater shrinkage than the blend containing slag B. The addition of sulfates (C_140S_c\$) had no effect discernible effect, although early age hydration appeared to be accelerated. The increase in reactivity per gram of clinker could be

attributed to two distinct effects. Firstly, because of the hydration of the slag itself [85, 86, 283]. Secondly, there is also the aforementioned filler effect [91, 92, 93], with an increase of the W/C of the blends and the provision of nucleation sites, promoting early-age clinker hydration [284]. This is illustrated in Figure 5-11 where the blend $C_1$40Q contained 40% quartz (which was shown to be unreactive in Figure 3-3) in place of GGBS; any increased reactivity is therefore attributed to the filler effect only to this level of replacement.

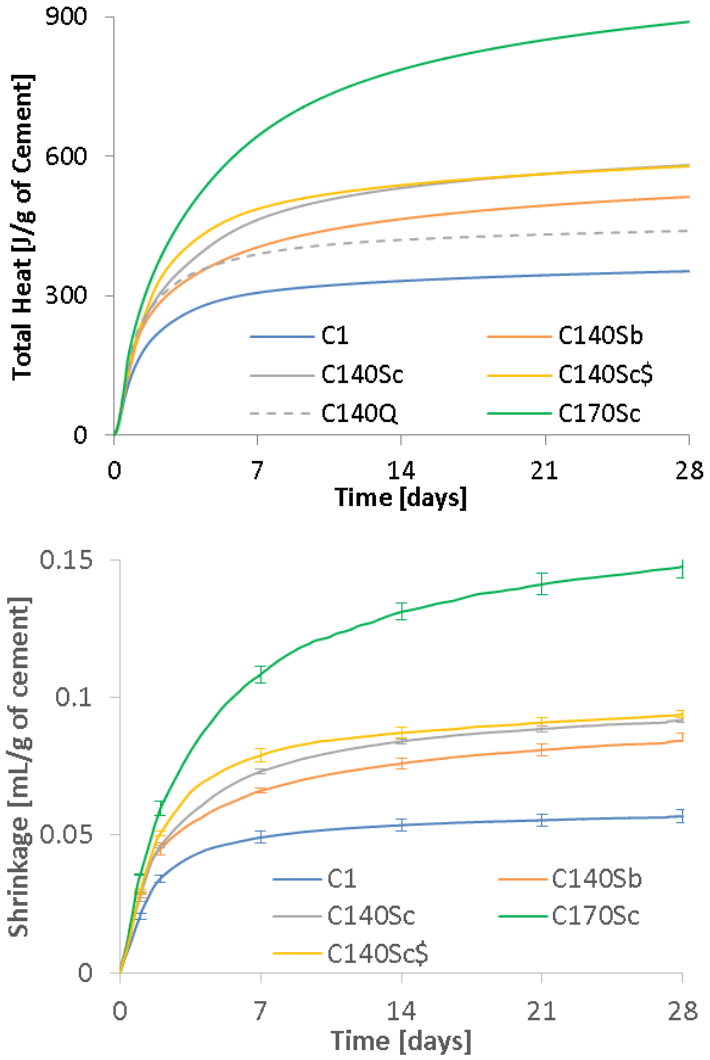

Figure 5-11 – Hydration Kinetics by Means of Calorimetry (top) and Chemical Shrinkage (bottom)

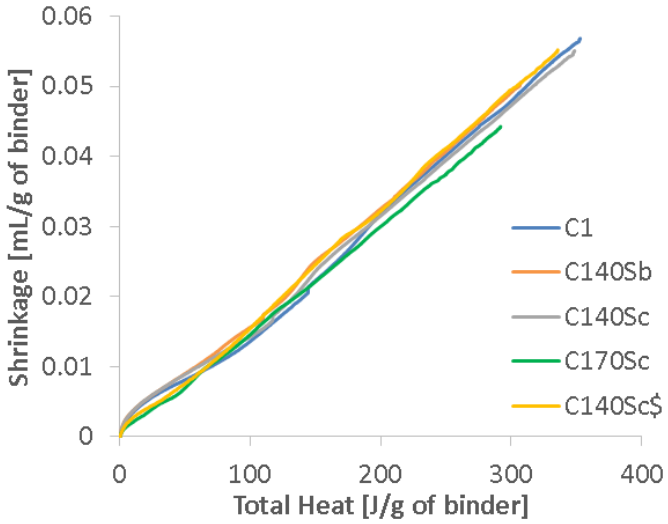

Figure 5-12 – Shrinkage Evolution Plotted Against Heat Evolution

In Figure 5-13, showing the heat evolution rate, it can be seen that the neat system was dominated by one peak, associated with alite hydration, followed by a very slight hump after 1 day, indicative of secondary aluminate reaction upon sulfate depletion [46, 47, 48]. The addition of slag was accompanied by an increase in the maximum heat rate of the alite phase; characteristic of the filler effect exacerbating clinker hydration. This increase in C_3S hydration rate was too slight to be determined by XRD (Figure 5-4). The greater the slag content, the greater was this effect [81]. Furthermore, an additional peak was observed soon after the onset of the deceleration of alite hydration; this peak (labelled A) is analogous to the faint hump seen in the neat system C_1, and is due to the hydration of the aluminate phase under the influence of the slag [3]. The occurrence of peak A was not constant in the slag blends. At 40% slag content, peak A arose after 18h and 22.5 hours for C_140S_c and C_140S_b respectively. Since both slags had the same particle size distributions, the known impact of particle fineness on the filler effect can be discounted [285]. Thus, this difference was likely dependent on slag composition, with the aluminium-rich slag C showing a slightly quicker reaction. At 70% slag content this peak occurred earlier, with it almost coinciding with the maximum heat rate of C_3S, where the filler effect was greater. The addition of anhydrite in C_140S_c\$ caused a delay in the hydration of the aluminates [286], as previously demonstrated by Richardson et al. [46].

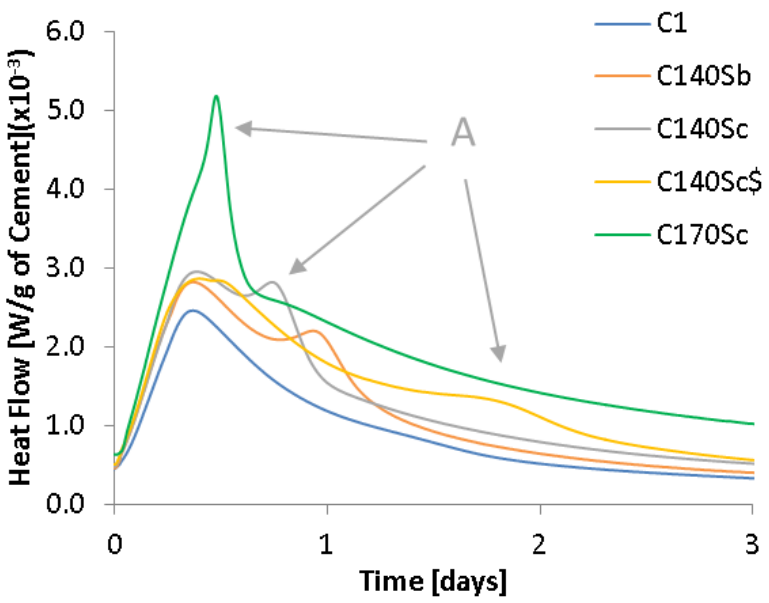

Figure 5-13 – Heat Evolution Rate of the Investigated Systems

From Figure 5-11, it was possible to separate the heat evolved from slag hydration from that of the clinker. The difference in heat evolution between the quartz blend, $C_1$40Q, and the neat system, C_1, is due solely to the filler effect. Therefore, the difference in heat evolution between a quartz- and slag-blend is due to the hydration of the slag itself, and this has been plotted in Figure 5-14, normalised to the slag content. Slag C was more reactive than slag B when comparing blends $C_1$40S_b and $C_1$40S_c. Increasing the slag content in blend $C_1$70S_c reduced the reactivity of the slag at later ages. This confirms the SEM-BSE image analysis.

At very early ages (less than 1 day), apparent zero values of heat released from the hydration of the slag was observed. This is likely to be the result of different interaction between the quartz, or slag, with the clinker; the very different composition between the quartz and slag would result in changes in the nature of the hydrates formed, most likely aluminates, and therefore resulting in minor changes in heat released at early stages. This suggests that the reactivity of slags remain low at very early ages confirming the SEM results. Slag C, the more reactive of the two slags, only reached a degree of hydration of 26 % after 1 day.

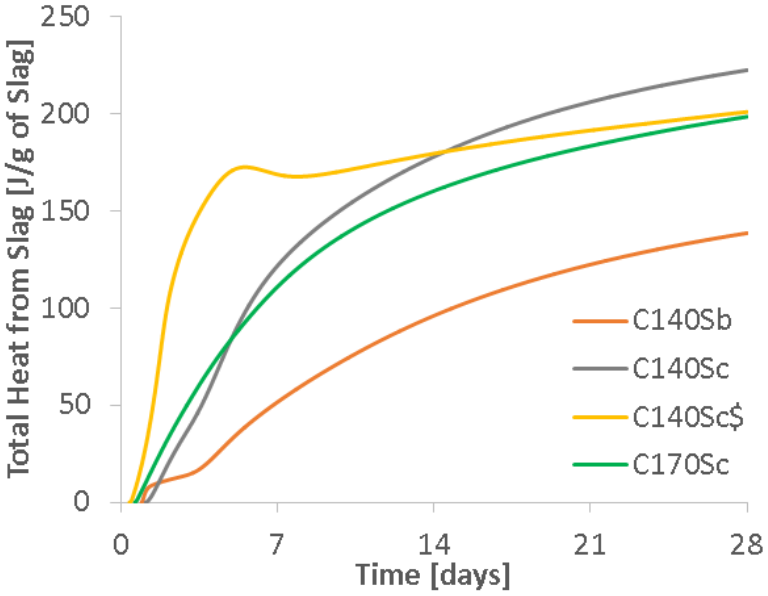

Figure 5-14 – Heat Evolved by the Hydration of Slags in Blended Systems

More interestingly, sulfate addition in blend $C_1$40S_c\$ led to the appearance of an apparent maximum after 3-4 days. This was a consequence of a change in hydration kinetics of the aluminates in the presence of sulfates, as shown in the calorimetry traces shown in Figure 5-15. In blend $C_1$40S_c\$, peak A was observed after 2 days, whilst in the equivalent quartz blend ($C_1$40Q\$) the same peak appeared 5 days into the hydration. By comparison, in the blends not including additional sulfate ($C_1$40S_c and $C_1$40Q) peak A appeared after about 1 day of hydration. The difference in time explains the observed maximum following subtraction of the trace for $C_1$40Q. Because peak A is associated with aluminate hydration as sulfate is depleted, this would suggest an interaction between the sulfates and the slag allowing for a faster hydration of the sulfate and consumption of the aluminates [60, 75, 287]

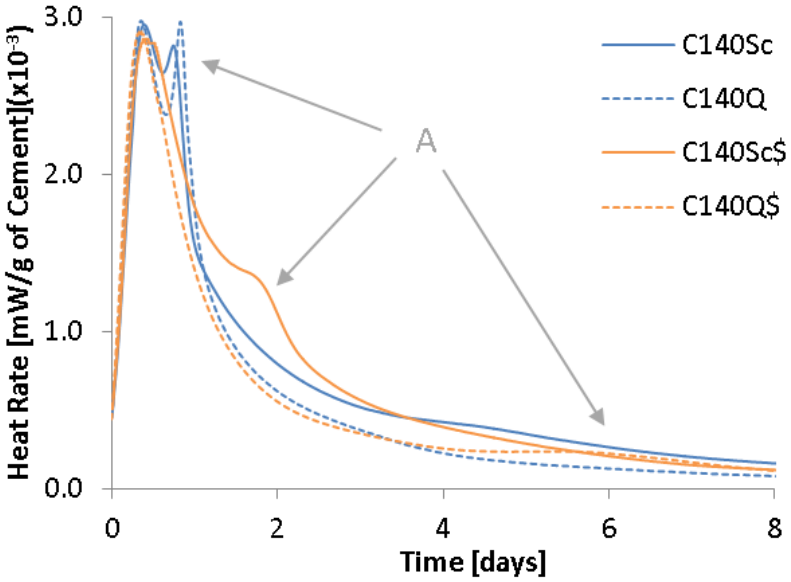

Figure 5-15 – Heat Evolution Rate of $C_1$40S_c\$ Compared to $C_1$40Q\$

This change in the kinetics of the aluminate hydration in the presence of sulfates was confirmed by XRD and is shown in Figure 5-16. In blends containing no added sulfate, C_3A hydration was fast, with only traces remaining in both blends $C_1$40Q and $C_1$40S_c. Upon sulfate addition, C_3A hydration was delayed, however, more so in blend $C_1$40Q\$, where C_3A was present still after 7 days of hydration; confirming the calorimetric observations.

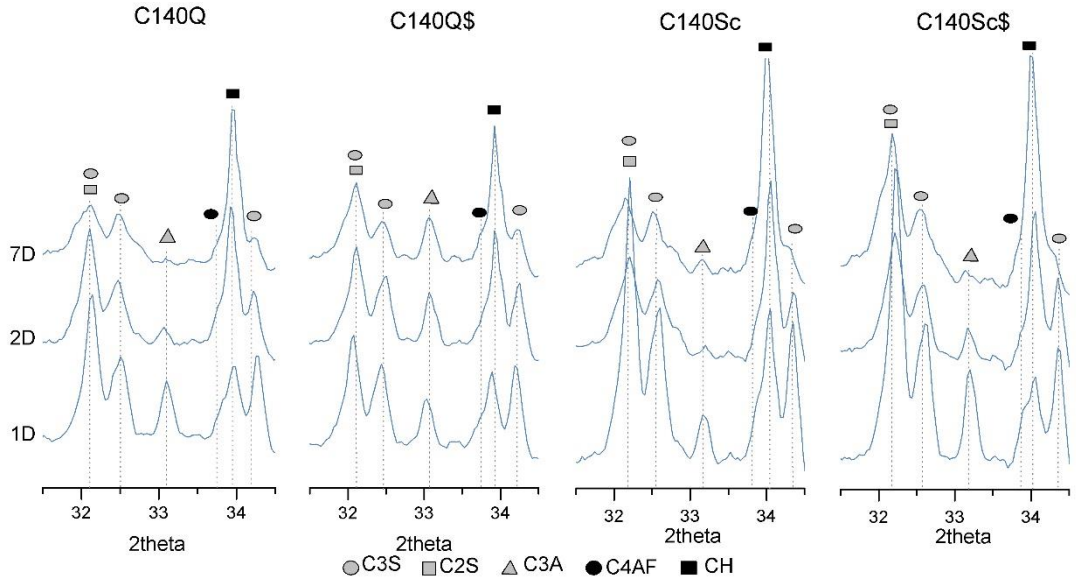

Figure 5-16 – Effect of Sulfate Addition on the Hydration of C_3A in Blends $C_1$40Q and $C_1$40S_c

Figure 5-17 further highlights the interplay between slag composition and sulfates, by following the hydration of blends $C_1 40 S_c$ and $C_1 40 S_b$ on the one side, plus their sulfated analogues on the other, containing 3 % of sulfates by weight of binder. Evidently, C_3A hydration was delayed in the slag composites prepared with added sulfates, the extent of which was greatest in blend $C_1 40 S_b$\$. Of the two slags, slag B was the more deficient in alumina and the least reactive. This confirms that alumina from slag contributed to the formation of the aluminate hydrates; sulfates was more rapidly consumed in blends prepared with the alumina rich slag C allowing for the faster dissolution of C_3A.

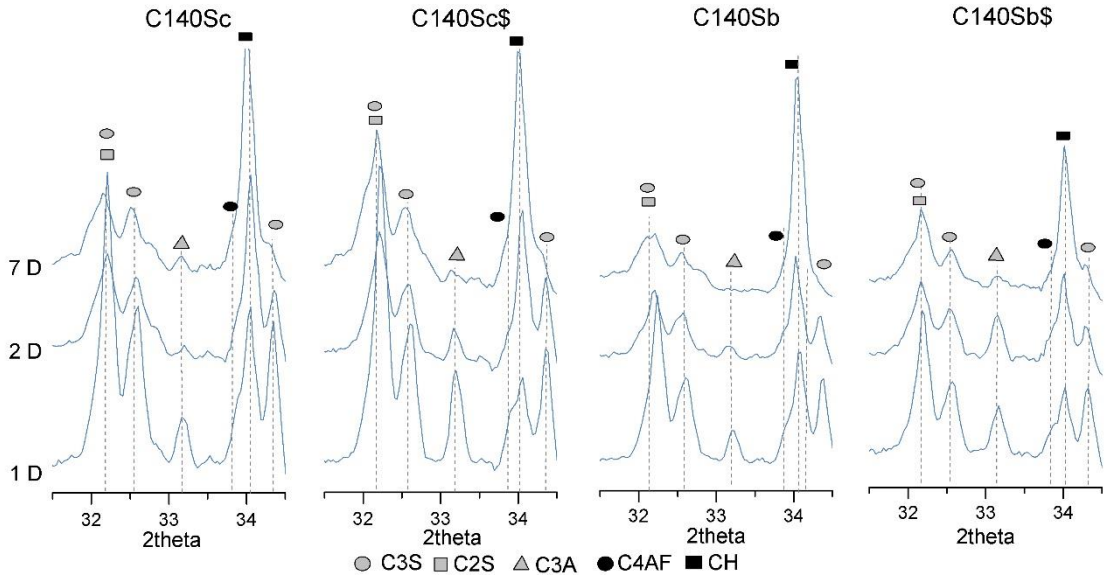

Figure 5-17 – Impact of the Alumina content of the Slag in Blends With and Without Additional Sulfates

With the degree of the hydration of the slag and the clinker quantified separately, it was possible to measure a weighted degree of hydration, combining the two techniques together. This is plotted in Figure 5-18. With cement hydration being fast compared to slags, C_1 showed the greatest degree of hydration; its rate was fast during the first 7 days, with 80 % of the clinker having dissolved, and decreased with time. The slower hydration kinetics of the slag meant that the overall degree of hydration was lower in all the slag composite cements investigated. However, the hydration rate was greater in the composite systems beyond 7 days of curing. With most of the clinker dissolved, the

increased hydration rate was because of slag dissolution [84, 85]. This effect was seen in Figure 5-11.

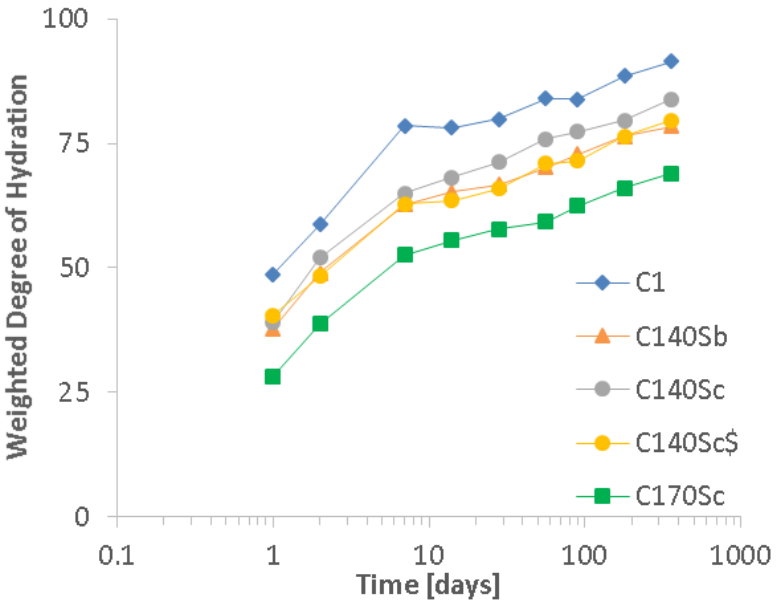

Figure 5-18 – Weighted Degree of Hydration of The investigated Blends

The extent of shrinkage was plotted against the weighted degree of hydration in Figure 5-19. At lower degrees of hydration, the shrinkage evolved along one regression line for all systems. This effect remained true for degrees of hydration up to 60 % for blends containing 40 % slag, and up to 50 % for blend C_170S_c. Compared to the figure just above, the aforementioned degrees of hydration for slag systems are reached after just 7 days of hydration. Beyond that point, a change of slope was observed in the blended systems such that shrinkage was greater per unit of hydration; by then much of the clinker had reacted and, therefore, the observed increase in shrinkage per unit of hydration is attributed to the hydration of the slag.

This suggest a change in hydrate composition or amounts. Ettringite is the phase richest in water. However, as all the C_3A and sulfates had been consumed in 7 days or less (Figure 5-6 and Figure 5-13), no more ettringite would be expected to precipitate. With AFm phases or hydrotalcite present in minute amounts, it was more likely that it was the C-S-H phases that had bound more water in the blended systems. This increase

in bound water in composite systems had previously been reported by Termkhajornkit and Nawa [288] and more specifically for slag containing cements by Ishida et al. [289].

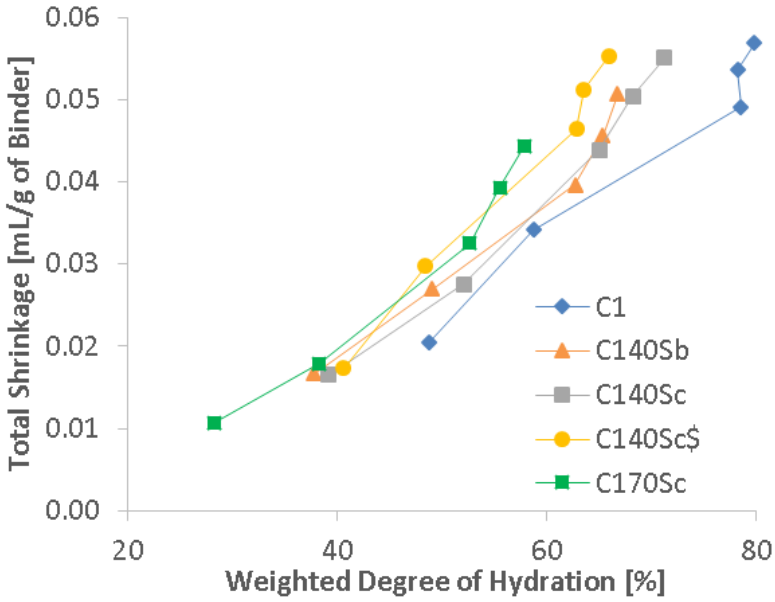

Figure 5-19 – Evolution of Shrinkage with Weighted Degree of Hydration

5.3 Hydration products

Figure 5-20 shows typical BSE micrographs of the neat system C_1, compared to the blended systems C_140S_b and C_170S_c. In the micrographs obtained from pastes cured for 2 days there was an intimate mixture of anhydrous material, hydrated phases and pores. At this early stage a high proportion of anhydrous material was visible; ranging in size from just a few microns to 20µm or more. The more noticeable hydrates included calcium hydroxide (CH) appearing light grey, and outer product (Op) C-S-H, appearing dark grey. Since slags hydrate more slowly than Portland cement clinker, a higher porosity was noticeable at this early age in the blend compared to the neat system C_1. At later ages (Figure 5-21), inner product C-S-H was more abundant, surrounding the partially hydrated larger grains. The finer slag particles had fully reacted leaving only partially hydrated larger ones with characteristic hydration rims. With increasing hydration the total pore area reduced.

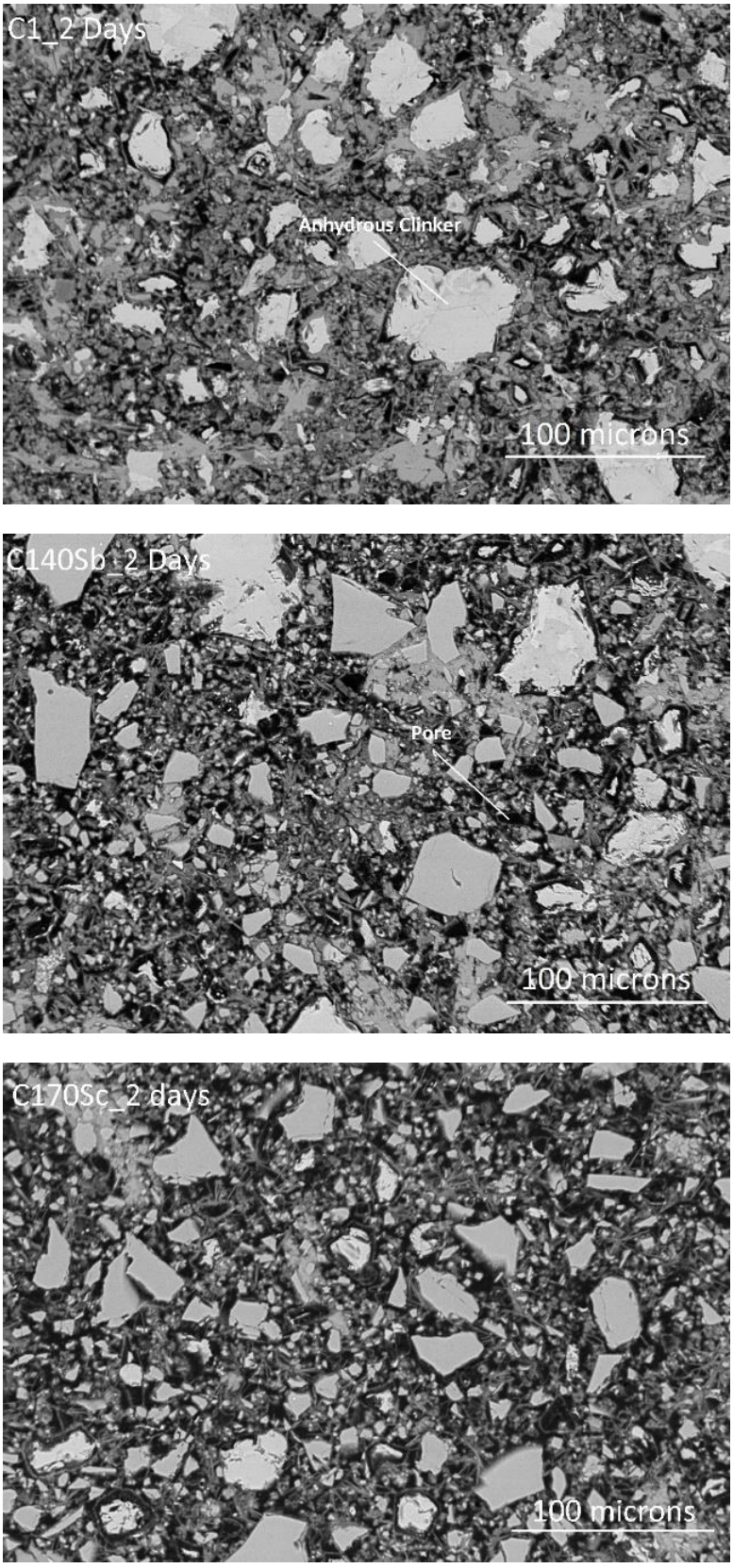

Figure 5-20 – Evolution of the Microstructure for C_1, C_140S_b and C_170S_c cured for 2 days

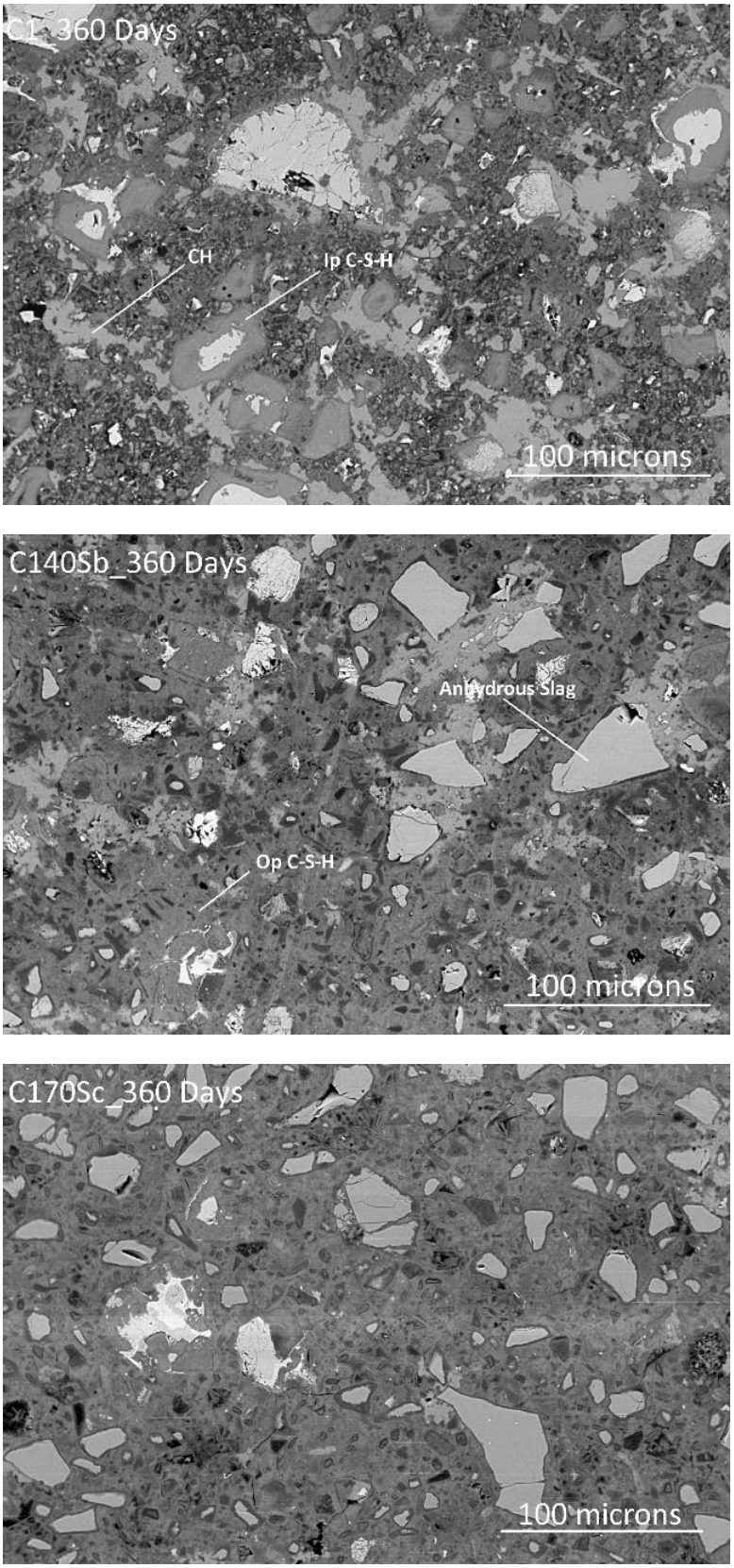

Figure 5-21 – Evolution of the Microstructure for C_1, C_140S_b and C_170S_c cured for 360 days

The evolution of porosity with time is plotted in Figure 5-22. After just one day of curing, the porosity was greater in the slag blended systems, and increased with slag loading. Porosity was always found to be the lowest in the neat system up to 28 days of hydration. In response, C_1 was always the strongest during the first 28 days of curing (Figure 5-3). However, beyond 28 days of curing, the porosity showed no appreciable decrease after 28 days of curing, by which time most of the clinker phases had reacted (Figure 5-9).

In the slag blended systems, the porosity evolution was such that after 28 days of curing, the differences in porosity between the slag composite cements and the neat system C_1 had lessened, where slags continued to hydrate filling pore space with hydrates. Eventually, after prolonged curing, all the investigated systems showed comparable porosities. Furthermore, sulfate addition had no noticeable effect on the porosity, despite the greater potential of forming the lesser dense phase ettringite.

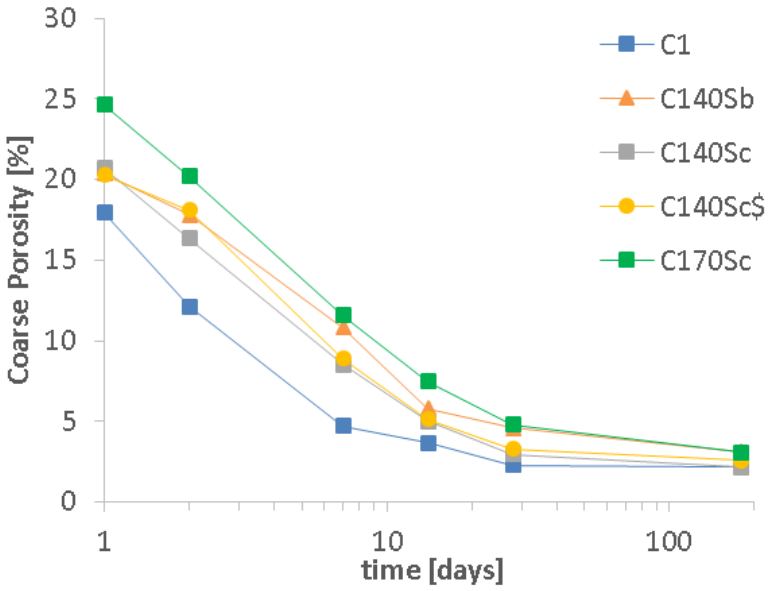

Figure 5-22 – Evolution of the Porosity with Time of the Investigated Systems, Measured by SEM-BSE

5.3.1 C-S-H Composition

The chemical composition of C-S-H was examined by SEM-EDX from Al/Ca against Si/Ca atomic plots (Figure 5-23). The Al/Si ratios were determined from the slope of the

line originating from the origin drawn through the point with the lowest measured Al/Ca to best avoid intermixing with other phases. The Ca/Si was taken as the point along that same line having the highest Si/Ca ratio.

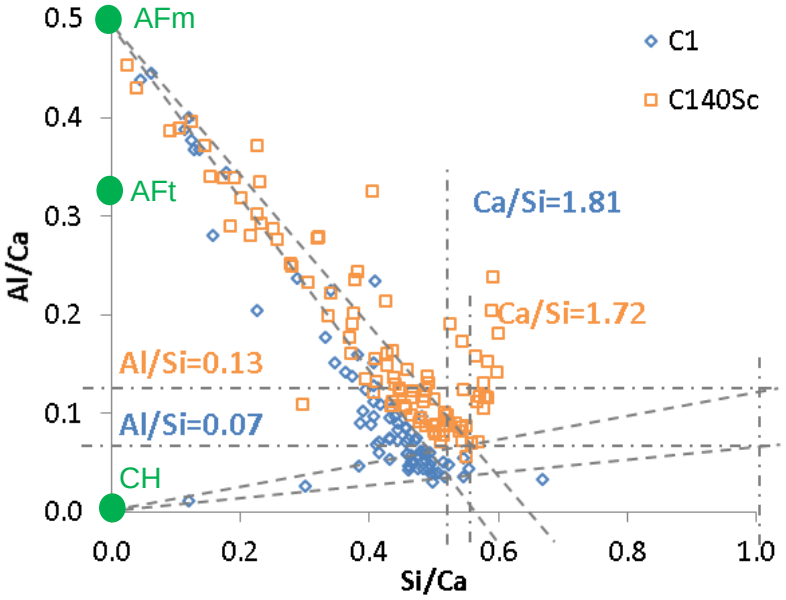

Figure 5-23 – Al/Ca v Si/Ca for C_1 and $C_1 40S_c$ Cured for 180 Days

The Ca/Si and Al/Si ratios of C_1 were shown to be constant over time, with a Ca/Si ≈ 1.8 and Al/Si ≈ 0.06 (Table 5-2). Clinker replacement resulted in changes to C-S-H composition. In the case of blend $C140S_b$ the Ca/Si ratio decreased to about 1.6 and remained approximately constant. The Al/Si ratio also remained constant, with a value close to 0.1. These values are similar to those in the literature; where the effect of slag on C-S-H composition and morphology are well reported and a C-S-H with a lower Ca/Si and higher Al/Si atomic ratio is ultimately formed [29, 78, 88, 290]

Higher alumina contents in slag C resulted in greater aluminium incorporation in the C-S-H in blend $C_1 40S_c$. The Al/Si averaged 0.13 and again remained unchanged during hydration. The Ca/Si of the C-S-H was higher than for the equivalent blend made with slag B, due to the higher CaO/SiO_2 of the slag. Blend $C_1 70S_c$ had the lowest Ca/Si and highest Al/Si ratios of all the investigated systems.

Table 5-2 – Various Atomic Ratios of the Outer Product C-S-H Phase (error= ±0.005)

	days	C_1	C_140S_b	C_140S_c	C_140S_c\$	C_170S_c
	1	1.85	1.61	1.67	1.78	1.43
Ca/Si	**28**	1.82	1.56	1.65	1.75	1.43
	180	1.81	1.59	1.72	1.72	1.39
	1D	0.06	0.12	0.14	0.08	0.17
Al/Si	**28D**	0.07	0.11	0.12	0.13	0.15
	180D	0.06	0.09	0.12	0.12	0.15
	1D	0.07	0.05	0.05	0.09	0.05
S/Ca	**28D**	0.05	0.04	0.04	0.05	0.03
	180D	0.04	0.01	0.02	0.04	0.01

The addition of sulfate did lower the Al/Si ratio at 1 day, all the while increasing the Ca/Si ratio. At this early stage, there was still some residual anhydrite in the paste and so ettringite was preferentially precipitated over the AFm phases. The aluminium concentration in solution was thus defined by the low solubility of ettringite [284]. Therefore aluminium incorporation into the C-S-H remained low. Additionally the S/Ca atomic ratio increased (Table 5-2) in C_140S_c\$, in line with similar, previous studies [278, 281, 291, 292]. The coupled increase of both Ca and S content in the C-S-H suggests the absorption of calcium sulfate on C-S-H, as predicted by Labbez et al. [282].

5.3.2 **Effect of Slag Composition and Added Sulfate**

The ettringite contents, as determined by XRD-Rietveld, are summarised in Figure 5-24. All hydrating systems quickly reached a stable plateau within the first few days of hydration. In the neat system, C_1, 17g of ettringite was produced from 100g of cement. Slag addition reduced the ettringite content, with both slags behaving similarly. Therefore, the lower sulfate content of these blends dominated over the increased aluminium content. The addition of sulfate in blend C_140S_c\$ led to an increase in ettringite content, exceeding those of C_1.

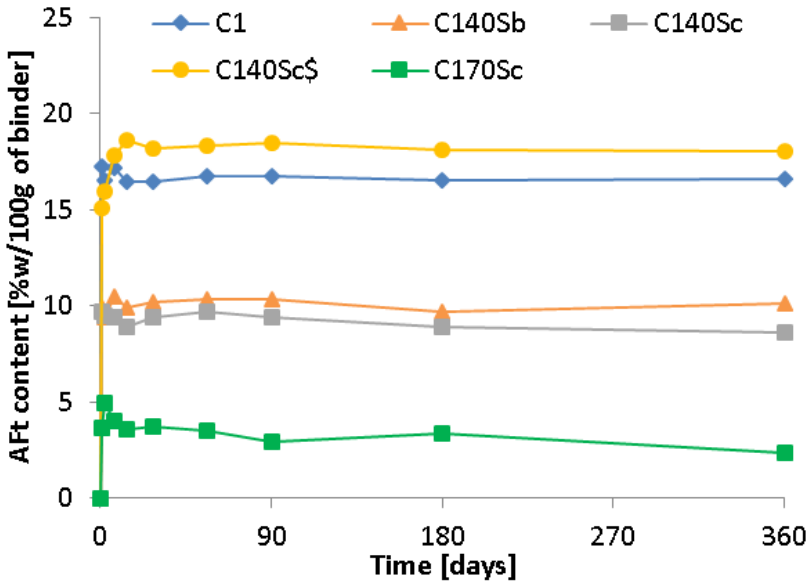

Figure 5-24 – Evolution of Ettringite of the Investigated Blends (/100g of Binder) [±2 %]

The addition of slag to blends altered the chemistry of the hydration products, and Figure 5-25 shows the evolution of the AFt and AFm phases in all the systems, as measured by XRD. Throughout the study ettringite was present in the neat system. As hydration proceeded, hemicarboaluminate (Hc) was formed beyond 7 days and progressively transformed to monocarboaluminate (Mc), agreeing with previous studies [42, 281, 293].

Upon the addition of slag, provision of aluminium led to the formation of hemicarboaluminate within one day. In the case of C_140S_b, the subsequent progressive conversion of Hc to Mc started after 7 days of hydration and was almost complete after a year. In the more Al-rich C_140S_c, Hc persisted and its conversion to Mc was only partial. The addition of sulfates in blend C_140S_c\$ further upset the AFm-carboaluminate distribution. The reflections for ettringite were more intense, but at the expense of the carboaluminate phases. Just like its sulfate free equivalent, after 7 days of hydration, there was a strong Hc reflection, but this was converted to Mc as hydration progressed.

The presence of hemicarboaluminate and its subsequent conversion to monocarboaluminate was a feature present in blend C_170S_c too. That same blend further

showed the formation of monosulfate after 180 days of curing, and the ettringite signals had dampened. With such a high slag loading, the added aluminium was great enough as to favour monosulfate formation at the expense of ettringite at later ages of hydration. However, the conversion was too slight to be quantified by XRD analysis. There was no indication of the conversion of ettringite to AFm in the blends prepared with 40 % slag, where limestone levels were sufficient to stabilize ettringite [5, 42, 294].

In the neat blends, the overall peak shapes of the AFm phases were mostly well defined making their identification easy. The overall shapes of the phases were ill defined in the slag blends, particularly in blend C_170S_c; additional unidentified peaks were present, most likely either a hydroxyl –AFm or monosulfate type solid solution [42]. As such, care should be taken when assigning reflections to the AFm phases, as their low crystallinity and variability in composition can result in peak shifts and changes in intensity [41, 42]. Hydrotalcite (Ht) was present in the blended systems only at later stages of hydration, due to the higher magnesium content of the slags.

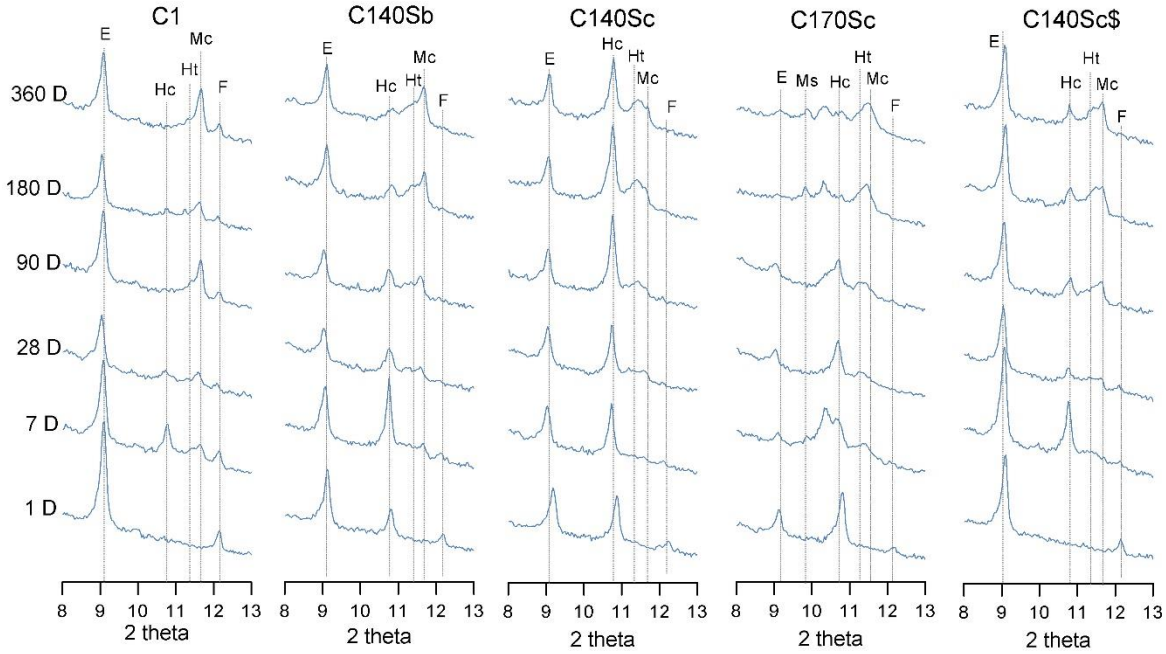

Figure 5-25 – XRD Patterns from 8-13 2theta Highlighting the AFm Phases (E -ettringite, Ms – monosulfate, Hc - hemicarboaluminate, Mc - monocarboaluminate, F - ferrite)

The effect of slag on the AFm phase distribution is further highlighted in Figure 5-26, showing blends where the slag fraction has been replaced with quartz. In blend $C_1$40Q, ettringite was present after just 1 day of hydration and hemicarboaluminate precipitated after 2 days. Compared to its slag-containing cousin, hemicarboaluminate was present after just 1 day with much stronger peak intensities. C_3A hydration (Figure 5-16) was comparable between blends $C_1$40Q and $C_1$40S_c suggesting that the slag acts as an Al_2O_3 reservoir promoting earlier hemicarboaluminate precipitation in the slag blend. When adding sulfates, in blend $C_1$40Q\$, ettringite continuously precipitated, highlighting the slower dissolution of C_3A, and hemicarboaluminate was never present. In comparison to the sulfated slag blend, ettringite showed the strongest peak intensities and was present in full by 2 days (Figure 5-24), and hemicarboaluminate was present in minor quantities after just 2 days of hydration. C_3A hydration was delayed in blend $C_1$40Q\$ (Figure 5-16); where there was too little alumina to compensate for the additional sulfate, thus preventing any AFm precipitation within 7 days of hydration. This confirms the role of slag alumina content on the hydrates formed.

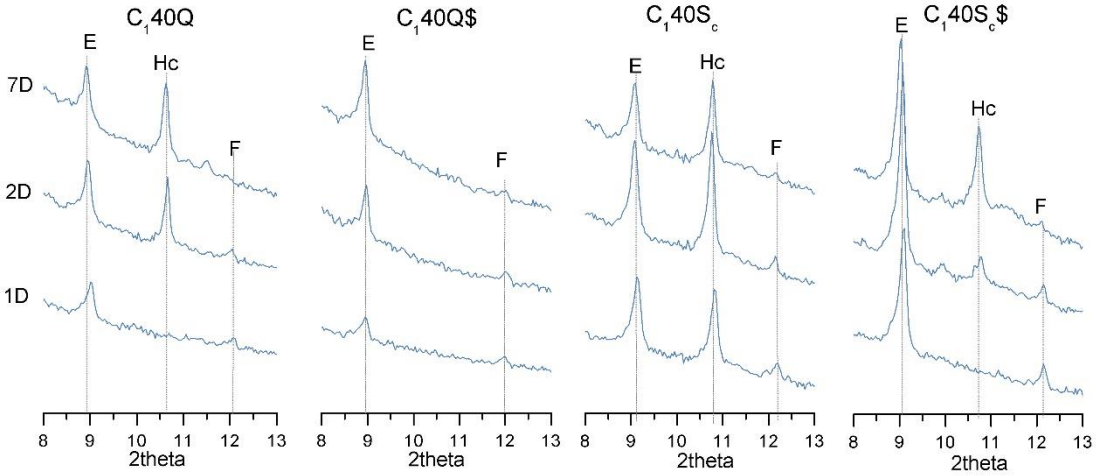

Figure 5-26 – Influence of Slag on AFm Distribution at Early Ages Compared to Quartz Blends

The impact of the differing contents of alumina between the two slags can again be elucidated to a greater extent by comparing blends $C_1$40S_b and $C_1$40S_c with, or without, added sulfate. The evolution of AFm phases in all the systems was already observed in Figure 5-25, and the slag blends showed the formation of AFm after just 1 day of curing.

In the presence of sulfates (Figure 5-27), AFm was absent after 1 day of curing for both $C_1 40 S_b \$$ and $C_1 40 S_c \$$. However, as hydration progressed, hemicarboaluminate formed after 2 days of hydration in blend $C_1 40 S_c \$$ only, and a strong reflection was seen after 7 days of curing. In blend $C140 S_b \$$, hemicarboaluminate hesitantly started precipitating after 7 days of hydration, again because of its lower alumina content twinned with its lower reactivity.

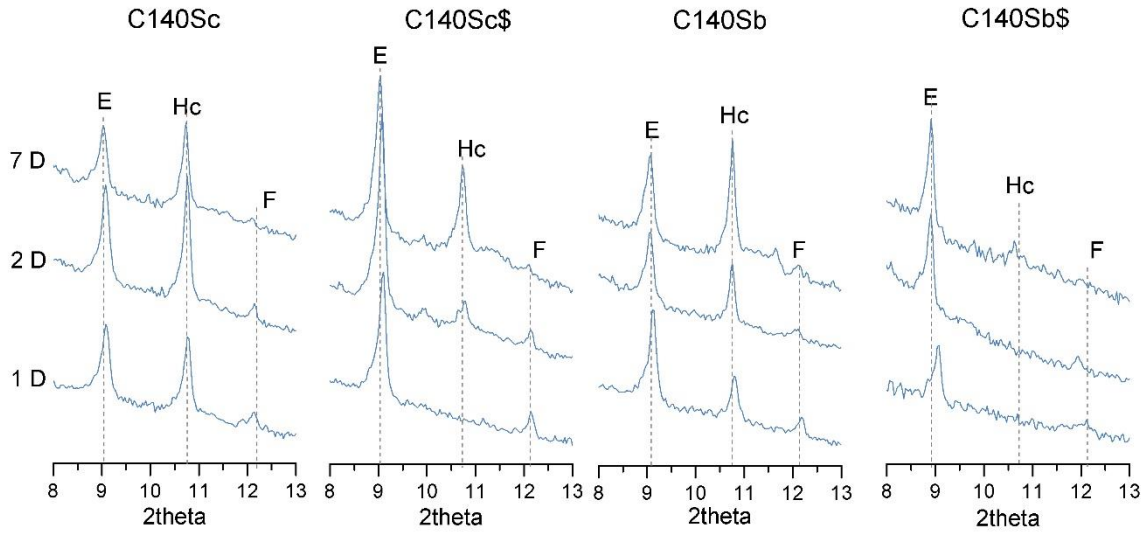

Figure 5-27 – Impact of Slag Composition in the Formation of Aluminate Hydrates, and the Impact of Sulfates

These results can be explained by the findings of Matschei et al. [41]. The hydration of C_3A with sulfates produces ettringite and sulfate-AFm phases. In the quartz blend spikes with sulfate, the SO_3/Al_2O_3 was sufficiently high enough for only ettringite to precipitate. With the slag blend, more aluminium was available supplied by the slag, effectively reducing the overall SO_3/Al_2O_3 allowing for more AFm to precipitate at the expense of ettringite. With calcite in the system, added to the clinker, carboaluminate AFm phases are predicted to precipitate over sulfate AFm, as they are more stable in the presence of calcite.

5.3.3 **Slag Hydration Rims**

Slag hydration is associated with the formation of a hydrotalcite-like phase. Unlike pure hydrotalcite $Mg_6Al_2(OH)_{16}.CO_3.{}_4H_2O$, where the Mg/Al is equal to 3, a ratio closer to

2 is more common in slag cement blends [295]. Mg/Al ratios were obtained from the slope of the line of best fit when plotting Mg/Si against Al/Si (Figure 5-28 through Figure 5-31). The Al/Si of the C-S-H akin to the slag hydration rims was taken as the intersection of the slope with the axis. Data were obtained from slag hydration rims on samples cured for 180 days, where the rims were sufficiently large enough to be measured with minimal interference from the surrounding hydrates. The Mg/Al of the slag rims was highest in blend $C_140S_{b,}$ at 2.67. Replacement of slag B with slag C led to a slight reduction in the Mg/Al ratio of the hydrotalcite, to 2.01.The same ratio was further lowered by increasing the slag content to 70 % due to the greater availability of aluminium from the slag. XRD patterns showed only slight traces of hydrotalcite in the neat system C_1 (Figure 5-25). However, it was not possible to observe hydrotalcite by SEM, because it was being finely intermixed with the C-S-H and therefore no EDX analysis could be performed.

For a given level of replacement, the reduction in Mg/Al for the blend containing slag C was likely due to differences in slag composition. Slag C contained more aluminium and magnesium than slag B, but had a lower bulk Mg/Al ratio (0.89 versus 1.19). The increased aluminium content may explain the higher levels of calcium hemicarboaluminate hydrate and the increased aluminium incorporation into the outer product C-S-H. However, with magnesium remaining immobile [296] and not being incorporated into C-S-H but rather finely intermixed [76], the lower initial bulk Mg/Al led to a lower Mg/Al ratio in the hydrotalcite. This observation is in line with those of Ben Haha et al. who measured a much lower Mg/Al for the hydrotalcite like phase when the bulk Mg/Al of the anhydrous slag was much lower [68]. Furthermore as the MgO content increases in a blend, more hydrotalcite is expected to form, requiring a greater amount of Al, but also potentially reducing porosity and improving strength [69]. Although poorly resolved in XRD patterns [297], there appears to be a greater, albeit broad, hydrotalcite reflection indicating a greater amount of hydrotalcite in blends using slag C.

However, when extra sulfates were added, there was a marked increase in the hydrotalcite Mg/Al ratio, due to aluminium being incorporated in hydrate phases

elsewhere. The addition of calcium sulfate resulted in a lower Al/Si of the outer product C-S-H at early ages only to increase as hydration proceeded, plus a higher Ca/Si leading the lower observed CH content in blend $C_140S_c\$$. The lower Al/Si in the C-S-H was caused by the reaction of alumina in solution to form the low soluble ettringite quickly. As a result, less alumina was available in solution for the formation of the hydrotalcite phase, resulting in the observed increase in the Mg/Al.

The Al/Si ratio of the C-S-H within the slag hydration rims estimated comparable values than those measured for the outer product C-S-H of the blended systems since the slags are richer than the clinker in aluminium.

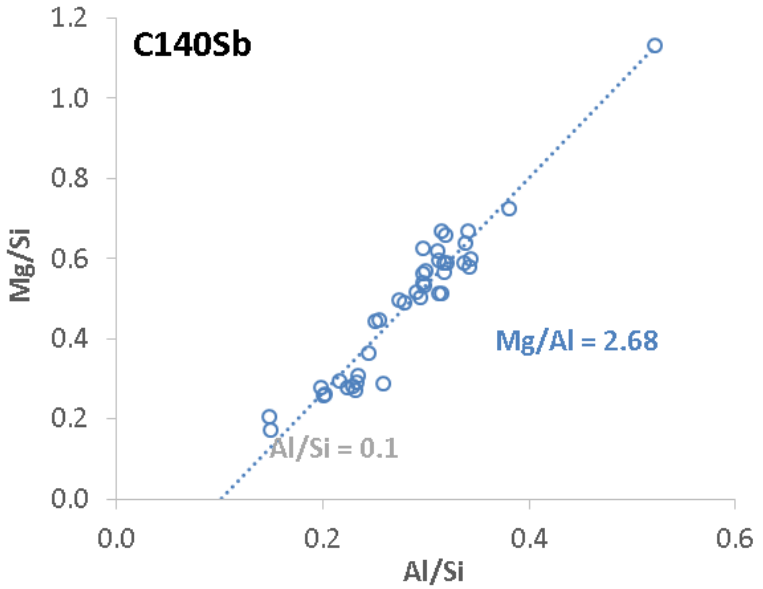

Figure 5-28 – Mg/Si v Al/Si for blend C_140S_b cured for 180 days

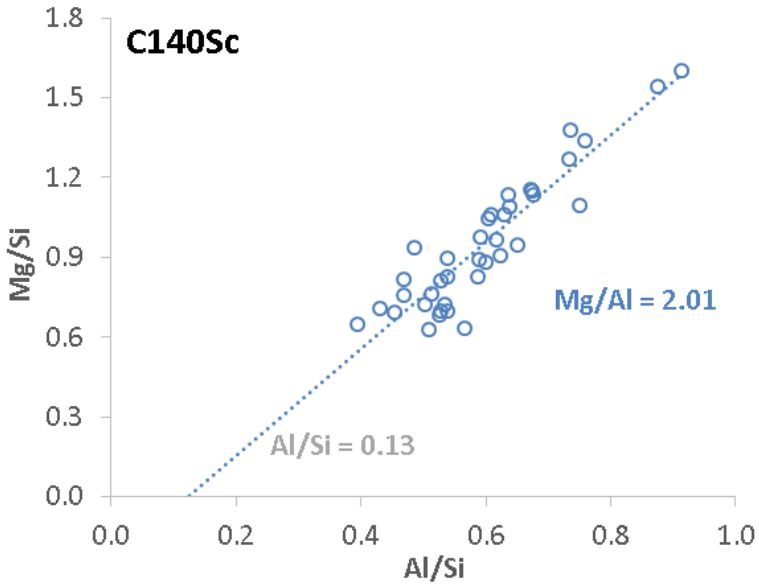

Figure 5-29 – Mg/Si v Al/Si for blend $C_1 40 S_c$ cured for 180 days

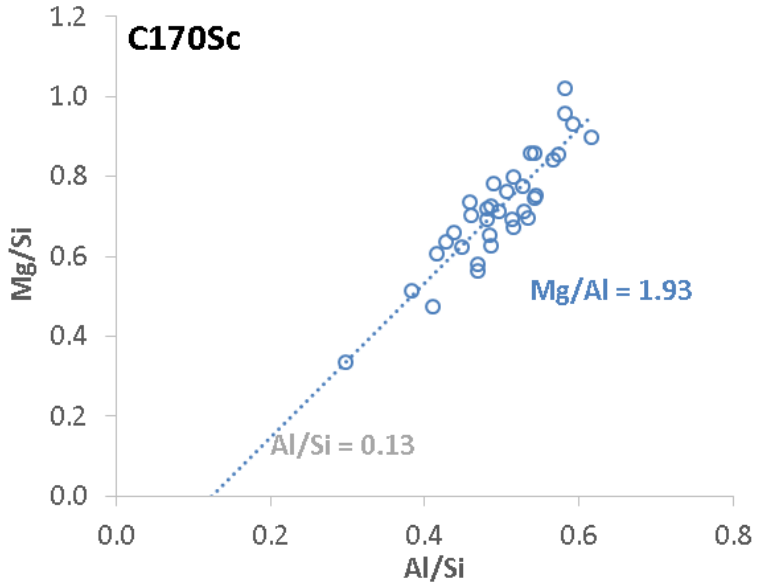

Figure 5-30 – Mg/Si v Al/Si for blend $C_1 70 S_c$ cured for 180 days

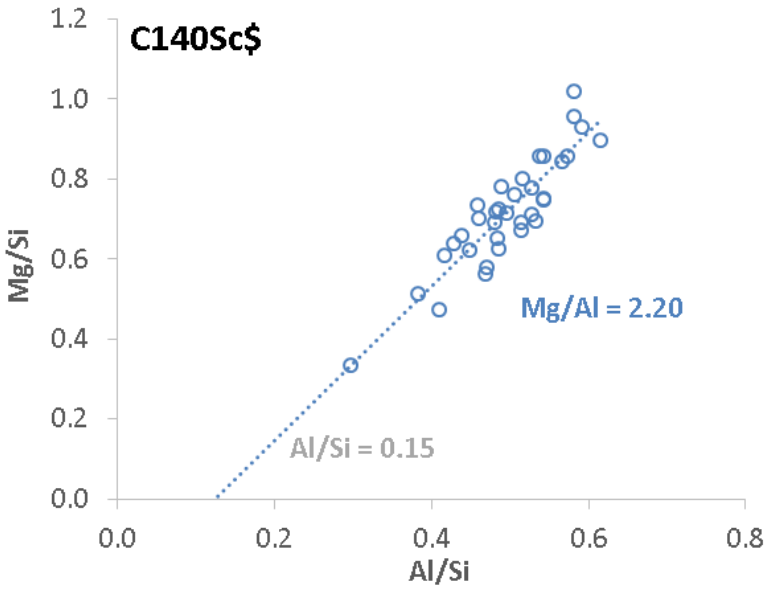

Figure 5-31 – Mg/Si v Al/Si for blend C_140S_c\$ cured for 180 days

5.4 Discussion

Figure 5-32 shows a clear negative correlation between porosity and compressive strength. Only the coarser porosity was evaluated using this approach, as the finer porosity was invisible to the SEM. This suggests that the coarse porosity dominates the compressive strength, independent of the mix designs, which is in agreement with previous observations [5, 50, 298, 299].

At later ages (180 days) the samples are characterized by a similar low coarse porosity and high compressive strength. However, data from Figure 5-14 and Figure 5-18 show that the total degree of hydration was lower in the slag blends. This was confirmed by thermodynamic modelling (provided by Maciej Zajac, Figure 5-33), which showed clinker replacement with slag to reduce the total volume of hydrates. It was assumed that the cement had reached 100% degree of hydration and that slag, using the composition of slag C, had reached a degree of hydration 70%, corresponding to the situation after roughly 360 days of hydration. The C-S-H phase was modelled having a Ca/Si of 1.6 and an Al/Si of 0.1 (Table 5-2). However, as shown, the capillary porosity and, therefore, the strength does not change. This implies that the capacity of the hydrates to fill the pore space in C_1 and slag blended cement is different. It is known that the properties of

the C-S-H phase are modified in the presence of slag, for example the microstructure [29, 290] improving space filling.

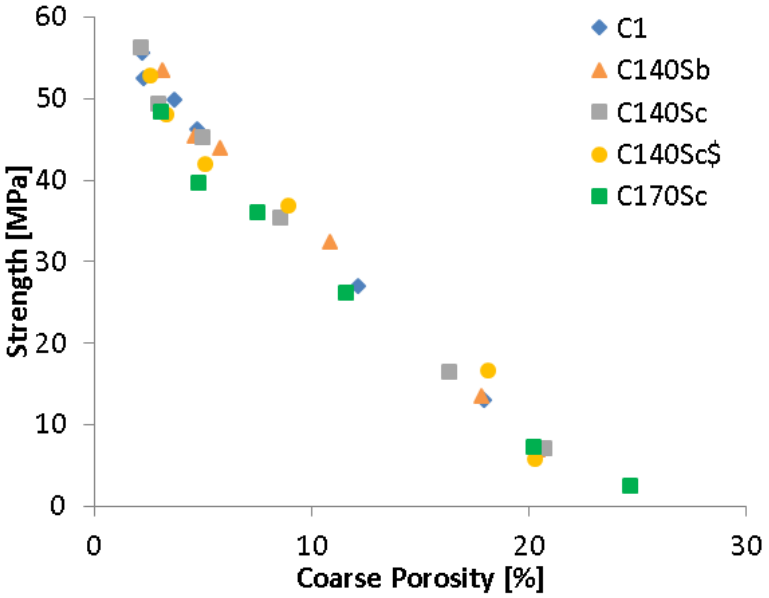

Figure 5-32 – Relationship Between Strength and Coarse Porosity

Thermodynamic modelling confirmed XRD observations (Figure 5-25). As the slag content increased, ettringite and CH contents continually decreased as the clinker phases and sulfate contents were diluted. With respect to the aluminate hydrates, AFm phases gradually replaced AFt. Furthermore, as the slag content increased, the increasing amount of aluminium provided by the slag favoured the formation of monosulfate around 70% slag and ultimately stratlingite C_2ASH_8. Hydrotalcite continuously increased with slag loading as the magnesium content increased.

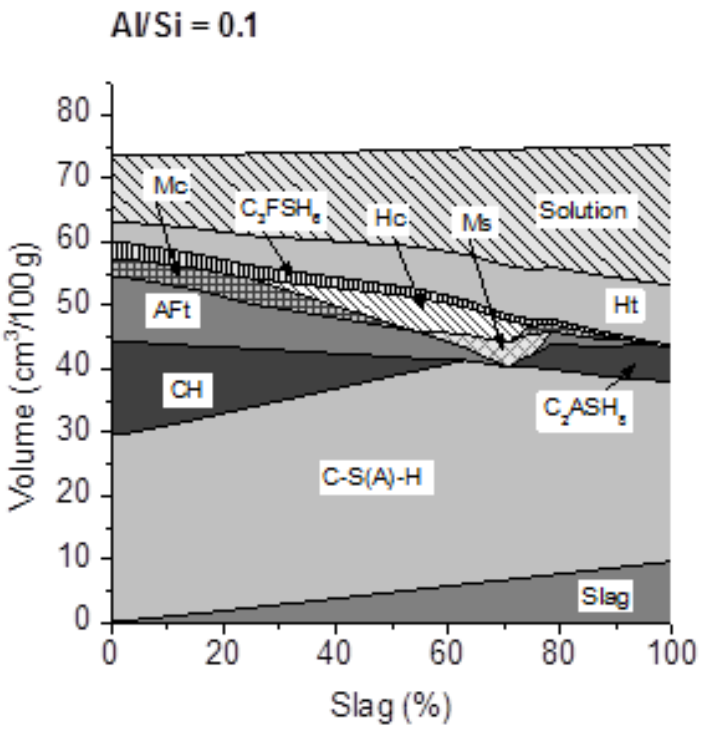

Figure 5-33 – Modelled phase assemblage change when a part of OPC is replaced by the slag assuming complete reaction of the Portland cement and 70% reaction of slag C [Provided by Maciej Zajac]

This improved space filling can be gleaned at in Figure 5-34. Just like shrinkage, at early ages of hydration, the porosity evolution sat on a single regression line. Beyond degrees of hydration of 60 %, for blends containing 40 % slag, and beyond 40 % for blend C_170S_c, porosity decreased faster per unit of hydration. This effect was seen after 7 days of hydration, by which time much of the clinker had dissolved.

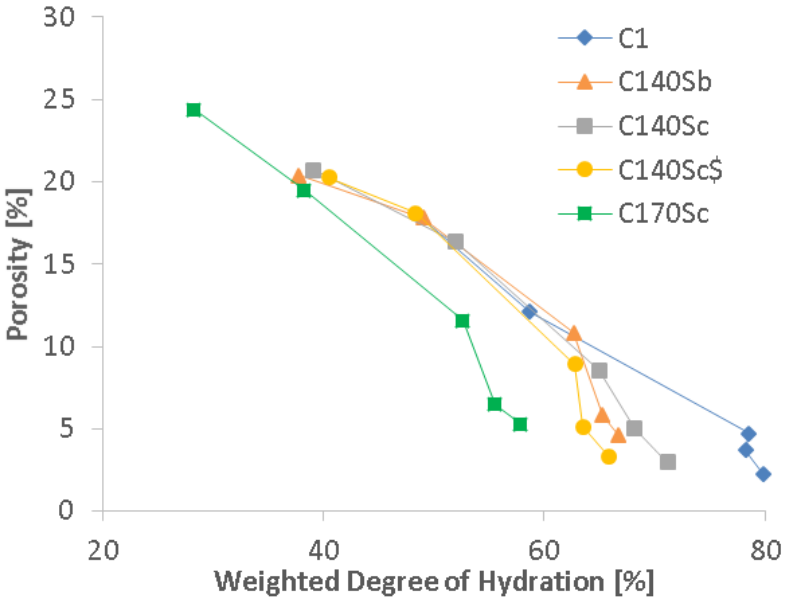

Figure 5-34 – Evolution of the Porosity and with Degree of Hydration

Figure 5-19 showed that more water had been bound in the hydrates per unit of hydration in the slag blends in the later stages of hydration, most likely by the C-S-H phase. The density of C-S-H depends muchly on its water content [300, 301]. Gallucci et al. [274] followed the density of the C-S-H phase in cement pastes cured at various temperatures. They found that at lower temperatures, the C-S-H had a lower apparent density and higher H_2O/SiO_2, resulting in an improved space filling of C-S-H and higher strength at later ages. Thomas et al. [301] have also shown that the density of the C-S-H gel reduced with increasing H_2O/SiO_2. Indeed, water rich C-S-H phases have a lower density [302]. Ishida et al. [289] further indicated that the apparent density of the C-S-H phase depended on the reaction degree of the slag. They also noted that the phase contained more gel and interlayer water at higher degrees of hydration, which implies a larger gel porosity. Termkhajornkit and Nawa [288] postulated that the C–S–H phase formed as a result of pozzolanic reaction has a greater specific volume of about 25 % for a replacement ratio of 25 % in comparison to the C-S-H in neat cement paste.

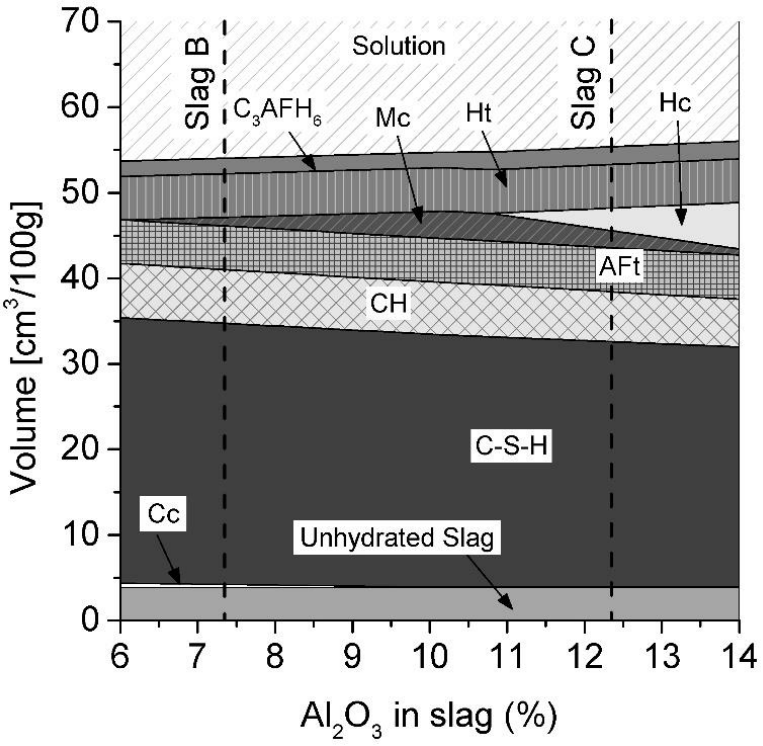

Figure 5-35 – Modelled phase assemblage of 40 % slag blends highlighting the Al_2O_3 content in slag (at the expense of SiO_2). All the cement was assumed reacted, and 70% of the slag had reacted [Provided by Maciej Zajac]

Figure 5-35 illustrates the effect of changing the Al_2O_3 content in the slag on the phase assemblage for slag blends whose slag content is the same (here, 40%). It was assumed that all the clinker had reacted and only 70% of the slag had reacted. The differences in phase assemblage here only reflect the changes in composition of the slag, ignoring any kinetic effect of the 2 slags. Increasing the Al_2O_3 content of the slag from that of Slag B (7.4 % Al_2O_3) to that of slag C (12.3 % Al_2O_3) leads to the formation of AFm phases (monocarboaluminate and hemicarboaluminate) while decreasing the total volume of the C-S-H phase, slightly increasing the total hydrate volume. With such a slight increase in volume, it is unlikely that the increasing the Al_2O_3 content would greatly affect the strength. As such the differences in strength (Figure 5-3) between blends C_140S_b and C_140S_c are due to the hydration kinetics of the slags (Figure 5-10).

Additionally, modelling results agree very well with the changes in the phase assemblage shown in Figure 5-24 and Figure 5-25. The limestone within the cement ensured that the ettringite content remained constant and that the formation of the

carboaluminates became increasingly prominent. Modelling reveals that the calcium demand for the formation of the additional AFm phases is rather limited. The model also predicted that increasing the Al_2O_3 content in the slag from 7 % to 12 % reduced the portlandite content. The modelled reduction in portlandite was experimentally observed in Figure 5-1 when substituting slag B with slag C. This suggests that the changes between samples C_140S_b and C_140S_c are related to changes in the C-S-H (Table 5-2).

Although C-S-H is the primary hydrate responsible for strength, the amount and type of aluminate hydrates formed also play a role in space filling [303]. It is important to note the effects associated with changes in AFm phases and ettringite. The stabilisation of ettringite with addition of extra sulfate leads to an increase in the volume of hydration products (Figure 5-36), and thus one would expect an increase in compressive strength. Nevertheless, comparing blends C_140S_c and C_140S_c\$, the latter has a slightly higher porosity, and lower compressive strength at later ages, despite a similar degree of hydration. This is true despite the lower density of ettringite which is much more prevalent in C_140S_c\$ (Figure 5-24 and Figure 5-35). Studies [278, 279] have shown that the addition of a small quantity of sulfates enhanced strength; but higher levels led to a decrease in strength. Gunay et al. [304] showed that the nucleation growth process of the C-S-H is modified as calcium sulfate is adsorbed on the C-S-H. The lower strength found here could be due to a reduced particle force between C-S-H as measured by Medala [305]. Sersale et al. [306] found that the mechanical resistance and amount of porosity varied with sulfate content. This study suggests that the sulfate can have a negative impact on the filling capacity of the C-S-H as already shown in the literature [281].

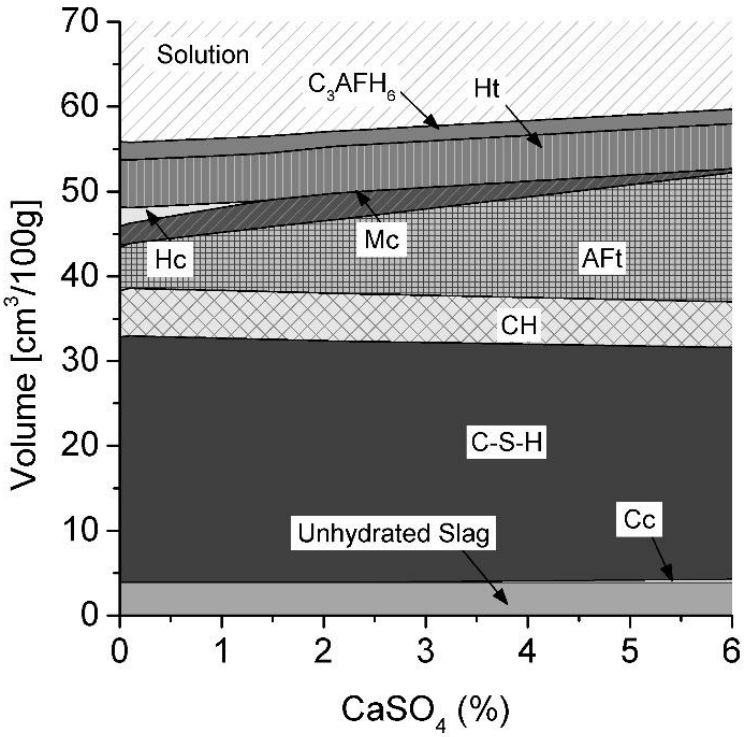

Figure 5-36 – Modelled phase assemblage of 40 % slag blends, highlighting the effect of sulfate content. It was assumed that all the clinker had reacted, and 70% of the slag had reacted. [Provided by Maciej Zajac]

5.5 Summary

1. Slag hydration was slower compared to that of cements. Still, after 180 days of curing, 40% slag blends achieved comparable strengths to that of a neat system.
2. The overall hydration kinetics of the clinker seemed unaffected by the presence of slag. However, the hydration of the individual clinker phases was affected; hydration of C_3S C_3A and C_4AF was accelerated and hydration of C_2S was retarded. Sulfates further exacerbated C_3S hydration.
3. Slag hydration kinetics were dependent on slag composition and loading. At 40% slag content, the alumina rich slag C was shown to be the more reactive than slag B, with the former having the higher CaO/SiO_2 ratio. The addition of sulfates had no effect on slag hydration, however its reactivity was dampened by increasing the slag content.
4. Slag addition affected C-S-H composition, reducing the Ca/Si ratio and increasing the Al/Si ratio. The extent of these changes was dependent upon slag

composition and loading. Sulfates further affected the composition such that the apparent Ca/Si of the C-S-H increased as calcium sulfates were adsorbed on its surface. The data further suggests that more water had been bound by the C-S-H phase in the slag composite systems.

5. Slag blended systems favoured the formation of AFm phases over ettringite, as the sulfate content was diluted, and aluminium from slag was shown to contribute to the formation of calcium aluminate hydrates. In the 40 % slag blends, Slag C favoured the formation of hemicarboaluminate over monocarboaluminate due to its higher aluminium content. At 70% slag content, monosulfate was observed after prolonged curing periods.
6. The composition of the slag also had an effect on the hydrotalcite-like phase seen in all blended systems, with the Mg/Al ratio differing between blends. More interestingly, the addition of extra sulfates resulted in an increase in the Mg/Al ratio of hydrotalcite as more alumina was consumed to form ettringite.
7. Modelling showed a decrease in paste volume with an increase in slag content. The addition of sulfates favoured the formation of ettringite, increasing the total solid volume.

Chapter 6

Impact of Slag Composition and Loading, Plus Additional Sulfate, on the Sulfate Resistance of Slag Composite Cements

6.1 Macroscopic and Microscopic Observations

6.1.1 Expansion

Figure 6-1 summarises the expansion of mortar prisms exposed to sulfates. From a very early age the neat system C_1 showed continual expansion, the rate of which increased after 48 weeks of exposure to sulfates. Of all the mortars exposed to sulfates, only the neat system showed macroscopic damage, with cracking occurring at the corners of the sample (appendix A.1). In contrast, all the slag blended systems showed very limited expansion during the testing period. Little difference was observed between blends C_140S_b and C_140S_c, despite the differing aluminium content of the slag. The presence of additional anhydrite in blend $C_140S_c\$$ did appear to improve sulfate resistance, reducing expansion. Blend C_170S_c proved to be the most resistant, showing the least expansion. Evidently, none of the mortars showed any signs of damage. The expansion measurements of the remaining samples is shown in appendix A.3.

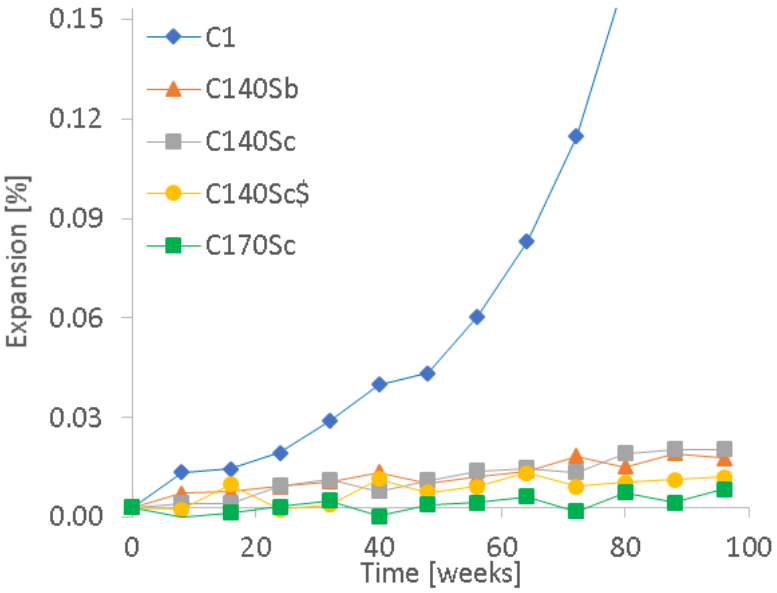

Figure 6-1 – Linear Expansion of Mortar Prisms exposed to 3 $g.L^{-1}$ of Na_2SO_4

Images of the paste samples can be found in appendix A.2. Their smaller size allowed for faster disintegration upon sulfate attack. The neat system showed damage after just 56 days of curing in a sulfate solution. The sample continuously deteriorated with the surface of C_1 samples effectively spalling. By 360 days of curing in sulfates, the neat sample had to be handled with care so as to prevent undesirable damage.

Much like the mortar prisms, all the slag pastes showed greater resistance. It took nearly 6 months to see any signs of damage in blend C_140S_c where cracks had formed on the faces of the cylinders, which gradually widened with time. No damage was seen along the length of the samples. Resistance of the 40 % slag blend was improved by either substituting slag C for B, with slag B being poorer in aluminium, or by adding sulfates. Resistance was also improved by increasing the slag content to 70 % by weight.

6.1.2 **SEM-BSE imaging**

SEM-BSE images of the surfaces of paste samples exposed to sulfates for 360 days (Figure 6-2 through Figure 6-6) provided further insight into any damage. The neat paste C_1 was the most prone to damage, with evidence of heavy cracking, increasing porosity. A layer of a calcium carbonate polymorph was observed just below the surface, at a depth of 100µm (Figure 6-7). There was no evidence of calcium hydroxide (CH), with it most likely either having leached or reacted with sulfates, to form ettringite or gypsum. Furthermore, the greylevel of the C-S-H phase was darkest at the very surface and progressively grew brighter deeper into the sample.

Generally, the blended systems showed greater resistance against sulfate attack. However, despite there being no evidence of expansion (Figure 6-1), BSE imaging showed evidence of deterioration. Of all the slag blended systems, blend C_140S_b appeared to have the greatest increase in porosity, at greater depths, while C_140S_c showed cracking due to the attack. The addition of sulfate, in blend C_140S_c\$, suppressed any cracking affirming the potential benefit of additional sulfate [11, 13, 16, 188]. Like in C_1, all the slag cement pastes were depleted in calcium. Only Blend C_140S_c\$ showed

minimal CH clusters at a depth greater than 500µm. Many samples showed surface deposits of calcium carbonate (Figure 6-8) [121].

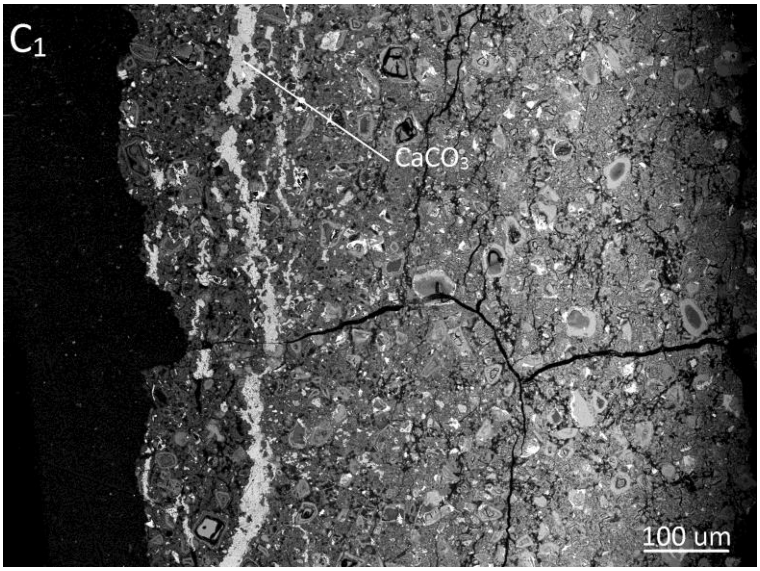

Figure 6-2 – SEM-BSE observations of Paste C_1, Exposed for 360 Days

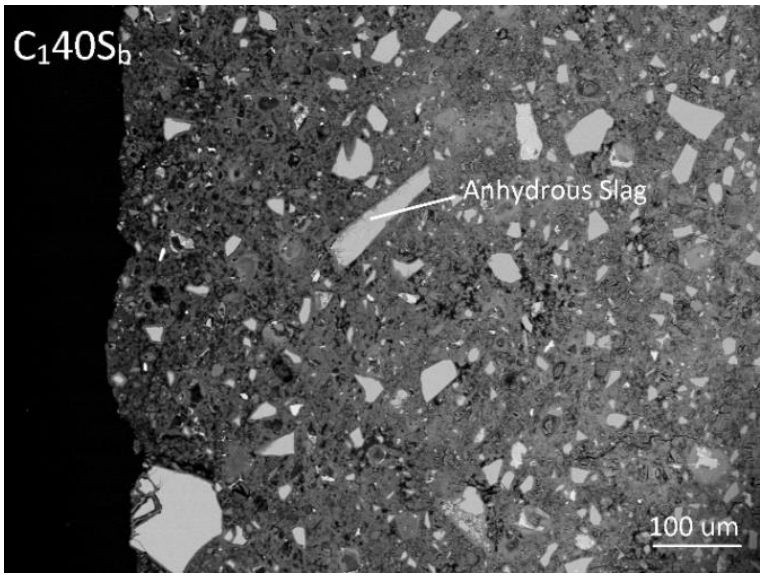

Figure 6-3 – SEM-BSE observations of Paste C_140S_b, Exposed for 360 Days

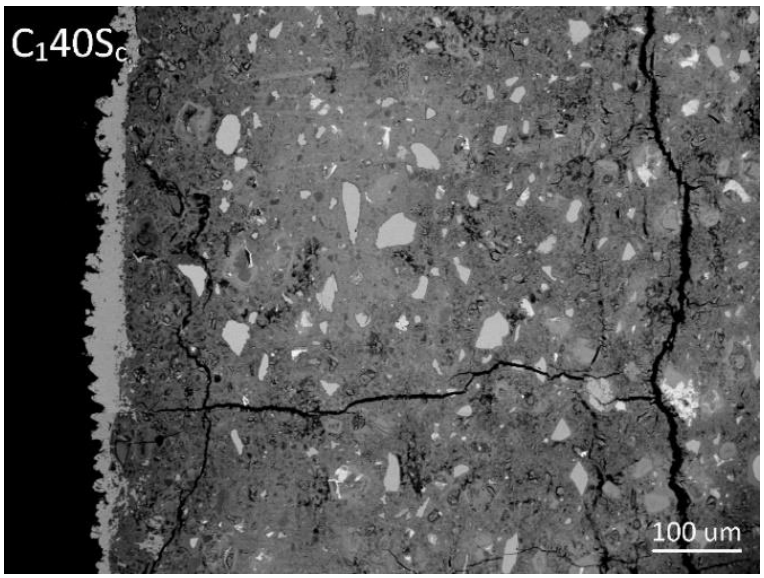

Figure 6-4 – SEM-BSE observations of Paste $C_1 40 S_c$, Exposed for 360 Days

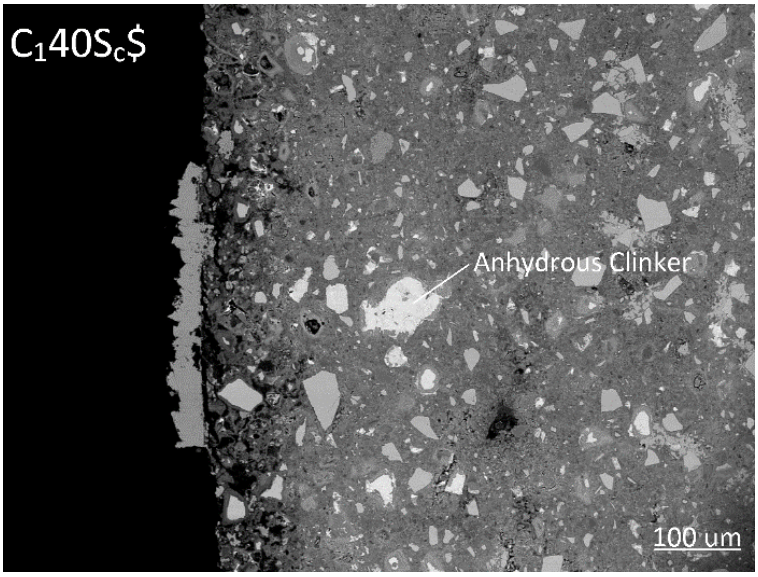

Figure 6-5 – SEM-BSE observations of Paste $C_1 40 S_c$\$, Exposed for 360 Days

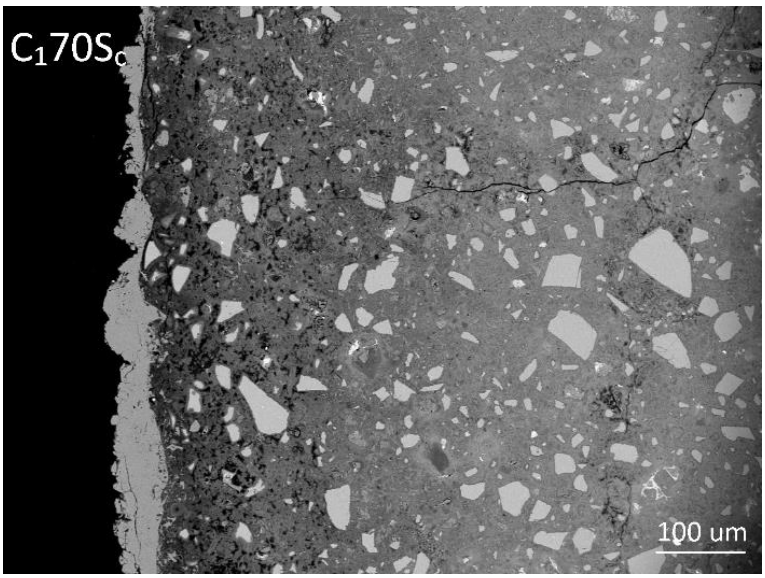

Figure 6-6 – SEM-BSE observations of Paste $C_1 70 S_c$, Exposed for 360 Days

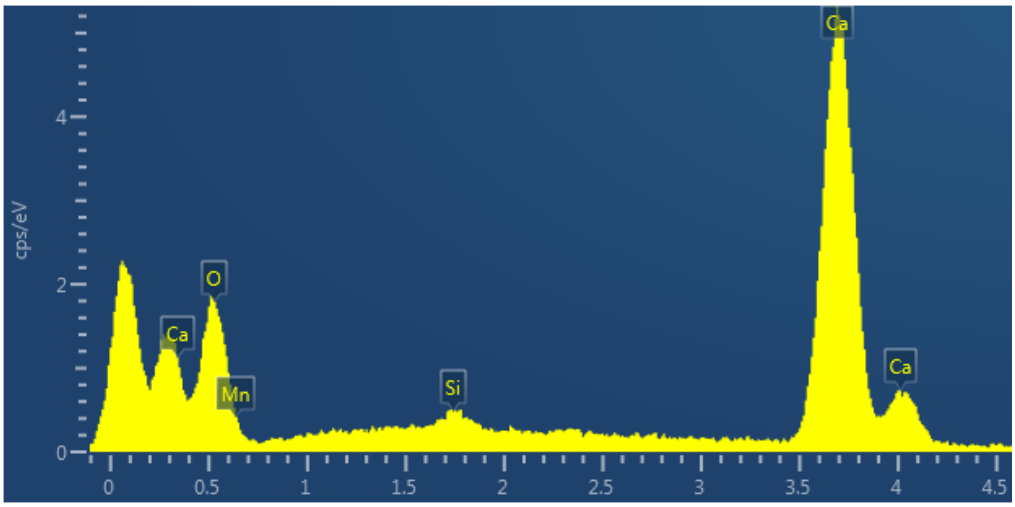

Figure 6-7 – EDX spectra of $CaCO_3$ Vein in C_1

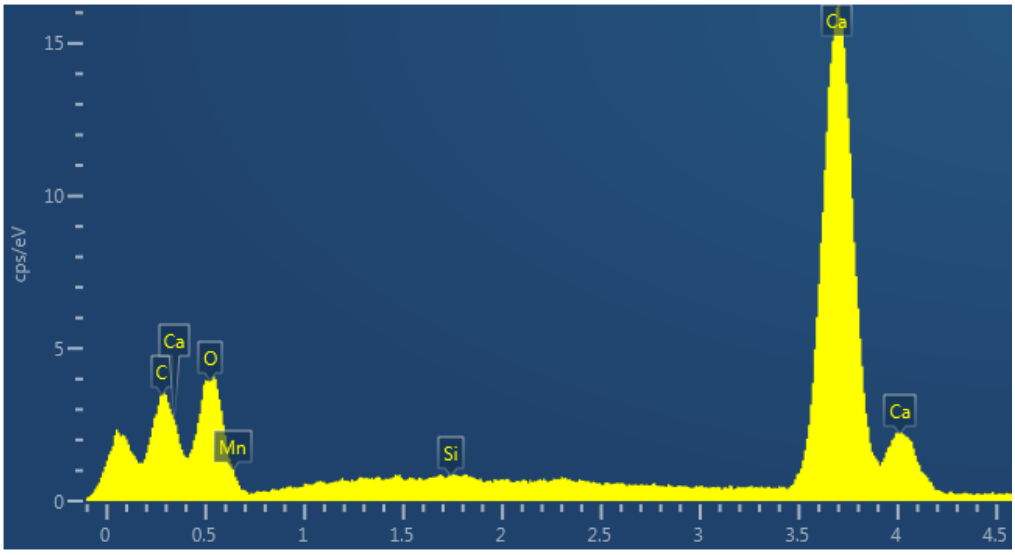

Figure 6-8 – EDX spectra of $CaCO_3$ Deposit in C_140S_c

6.2 Hydration Kinetics

Slags are known to be activated by sulfates. However, their hydration remains slow in the presence of sulfates alone and an additional activator is often used. As such, we can suppose that slag hydration may be exacerbated as sulfates penetrate through the matrix. As slags are inherently richer in aluminium compared to cement, this may have serious consequences on the resistance of slag composite cements subjected to sulfate attack. The impact of external sulfates on slag hydration was checked for blend C_140S_c cured for 360 days in a sulfate solution. As seen in Figure 6-9, slag hydration was in fact not exacerbated at later ages upon exposure to sulfates in the degraded zone, much like

in blend $C_1 40 S_c \$$. This suggests that clinker has the greater potential in activating slags. Furthermore, in the degraded zone, the pH of the pore solution would have dropped, due to calcium leaching, potentially slowing down slag hydration. With respect to the clinker, 80 % or more of it had reacted by the time samples were transferred into a sulfate bath. As such, the impact of sulfates on their hydration would be negligible.

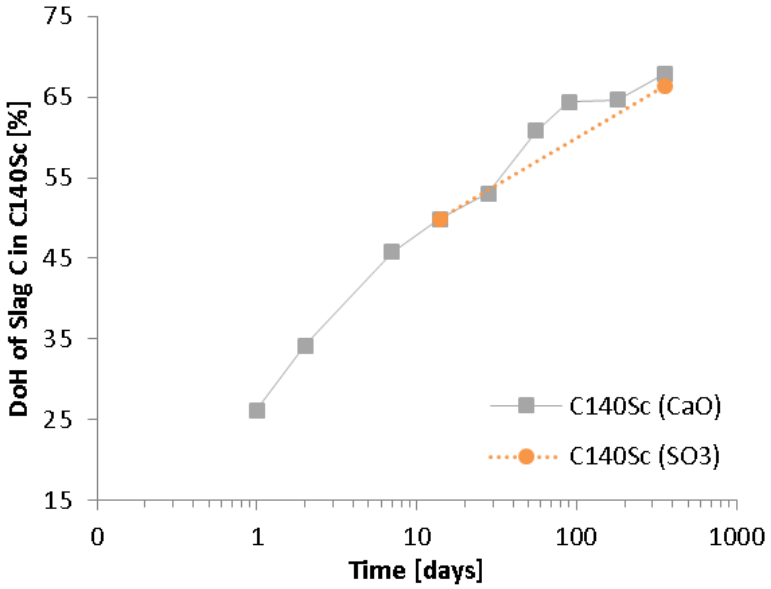

Figure 6-9 – Degree of Hydration of Slag C in Blend $C_1 40 S_c$ Curing in Lime or a Sulfate solution (in the Degraded Zone)

6.3 Sulfate Profile

Figure 6-10 through Figure 6-14 show the evolution of the sulfate profile with time and the profiles for all the investigated systems obtained by the end of the testing period are compared against one another in Figure 6-15. The sulfate profiles were taken as the average of 144 points measured by SEM-EDX analysis. The data was then treated to remove any points associated with porosity, anhydrous material and calcium hydroxide.

In the neat system, the very surface of the sample was gradually enriched in sulfates for periods up to 90 days. Beyond 90 days of exposure, however, the greatest sulfate content was no longer observed at the very edge of the sample but rather at a depth of 0.5 mm and 1 mm, after 180 and 360 days of curing in a sulfate solution respectively.

With time, the sulfate content actually decreased at the surface, and the maximum sulfate content increased at greater depths.

Similar evolutions were observed in the blended systems such that the surface was the richest initially. The sulfate content was highest near the surface up to 90 days of curing for blends C_140S_b and C_140S_c. Prolonging the exposure time led to a depletion of bound sulfates at the surface and more had penetrated at greater depths. For blend C_140S_c\$, the sulfate content was highest near the surface after only 56 days, rather than 90. This was also true for blend C_170S_c; the surface of the blend was particularly depleted of sulfates by 90 days.

By the end of the testing period, all samples showed slight sulfate depletion near the surface, rising to a maximum at depths of 0.5 mm, for blends C_140S_c, C_140S_c\$ and C_170S_c, and 1 mm for blends C_1 and C_140S_b. As the slag content increased, the total amount of bound sulfates decreased. The sulfate content then gradually fell back to background levels to a depth between 2 and 3.5 mm, with the CEM I system showing the greatest penetration depth.

These profiles are typical of samples exposed for extended periods to sulfate attack [14, 107, 124, 200]. Stroh et al. [200] measured the profiles on concretes buried in a sulfate rich soil for 19 years. A concrete with only cement as a binder showed no sulfates in the first outer 1.5 mm, with levels rising and then persisting to a depth over 15 mm from the surface. A concrete prepared with cement and 80% slag however showed only a 4 mm thick band of sulfates, with no sulfates in the first 1 mm.

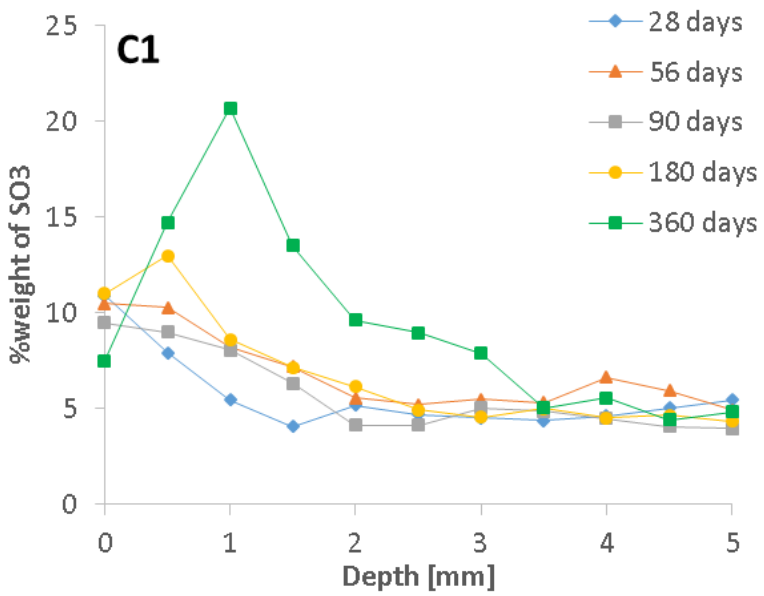

Figure 6-10 – Evolution of the Sulfate Profile with Time for C_1

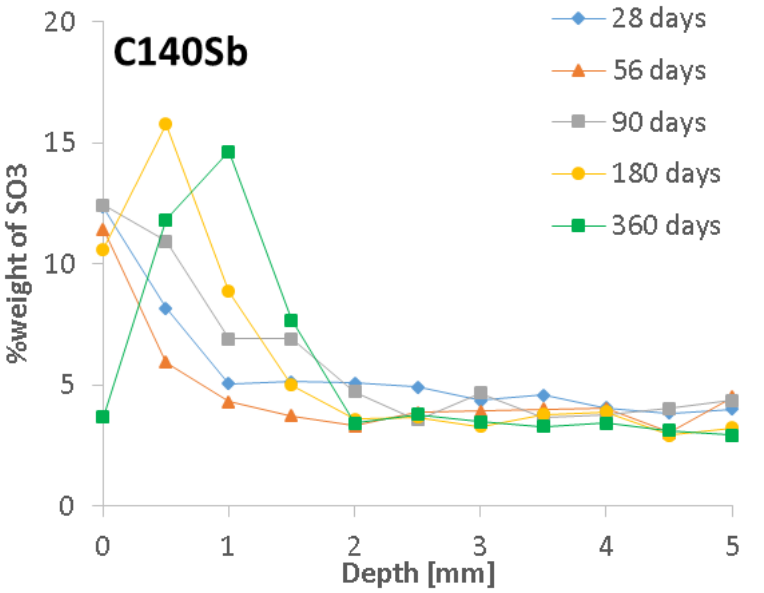

Figure 6-11 – Evolution of the Sulfate Profile with Time for C_140S_b

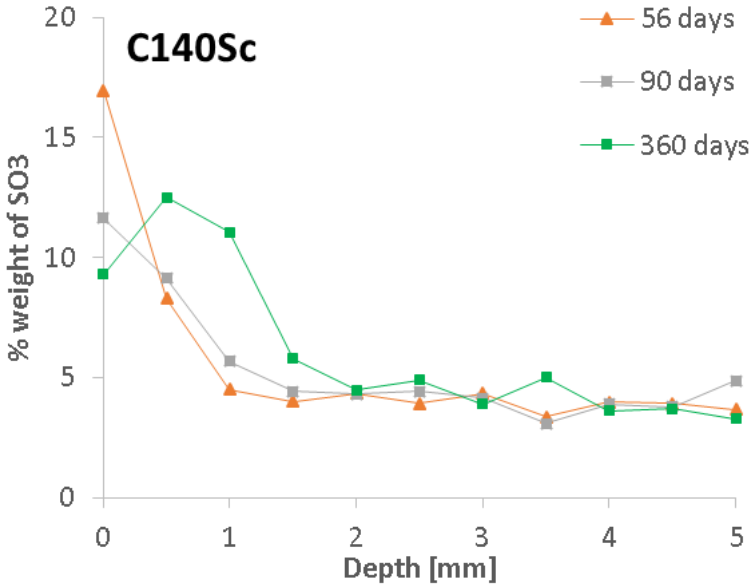

Figure 6-12 – Evolution of the Sulfate Profile with Time for $C_1 40 S_c$

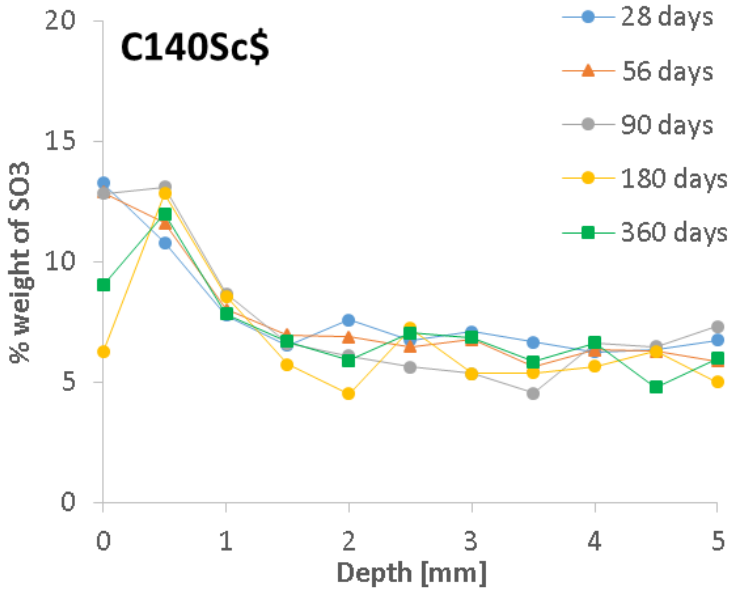

Figure 6-13 – Evolution of the Sulfate Profile with Time for $C_1 40 S_c$\$

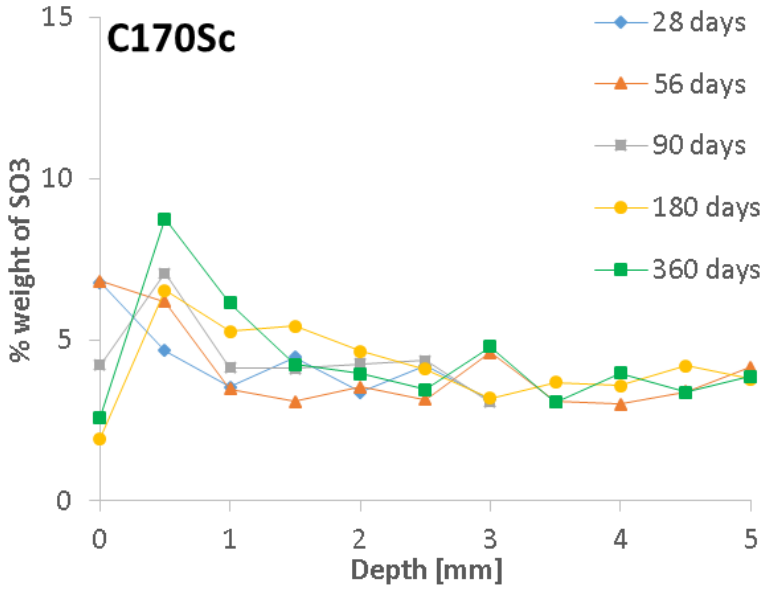

Figure 6-14 – Evolution of the Sulfate Profile with Time for $C_1 70S_c$

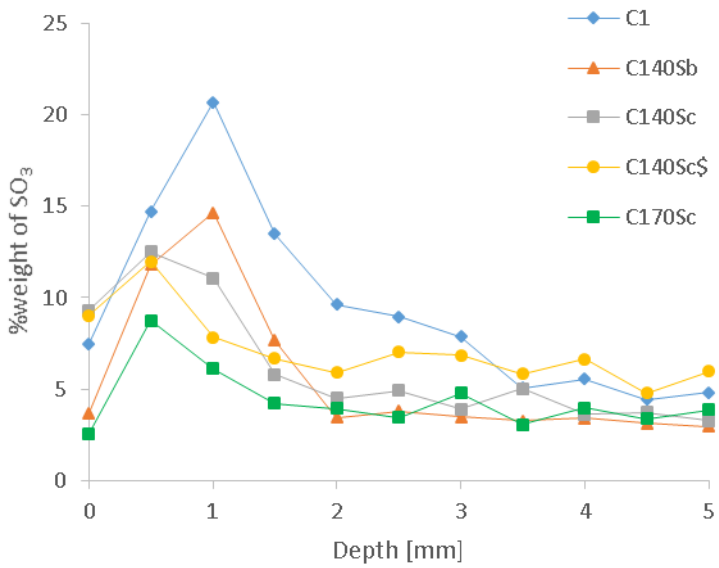

Figure 6-15 – Sulfate Profile Measured on Paste Samples, After 360 days of Curing Exposed to a Sulfate Solution

6.4 Hydrates

6.4.1 C-S-H and Calcium Hydroxide

Figure 6-16 illustrates the gradual leaching of calcium hydroxide from within the outer 1 mm of the pastes exposed to Na_2SO_4, it having either leached out of the samples or having reacted with sulfates to produce gypsum, or ultimately ettringite. Depletion was initially very fast, i.e. near 50% of the portlandite had leached (or reacted) after just 2

weeks of exposure for all systems, and more gradually thereafter. Despite this, up to 90 days of curing in sulfates, the neat system was the richest in calcium hydroxide, after which all systems had comparable levels of portlandite.

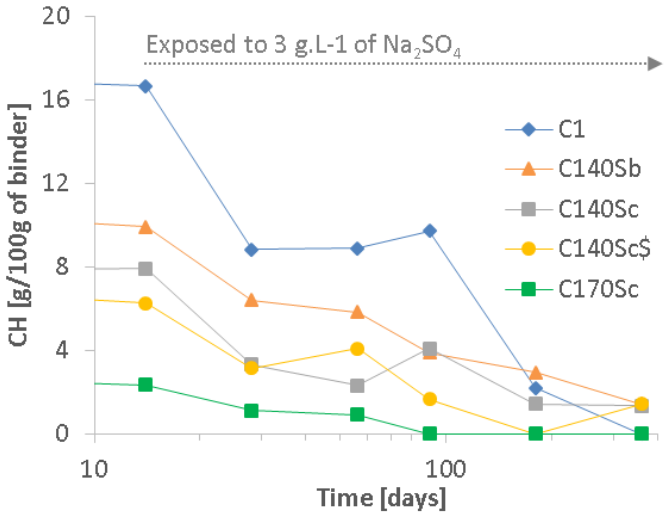

Figure 6-16 – Leaching of Calcium Hydroxide, Measured on Pastes Exposed to a Sulfate Solution, Measured From the Outer 1 mm of Pastes Exposed to Sulfates

Figure 6-17 through Figure 6-21 illustrate the changes in composition of the C-S-H phases with time as a function of depth for each sample. The Ca/Si ratio and Al/Si ratio were measured from Al/Ca against Si/Ca atomic plots as detailed in chapter 5. The Al/Si ratios were determined from the slope of the line originating from the origin drawn through the point with the lowest measured Al/Ca to best avoid intermixing with other phases. The Ca/Si was taken as the point along that same line having the highest Si/Ca ratio. The full set of data can be found in appendix A.4.

The neat system showed almost no calcium leaching after curing in the presence of sulfates for 180 days. Decalcification had only occurred beyond 6 months of curing, and C-S-H was affected to a depth of 1.5 mm [126, 127]. Similarly, no changes were seen in the Al/Si ratio of the C-S-H initially, and more aluminium was bound by the phase by the end of the testing period.

All the slag blends were more prone to decalcification; all showed some calcium leaching from C-S-H by 28 or 56 days of curing of less. However, decalcification was only limited to the first 0.5 mm of the sample. Similarly, the Al/Si of C-S-H increased in conjunction with its decrease in Ca/Si. This effect was greatest in blends using the alumina rich slag C.

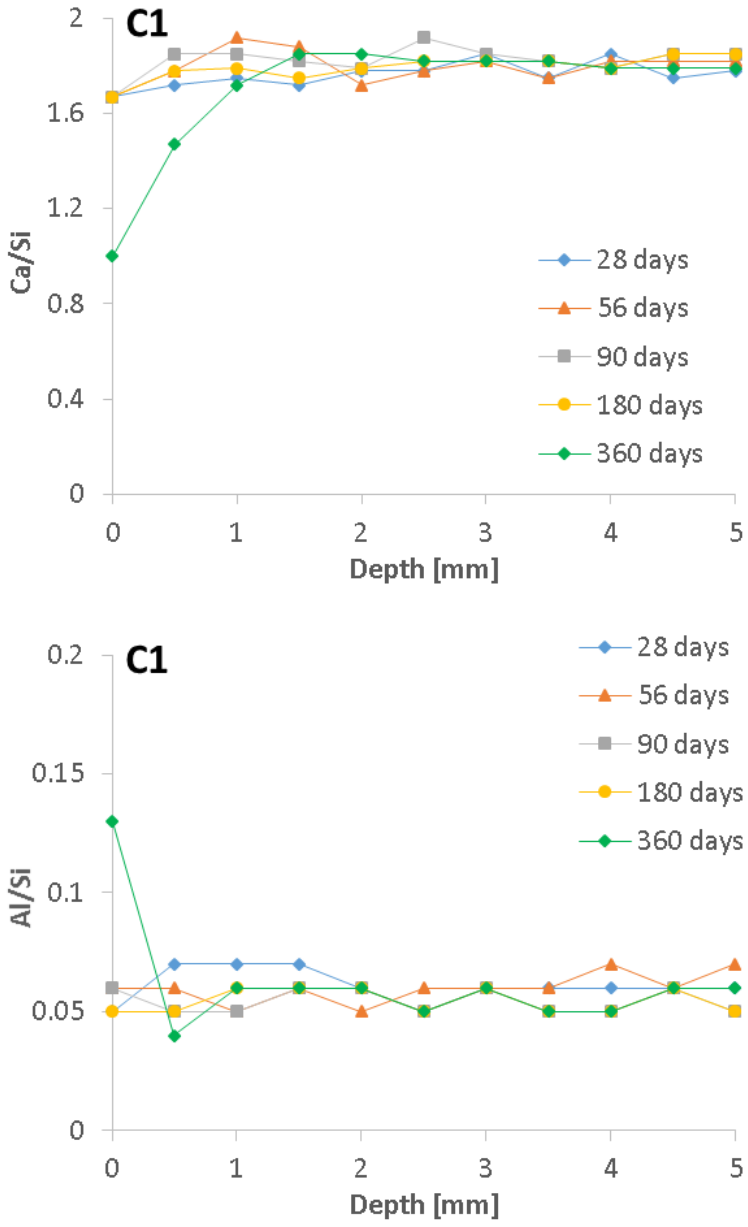

Figure 6-17 – Changes in Ca/Si and Al/Si of the C-S-H Phase With Time, For Pastes C_1 Exposed to a Sulfate Solution (± 0.05)

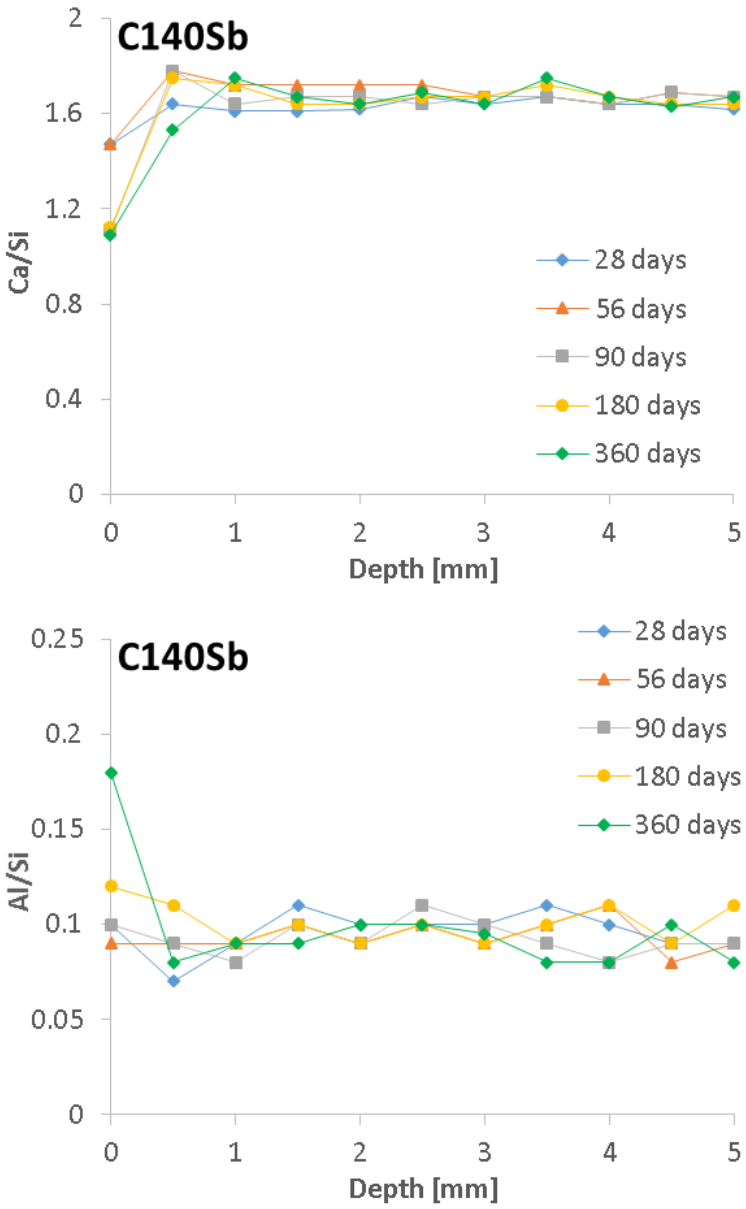

Figure 6-18 – Changes in Ca/Si and Al/Si of the C-S-H Phase With Time, For Pastes C_140S_b Exposed to a Sulfate Solution (± 0.05)

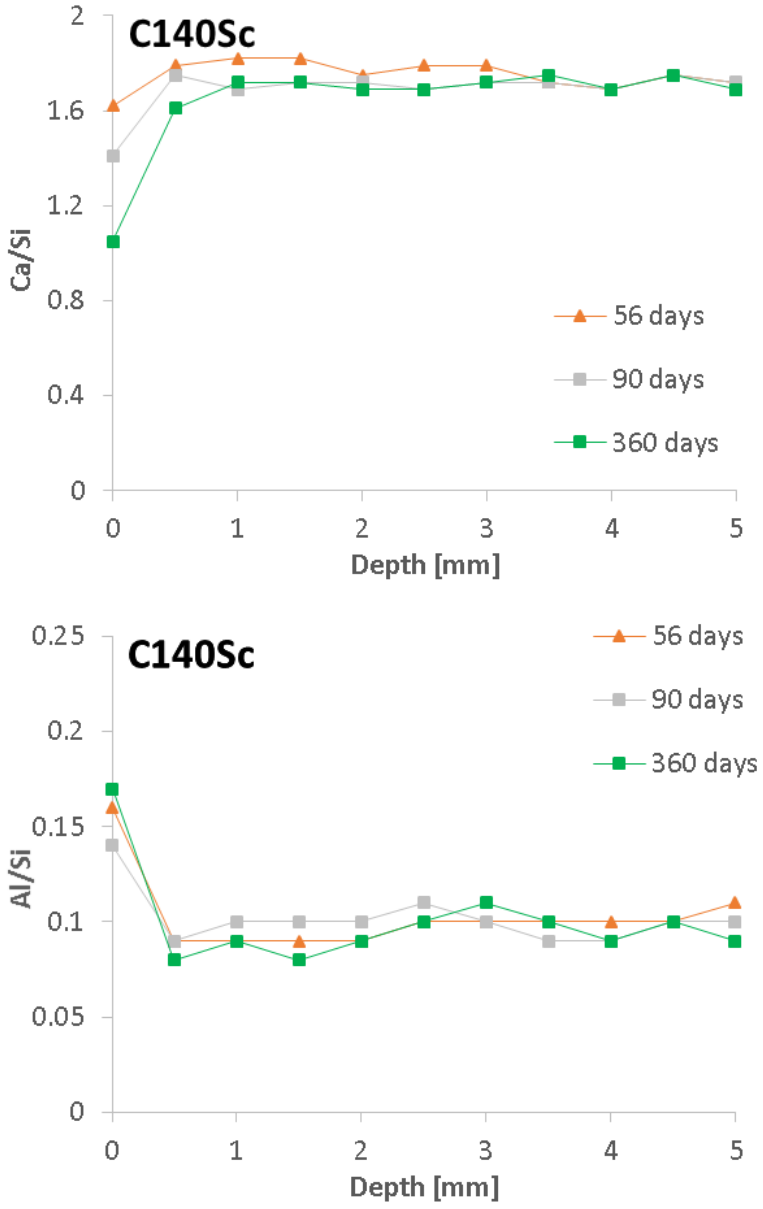

Figure 6-19– Changes in Ca/Si and Al/Si of the C-S-H Phase With Time, For Pastes C_140S_c Exposed to a Sulfate Solution (± 0.05)

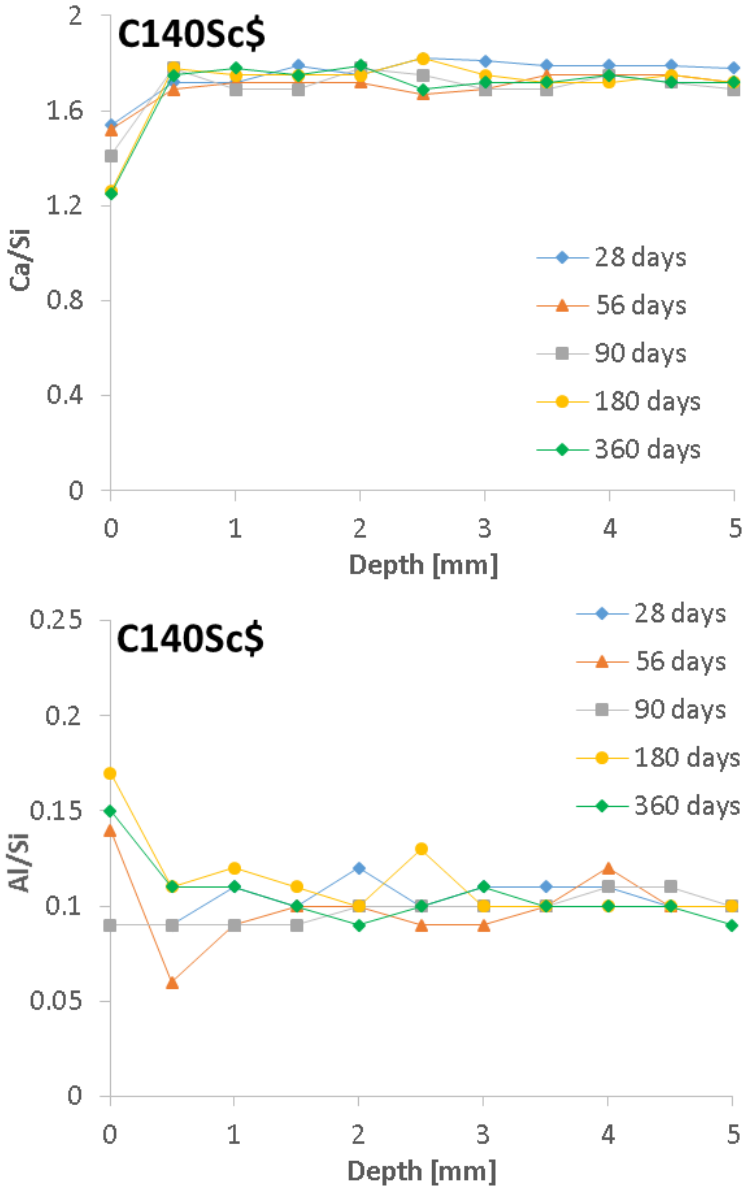

Figure 6-20 – Changes in Ca/Si and Al/Si of the C-S-H Phase With Time, For Pastes $C_1 40 S_c$ Exposed to a Sulfate Solution (± 0.05)

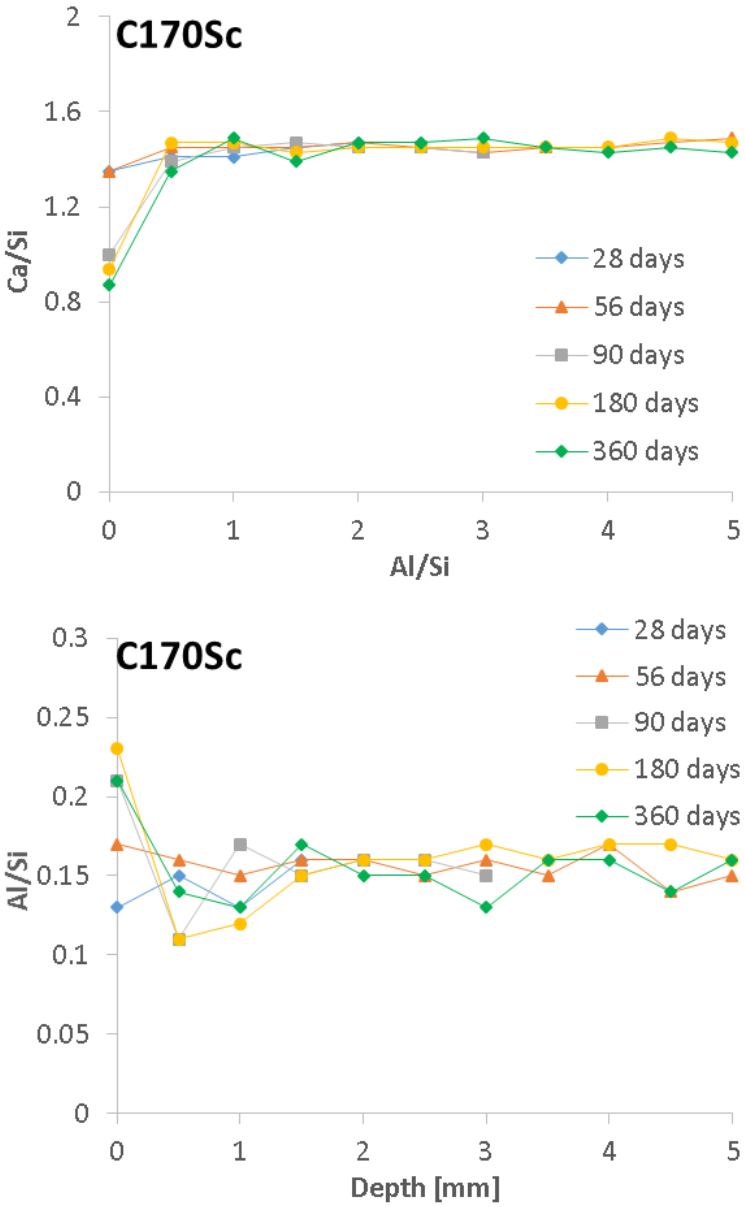

Figure 6-21 – Changes in Ca/Si and Al/Si of the C-S-H Phase With Time, For Pastes C_170S_c Exposed to a Sulfate Solution (± 0.05)

By the end of the testing period (Figure 6-22), all the samples showed evidence of C-S-H decalcification. Proportionally, this effect was greatest in the neat system despite the late onset of calcium release. The deeper penetration was most likely related to the advanced deterioration the samples exhibited. In all the slag blended systems, decalcification had only occurred to a depth of 0.5 mm.

More aluminium was bound within the C-S-H in slag cement blends, where the Ca/Si was lower [29, 88, 290]. There was no dealumination of the C-S-H, and rather more

aluminium was bound by C-S-H. This was a direct response of the lowered Ca/Si in the decalcified C-S-H, allowing for more aluminium to be bound by the phase [307].

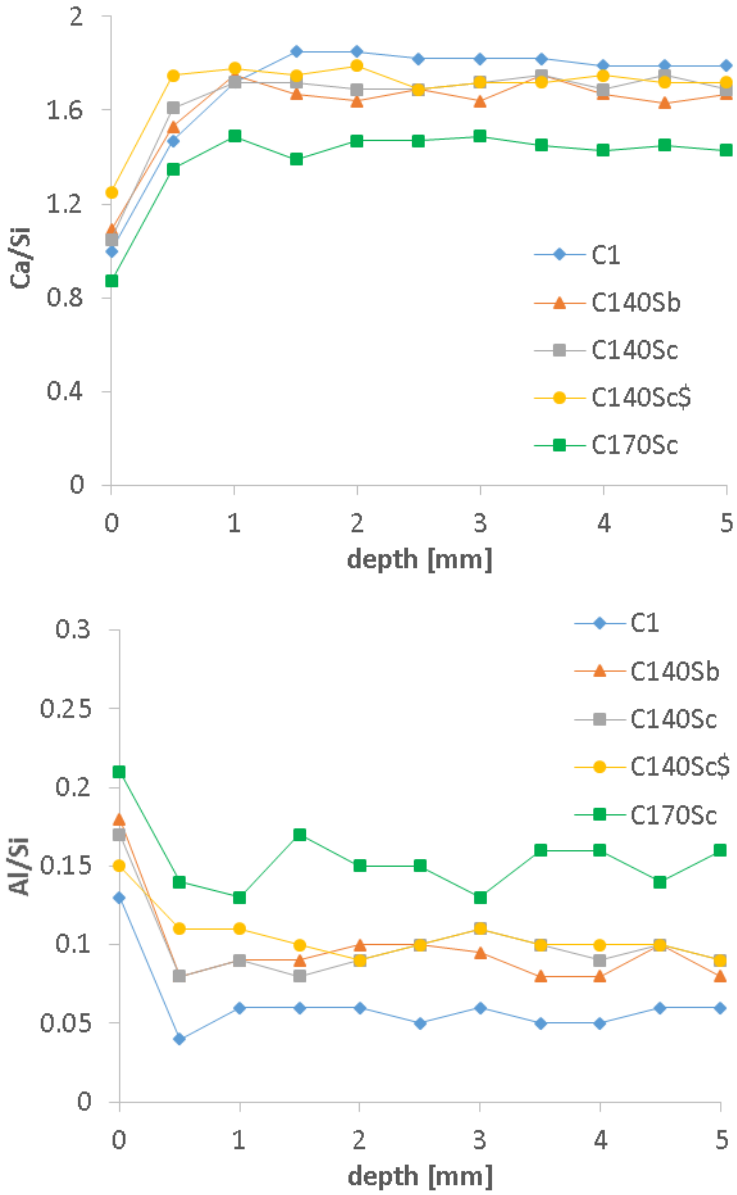

Figure 6-22 – Changes in Ca/Si and Al/Si of the C-S-H Phase Measured on all Pastes Exposed to a Sulfate Solution for 360 days (± 0.05)

6.4.2 Ettringite – AFm distribution – Gypsum

Figure 6-23 compares the evolution of the ettringite and AFm phases in samples cured in a sulfate solution (in blue). Before exposure all samples showed the formation of ettringite with carbonate AFm phases only (in grey), present in all samples after 14 days of hydration. Upon sulfate exposure, the ettringite content increased in all systems.

The reflections of the phase was greatest in the neat system, and decreased with slag loading, a plausible reason of the improved resistance of slag cements to sulfate attack. At 40 % replacement, the reflections were greatest in blends using slag C, richest in alumina. In response, the carbonate AFm were consumed; most of it had been consumed after just 90 days of curing. Only in blend C_140S_c did carbonate AFm phases persist beyond 90 days of curing in sulfates. Ettringite was the only sulfated aluminate hydrate present in the neat system C_1, whereas monosulfate had also precipitated in all the slag blended systems. More monosulfate had precipitated as the overall Al_2O_3 content of a blend increased. The addition of sulfates had no effect on the formation of monosulfate at later stages of attack in blend C_140S_c\$.

Hydrotalcite was still clearly evident in all the slag blended systems, with the blends prepared with the magnesium-rich slag C showing more intense reflections. The strongest reflections were seen at a higher slag loading, in blend C_170S_c.

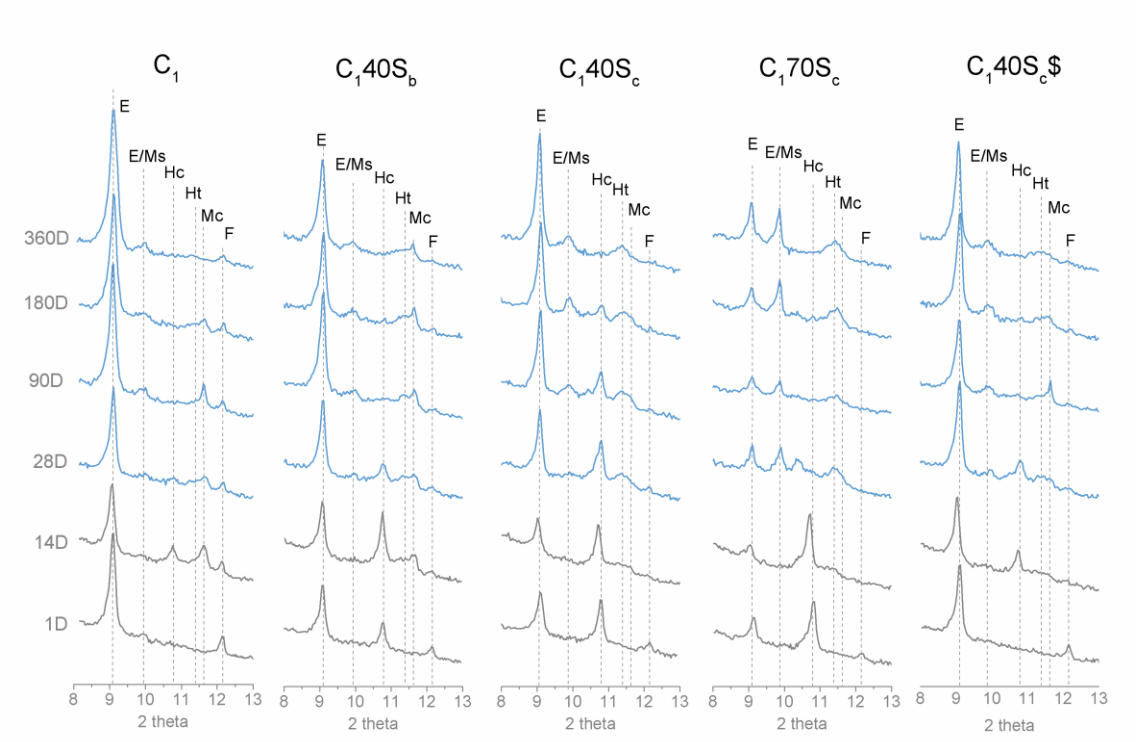

Figure 6-23 – XRD Tracings of the Outer 1 mm of Pastes Cured in a Na_2SO_4 Solution. The Grey Tracings are Those Obtained on Samples Before Exposure to Sulfates (E - Ettringite, Ms - monosulfate, Hc - Hemicarboaluminate, Mc - Monocarboaluminate, Ht - Hydrotalcite)

EDX analysis provided an even greater insight on how the sulfates were bound to cement hydrates. S/Ca and Al/Ca plots were obtained for all systems, from the surface of the samples down to a depth of 5 mm, in increments of 0.5 mm. The data set can be found in appendix A.5 to a depth of 3 mm (background levels). Some of these are plotted in Figure 6-24 through Figure 6-28, focusing on the surface of the samples, at the depth where the greatest amount of sulfate was bound (Figure 6-15), and at a depth of 5 mm.

At the surface of the investigated systems, no clear trend indicative of the presence of ettringite or monosulfate phases was noticeable. Sulfates were, however, still present in blends C_1, C_140S_c and C_140S_c\$. In contrast, blends C_140S_b and C_170S_c looked particularly depleted in sulfates.

Moving on to the point where the sulfate content was highest (Figure 6-15), the neat system, C_1, showed ettringite and gypsum intermixed with C-S-H. This was also true for blend C_140S_b. In blends C_140S_c and C_140S_c\$, both ettringite and monosulfate were intermixed with C-S-H and no gypsum was observed. In Blend C_170S_c, only monosulfate appeared to be intermixed with C-S-H.

Deeper within the samples, where sulfate levels reached background levels, C-S-H was intermixed with both ettringite and AFm phases in blend C_1. In all slag blend systems, AFm phases were much more prevalent, most likely a combination of hemicarboaluminate, monocarboaluminate and monosulfate (Figure 6-23). This can be checked against XRD tracings of the pastes immersed in limewater (Figure 5-25).

In all cases, a shift in the points to higher Al/Ca was observed near the surface caused by the leaching of calcium bound to the C-S-H phase [132].

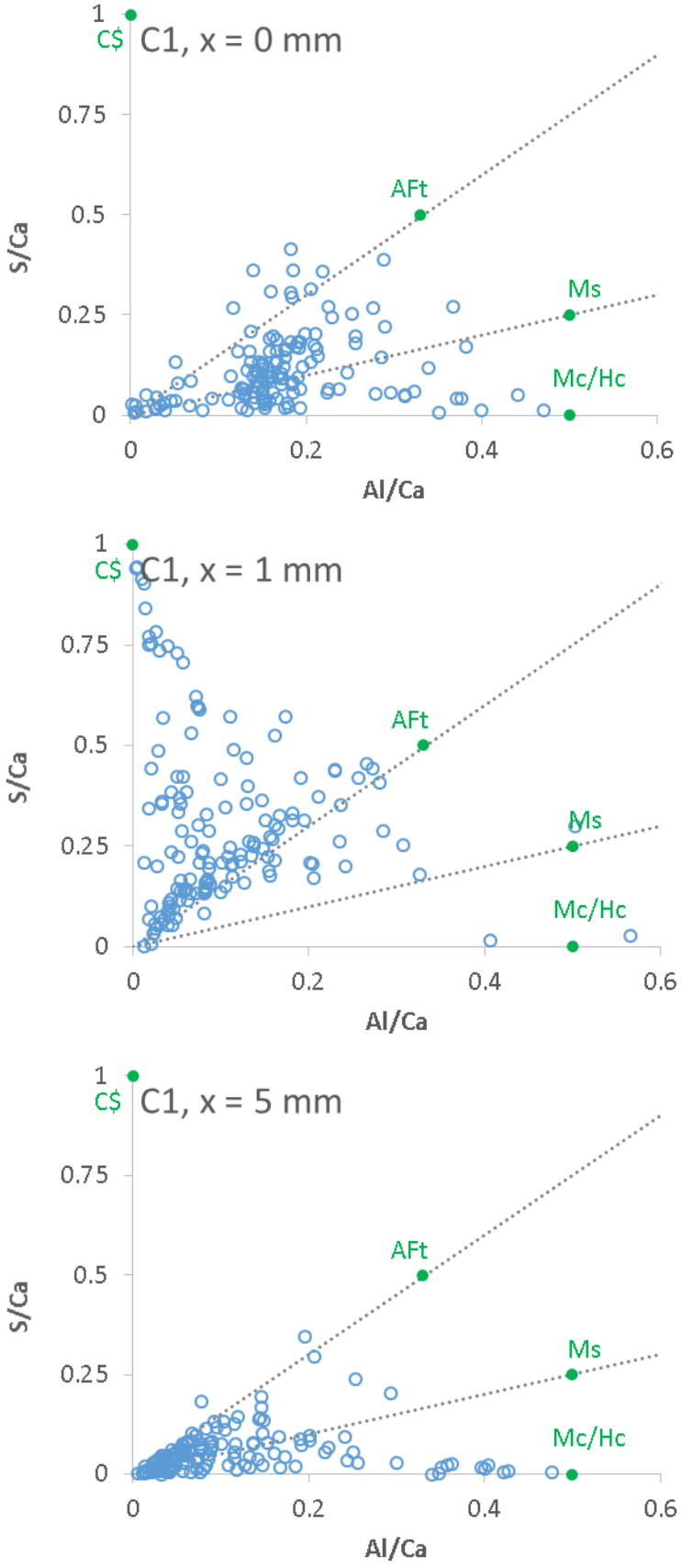

Figure 6-24 – Variations in S/Ca v Al/Ca as a Function of Depth for C_1 Exposed to a Sulfate Solution, after 360 Days

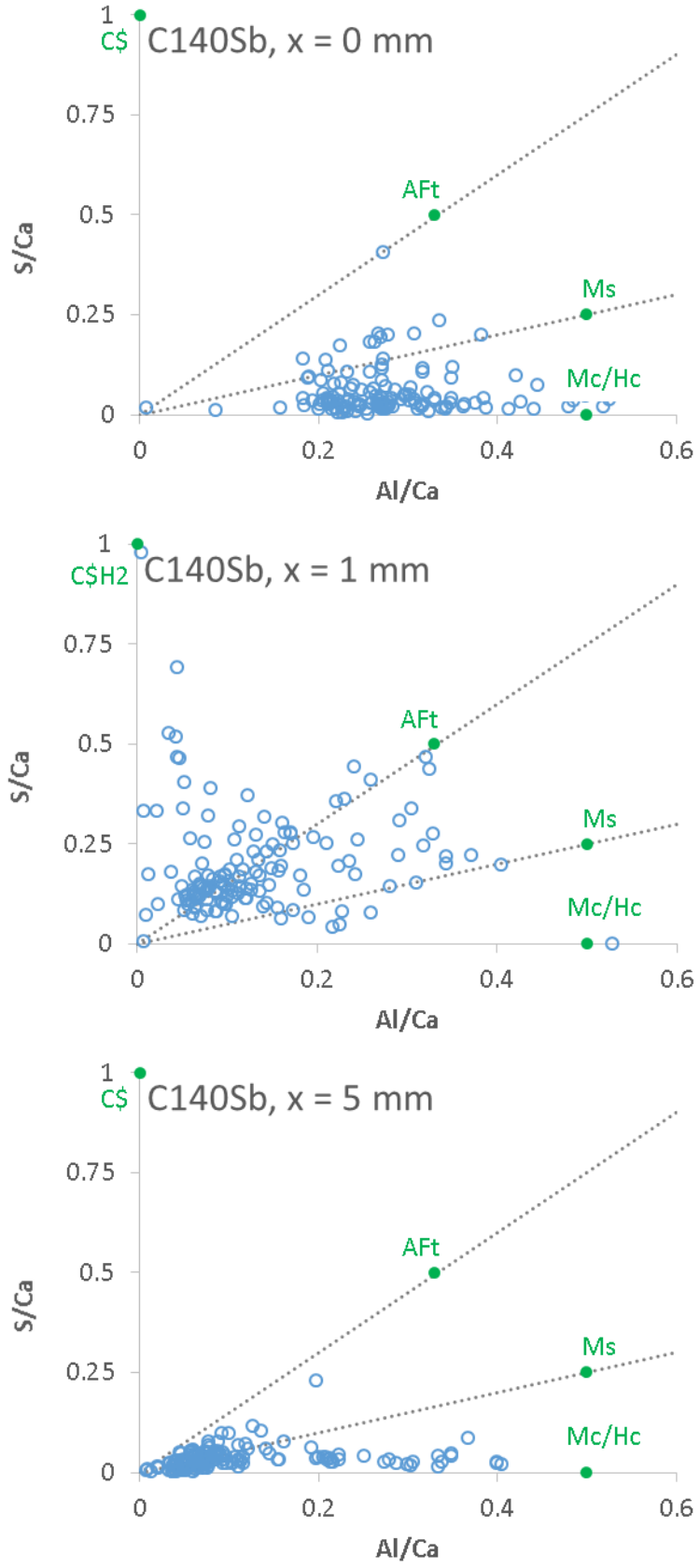

Figure 6-25 – Variations in S/Ca v Al/Ca as a Function of Depth for $C_1 40S_b$ Exposed to a Sulfate Solution, after 360 Days

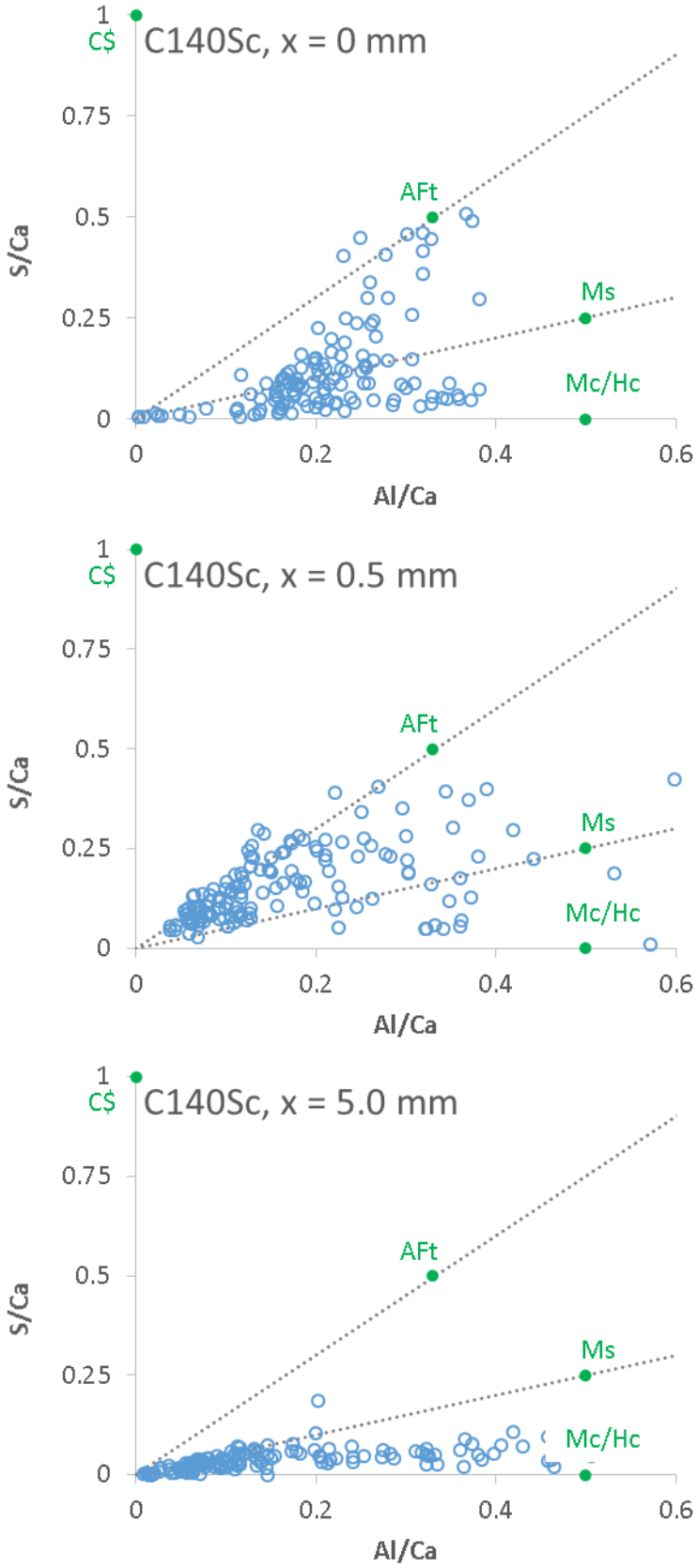

Figure 6-26 – Variations in S/Ca v Al/Ca as a Function of Depth for $C_1 40S_c$ Exposed to a Sulfate Solution, after 360 Days

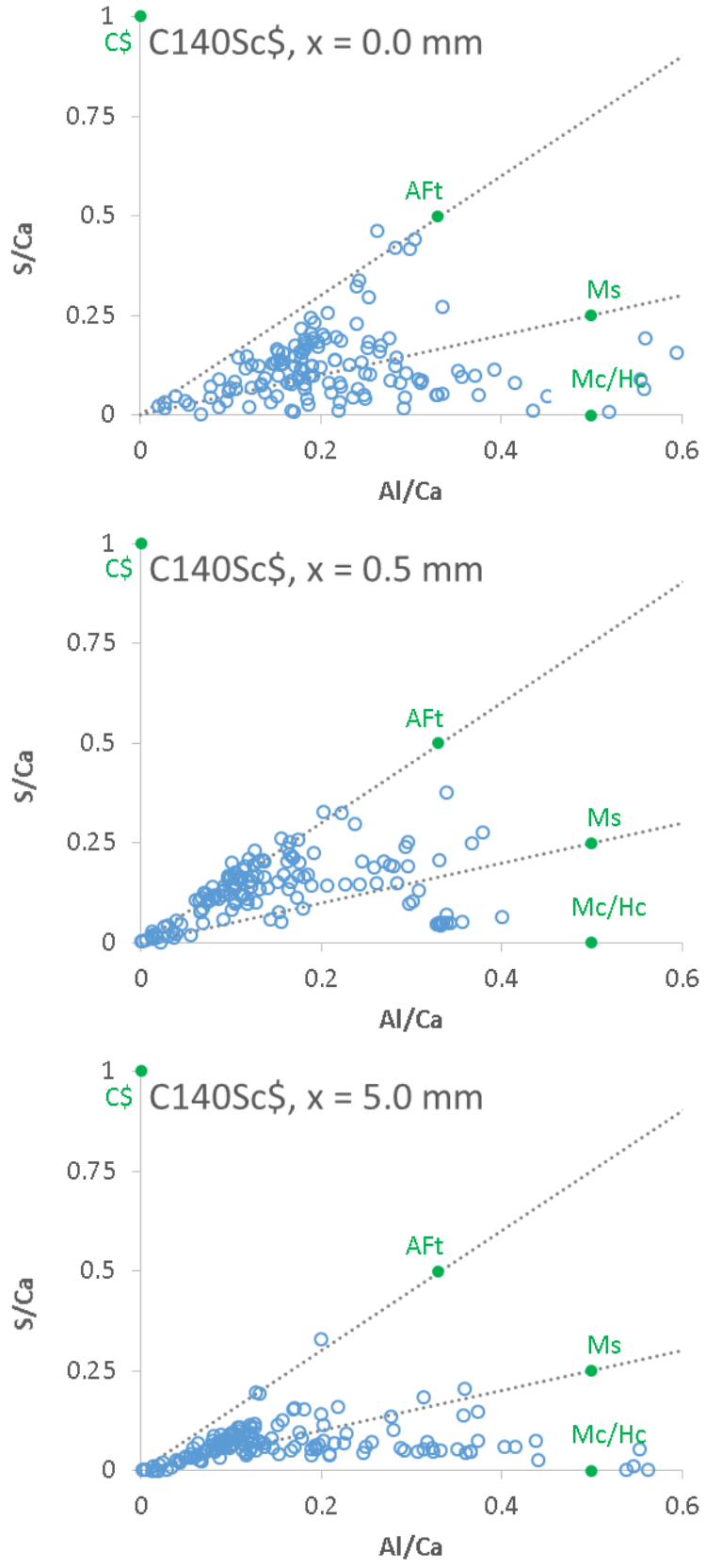

Figure 6-27 – Variations in S/Ca v Al/Ca as a Function of Depth for $C_1 40 S_c$\$ Exposed to a Sulfate Solution, after 360 Days

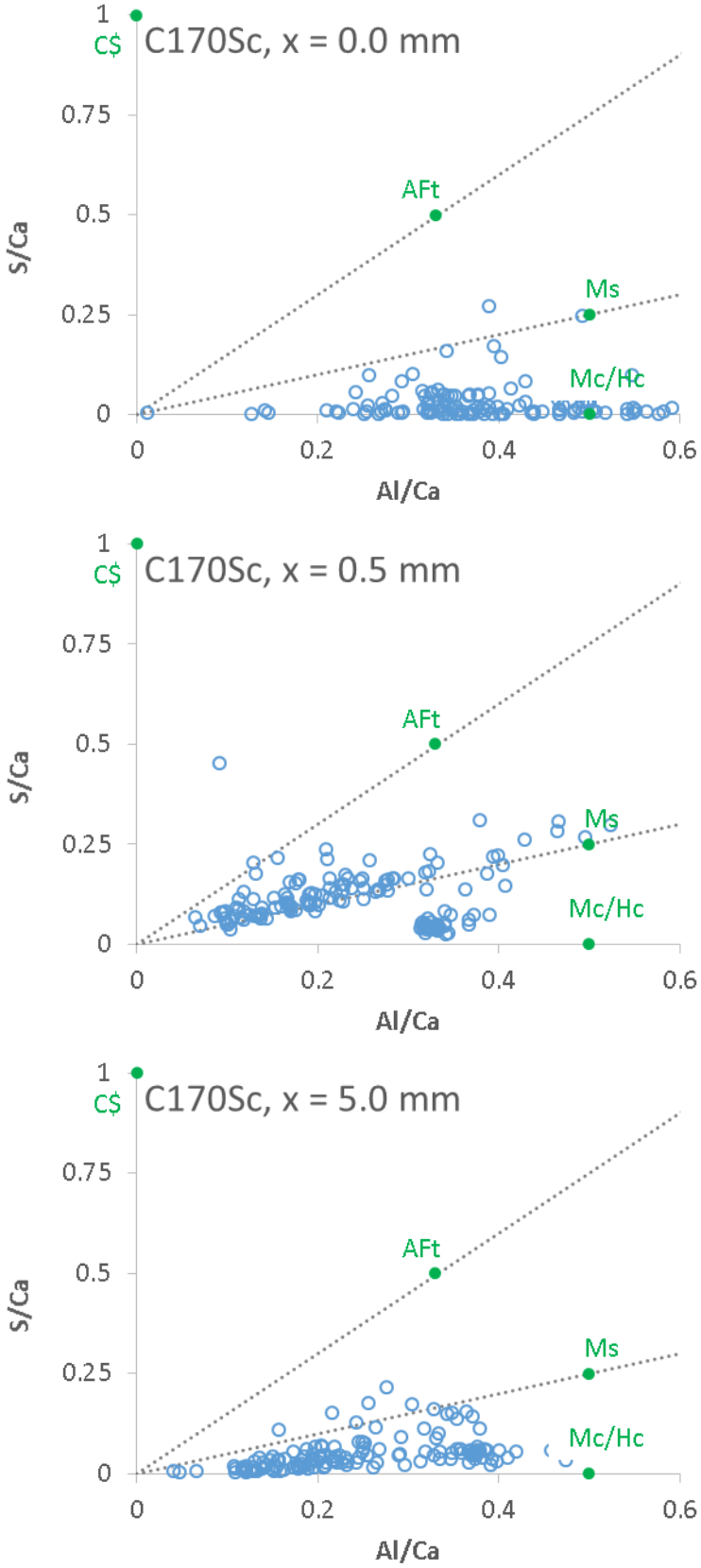

Figure 6-28 – Variations in S/Ca v Al/Ca as a Function of Depth for C_170S_c Exposed to a Sulfate Solution, after 360 Days

Figure 6-29 shows the evolution of ettringite in the pastes exposed to a sulfate solution. All samples showed an increase in ettringite content with time, yet it was the neat C_1 system which showed both the highest ettringite levels and the greatest increase in ettringite content. As cement was replaced with slag, less ettringite precipitated. At 40% replacement, the use of slag C yielded slightly more ettringite compared to slag B; at just over 23% by weight, for blends C_140S_c and C_140S_c\$. Very little ettringite had precipitated in blend C_170S_c. It is interesting to note the kinetics of ettringite precipitation. Most of the ettringite had formed within 3 months of exposure for all systems, after which evolution appeared to be stagnating. Of all the slag blended systems, only blend C_140S_c showed an appreciable amount of ettringite formation, owing to the more carbonate AFm phases being present at later ages. The lower ettringite content in the blended systems may very well be a factor in improved resistance of the slag blends.

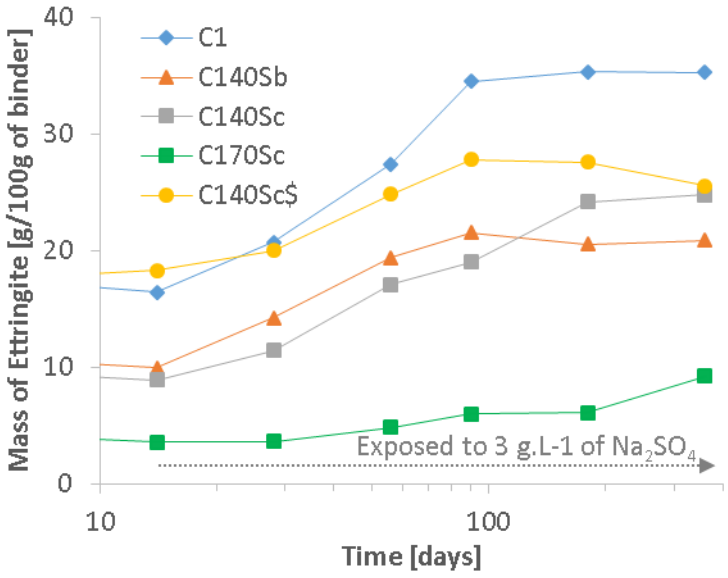

Figure 6-29 – Ettringite Evolution within the outer 1mm (± 2%) in all Pastes Exposed to a Sulfate Solution

6.4.3 Hydrotalcite

Figure 6-30 through Figure 6-33 highlight the changes in composition of the hydrotalcite phase upon exposure to sulfates for 360 days, comparing measurements taken near the edge of the sample (in orange) and at background levels (in blue). At background levels, the Mg/Al ratios varied from 1.78 to 2.11 depending on the slag blend;

Ben Haha et al. [68, 78] measured Mg/Al as low as 1.3 in alkali activated systems where the Mg/Al of the slag was low.

Changes in the Mg/Al ratios were minimal upon exposure to the sulfate solution. This indicates that the aluminium bound to the hydrotalcite was not readily available to react with sulfates [121, 187].

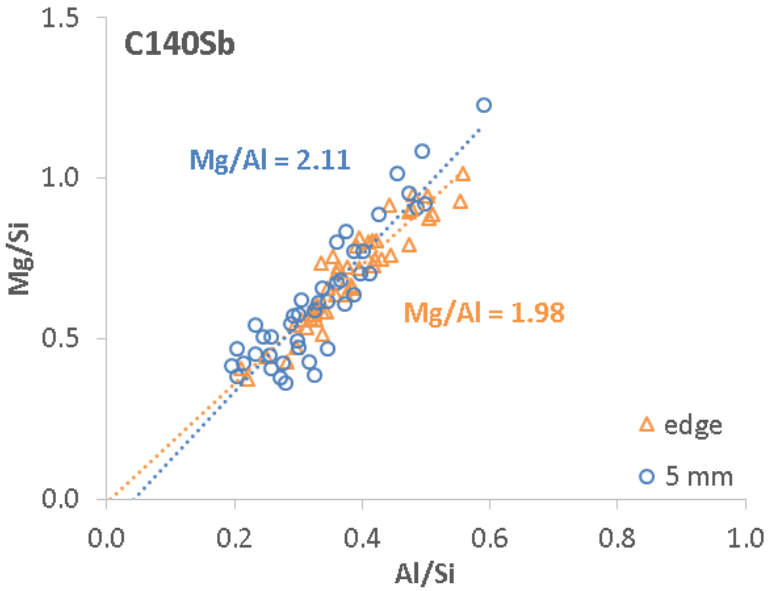

Figure 6-30 – Mg/Si v Al/Si for Blend C_140S_b Cured in a Sulfate Solution for 360 Days

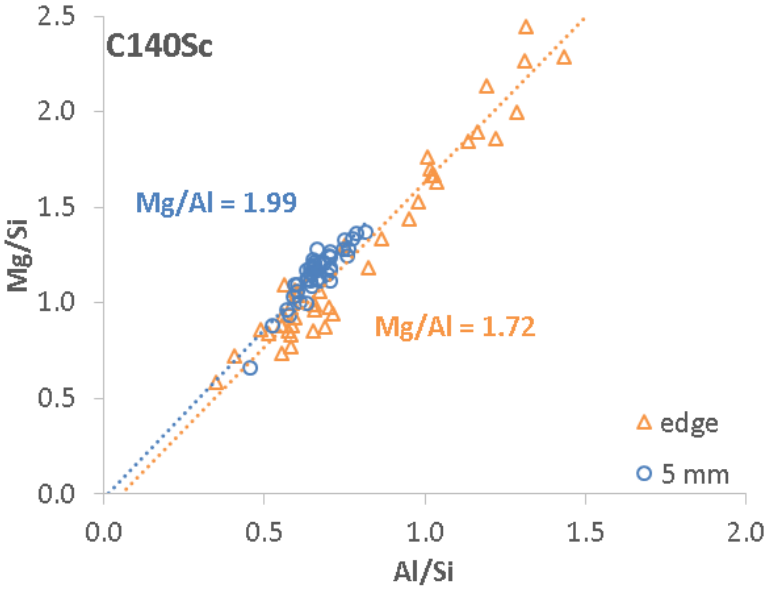

Figure 6-31 – Mg/Si v Al/Si for Blend C_140S_c Cured in a Sulfate Solution for 360 Days

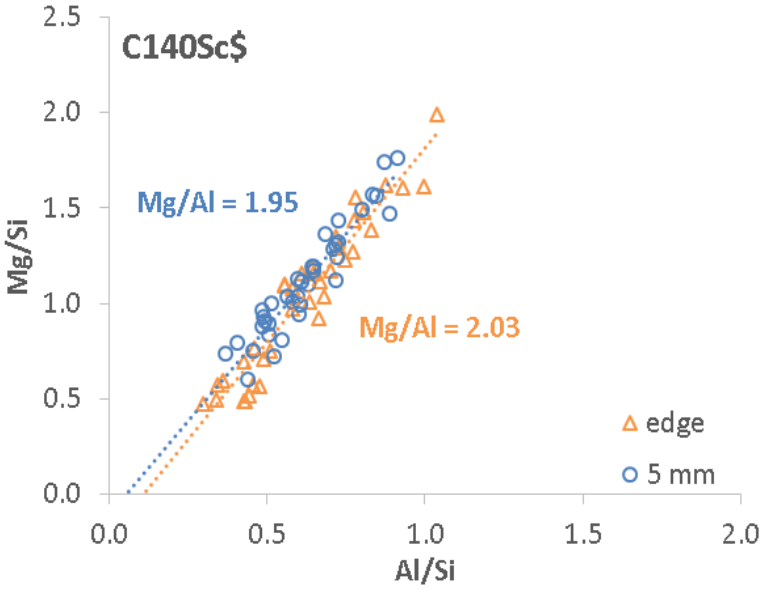

Figure 6-32 – Mg/Si v Al/Si for Blend $C_1 40 S_c \$$ Cured in a Sulfate Solution for 360 Days

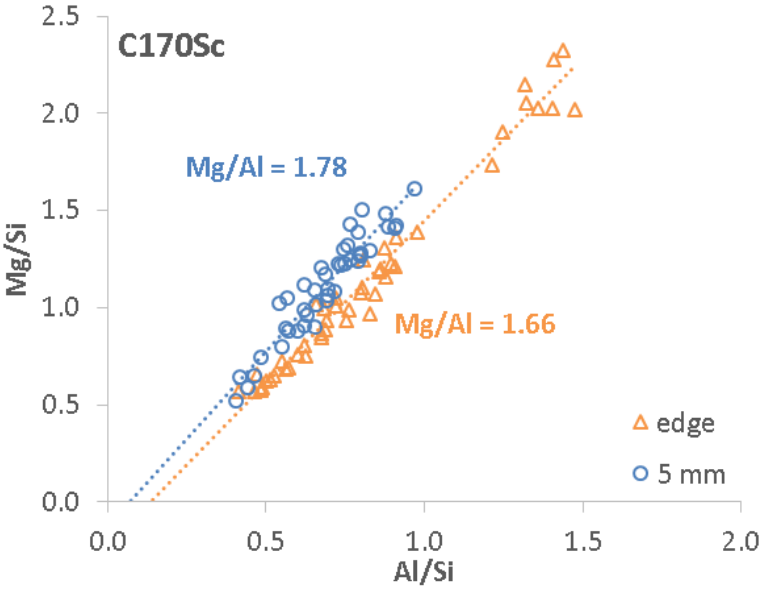

Figure 6-33 – Mg/Si v Al/Si for Blend $C_1 70 S_c$ Cured in a Sulfate Solution for 360 Days

6.5 Discussion

6.5.1 Macroscopic and Microscopic Observations

It is quite evident that the neat cement was the most prone to damage, with it having expanded the most by the end of the testing period. SEM-BSE observations confirmed the susceptibility of C_1 exposed to sulfate, with the system being heavily cracked. Furthermore, the neat paste had deteriorated the most. In contrast all the slag blends showed greater resistance, marked by their respective lower expansion. The impact of slag composition cannot be differentiated by expansion of mortar prisms alone within this

testing period. However, damage was perceived through SEM-BSE and visual observations of the pastes (Figure 6-2 through Figure 6-6, plus appendix A.2). The pastes prepared for characterisation disintegrated faster because of their smaller size. The neat system had deteriorated the fastest and showed signs of cracking along the side of the cylinders. Blend C_140S_c was the least resistant of all the slag blends, with the samples exhibiting cracks along the edge of the faces of the cylinders. These cracks were minimal in $C_140S_{b,}$ and served as the only physical indication that using slags richer in aluminium is undesirable in specimens exposed to sulfates. Similarly, adding sulfates into the mix limited damaged, agreeing with previous studies [12, 16, 185, 188]; the added sulfates bound more aluminium in ettringite prior to attack (Figure 5-24 and Figure 6-29), and the percentage increase of ettringite in the sulfated slag blend was lesser compared to C_140S_c, thus improving resistance. As expected, the blend C_170S_c showed the greatest resistance to sulfates.

The absence of CH and the darkening of the greylevel associated with the C-S-H phase near the edge of the sample is indicative of calcium leaching. Calcium leaching from portlandite, and ultimately C-S-H is not, as such, a direct cause of sulfate attack; any contact with an outside source of water will lead to an outward flow of calcium ions [123, 126, 132, 133]. Planel et al. [123] stated that leaching kinetics are similar for calcium when samples are exposed to either a sulfate solution or deionized water. El Hachem et al. [125] had, however, noticed that a highly concentrated solution may accelerate leaching.

The formation of a thin carbonation layer over time also has to be considered. Curing conditions that favour the formation of a thin carbonate layer typically show improved resistance, with the layer resisting sulfate ingress [187, 203]. However, the carbonate layer here appeared discontinuous. It was not distinguishable whether or not sample preparation would have removed the layer, but still samples where sulfate ingress is slow and resistance high, it can be gleaned that the formation of a carbonate will have time to

form, improving resistance. In the case of C_1 the damage was so severe that the carbonates actually formed in opened cracks.

6.5.2 **Sulfate Profile**

Following the evolution with depth, the very edge of all samples was depleted in sulfates. This was of a direct consequence of leaching of the calcium species marked by the lowered calcium hydroxide content and Ca/Si of the C-S-H phase (Figure 6-16 and Figure 6-22). In this zone, the pH would have been lowered to levels below that required to stabilize ettringite, e.g. below 10.7 [131, 134, 308, 309].

Interestingly, sulfate depletion typically occurred sooner in the slag blends. This effect occurred the earliest in blends $C_140S_c\$$ and C_170S_c. This may have been in response to their lower portlandite content (Figure 5-1 and Figure 6-16). Indeed it is CH that is responsible for the high pH of the pore solution to values above that required to stabilise the hydrates [131]. Upon its leaching, the pH of the solution would have dropped, destabilising the sulfate containing hydrates [131].

The sulfate content then increased to a maximum at a depth of either 0.5 mm for all slag systems using slag C, and to a depth of 1 mm for blend C_140S_b and C_1. The greater penetration depth seen in the latter two blends was likely due to an increase in permeability of the sample suggested in Figure 6-2, where the mentioned systems showed increased porosity and cracking during sulfate attack facilitating sulfate ingress. The greater amount of sulfate bound in the neat system can be linked to its higher overall calcium content, as all sulfate phases in cement contain calcium [107]. In comparison, slags are deficient in calcium reducing the binding capacity of the slag composite systems. The lesser amount of sulfate bound in the slag blended systems was further compounded by the nature of the calcium aluminate sulfate hydrate. XRD and EDX (Figure 6-23 and Figure 6-24) analysis confirmed the co-existence of monosulfate and ettringite in slag composite cements, with monosulfate having a lower S/Ca ratio than ettringite.

6.5.3 Hydrates

6.5.3.1 C-S-H and CH

The stability of the C-S-H phase was shown in Figure 6-22. As expected, the phase had decalcified during attack in all systems, as previously suggested by the SEM observations (Figure 6-2). The extent of decalcification was greatest in the neat system by the end of the testing period. However, during testing, the slag blends showed earlier signs of decalcification. This earlier onset in the blended systems was most likely because of the lower CH content of the blends, effectively reducing the pH of the pore solution. As such the C-S-H was more prone to attack. Note that this effect typically occurred on the very edge of the sample.

With the decalcification of C-S-H, the Al/Si had increased near the surface of the sample for each system. For all samples, from a depth of 0.5 mm to 5 mm, the Al/Si was however constant, and no dealumination had occurred. This goes against a study carried out by Heinz et al. [310]. who measured dealumination of C-S-H in PFA systems . Still, the Al/Si never dropped below 0.1, a value greater than expected in a neat system by any means. Only in blend C_170S_c was the Al/Si of the C-S-H phase greater than 0.1 and yet the phase appeared to be stable. As such, any availability of aluminium from C-S-H can be discounted in slag composite cements.

6.5.3.2 Ettringite – AFm Distribution - Gypsum

The reaction of external sulfates with hydrates led to a redistribution of the AFm phases and ettringite. As expected the main antagonist of sulfate attack, ettringite, had precipitated at the expense of the carbonate AFm phases (Figure 6-23). The amount of ettringite precipitated differed between all blends and lowered as the slag content increased. This is likely because of the lowered carbonate AFm content, which readily react with sulfates, in blended systems due to the dilution of C_3A. Blends C_140S_c and $C_140S_c\$$ had both precipitated the same amount of ettringite, where both blends had comparable aluminium levels. However, the percentage increase of ettringite in blend $C_140S_c\$$ was lower compared to C_140S_c, as explained previously.

Less ettringite had formed in blend $C_1 40S_b$ compared to blend $C_1 40S_c$. This demonstrates that the aluminium from slag contributed to ettringite precipitation. However, the limited amount of ettringite formed in $C_1 70S_c$ would suggest that much of the aluminium was unavailable to react in a calcium poor system. The reduced amount of ettringite formed by the end of the testing period was further compounded by the formation of monosulfate which holds aluminium in its structure. More interestingly was the kinetics of ettringite precipitation. Ettringite precipitation was fast in the first 3 months of curing. Beyond that, and the ettringite evolution was much slower. This may be explained by the lack of carbonate AFm phases, readily providing aluminium, after 90 days of curing in a sulfate solution (Figure 6-23). Only $C_1 40S_c$ showed appreciable ettringite precipitation beyond 90 days of curing in sulfates; the blend still contained carbonated AFm phases.

The formation of 'secondary' monosulfate in slag blends exposed to sulfates had previously been noticed by Fernandez-Altable [187]. There was a positive correlation between the amount of monosulfate precipitated and the overall alumina content of a blend; monosulfate reflections were stronger in blends using slag C at 40% replacement and strongest in blend $C_1 70S_c$. This was confirmed again in Figure 6-24 through Figure 6-28 where the atomic ratio S/Ca was plotted against Al/Ca. At the depth where the sulfate content was highest, the distribution of the points shifted such that monosulfate dominated over ettringite as the slag content increased. The presence of monosulfate is indicative that the $/Al of the pore solution may be lower in the slag blends. This explanation also requires that another source of aluminium is available. It should also be stated that the formation of secondary monosulfate is only a temporary shield against sulfate attack as, with time, the sulfate content in the pore solution is bound to increase; secondary monosulfate will then be converted to ettringite [41]. This suggests that any extra aluminium would react with sulfate to form monosulfate prior to ettringite, and is the reason behind a delay in expansion offset in slag blended systems.

Sulfates had also been bound with calcium to form gypsum in blends C_1 and C_140S_b (Figure 6-24 and Figure 6-25). Its presence was, however, a surprise. Several studies have found its formation during sulfate attack, though the studies relied on strongly concentrated solutions [115, 116, 117, 118]; the sulfate concentration must typically be high to stabilize gypsum in an alkaline environment, e.g. in the pore solution. [119, 120]. Tian et al. [116] stated that gypsum can lead to expansion. Other studies have seen the formation of gypsum in cracks [121, 122] and as such its impact on expansion can be debated. Planel et al. [123] however have noticed the presence of gypsum in cement pastes exposed to a much lower concentration, set at 0.015 $mol.L^{-1}$ (2.1 $g.L^{-1}$) of Na_2SO_4. This is supported by other studies [124, 125].

The data hinted that the sulfate phases may be less stable in the slag blended systems during attack (Figure 6-24 through Figure 6-28). However the data plotted relied on calcium which is soluble. For a better observation, Si would prove a better denominator owing to its lower solubility. The S/Si atomic ratio was therefore plotted against Al/Si, measured on pastes cured for 360 days in the presence of sulfates (Figure 6-34 through Figure 6-38).

The neat system C_1 clearly showed ettringite as the principle sulfate hydrate at the very surface based on the point distribution (see arrow in Figure 6-34 at x = 0.0 mm). The base of the arrow represents the composition of the C-S-H phase and it is apparent that the Al/Si of the phase has increased near the surface when compared to measurements taken at a depth of 1 and 5 mm. This was plotted already in (Figure 6-17). At those greater depths, the lower Al/Si allowed for the tail of points akin to ettringite to sit closer to the ideal stoichiometric S/Al atomic ratio of the hydrate (S/Al = 3). Furthermore, it can also be gleaned that the S/Si of the C-S-H phase was lower near the surface and higher where the sulfate content was measured to be the highest (Figure 6-15). In sulfate rich solutions, sulfates can be bound to the C-S-H phase [292] . During attack, the C-S-H phase decalcified removing any sulfate bound to it.

For all the composite systems prepared with 40% slag, ettringite was present too near the surface after a prolonged period of attack. Again, the C-S-H phase was rich and poor in alumina and sulfur respectively near the surface. At the depth where the overall sulfate content was highest, ettringite points were clearly sitting on the slope representing the ideal S/Al ratio of ettringite. At a depth of 5 mm, blend C_140S_b showed on intimate mixture of ettringite and AFm phases, whereas the latter appeared to dominated in C_140S_c and $C_140S_c\$$.

In blend C_170S_c, the same shift in points was observed indicating an uptake and release of alumina and sulfate respectively. However, at all depths, AFm phases always dominated. This observation agrees with the very low ettringite contents measured previously (Figure 6-29).

The issue of sulfate hydrate stability came about the fact that the phases are stable at high pH [131]. With the lower portlandite content of the blended systems twinned with its leaching (Figure 5-1 and Figure 6-16), the pH of the pore solution in slag systems would systematically be lower than that of a neat system. Consequently, ettringite would be more prone to decompose in slag cements. Still, ettringite was observed suggesting that the pH was maintained. If decomposition had occurred, then the effect was limited.

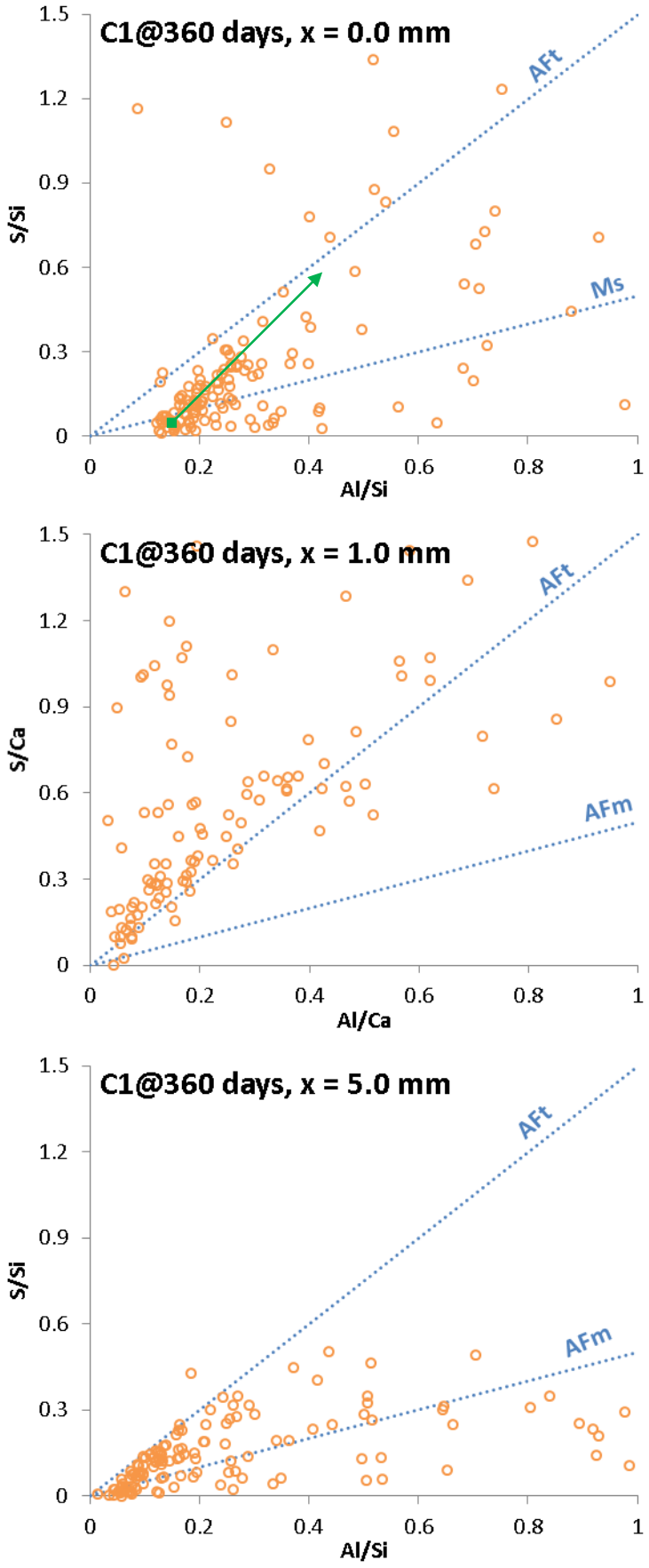

Figure 6-34 – Variations in S/Si v Al/Si as a Function of Depth for C_1 Exposed to a Sulfate Solution, after 360 Days

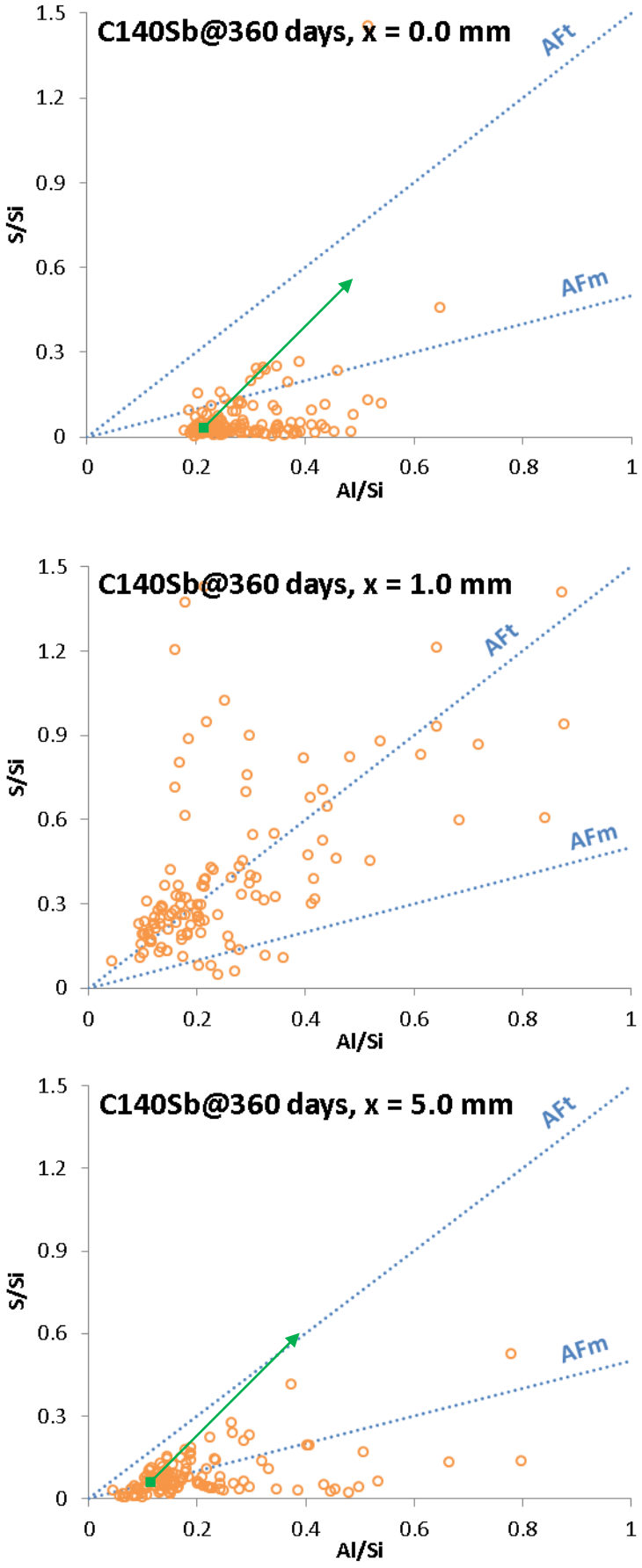

Figure 6-35 – Variations in S/Si v Al/Si as a Function of Depth for C_140S_b Exposed to a Sulfate Solution, after 360 Days

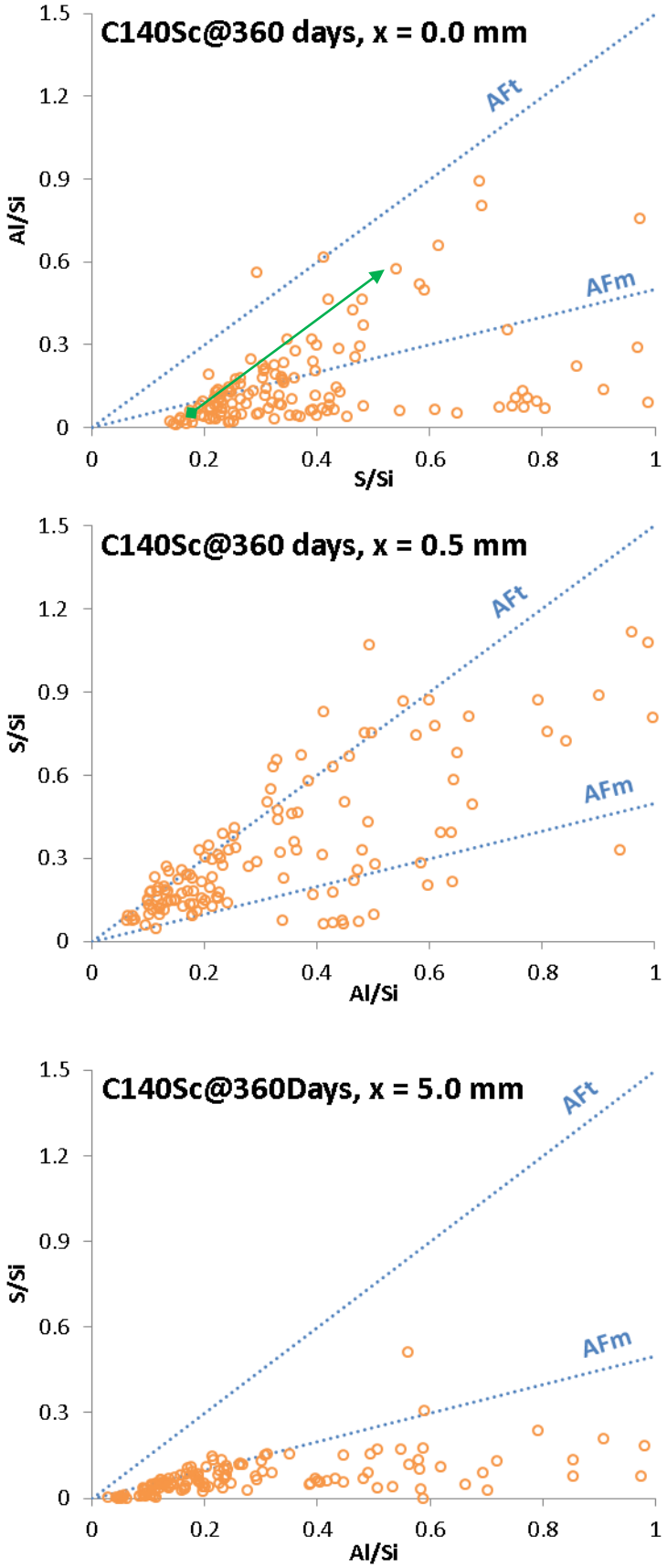

Figure 6-36 – Variations in S/Si v Al/Si as a Function of Depth for $C_1 40S_c$ Exposed to a Sulfate Solution, after 360 Days

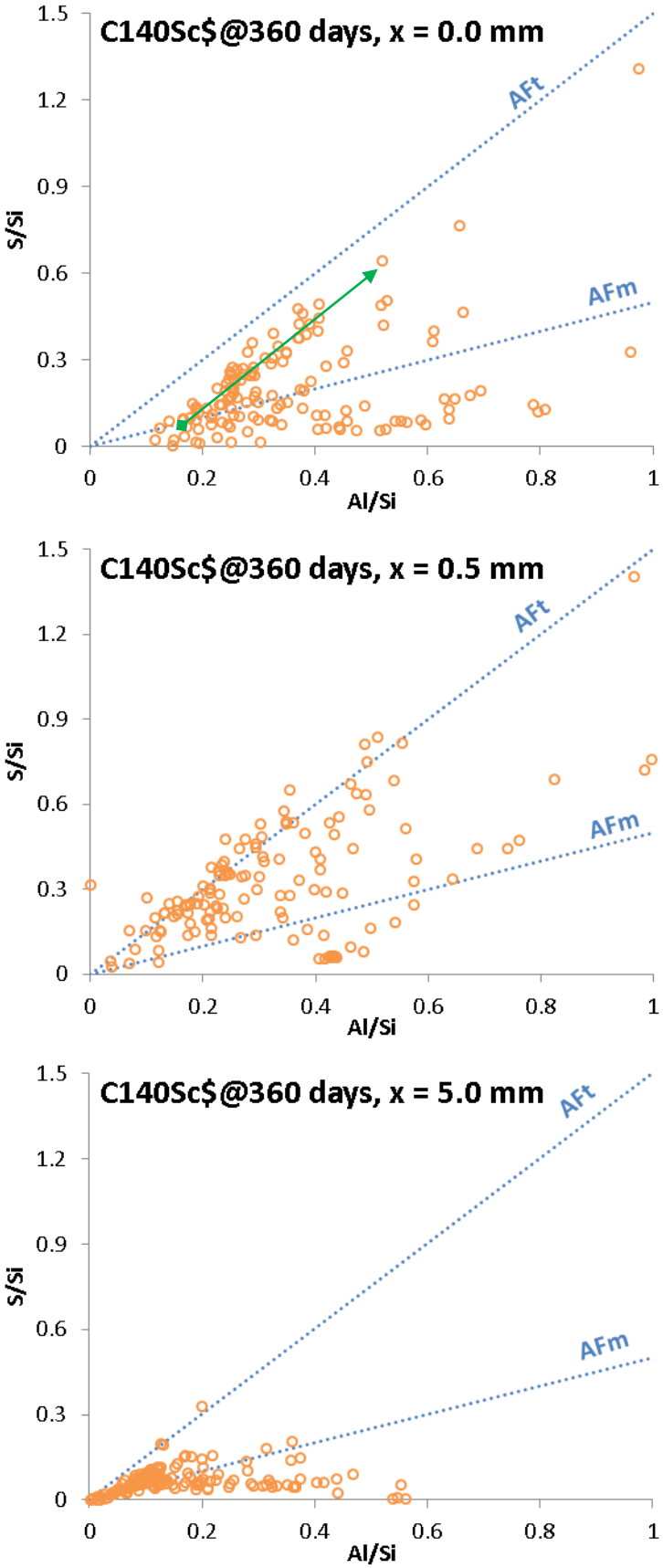

Figure 6-37 – Variations in S/Si v Al/Si as a Function of Depth for $C_1 40 S_c$ Exposed to a Sulfate Solution, after 360 Days

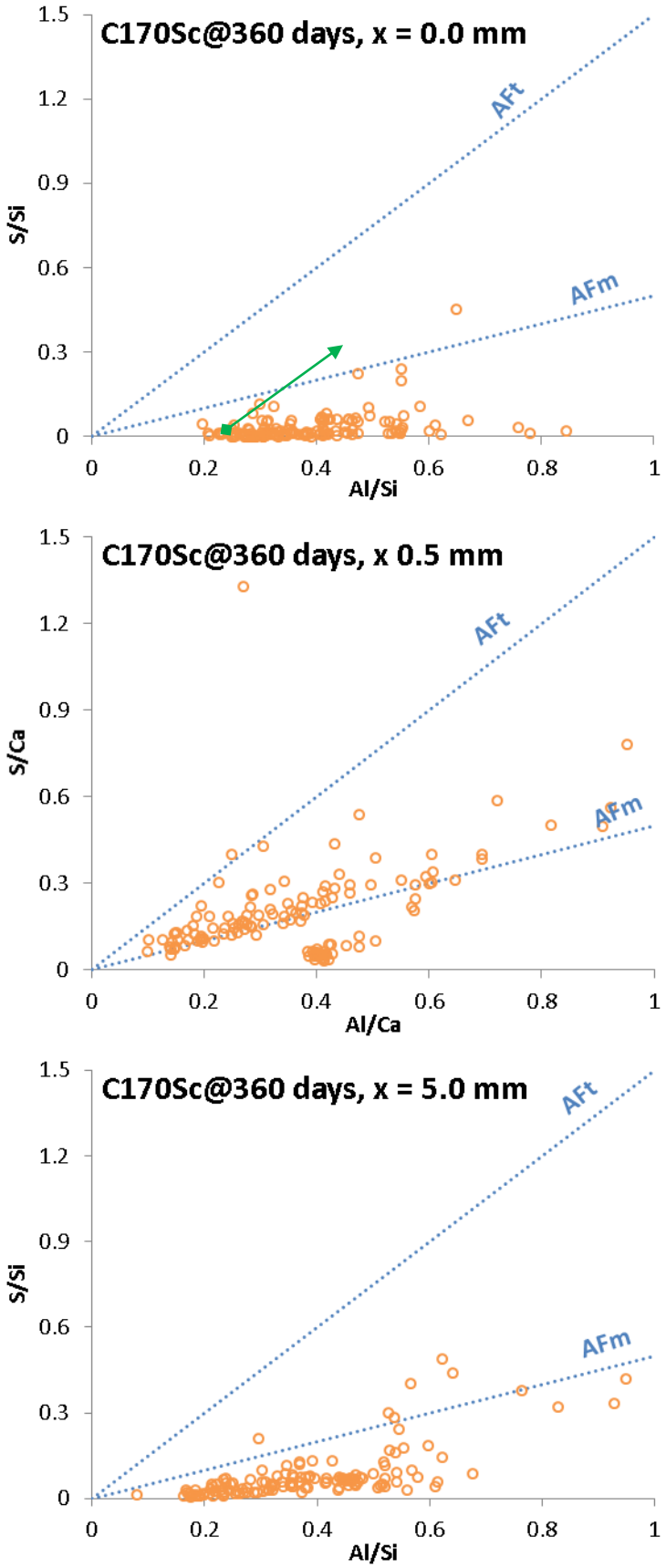

Figure 6-38 – Variations in S/Si v Al/Si as a Function of Depth for $C_1$70S_c Exposed to a Sulfate Solution, after 360 Days

6.5.3.3 Hydrotalcite

Much like the C-S-H phase, hydrotalcite also appeared to be stable in the presence of sulfates. The shifts in Mg/Al ratio were too slight to confirm any contribution of aluminium by the phase. Komljenović et al. [186] found that alkali activated slag (AAS) systems performed better than a CEM II/A-S system, and that the aluminium in AAS was already bound to hydrotalcite and C-S-H neither of which released aluminium upon immersion in a sulfate solution.

With the C-S-H phase and hydrotalcite effectively providing refuge for aluminium from sulfates, any supply of aluminium to promote ettringite formation must come from the slag itself.

It is also interesting to note the changes in the Mg/Al ratio of the hydrotalcite with time [68, 78]. The Mg/Al ratio measured in chapter 5 (Figure 5-28 through Figure 5-31) was measured on samples cured for 180 days, which was higher compared to the ratios measured here after 360 days of curing. This implies a greater affinity between aluminium and hydrotalcite, regardless of the presence of sulfates.

6.5.4 Aluminium Distribution

By adopting a mass balance approach [19, 187], the amount of aluminium released by the raw materials can be tentatively determined and distributed among the aluminium containing hydrates. As such, an idea of how much aluminium available to react with sulfate to produce ettringite can be formed. Aluminium was distributed following the proposed steps:

1. The atomistic composition (Table 6-1) of the clinker phases, plus slags, were determined by EDX analysis. Hydration kinetics was measured by XRD and SEM-BSE image analysis for the clinker and slag fraction respectively, and the amount of each element released was calculated.

2. All the Si was distributed into C-S-H, and its aluminium demand was calculated from the Al/Si.

3. All the Mg released was incorporated into a hydrotalcite-like phase (Ht). From the Mg/Al of the slag hydration rims, the Al demand was calculated. It was assumed that Mg/Al = 2 in C_1.

4. The ettringite content was experimentally determined by quantitative XRD, and the required Al demand was subtracted from the remaining content.

5. The remaining Al was assumed to be in AFm phases. XRD investigations have shown that only carbonate AFm, which was assumed to be monocarboaluminate (Mc), with it being the long term stable AFm hydrate.

Table 6-1 – Atomistic Composition of the Clinker Phases

C_3S	$(Ca_{2.900}\,Mg_{0.061}\,Fe_{0.02}\,Na_{0.007}\,K_{0.013})(Al_{0.055}\,Si_{0.940}\,S_{0.003})\,O_{4.959}$
C_2S	$(Ca_{1.950}\,Na_{0.010}\,K_{0.040})(Mg_{0.011}\,Fe_{0.016}\,Al_{0.102}\,Si_{0.898}\,S_{0.006})\,O_{3.971}$
C_3A	$(Ca_{2.972}\,Mg_{0.028}\,Na_{0.016}\,K_{0.027})(Al_{1.628}\,Fe_{0.135}\,Si_{0.216})\,O_{6.006}$
C_4AF	$(Ca_{1.982}\,Na_{0.006}\,K_{0.012})(Al_{0.880}\,Mg_{0.188}\,Fe_{0.523}\,Si_{0.397})\,O_{4.324}$
Slag B	$Ca_{2.524}\,Na_{0.024}\,K_{0.053}\,Si_{2.457}\,Al_{0.539}\,Mg_{0.762}\,S_{0.087}\,O_{9.322}$
Slag C	$Ca_{2.628}\,Na_{0.043}\,K_{0.036}\,Si_{2.212}\,Al_{0.995}\,Mg_{0.931}\,S_{0.139}\,O_{9.948}$

The aluminium distribution in all the investigated systems is summarised in Figure 6-39, for samples cured in lime water for 360 days. As such the aluminium distribution is representative to that expected at the end of the testing period for samples cured in the lime solution. The size of each pie for the different systems is reflective of the total aluminium present in each system, increasing as slag is incorporated to cement. The individual figures are the actual calculated amount of aluminium in each phase, expressed as Al_2O_3.

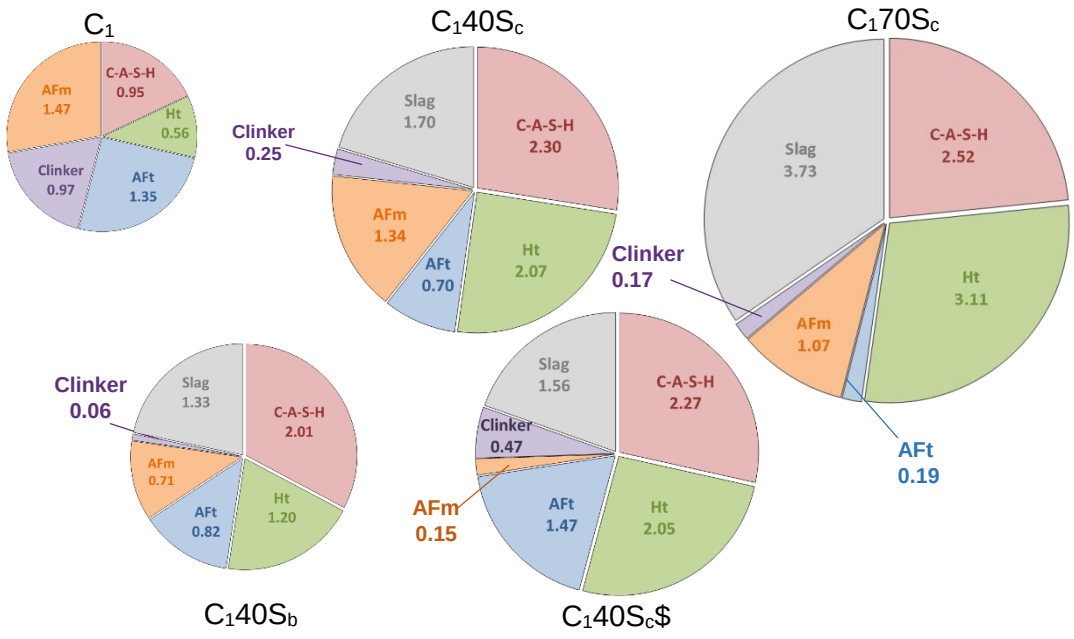

Figure 6-39 – Distribution of Aluminium in Hydrated Slag Cement Pastes Cured for 360 Days in a lime solution
(Ht – hydrotalcite; AFm – monocarboaluminate; AFt – ettringite)

In the neat system C_1, almost a third of all of the aluminium was bound to the AFm phase. Even after a year of curing, the neat system was the richest in AFm compared to all slag blends. This aluminium is readily available to react to form ettringite [121], making the system susceptible to sulfate attack (Figure 6-1 and Figure 6-2). The remaining aluminium was distributed between C-S-H, AFt, and hydrotalcite, with some remaining in anhydrous clinker. The role of C_3A in sulfate attack is known and reducing its content results in better resistance [105], achieved by blending cement with slag.

At 40% replacement, the AFm content was effectively lowered. However, slags can promote the formation of AFm, the impact of which would be limited by their hydration kinetics and composition. More AFm was seen in blend C_140S_c, to a value almost to that seen in C_1, because of the faster hydration kinetics, plus overall Al_2O_3 content, of the slag compared to blend C_140S_b; this made blend C_140S_c more vulnerable to sulfate attack (Figure 6-2, appendix A.2). The addition of sulfates reallocated AFm-bound aluminium to ettringite, subsequently improving resistance.

Blend C_170S_c was rich in carbonate AFm, more so than blend C_140S_b but less so than blend C_140S_c, and the blend showed no sign of damage. The ettringite content remained low in this system after attack (Figure 6-29), and rather monosulfate had preferentially formed. The increased aluminium content of the blend had not lead to greater damage, but rather offered protection. However, as explained, this may only be a temporary effect.

In all the blended systems, much of the released aluminium had been bound to C-S-H in response to a lower Ca/Si (Figure 6-22) [29, 88, 290] and up to 2/3 of the total aluminium content was bound by it. The amount of aluminium bound by C-S-H was rather dependent on the level of replacement rather than the composition of the slag; all the blends with 40% slag had comparable Ca/Si ratios (Figure 6-22) and similar levels of aluminium were incorporated into C-S-H. Only by increasing the slag content, therefore, reducing the Ca/Si of the C-S-H phase, had more aluminium been bound. Gollop and Taylor [16] had previously argued the impact of C-S-H composition on sulfate attack to conclude that blends whose slag content is low will have a C-S-H phase with a Ca/Si ratio comparable to that of a neat system, limiting the amount of aluminium bound to it. Hence any aluminium that has not been bound, which could have been if the slag content was higher, could potentially be used to form ettringite.

The impact of magnesium should not be dismissed either when assessing sulfate resistance of slag blended systems, with the phase effectively hiding aluminium in its structure from sulfates (Figure 6-30 through Figure 6-33). Slag B had the lowest magnesium twinned with the highest Mg/Al ratio, limiting the aluminium bound to the phase to 1.52 g of Al_2O_3. More aluminium had been bound by the phase in blends C_140S_c and C_140S_c\$ because of the higher magnesium content of the slag and lower Mg/Al ratio of the hydrotalcite phase. Increasing the slag content further increased the total amount of aluminium bound simply because of the greater amount of hydrotalcite that had formed, as seen by the XRD tracings in Figure 6-23, paired with further lowering of the

Mg/Al ratio. Together with C-S-H, up to half and more of the total aluminium content in a blend can be made inaccessible to sulfates.

However, XRD and EDX investigations showed the formation of monosulfate with ettringite in slag blended systems (Figure 6-23) even where the sulfate content was measured to be the highest [187]. This suggests an availability of aluminium from the slag itself, as any aluminium in C-S-H and hydrotalcite was effectively secure. Indeed much of the aluminium in the slag had yet to be released; up to 2/3 of all the alumina in blend C_170S_c was still bound by the slag. The progressive hydration of the slag continuously fed aluminium to form monosulfate keeping the $/Al ratio low [41]. The slow release of aluminium was most likely the underlying cause of the slow precipitation kinetics of ettringite beyond 90 days of hydration, by which time most of the carbonate AFm phases would have been consumed (only C_140S_c had carbonate AFm phases remaining beyond 90 days of curing in the presence of sulfates). Eventually if the process of forming ettringite is too slow, the continual leaching of calcium would result firstly in an unavailability of the element to form ettringite and secondly in a decrease in pH such that ettringite formation may even be further hindered. Kunther et al. have very recently established that ettringite crystallisation pressure reduced with reduced calcium contents [311]. As such, sulfates have to penetrate deeper into the sample to cause damage in the blended systems. It has been previously suggested that at low levels of replacement, the resistance of a blend is dependent on the original AFm content; at higher levels of replacement, however, the resistance was dependant on the overall Al_2O_3 content [187].

6.6 Summary

1. All the slag blended systems showed greater resistance to sulfate attack compared to the neat system C_1. Visual observations confirmed that alumina-rich slags performed worse in blends prepared with 40% slag. Similarly, the addition of sulfates, and changes in the slag composition and loading improved resistance.
2. All samples showed leaching of calcium hydroxide and decalcification of the C-S-H. Decalcification had occurred earlier in the slag blends compared to C_1, possibly

because of the lower pH of the pore solution in the composite systems. In response to the reduced Ca/Si, more aluminium had been bound to the phase. There was a general trend such that, as the CH content decreased, decalcification occurred faster.

3. The sulfate content increased initially at the surface of the sample and decreased after prolonged exposure times. This was the result of calcium leaching as all sulfate hydrates contain calcium. Sulfates penetrated deeper into the sample such that the maximum content was found at either 0.5 mm or 1 mm depths.
4. The neat system was the richest in ettringite, with gypsum also present, after attack. Increasing the slag content reduced the amount of ettringite, although alumina from slag contributed to AFt formation. Furthermore, slag blends allowed for the formation of monosulfate, suggesting an availability of aluminium such that the $/Al of the solution was low enough to allow monosulfate precipitation
5. Despite the higher alumina content of blended systems, much of it was distributed between C-S-H and hydrotalcite. These phases together contained up to half of all the aluminium in slag cement. Aluminium bound to these phases was unavailable to react with sulfates. The only remaining plausible source of aluminium was therefore from the slag itself.
6. There is no evident link between alumina availability and expansion upon ettringite formation. When comparing C_1 with C_140S_c, both had comparable alumina contents bound to ettringite and yet less had formed. This was partly due to the formation of monosulfate during the testing the period. When considering depleting calcium availability, the calcium content on ettringite formation must also be taken into account as 2 moles of calcium must be provided to form ettringite from AFm phases.

Chapter 7

Conclusions and Further Work

7.1 Impact of Slags and their Compositions on Hydration Kinetics

The hydration kinetics of the slag composite systems were followed by both qualitative and quantitative techniques. Slag hydration was quantitatively measured by SEM-BSE and showed that its hydration was slow. After 1 day of curing, only 20 to 25 % of the slag had reacted, and no more than 70 % had reacted after 1 year in blends prepared with 40 % slag. Slag C was shown to be the more reactive of the two slags, and its reactivity lessened with increased slag loading. These differences in kinetics were most likely because of a change in composition. In contrast, cement hydration was fast, and 80 % of the clinker had reacted by 7 days in all systems. Its hydration was not particularly further exacerbated due to the presence of slags, only at very early ages. With respect to the individual clinker phases however, all were accelerated in the presence of slag, with the exception of belite whose hydration was retarded. Despite this, the overall degree of hydration for any given day remained unchanged. The addition of sulfates retarded C_3A hydration. Quantitative and qualitative evaluation of hydration typically agreed well.

7.2 Impact of Slag and Their Composition of Microstructural Features

7.2.1 C-S-H

The neat cement was characterised by having a calcium rich C-S-H phase with an average Ca/Si of 1.8 and an Al/Si of 0.6, both of which remained constant during hydration. In contrast, the C-S-H phase in the slag cements was deficient in calcium. In blends prepared with 40% slag, The Ca/Si was marginally lower (Ca/Si ~ 1.6-1.7) and did not differ greatly between blend $C140S_b$ and $C140S_c$. This was due to the fact that both slags B and C had similar calcium contents. The Ca/Si was lowest in blend C_170S_c, with readings as low as 1.4. The addition of calcium sulfate in blend C_140S_c\$ made no

discernible changes to the ratio at later ages, but had increased it at early ages as calcium sulfate temporarily sorped to the phase.

In response to the lower Ca/Si of the phase in the slag blends, more alumina was bound by the C-S-H phase. When comparing blends C_140S_b and C_140S_c, the latter showed a higher Al/Si as slag C was the richest in alumina. As expected, the C-S-H phase in blend C_170S_c had bound the most amount of Al_2O_3 due to the much lower Ca/Si of the C-S-H phase in the blend, having formed in an alumina rich environment. Added sulfates had again affected the early age composition of the C-S-H phase only where the Al/Si was low after just 1 day of curing; the alumina content in solution was controlled by the low solubility of ettringite in the early stages of hydration.

7.2.2 **Calcium Hydroxide**

The calcium hydroxide contents were lower in all the slag blended systems compared to the neat cement, the contents of which depended on slag composition and loading. In blends prepared with 40% slag, blend C_140S_b was the richest in CH and blend C_140S_c\$ the poorest. The differing CH contents between blends C_140S_b and C_140S_c was most likely due to the differences in hydration kinetics of the slags rather than composition, with the latter being the more reactive. As such, slag C would have consumed more calcium hydroxide during the early stages of hydration. In blend C_140S_c\$, the CH content was lowered further due to the initially higher Ca/Si of the C-S-H phase. Naturally, blend C_170S_c was the poorest in CH.

7.2.3 **Hydrotalcite**

A hydrotalcite-like phase was also prominent in the slag composite cements and the Mg/Al of the phase varied with slag composition and time. At 180 days of curing, the Mg/Al atomic ratio ranged from 2.68 for blend C_140S_b to 1.93 for blend C_170S_c. Generally, as more aluminium was available more was bound to the phase. As hydration proceeded, from 180 to 360 days of curing, the Mg/Al decreased slightly highlighting the affinity of aluminium to react with magnesium. Interestingly, the addition of sulfates in

blend $C_1 40 S_c \$$ at the start of the reaction led to an increase in the Mg/Al of the hydrotalcite phase. This was the result of aluminium reacting with sulfates to form ettringite over hydrotalcite

7.2.4 **Aluminate Hydrates**

With respect to aluminate hydrates, the slag blended systems were typically poorer in AFm phases (hemi- or monocarboaluminate here) and ettringite compared to C_1. This was due to the fact that the clinker content was diluted, although the alumina provided by slags can contribute to their formation. Similarly, the sulfate contents were also diluted lowering the ettringite content.

The main AFm phases present in normal curing conditions were carbonate-AFm, initially hemicarboaluminate which later converted either fully or partially to monocarboaluminate depending on binder composition. When comparing all the slag cements, blend $C_1 40 S_c$ was the richest in carbonate-AFm. The addition of sulfate in blend $C_1 40_c \$$, correcting for the sulfate imbalance created when adding slags, promoted ettringite precipitation over carbonate-AFm.

7.3 **Impact of Slags and Their Compositions on Strength and Porosity**

The neat system was the strongest of all the systems at early ages. However, by 28 days, the difference in strength between C_1 and the 40% slag systems were greatly minimised such that, by 180 days of curing, all had comparable strengths. This was due to the slow but continual hydration of the slags. Blend $C_1 70 S_c$ was marginally weaker after 6 months of curing. This improvement in strength exhibited by the slag systems remained true despite the lower volume of the solid phases. Furthermore, slag composition had little impact on strength, and hydration kinetics was more important. Additional sulfates promoted ettringite formation increasing the solids volume. However, excess sulfates affected the C-S-H, weakening it.

Generally, strength and porosity showed good correlation. What was most interesting was the evolution of porosity with hydration. It was seen that the porosity

decreased faster after 7 days of curing in the blended systems with respect to the degree of hydration of the slag cements. Similarly, more shrinkage had occurred per unit of hydration after 7 days. This increase in shrinkage suggested that more water had been bound to the C-S-H phase. A water rich C-S-H would have a lower density and is perhaps an underlying cause for improved mechanical strength of the blended systems despite a lower hydration degree of the slag.

7.4 Impact of Slags and their Composition on Sulfate Resistance

Serving as reference, the neat system was the richest in ettringite after attack with the bulk of it having formed quickly, in less than 90 days. As such, the neat system was the first to show signs of damage in the form of surface cracks, later promoting sulfate ingress. Mass balance calculations showed that the amount of deleterious ettringite that has formed can be linked to the availability of aluminium bound in AFm phases which are easily converted to ettringite in the presence of sulfates; almost 2/3 of all total aluminium was bound to the AFm phase. With the clinker hydrates almost depleted, little more was expected to be released.

7.4.1 Impact of Slag Composition in 40% Slag Blends on Sulfate Resistance

The expansion of all the 40% slag blends was in fact quite comparable. Only by observing the pastes was it revealed that the use of the alumina rich slag C led to greater damage by the end of the testing period. Compared to C_1, less ettringite had formed in blends C_140S_b and C_140S_c. The latter of the slag blends, however, was ultimately the richest in ettringite owing to the higher alumina content of the slag. Kinetically, ettringite formation was fast too with the bulk of ettringite forming in 90 days again. Beyond that, ettringite levels increased slightly in blend C_140S_c where carbonate AFm persisted, but remained constant in blend C_140S_b. In the absence of carbonate AFm, ettringite levels were controlled by the $/Al ratio of the pore solution which itself depended on sulfate ingress and aluminium release from the slag. Monosulfate had also formed during attack, the amount of which was greatest when using the alumina rich slag C.

Based on microstructural developments, both of the 40 % slag blends showed comparable amounts of alumina bound the C-S-H phase and ettringite, but much more was bound to hydrotalcite in blend C_140S_c, all of which was observed to be unavailable to react with sulfates. The main difference was the AFm contents between the slag blends, with much more available in blend C_140S_c. In fact, AFm contents in C_140S_c were similar to those in C_1 and yet ettringite levels and resistance were different. This can be attributed to the formation of monosulfate during attack limiting ettringite formation. Furthermore, ettringite crystallisation pressure is reduced in calcium deficient systems so it can be suspected that the potential for damage was lower.

7.4.2 **Impact of Added Sulfates**

The addition of sulfates was proven to improve sulfate resistance of blend C_140S_c\$. The blend was richer in ettringite before attack occured and the percentage increase of ettringite had therefore lessened after. Expansion was only slightly minimised despite this effect, although pastes showed cracking after 360 days of exposure. Both blends C_140S_c and C_140S_c\$ had evolved the same amount of ettringite after attack suggesting that the sulfates had no great influence during actual sulfate attack other than binding more aluminium in ettringite prior to sulfate exposure. The main differences, with respect to microstructure, compared to blend C_140S_c was an slight increase in the Mg/Al ratio and reduced AFm contents. But because the release of alumina from hydrotalcite, plus that of the AFm phases, was redistributed to ettringite the effect was nullified. Similar levels of monosulfate even appeared to have formed when comparing blends C_140S_c and C_140S_c\$.

7.4.3 **Impact of slag Loading**

The mortar prisms prepared with C_170S_c as binder has shown the least expansion, and the complimentary paste showed great resistance too. With respect to ettringite formation, the slag rich blend had evolved the least during sulfate exposure.

The low amount of ettringite formed seems contradictory at first as the amount of AFm was greater when compared to blend $C_1 40S_b$, but still less than $C_1 40S_c$. As such, the ettringite content after attack should theoretically be between that of $C_1 40S_b$ and $C_1 40S_c$. This was due firstly to the formation of monosulfate, for which alumina was provided by the slag, and secondly due to changes in the microstructure.

Despite much more aluminium available from the slag, most of which was bound to the C-S-H phase and hydrotalcite, leaving surprisingly little to form AFm hydrates providing a first level of replacement. Furthermore, calcium contents were the lowest with most of it leaching from the outer layer by the end of the testing period making further ettringite formation difficult, thus further reducing ettringite growth and crystallisation pressure.

7.4.4 **Final Comments**

The presented work followed the hydration of slag cement blends in both controlled conditions and in an aggressive media in the form of sodium sulfate. The impact of slag incorporation has led to several key changes in the microstructure, all of which led to improved resistance, including:

1. A reduction in the overall calcium content leading to a calcium deficient C-S-H phase and a lower calcium hydroxide content
2. An increase in the alumina content of the C-S-H phase
3. The presence of a hydrotalcite phase varying in Mg/Al ratio
4. A reduced AFm content though the contents varied strongly between blends

Depending on slag loading and composition, the mentioned changes varied as described above. It was shown that alumina bound to C-S-H and hydrotalcite, was unavailable to react with ingressing sulfates to form ettringite. During attack, it was seen that monosulfate had also formed . This highlighted a change in the pore solution such that alumina from the slag itself was released keeping the $/Al ratio low. However this effect is only temporary; the slag blends will perform adequately as long as the $/Al remains stable. As soon as the $/Al is allowed to rise, ettringite will form.

Furthermore, the role of calcium needs attention where it was recently shown that ettringite crystallisation pressure is lower in calcium deficient systems. Over time, calcium will continuously leach further lowering the potential for ettringite growth. As such, there are two mechanisms to be considered during attack. Firstly ettringite precipitation and, secondly, calcium leaching. It can be supposed, therefore, that as slags are introduced the main failure mechanism may likely sway from the former to the latter.

7.5 Further work and Recommendations

With respect to the work presented here, more work could have been aimed towards the C-S-H phase. As much as the data suggest that more water is bound by this phase, effectively reducing its density and improving space filling, this is not entirely proven. ^{1}H NMR may have very well demonstrated this effect, or possibly even SANS measurements. Although volume balance can be found in the literature to tentatively assess C-S-H density, any attempts in assessing the water content, and in turn density, here proved inconclusive. This may have been the result of freeze drying samples.

Similarly, porosity was only followed by SEM-BSE imagery. This has a drawback of only measuring the coarser porosity. Pore refinement can be expected in slag blended systems and MIP measurements would have been an ideal complement with respect to sulfate ingress and calcium leaching. Furthermore, crystallisation pressure has an inverse relationship with pore size (pressure is greater in smaller pores) and relating pore size to pressure in composite systems has yet to be seen. To maintain crystal growth in smaller pores, however, the supersaturation degree has to be higher. Otherwise the smaller ettringite crystal will dissolves in favour of larger ones, provided the pores are connected. However, the degree of supersaturation with respect to ettringite has to be estimated first, either through modelling or experimental investigations. It would be interesting to model which phases would have formed taking into account sulfate ingress and slag dissolution.

It is also accepted that it is the aluminium content that determines whether or not a slag is suitable for use in sulfate laden areas. However, the data probed that calcium also becomes rare as the slag content increase as slags are inherently poor in calcium compared to Portland cement. During attack, calcium is either leached out of the sample or consumed to form ettringite, sourced from calcium hydroxide and possibly C-S-H. If too little is available then ettringite cannot form at the expense of AFm phases. As such, it is insufficient to rely only on the aluminium content of the slag, but also on its calcium content.

Sulfate resistance was assessed using an ideal lab controlled solution, here a sodium sulfate solution. Simple changes in approach could have led to very different results. Slag systems were characterised by having a lower pH, which would increase the likelihood of C-S-H decalcification. Changes in the experimental approach could have been adopted to accentuate leaching, hence changing the behaviour of the samples subjected to attack, increasing the renewal of the solution and its volume could have demonstrated this effect, as well as substituting Na_2SO_4 for $MgSO_4$. Magnesium sulfate has a very different attack mechanism and attack more readily calcium hydroxide and C-S-H. Furthermore, macroscopic damage was assessed only by expansion and visual observations, but do not provide any information of any other structural changes. The impact of leaching and decalcification could have been perhaps followed by changes in the dynamic modulus.

References

[1] J. S. DAMTOFT, J. LUKASIK, D. HERFORT, D. SORRENTINO and E. GARTNER, "Sustainable Development and Climate Change Initiatives," *Cement and Concrete Research,* vol. 38, no. 2, p. 115/127, 2008.

[2] M. SCHNEIDER, M. T. M. ROMER and H. BOLIO, "Sustainable Cement Production at Present and Future," *Cement and Concrete Research, ,* vol. 41, no. 7, pp. 642-650, 2011.

[3] B. LOTHENBACH, K. SCRIVENER and R. D. HOOTON, "Supplementary Cementitious Materials," *Cement and Concrete Research,* vol. 41, pp. 1244-1256, 2011.

[4] M. WHITTAKER, M. ZAJAC, M. BEN HAHA, F. BULLERJAHN and L. BLACK, "The Role of the Alumina Content of Sag, Plus the Presence of Additional Sulfate on the Hydration and Microstructure of Portland cement-Slag Blends," *Cement and Concrete Research,* vol. 66, 2014.

[5] K. DE WEERDT, M. BEN HAHA, G. LE SAOUT, K. KJELLSEN, H. JUSTNES and B. LOTHENBACH, "Hydration Mechanisms of Ternary Portland Cements Containing Limestone Powder and Fly Ash," *Cement and Concrete Research,* vol. 41, pp. 279-291, 2011.

[6] F. DESCHNER, F. WINNEFELD, B. LOTHENBACH, S. SEUFERT, P. SCHWESIG, S. DITTRICH, F. GOETZ NEUNHOEFFER and J. NEUBAUER, "Hydration of Portland Cement with High Replacement by Siliceous Fly Ash," *Cement and Concrete Research,* vol. 42, pp. 1389-1400, 2012.

[7] H. G. SMOLCZYK, "Slag Structure and Identification of Slags," *Proceedings of the 7th International Congress on the Chemistry of Cement ,* vol. III, pp. 1/3-1/17, 1980, Paris.

[8] A. BOUGARA, C. LYNSDALE and N. B. MILESTONE, "Reactivity and Performance of Blast furnace Slags of Different Origin," *Cement and Concrete Composites,* vol. 32, pp. 319-324, 2010.

[9] D. G. MANTEL, "Investigation into the Hydraulic Activity of Five Granulated Blast Furnace Slags with Eight Different Portland Cements," *ACI Materials Journal,* vol. 91, no. 5, pp. 471-477, 1994.

[10] BS EN 197-1:2011, "Cement part I: Composition, Specifications and Conformity for Common Cements," *British Standard Institution,* 2011.

[11] D. D. HIGGINS, "Increased Sulfate Resistance of GGBS Concrete in the Presence of Carbonate," *Cement and Concrete Composites,* vol. 25, no. 8, pp. 913-919, 2003.

[12] D. D. HIGGINS and N. J. CRAMMOND, "Resistance of Concrete Containing GGBS to the Thaumasite Form of Sulfate Attack," *Cement and Concrete Composites,* vol. 25, pp. 921-929, 2003.

[13] R. D. HOOTON and J. J. EMERY, "Sulfate Resistance of a Canadian slag Cement," *ACI Materials Journal,* vol. 87, no. 6, pp. 547-555, 1990.

[14] W. KUNTHER, B. LOTHENBACH and K. L. SCRIVENER, "On the Relevance of Volume Increase for the Length Changes in Mortar Bars in Sulfate Solution," *Cement and Concrete Research,* vol. 46, pp. 23-29, 2013.

[15] F. W. LOCHER, "The Problem of the Sulfate Resistance of Slag Cements," *Zement-Kalk-Gibs (Weisbaden),* vol. 9, pp. 395-401, 1966.

[16] R. S. GOLLOP and H. F. W. TAYLOR, "Microstructural and Microanalytical Studies of Sulfate Attack, V, Comparison of Different Slag Blends," *Cement and Concrete Research,* vol. 27, pp. 1029-1044, 1996.

[17] P. K. MEHTA, "Effect of Fly Ash Composition on Sulfate Resistance of Cement," *Proceedings of the American Concrete Institute,* vol. 83, no. 6, pp. 994-1000, 1986.

[18] ASTM C150/C150M-12, "Standard Specification for Portland Cement," *American Society for Testing and Materials, ASTM C150/C150M-12, 04.01,* 2012.

[19] H. W. F. TAYLOR, Cement Chemistry, London: Academic Press Limited, 1992.

[20] A. CRUMBIE, G. WALENTA and T. FULLMAN, "Where is the Iron? Clinker Microanalysis with XRD Rietveld, Optical Microscopy/Point Counting, Bogue and SEM-EDS Techniques," *Cement and Concrete Research,* vol. 36, pp. 1542-1547, 2006.

[21] I. MAKI and K. GOTO, "Factors Influencing the Phase Constitution of Alite in Portland Cement Clinker," *Cement and Concrete Research,* vol. 12, pp. 301-308, 1982.

[22] I. G. RICHARDSON and G. W. GROVES, “Microstructure and Microanalysis of Hardened Ordinary Portland Cement Pastes,” *Journal of Material Science,* vol. 28, pp. 265-277, 1993.

[23] I. ODLER and H. DORR, “Early Hydration of Tricalcium Silicate I. Kinetics of the Hydration Process and the Stoichiometry of the Hydration Kinetics,” *Cement and Concrete Research,* vol. 9, pp. 239-248, 1979.

[24] I. G. RICHARDSON, “Tobermorite/Jennite- and Tobermorite/Calcium Hydroxide-based Models for the Structure of C-S-H: Applicability to Hardened Pastes of Tricalcium Silicate, β-Dicalcium Silicate, Portland Cement, and Blends of Portland Cement with Blast-Furnace Slag, Metakaolin, or Silica Fume,” *Cement and Concrete Research,* vol. 34, pp. 1733-1777, 2004.

[25] X. CONG and R. J. KIRKPATRICK, “29Si MAS NMR Study of the Structure of Calcium Silicate Hydrate,” *Advanced Cement Based Materials,* vol. 3, pp. 144-156, 1996.

[26] K. FUJII and W. KONDO, “ Estimation of Thermochemical Data for Calcium Silicate Hydrate (C-S-H),” *Journal of the American Ceramic Society, (),* vol. 66, no. 12, pp. C220-221, 1983.

[27] I. G. RICHARDSON, “The Calcium Silicate Hydrates,” *Cement and Concrete Research,* vol. 38, pp. 137-158, 2008.

[28] I. G. RICHARDSON, A. R. BROUGH, R. BRYDSON, G. W. GROVES and C. M. DOBSON, “Location of Aluminium in Substituted Calcium Silicate Hydrate (C-S-H) Gels as determined by 29Si and 27Al NMR and EELS,” *Journal of the American Ceramic Society,* vol. 76, pp. 2285-2288, 1993.

[29] I. G. RICHARDSON and G. W. GROVES, “Microstructure and Microanalysis of Hardened Cement Pastes Involving Gound Granulated Blast-Furnace Slag,” *Journal of Material Science,* vol. 27, pp. 6204-6212, 1992.

[30] S.-Y. HONG and F. P. GLASSER, “Alkali Binding in Cement Pastes Part I: the C-S-H Phase,” *Cement and Concrete Research,,* vol. 29, pp. 1893-1903 , 1999.

[31] S.-Y. HONG and F. P. GLASSER, “ Alkali Sorption by C-S-H and C-A-S-H gels Part II: Role of Alumina,” *Cement and Concrete Research,* vol. 32, pp. 1101-1111, 2002.

[32] I. G. RICHARDSON, “The Nature of the Hydration Products in Hardened Cement Pastes,” *Cement and Concrete Composites,* vol. 22, pp. 97-113, 2000.

[33] F. LEA, Lea's Chemistry of Cement, P. Hewlett, Ed., Oxford: Butterworth-Heinemann, 1988.

[34] J. BENSTED, “Some Applications of Conduction Calorimetry to Cement Hydration,” *Advances in Cement Research,* vol. 1, pp. 35-44, 1987.

[35] S. GONI, F. PUERTAS, M. SOLEDAD HERNANDEZ, M. PALACIOS, A. GUERRERO, J. S. DOLADO, B. ZANGA and F. BARONI, “Quantitative Study of Hydration of C3S and C2S by Thermal Analysis,” *Journal of Thermal Analysis and Calorimetry,* vol. 102, no. 3, pp. 965-973, 2010.

[36] G. BYE, Portland Cement, 3rd Edition, London: ICE Publishing, London, 2011.

[37] Y. TAKEUCHI, F. NISHI and I. MAKI, “Crystal-Chemical Characterization of the 3 CaO.Al2O3 Solid-Solution Series,” *Zeitschrift fur Kristallographie,* vol. 152, pp. 259-307 , 1980.

[38] P. K. MEHTA and M. P. J. MONTEIRO, Concrete: Microstructure, Properties, and Materials, 3rd edition, United States of America: McGraw-Joll, 2006.

[39] N. TENOUTASSE, “The Hydration Mechanism of C3A and C3S in the Presence of Calcium Chloride and Calcium Sulfate,” in *5th International Symposium on the Chemistry of Cement*, Tokyo, 1968.

[40] H. MINARD, S. GARRAULT, L. REGNAUD and A. NONAT, “Mechanisms and Parameters Controlling the Tricalcium Aluminate Reactivity in the Presence of Gypsum,” *Cement and Concrete Research,* vol. 37, pp. 1418-1426, 2007.

[41] T. MATSCHEI, B. LOTHENBACH and F. P. GLASSER, “The AFm Phase in Portland Cement,” *Cement and Concrete Research,* vol. 37, pp. 118-130, 2007.

[42] B. LOTHENBACH, G. LE SAOUT, E. GALLUCCI and K. SCRIVENER, “Influence of Limestone on the Hydration of Portland Cements,” *Cement and Concrete Research,* vol. 38, pp. 848-860, 2008.

[43] T. MATSCHEI, B. LOTHENBACH and F. GLASSER, “The Role of Calcium Carbonate in Cement Hydration,” *Cement and Concrete Research,* vol. 37, pp. 551-558, 2007.

[44] M. COLLEPARDI, S. MONOSI and G. MORICONI, “Tetracalcium Aluminoferrite Hydration in the Presence of Lime and Gypsum,” *Cement and Concrete Research,* pp. 431-437, 1979.

[45] J. W. BULLARD, H. M. JENNINGS, R. A. LIVINGSTON, A. NONAT, G. W. S. J. S. SCHERER, K. L. SCRIVENER and J. J. THOMAS, "Mechanisms of Cement Hydration," *Cement and Concrete Research,* vol. 41, pp. 1208-1223, 2011.

[46] I. G. RICHARDSON, C. R. WILDING and M. J. DICKSON, "The Hydration of Blastfurnace Slag Cements," *Advances in Cement Research,* vol. 2, no. 8, pp. 147-157, 1989.

[47] C. HESSE, F. GOETZ-NEUNHOEFFER and J. NEUBAUER, "A New Approach in Quantitative in-Situ XRD of Cement Paste: Correlation of Heat Flow Curves with Early Hydration Reactions," *Cement and Concrete Research,* vol. 41, pp. 123-128, 2011.

[48] W. LERCH, "The Influence of Gypsum on the Hydration of Reactions of Portland Cement," *Proceedings of the American Society for Testing Materials,* vol. 46, pp. 1252-1292, 1946.

[49] S. MINDESS, J. F. YOUNG and D. DARWIN, Concrete, 2nd Edition, New Jersey: Prentice Hall, 2002.

[50] M. ROBLER and I. ODLER, "Investigations on the Relationship Between Porosity, Structure and Strength of Hydrated Portland Cement Pastes I. Effect of Porosity," *Cement and Concrete Research,* vol. 15, pp. 320-330, 1985.

[51] T. C. POWERS and T. L. BROWNYARD, "Studies of the Physical Properties of Hardened Portland Cement Pastes (Part 9)," *Procdeedings of the American Concrete Institute,* vol. 18, pp. 933-992, 1947.

[52] E. KNAPEN, O. CIZER, K. VAN BALEN and D. VAN GEMERT, "Effect of Free Water Removal from Early-Age Hydrated Cement Pastes on Thermal Analysis," *Construction and Building Materials,* vol. 23, pp. 3431-3438, 2009.

[53] D. SNOECK, L. F. VELASCO, A. MIGNON, S. VAN VLIERBERGHE, P. DUBRUEL, P. LODEWYCKX and N. DE BELIE, "The Influence of Different Drying Techniques on the Water Sorption Properties of Cement-Based Materials," *Cement and Concrete Research,* vol. 64, pp. 54-62, 2014.

[54] M. M. C. CANUT, *Pore Structure in Blended Cement Pastes,* Technical University of Denmark: PhD Thesis, 2011.

[55] J. BENSTED and P. BARNES, Structure and Performance of Cements, 2nd edition, London: Spon Press, 2002.

[56] A. R. LEE, Blastfurnace and Steel Slag, London: Edward Arnold Publishers, 1974.

[57] I. G. RICHARDSON, A. R. BROUGH, G. W. GROVES and C. M. DOBSON, "The Characterisation of Hardened Alkali-Activated Blast-Furnace Slag Pastes and the Nature of the Calcium Silicate Hydrate (C-S-H) Phase," *Cement and Concrete Research,* vol. 24, pp. 813-829, 1994.

[58] D. M. ROY and G. M. IDORN, "Hydration, Structure, and Properties of Blast Furnace Slag Cements, Mortars, and Concrete," *American Concrete Institute,* vol. 79, pp. 444-457, 1982.

[59] M. BEN HAHA, G. LE SAOUT, F. WINNEFELD and B. LOTHENBACH, "Influence of Activator Type on Hydration Kinetics Hydrate Assemblage and Micostructural Development of Alkali Activated Blast Furnace Slags," *Cement and Concrete Research,* vol. 41, pp. 301-310, 2001.

[60] T. MATSCHEI, F. BELLMANN and J. STARK, "Hydration Behaviour of Sulphate-Activated Slag Cements," *Advances in Cement Research,* vol. 17, pp. 167-178, 2005.

[61] S. SONG, D. SOHN, H. M. JENNINGS and T. O. MASON, "Hydration of Alkali-activated Ground Granulated Blast Furnace Slag," *Journal of Materials Science,* vol. 35, pp. 249-257, 2000.

[62] K. L. SCRIVENER and A. NONAT, "Hydration of Cementitious Materials, Present and Future," *Cement and Concrete Research,* vol. 41, pp. 651-665, 2011.

[63] S. M. ROIAK and J. C. CHKOLNIK, "Influence des Particularites Physiques et Chimiques Des Laiteris de Haut fourneau sur Leur Activite Hydrauliques," *Proceedings of the 7th International Congress on the Chemistry of Cement,* vol. III, pp. III-74 - III-77, 1980, Paris.

[64] H. UCHIKAWA and S. UCHIDA, "Effect of Character of Glass Phase in Blending Components on their Reactivity in Calcium Hydroxide Mixture," *8th International Congress on the Chemistry of Cement,* vol. 4, pp. 245-250, 1986,Rio de Janeiro.

[65] E. DEMOULIAN, P. GOURDIN, F. HAWTHORN and C. VERNET, "Influence de la composition chimique et de la texture des laitiers sur leur hydraulicité," *Proceedings of the 7th International Congress on the Chemistry of Cement,* vol. III, pp. III-89 - III-94, 1980, Paris.

[66] P. Z. WANG, R. TRETTING, V. RUDERT and T. SPANIOL, "Influence of Al2O3 Content on hydraulic reactivity of Granulated Blast-Furnace Slag, and the Interaction Between Al2O3 and CaO," *Advances in Cement Research,* vol. 16, pp. 1-7, 2004 .

[67] T. ITOH, “Rapid Discrimination of the Character of the Water-Cooled Blast Furnace Slag Used for Portland slag Cement,” *Journal of Materials Science,* vol. 39, pp. 2191-2193, 2004 .

[68] M. BEN HAHA, B. LOTHENBACH, G. LE SAOUT and F. WINNEFELD, “Influence of the Slag Chemistry on the Hydration of Alkali-Activated Blast-Furnace Slag – Part II: Effect of Al2O3,” *Cement and Concrete Research,* vol. 42, pp. 74-83, 2012.

[69] M. BEN HAHA, B. LOTHENBACH, G. LE SAOUT and F. WINNEFELD, “Influence of the Slag Chemistry on the Hydration of Alkali-Activated Blast-Furnace Slag – Part I: Effect of MgO,” *Cement and Concrete Research,* vol. 41, pp. 955-963, 201.

[70] P. K. MEHTA, Pozzolanic and Cementitious By-Products in Concrete: Another Look, edited by Malhotra, V.M., Proceedings of the Third International Conference on the use of Fly Ash, Silica Fume, Slag, and Natural Pozzolans in Concrete, 1989, ed V. M. Malhotra, ACI, Farmington Hills, MI, ACI SP-114, Trondheim, Norway.

[71] M. REGOURD, “Caracteristiques et Activation des Produits d’Addition,,” *8th International Congress on the Chemistry of Cement,* vol. 3, pp. 199-229, Rio de Janeiro, 1986,.

[72] J. I. ESCALANTE-GARCIA, A. F. FUENTES, A. GOROKHOVSKY, P. E. FRAIRE-LUNA and G. MENDOZA-SUAREZ, “Hydration Products and Reactivity of Blast-Furnace Slag Activated by Various Alkalis,” *Journal of the American Ceramic Society,* vol. 86, pp. 2148-2153, 2003.

[73] A. M. RASHAD, Y. BAI, P. A. M. BASHEER, N. B. MILESTONE and N. C. COLLIER, “Hydration and Properties of Sodium Sulfate Activated Slag,” *Cement and Concrete Composites,* vol. 37, pp. 20-29, 2013.

[74] R. KUMAR, S. KUMAR, S. BADJENA and S. MEHROTRA, “Hydration of Mechanically Activated Granulated Blast furnace Slag,” *Metallurgical and Materials Transaction B,* vol. 36, pp. 873-883 , 2005.

[75] M. REGOURD, “Structure and Behaviour of Slag Portland Cement Hydrates,” *Proceedings of the 7th International Congress on the Chemistry of Cement,* vol. III, no. 2, pp. 2/10-12/26, 1980, Paris.

[76] J. M. RICHARDSON, J. J. BIERNACKI, P. E. STUTZMAN and D. P. BENTZ, “Stoichiometry of Slag Hydration with Calcium Hydroxide,” *Journal of the American Ceramic Society,* vol. 85, pp. 947-953, 2002.

[77] J. S. LUMLEY, R. S. GOLLOP, G. K. MOI and H. F. W. TAYLOR, “Degrees of Reaction of the Slag in Some Blends with Portland Cements,” *Cement and Concrete Research,* vol. 26, pp. 139-151, 1996.

[78] R. TAYLOR, R. G. RICHARDSON and R. M. D. BRYDSON, “Composition and Microstructure of 20-year-old Ordinary Portland-Ground Granulated Blast-Furnace Slag Blends Containing 0 to 100% Slag,” *Cement and Concrete Research,* vol. 40, pp. 971-983, 2010.

[79] S. D. WANG, K. L. SCRIVENER and P. L. PRATT, “Factors Affecting the Strength of Alkali-Activated Slag,” *Cement and Concrete Research,* vol. 24, pp. 1033-1043, 1994.

[80] J. BIJEN, “Benefits of Slag and Fly Ash,” *Construction of Building Materials,* vol. 10, no. 5, pp. 309-314, 1996.

[81] E. GRUYAERT, N. ROBEYST and N. BELIE, “Study of the Hydration of Portland Cement Blended With Blast-Furnace Slag By Calorimetry and Thermogravimetry,” *Journal of Thermal Analysis and Calorimetry,* vol. 102, no. 3, pp. 941-951, 2010.

[82] J. I. ESCALANTE, L. Y. GOMEZ, K. K. JOHAL, G. MENDOZA, H. MANCHA and J. MENDEZ, “Reactivity of Blast-Furnace Slag in Portland Cement Blends Hydrated Under Different Conditions,” *Cement and Concrete Research,* vol. 31, pp. 1403-1409, 2001.

[83] K. LUKE and F. P. GLASSER, “Internal Chemical Evolution of the Constitution of Blended Cements,” *Cement and Concrete Research,* vol. 18, pp. 495-502, 1988.

[84] V. KOCABA, E. GALLUCCI and K. L. SCRIVENER, “Methods for Determination of Degree of Reaction of Slags in Blended Cement Pastes,” *Cement and Concrete Research,* pp. 511-525, 2012.

[85] V. KOCABA, “Development and Evaluation of Methods to Follow Microstructural Development Of Cementitious Systems Including Slags,” PhD Thesis, 2009, Ecole Polytechnique Federal de Lausanne.

[86] I. PANE and W. HANSEN, “Investigation of Blended Cement Hydration by Isothermal Calorimetry and Thermal Analysis,” *Cement and Concrete Research,* vol. 35, pp. 1155-1164, 2005.

[87] B. KOLANI, L. BUFFO-CALAFFIERE, A. SELLIER, G. ESCADEILLAS, L. BOUTILLON and L. LINGER, "Hydration of Slag Blended Cements," *Cement and Concrete Composites,* vol. 34, pp. 1009-1018, 2012.

[88] I. G. RICHARDSON, "The nature of C–S–H in hardened cements," *Cement and Concrete Research,* vol. 29, p. 1131–1147, 1999.

[89] E. H. KADRI, S. AGGOUN, G. SCHUTTER and K. EZZIANE, "Combined Effect of Chemical Nature and Fineness of Mineral Powders on Portland Cement Hydration," *Materials and Structures,* vol. 43, pp. 665-673, 2010.

[90] J. I. ESCALANTE-GARCIA and J. H. SHARP, "Effects of Temperature on the Hydration of the Main Clinker Phases in Portland Cements: Part II, Blended Cements," *Cement and Concrete Research,* vol. 28, pp. 1259-1274, 1998.

[91] W. A. GUTTERIDGE and J. A. DALZIEL, "Filler Effect: The Effect of the Secondary Component on the Hydration of Portland Cement Part I. A Fine None-Hydraulic Filler," *Cement and Concrete Research,* vol. 20, pp. 778-782, 1990.

[92] W. A. GUTTERIDGE and J. A. DALZIEL, "Filler Effect: The Effect of the Secondary Component on the Hydration of Portland Cement Part II. Fine Hydraulic Binders," *Cement and Concrete Research,* vol. 20, pp. 778-782, 1990.

[93] E. BERODIER and K. SCRIVENER, "Understanding the Filler Effect on the Nucleation and Growth of C-S-H," *Journal of the American Ceramic Society,* pp. pp. 1-10, [DOI: 10.1111/jace.13177], 2014.

[94] S. J. BARNETT, M. N. M. S. G. SOUTSOS and J. H. BUNGEY, "Strength Development of Mortars Containing Ground Granulated Blast-Furnace Slag: Effect of Curing Temperature and Determination of Apparent Activation Energies," *Cement and Concrete Research,* vol. 36, pp. 434-440, 2006.

[95] A. ONER and S. AKYUZ, "An Experimental Study on Optimum Usage of GGBS for the Compressive Stength of Concrete," *Cement and Concrete Composites,* vol. 29, pp. 505-514, 2007.

[96] V. S. RAMACHANDRAN, "Alkali-Aggregate Expansion Inhibiting Admixtures," *Cement and Concrete Composites,* pp. 149-161, 1998.

[97] R. S. GOLLOP and H. F. W. TAYLOR, "Microstructural and Microanalytical Studies of Sulfate Attack IV – Reactions of a Slag Cement Paste with Sodium and Magnesium Sulfate Solutions," *Cement and Concrete Research,* vol. 26, pp. 1013-1028, 1996.

[98] H. F. W. TAYLOR, C. FAMY and K. L. SCRIVENER, "Delayed Ettringite Formation," *Cement and Concrete Research,* vol. 31, pp. 683-693, 2001.

[99] M. COLLEPARDI, "A State-of-the-Art Review on Delayed Ettringite Attack on Concrete," *Cement and Concrete Composites,* vol. 25, pp. 401-407, 2003.

[100] BS EN 206:2013, "Concrete – Specification, Performance, Production and Conformity," *British Standard Institution,* 2013.

[101] J. MARCHAND and J. P. SKALNY, Materials Science of Concrete: Sulfate Attack Mechanisms, special volume, American Ceramic Society, Ohio, 1999.

[102] J. SKALNY, Materials Science of Concrete III, American Ceramic Society, Ohio, 1992.

[103] P. K. MEHTA, "Sulfate Attack on Concrete – A Critical Review," in *Materials Science of Concrete III,American Ceramic Society*, J. SKALNY, Ed., 1992, pp. 105-130.

[104] RASHEEDUZZAFAR, O. S. B. AL-AMOUDI, S. N. ABDULJAUWAD and M. MASLEHUDDIN, "Magnesium-Sodium Sulfate Attack in Plain and Blended Cements," *Journal of Materials in Civil Engineering,* vol. 6(, no. 2, pp. 201-222, 1994.

[105] P. J. M. MONTEIRO and K. E. KURTIS, "Time to Failure for Concrete Exposed to Severe Sulfate Attack," *Cement and Concrete Research,* vol. 33, pp. 987-993, 2003.

[106] M. L. NEHDI, A. R. SULEIMAN and A. M. SOLIMAN, "Investigation of Concrete Exposed to Dual Sulphate Attack," *Cement and Concrete Research,* vol. 64, pp. 42-53, 2014.

[107] C. YU, W. SUN and K. SCRIVENER, "Mechanism of Expansion of Mortars Exposed in Sodium Sulphate Solutions," *Cement and Concrete Research,* vol. 43, pp. 105-111, 2013.

[108] J. SKALNY, J. MARCHAND and I. ODLER, Sulphate Attack on Concrete, London: Spon, 2002.

[109] W. G. HIME and B. MATHER, "'Sulfate Attack', or is it?," *Cement and Concrete Research,* vol. 29, pp. 789-791, 1999.

[110] M. EGLINGTON, "Resistance of Concrete to Destructive Agencies," in *Lea's Chemistry of Cement*, 4th ed., London, Butterworth-Heinemann, 1998, pp. 299-342.

[111] I. ODLER and J. COLAN-SUBAUSTE, "Investigations on Cement Expansion Associated with Ettringite Formation," *Cement and Concrete Research,* vol. 29, pp. 731-735, 1999.

[112] B. LOTHENBACH, B. BARY, P. LE BESCOP, T. SCHMIDT and N. LETERRIER, "Sulfate Ingress in Portland Cement," *Cement and Concrete Research,* vol. 40, pp. 1211-1225, 2010.

[113] G. J. VERBECK, "Field and Laboratory Studies of the Sulphate Resistance of Concrete, Research Bulletin 227," *Portland Cement Association,* 1967.

[114] C. OUYANG, A. NANNI and W. F. CHANG, "Internal and External Sources of Sulfate Ions in Portland Cement Mortar: Two Types of Chemical Attack," *Cement and Concrete Research,* vol. 18, pp. 699-709, 1998.

[115] M. SANTHANAM, M. D. COHEN and J. OLEK, "Effects of Gypsum Formation on the Performance of Cement Mortars During External Sulfate Attack," *Cement and Concrete Research,* vol. 33, pp. 325-332, 2003.

[116] B. TIAN and M. D. COHEN, "Does Gypsum Formation During Sulphate Attack on Concrete Lead to Expansion," *Cement and Concrete Research,* vol. 30, pp. 117-123, 2000.

[117] M. A. GONZALEZ and E. F. IRASSAR, "Ettringite Formation in Low C3A Portland Cement Exposed to Sodium Sulfate Solution," *Cement and Concrete Research,* vol. 27, pp. 1061-1072, 1997.

[118] J. G. WANG, "Sulfate Attack on Hardened Cement Paste," *Cement and Concrete Research,* vol. 24, pp. 735-742, 1994.

[119] F. BELLMANN, B. MOSER and J. STARK, "Influence of Sulfate Solutions Concentration on the Formation of Gypsum in Sulfate Resistance Test Specimen," *Cement and Concrete Research,* vol. 36, pp. 358-363, 2006.

[120] D. DAMIDOT and F. P. GLASSER, "Thermodynamic Investigation of the CaO-Al2O3-CaSO4-H2O system at 25°C and the Influence of Na2O3," *Cement and Concrete Research,* vol. 23, pp. 221-238, 1993.

[121] R. S. GOLLOP and H. F. W. TAYLOR, "Microstructural and Microanalytical Studies of Sulfate Attack I – Ordinary Portland Cement Paste," *Cement and Concrete Research,* vol. 22, pp. 1027-1038, 1992.

[122] T. SCHMIDT, B. LOTHENBACH, M. ROMER, J. NEUENSCHWANDER and K. SCRIVENER, "Physical and Microstructural Aspects of Sulfate Attack on Ordinary and Limestone Blended Portland Cements," *Cement and Concrete Research,* vol. 39, pp. 1111-1121, 2009.

[123] D. PLANEL, J. SERCOMBE, P. LE BESCOP, F. ADENOT and J.-M. TORRENTI, "Long-Term Performance of Cement Paste During Combined Calcium Leaching-Sulfate Attack: Kinetics and Size Effect," *Cement and Concrete Research,* vol. 36, pp. 137-143 , 2006.

[124] A. CHABRELIE, Mechanisms of Degradation of Concrete by External Sulfate Ions Under Laboratory and Field Conditions, PhD Thesis, EPFL, 2010.

[125] R. EL-HACHEM, E. ROZIERE, F. GRONDIN and A. LOUKILI, "New Procedure to Investigate External Sulphate Attack on Cementitious Materials, Cement and Concrete Composites," vol. 34, pp. 357-364, 2012.

[126] F. ADENOT and M. BUIL, "Modelling of the Corrosion of the Cement Paste By Deionized Water," *Cement and Concrete Research,* vol. 22, pp. 489-496, 1992.

[127] E. REVERTEGAT, C. RICHET and P. GEGOUT, "Effect of pH on the Durability of Cement Pastes," *Cement and concrete Research,* vol. 22, pp. 259-272, 1992.

[128] S. KAMALI, M. MORANVILLE and S. LECLERCQ, "Material and Environmental Parameters Effects on the Leaching of Cement Pastes: Experiments and Modelling," *Cement and Concrete Research,* vol. 38, pp. 575-585, 2008 .

[129] S. KAMALI, B. GERARD and M. MORANVILLE, "Modelling the Leaching Kinetics of Cement-Based Materials – Influence of Materials and Environment," *Cement and Concrete Composites,* vol. 25, pp. 451-458, 2003.

[130] E. ROZIERE and A. LOUKILI, "Performance-based Assessment of Concrete Resistance to Leaching," *Cement and Concrete Composites,* vol. 33, no. 4, pp. 451-456, 2011.

[131] A. GABRISOVA and J. HAVLICA, "Stability of Calcium Sulphoaluminate Hydrates in Water Solutions With Various pH values," *Cement and Concrete Research,* vol. 21, pp. 1023-1027, 1991.

[132] C. CARDE and R. FRANCOIS, “Effect of the Leaching of Calcium Hydroxide from Cement Paste on Mechanical and Physical Properties,” *Cement and Concrete Research,* vol. 27, pp. 539-550, 1997.

[133] E. ROZIERE, A. LOUKILI, R. EL-HACHEM and F. GRONDIN, “Durability of Concrete Exposed to leaching and External Sulphate Attacks,” *Cement and Concrete Research,* vol. 39, pp. 1188-1198, 2009.

[134] P. W. BROWN and H. F. W. TAYLOR, “The Role of Ettringite in External Sulfate Attack,” in *Materials Science of Concrete: Sulfate Attack Mechanism, Special Volume*, J. Marchand and J. Skalny ed., Westerville, OH, The American Ceramic Society, 1999, pp. 73-98.

[135] P. K. MEHTA, “Mechanism of Expansion Associated with Ettringite Formation,” *Cement and Concrete Research,* vol. 3, pp. 1-6, 1973.

[136] P. K. MEHTA and S. WANG, “Expansion of Ettringite by Water Adsorption,” *Cement and Concrete Research,* vol. 12, pp. 121-122, 1982.

[137] H. LAFUMA, “Theorie de L’expansion des Liants Hydrauliques,” *la revue des materiaux de construction et de travaux publics,* pp. Part 1, 243, pp. 441-444,1929 ; part 2, 244, pp. 4-8, 1930.

[138] M. D. COHEN, “Modeling of Expansive Cements,” *Cement and Concrete Research,* vol. 13, pp. 519-528, 1983.

[139] C. W. CORRENS, “Growth and Dissolution of Crystals under Linear Pressure,” *Discussions of the Faraday Society,* vol. 5, pp. 267-271, 1949.

[140] G. W. SCHERER, “Stress from Crystallisation of Salt,” *Cement and Concrete Research,* vol. 34, pp. 1613-1624, 2004.

[141] G. W. SCHERER, “Crystallisation in Pores,” *Cement and Concrete Research,* vol. 29, pp. 1347-1358, 1999.

[142] R. J. FLATT, “Salt Damage in Porous Materials: How High Supersaturations are Generated,” *Journal of Crystal Growth,* vol. 242, pp. 435-454, 2002.

[143] R. J. FLATT and G. W. SCHERER, “Thermodynamics of Crystallization Stresses in DEF,” *Cement and Concrete Research,* vol. 38, pp. 325-336, 2008.

[144] W. MULLAUER, R. E. BEDDOE and D. HEINZ, “Sulfate Attack Expansion Mechanisms,” *Cement and Concrete Research,* vol. 52, pp. 208-215, 2013.

[145] Thaumasite Expert Group, “Thaumasite Expert Group Report One-Year Review, prepared by Professor L A Clark and BRE,” http://www.planningportal.gov.uk/uploads/odpm/4000000009287.pdf, accessed August 2014, 2000.

[146] Thaumasite Expert Group, “Thaumasite Expert Group Report: Review After Three Years Experience, prepared by Professor L A Clark and BRE,” http://www.planningportal.gov.uk/uploads/odpm/4000000009288.pdf, accessed August 2014, 2002.

[147] T. SCHMIDT, B. LOTHENBACH, M. ROMER, K. SCRIVENER, D. RENTSCH and R. FIGI, “A Thermodynamic and Experimental Study of the Conditions of Thaumasite Formation,” *Cement and Concrete Research,* vol. 38, pp. 337-349, 2008.

[148] M. T. BLANCO-VARELA, J. AGUILERA and S. MARTINEZ-RAMIREZ, “ Effect of Cement C3A content, Temperature and Storage Medium on Thaumasite Formation in Carbonated Mortars,” *Cement and Concrete Research,* vol. 36, pp. 707-715, 2006.

[149] Q. ZHOU, J. HILL, E. A. BYARS, J. C. CRIPPS, C. J. LYNSDALE and J. H. SHARP, “The role of pH in Thaumasite Sulfate Attack,” *Cement and Concrete Research,* vol. 36, pp. 160-170, 2006.

[150] E. F. IRASSAR, “Sulfate Attack on Cementitious Materials Containing Limestone Filler – A Review,” *Cement and Concrete Research,* vol. 39, pp. 241-254, 2009.

[151] S. SAHU, S. BADGER and N. THAULOW, “Evidence of Thaumasite Formation in Southern California Concrete,” *Cement and Concrete Composites,* vol. 24, pp. 379-384, 2002.

[152] S. DIAMOND, “Thaumasite in Orange County, Southern California: an Inquiry into the Effect of Low Temperature,” *Cement and Concrete Composites,* vol. 25, pp. 1161-1164, 2003.

[153] H. JUSTNES, “Thaumasite Formed by Sulfate Attack on Mortar with Limestone Filler,” *Cement and Concrete Composites,* vol. 25, pp. 955-959, 2003.

[154] A. M. RAMEZANIANPOUR and R. D. HOOTON, “Thaumasite Sulfate Attack in Portland and Portland-Limestone Cement Mortars Exposed to Sulfate Solution,” *Construction and Building Materials,* vol. 40, pp. 162-173, 2013.

[155] P. NOBST and J. STARK, “Investigations on the Influence of Cement Type on Thaumasite Formation,” *Cement and Concrete Composites,* vol. 25, pp. 899-906, 2003.

[156] J. AGUILERA, S. MARTINEZ-RAMIREZ, I. PAJARES-COLOMO and M. T. BLANCO-VALERA, “Formation of Thaumasite in Carbonated Mortars,” *Cement and Concrete Composites,* vol. 25, pp. 991-996, 2003.

[157] F. BELLMANN and J. STARK, “The role of Calcium Hydroxide in the Formation of Thaumasite,” *Cement and Concrete Research,* vol. 38, pp. 1154-1161, 2008.

[158] K. TORII, K. TANIGUCHI and M. KAWAMURA, “Sulfate Resistance of High Fly Ash Conctent Concrete,” *Cement and Concrete Research,* vol. 25, pp. 759-768, 1995.

[159] ASTM C1012/C1012M-13, “Standard Test Method for Length Change of Hydraulic-Cement Mortars Exposed to a Sulfate Solution,” *American Society for Testing and Materials, 04.01,* 2013.

[160] J. BENSTED, “Thaumasite – Background and Nature in Deterioration of Cements,” *Mortars and Concretes, Cement and Concrete Composites,* vol. 21, pp. 117-121, 1999.

[161] D. MACPHEE and S. DIAMOND, “Thaumasite in Cementitious Materials,” *Cement and Concrete Composites,* vol. 25, pp. 805-807, 2003.

[162] M. COLLEPARDI, “Thaumasite Formation and Deterioration in Historic Buildings,” *Cement and Concrete Composites,* vol. 21, pp. 147-154, 1999.

[163] D. E. MACPHEE and S. J. BARNETT, “Solution Properties of Solids in the Ettringite-Thaumasite Solid Solution Series,” *Cement and Concrete Research,* pp. 1591-1598, 2004.

[164] S. J. BARNETT, D. E. MACPHEE and N. J. CRAMMOND, “Extent of Immiscibility in the Ettringite-Thaumasite System,” *Cement and Concrete Composites,* vol. 25, pp. 851-855, 2003.

[165] D. DAMIDOT, S. J. BARNETT, F. P. GLASSER and D. E. MACPHEE, “Investigation of the CaO-Al2O3-SiO2-CaSO4-CaCO3-H2O system at 25°C by Thermodynamic Calculations,” *Advances in Cement Research,* vol. 16, pp. 69-76, 2004 .

[166] S. KOHLER, D. HEINZ and L. URBONAS, “Effect of Ettringite on Thaumasite Formation,” *Cement and Concrete Research,* vol. 36, pp. 697-706, 2006.

[167] J. BENSTED, “Thaumasite – Direct, Woodfordite and Other Possible Formation Routes,” *Cement and Concrete Composites,* vol. 25, pp. 873-877, 2003.

[168] N. J. CRAMMOND, “The Thaumasite Form of Sulfate Attack in the UK,” *Cement and Concrete Composites,* vol. 25, pp. 809-818, 2003.

[169] F. BELLMANN, W. ERFURT and H.-M. LUDWIG, “Field Performance of Concrete Exposed to Sulphate and Low pH Conditions from Natural and Industrial Sources,” *Cement and Concrete Composites,* vol. 34, pp. 86-93, 2012.

[170] K. PETTIFER and P. J. NIXON, “Alkali Metal Sulphate – A Factor Common to Both Alkali Aggregate Reaction and Sulphate Attack on Concrete,” *Cement and Concrete Research,* pp. 173-181, 1980.

[171] M. SANTHANAM, M. D. COHEN and J. OLEK, “Mechanism of Sulfate Attack: a Fresh Look Part I: Summary of Experimental Results,” *Cement and Concrete Research,* vol. 32, pp. 915-921, 2002.

[172] M. SANTHANAM, M. D. COHEN and J. OLEK, “Mechanism of Sulfate Attack: a Fresh Look Part II: Proposed Mechanisms,” *Cement and Concrete Research ,* vol. 33, pp. 341-346 , 2003.

[173] O. S. B. AL-AMOUDI, “Attack on Plain and Blended Cements Exposed to Aggressive Sulfate Environments,” *Cement and Concrete Composites,* vol. 24, pp. 305-316, 2002.

[174] R. S. GOLLOP and H. F. W. TAYLOR, “Microstructural and Microanalytical studies of Sulfate Attack III. Sulfate-Resisting Portland Cement: Reactions with Sodium and Magnesium Sulfate Ions,” *Cement and Concrete Research,* vol. 25, pp. 1581-1590, 1995.

[175] D. BONEN and M. D. COHEN, “Magnesium Sulfate Attack on Portland Cement Paste II. Chemical and Mineralogical Analyses,” *Cement and Concrete Research,* vol. 22, pp. 707-718, 1992.

[176] W. KUNTHER, B. LOTHENBACH and K. L. SCRIVENER, “Deterioration of Mortar Bars Immersed in Magnesium Containing Sulfate Solutions,” *Materials and Structures,* vol. 46, pp. 2003-2011, 2013.

[177] A. SKAROPOULOU, K. SOTIRIADIS, G. KAKALI and S. TSIVILIS, "Use of Mineral Admixtures to Improve the Resistance of Limestone Cement Concrete Against Thaumasite Form of Sulfate Attack," *Cement and Concrete Composites,* vol. 37, pp. 267-275, 2013.

[178] L. BARCELO, E. GARTNER, R. BARBARULO, A. HOSSACK, R. AHANI, M. THOMAS, D. HOOTON, E. BROUARD, A. DELAGRAVE and B. BLAIR, "A modified ASTM C1012 Procedure for Quantifying Blended Cements Containing Limestone and SCMs for Use in Sulfate-Rich Environments," *Cement and Concrete Research,* vol. 63, pp. 75-88, 2014.

[179] P. S. MANGAT and J. M. EL-KHATIB, "Influence of Fly Ash, Silica Fume and Slag on sulfate Resistance of Concrete," *ACI Materials Journal,* vol. 92, no. 5, pp. 542-552, 1995.

[180] F. IRASSAR and O. BATIC, "Effects of Low Calcium Fly Ash on Sulfate Resistance of OPC Cement," *Cement and Concrete Research,* vol. 19, pp. 194-202, 1989.

[181] K. TORII and M. KAWAMURA, "Effects of Fly Ash and Silica Fume on the Resistance of Mortar to Sulfuric Acid and Sulfate Attack," *Cement and Concrete Research,* vol. 24, pp. 361-370, 1994.

[182] E. R. DUNSTAN, "A Possible Method for Identifying Fly Ashes that will Improve the Sulfate Resistance of Concrete," *Cement, Concrete, and Aggregates,* vol. 2, no. 1, pp. 20-30, 1980.

[183] S. T. LEE, H. Y. MOON and R. N. SWAMY, "Sulfate Attack and Role of Silica Fume in Resisting Strength Loss," *Cement and Concrete Composites,* vol. 27, pp. 65-76, 2005.

[184] H.-W. SONG, S.-W. PACK, S.-H. NAM, J.-C. JANG and V. SARASWATHY, "Estimation of the Permeability of Silica Fume Cement Concrete," *Construction and Building Materials,* vol. 24, pp. 315-321, 2010.

[185] S. OGAWA, T. NOZAKI, K. YAMADA, H. HIRAO and R. D. HOOTON, "Improvement on Sulfate Resistance of Blended Cement with High Alumina Slag," *Cement and Concrete Research,* vol. 42, pp. 244-251, 2012.

[186] M. KOMLJENOVIĆ, Z. BAŠČAREVIĆ, N. MARJANOVIĆ and V. NIKOLIĆ, "External Sulfate Attack on Alkali-Activated Slag," *Construction and Building Materials,* vol. 49, pp. 31-39, 2013.

[187] V. FERNANDEZ-ALTABLE, Availability of Al2O3 in Slag Blended Cements: Sulphate Attack Implications, Final Conference of the NANOCEM Marie Curie Research Training Network, Villars-sur-Ollon, September 1-3, 2009.

[188] R. B. FREEMAN and R. L. CARRASQUILLO, "Adjustment in Gypsum Content for the Production of Sulfate-Resistant Blended Cements Containing High-Calcium Fly Ash," *ACI Materials Journal,* vol. 92, no. 4, pp. 411-418, 1995.

[189] H. HAYNES, R. O'NEILL, M. NEFF and P. K. MEHTA, "Salt Weathering Distress on Concrete Exposed to Sodium Sulfate Environment," *ACI Materials Journal,* vol. 105, no. 1, pp. 35-43, 2008.

[190] N. THAULOW and S. SAHU, "Mechanism of Concrete Deterioration due to Salt Crystallization," *Materials Characterisation,* vol. 53, pp. 123-127, 2004.

[191] C. RODRIGUEZ-NAVARRO, E. DOEHNE and E. SEBASTIAN, "How does Sodium Crystallize? Implications for the Decay and Testing of Building Materials," *Cement and Concrete Research,* vol. 30, pp. 1527-1534, 2000.

[192] N. TSUI, R. J. FLATT and G. W. SCHERER, "Crystallization Damage by Sodium Sulfate," *Journal of Cultural Heritage,* vol. 4, pp. 109-115, 2003.

[193] M. STEIGER and S. ASMUSSEN, "Crystallization of Sodium Sulfate Phases in Porous Materials: The Phase Diagram NaSO4-H2O and the Generation of Stresses," *Geochimica et Cosmochimica Acta,* vol. 72, pp. 4291-3406, 2008.

[194] D. McMAHON, P. SANDBERG, K. FOLLIARD and P. MEHTA, "Deterioration Mechanisms of Sodium Sulfate," in *Proceedings of the 7th International Congress on Deterioration and Conservation of Stone*, Lisbon, 1992.

[195] M. SAHMARAN, "Sodium Sulphate Attack on Blended Cements under Different Exposure Conditions," *Advances in Cement Research,* vol. 19, no. 2, pp. 47-56, 2007.

[196] E. F. IRASSAR, A. DI MAIO and O. R. BATIC, "Sulfate Attack on Concrete with Mineral Admixtures," *Cement and Concrete Research,* vol. 26, pp. 113-123, 1996.

[197] G. A. NOVAK and A. A. COLVILLE, "Efflorescent Mineral Assemblages Associated with Cracked and Degraded Residential Concrete Foundations in Southern California," *Cement and Concrete Research,* vol. 19, pp. 1-6, 1989.

[198] W. H. HARRISON, Sulphate Resistance of Buried Concrete: Third Report on a Long Term Investigation at Northwick Park and on Similar Concretes in Sulphate Solutions, Building Research Establishment, Publication BR 164, Garston, 1992.

[199] T. DRIMALAS, Laboratory and Field Evaluations of External Sulfate Attack, PhD Thesis, University of Texas, Austin, 2007.

[200] J. STROH, M.-C. SCHLEGEL, E. IRASSAR, B. MENG and F. EMMERLING, "Applying High Resolution SyXRD Analysis on Sulfate Attacked Concrete Field Samples," *Cement and Concrete Research,* vol. 66, pp. 19-26, 2014.

[201] RILEM TC 25-PEM, "Recommended Tests to Measure the Deterioration of Stone and to Assess the Effectiveness of Treatment Methods," *Materials and Structures,* vol. 13, pp. 175-253, 1980.

[202] C. FERRARIS, P. STUTZMAN, M. PELTZ and J. WINPIGLER, "Developing a More Rapid Test to Assess Sulfate Resistance of Hydraulic Cements," *Journal of Research of the National Institute of Standards and Technology,* vol. 110, pp. 529-540, 2005.

[203] P. S. MANGAT and J. M. EL-KHATIB, "Influence of Initial Curing on Sulphate Resistance of Blended Cement Concrete," *Cement and Concrete Research,* vol. 22, pp. 1089-1100, 1992.

[204] R. EL-HACHEM, E. ROZIERE, F. GRONDIN and A. LOUKILI, "Multi-Criteria Analysis of the Mechanism of Degradation of Portland Cement Based Mortars Exposed to External Sulphate Attack," *Cement and Concrete Research,* vol. 42, pp. 1327-1335, 2012.

[205] N. M. AL-AKHRAS, "Durability of Metakaolin Concrete to Sulfate Attack," *Cement and Concrete Research,* vol. 36, pp. 1727-1734 , 2006.

[206] M. SAHMARAN, O. KASAP, K. DURU and I. O. YAMAN, "Effects of Mix Composition and Water-Cement Ratio on the Sulfate Resistance of Blended Cements," *Cement and Concrete Composites,* vol. 29, pp. 159-167, 2007.

[207] R. P. KHATRI and V. SIRIVIVATNANON, "Role of Permeability in in Sulphate Attack," *Cement and Concrete Research,* vol. 27, pp. 1179-1189, 1997.

[208] B. BOURDETTE, E. RINGOT and J. P. OLLIVER, "Modelling of the Transition Zone Porosity," *Cement and Concrete Research,* vol. 25, pp. 741-751, 1995.

[209] J. P. OLLIVIER, J. C. MASO and B. BOURDETTE, "Interfacial Transition Zone in Concrete," *Advances in Cement Based Materials,* vol. 2, no. 1, pp. 30-38, 1995.

[210] A. BONAKDAR, B. MOBASHER and N. CHAWLA, "Diffusivity and Micro-Hardness of Blended Cement Materials Exposed to External Sulfate Attack," *Cement and Concrete Composites,* vol. 34, pp. 76-85, 2012.

[211] D. BONEN and S. L. SARKAR, "Replacement of Portlandite by Gypsum in the Interfacial Zone Related to Crystallization Pressure," *Ceramic Transaction, 95th Annual Meeting, Cement-Based Materials: Present, Future, and Environmental Aspects, ACI, Westerville, OH,* pp. 49-60, 1993.

[212] H. T. CAO, L. BUCEA, A. RAY and S. YOZGHATLIAN, "The Effect of Cement Composition and pH of Environment of Sulfate Resistance of Portland and Blended Cements," *Cement and Concrete Composites,* vol. 19, pp. 161-171 , 1997.

[213] P. W. BROWN, "An Evaluation of the Sulfate Resistance of Cements in a Controlled Environment," *Cement and Concrete Research,* vol. 11, pp. 719-727, 1981.

[214] J. ZHANG and G. W. SCHERER, "Comparison of Methods for Arresting Hydration," *Cement and Concrete Research,* vol. 41, pp. 1024-1036, 2011.

[215] N. C. COLLIER, J. H. SHARP, H. J. MILESTONE and I. H. GODFREY, "The Influence of Water Removal Techniques on the Composition and Microstructure of Hardened Cement Pastes," *Cement and Concrete Research,* vol. 38, pp. 737-744, 2008.

[216] L. ZHANG and F. P. GLASSER, "Critical Examination of Drying Damage to Cement Pastes," *Advances in Cement Research,* vol. 12, no. 2, pp. 79-88, 2000.

[217] Q. ZHOU, E. E. LACHOWSKI and F. P. GLASSER, "Metaettringite, a Decomposition Production of Ettringite," *Cement and Concrete Research,* vol. 34, pp. 703-710, 2004.

[218] L. KONECNY and S. J. NAQVI, "The Effect of Different Drying Techniques on the Pore Size Distribution of Blended Cement Mortars," *Cement and Concrete Research,* vol. 23, pp. 1223-1228, 1993.

[219] C. GALLE, “Effect of Drying on Cement Based Materials Pore Structure as Identified by Mercury Intrusion Porosimetry – a Comparative Study Between Oven, Vacuum and Freeze Drying,” *Cement and Concrete Research,* vol. 31, pp. 1467-1477, 2001.

[220] A. KORPA and R. TRETTIN, “The Influence of different Drying Methods on Cement Paste Microstructures as Reflected by Gas Adsorption: Compartions Between Freeze Drying (F-Drying), D-Drying, P-Drying and Oven Drying Methods,,” *Cement and Concrete Research, ,* vol. 36, pp. 634-649, 2006.

[221] H. F. W. TAYLOR and A. TURNER, “Reactions of Tricalcium Silicate Paste with Organic Liquids,” *Cement and Concrete Research,* vol. 17, pp. 613-623, 1987.

[222] G. LE SAOUT, T. FULLMAN, V. KOCABA and K. L. SCRIVENER, “Quantitative Study of Cementitious Materials by X-Ray Diffraction/Rietveld Analysis Using an External Method,” in *Proceedings of the 12th International Congress on the Chemistry of Cement*, Montreal.

[223] K. K. ALIGIZAKI, Pore Structure of Cement-Based Materials: Testing, Interpretation an Requirements, London and New York: Taylor and Francis, 2006.

[224] R. L. DAY and B. K. MARSH, “Measurement of Porosity in Blended Cement Pastes,” *Cement and Concrete Research,* vol. 18, pp. 119-122, 1988.

[225] L. WADSO, “Applications of an Eight-Channel Isothermal Conduction Calorimeter for Cement Hydration Studies,” *Cement International,* vol. 5, no. 3, pp. 94-101, 2005.

[226] L. WADSO, “Operational Issues in Isothermal Calorimetry,” *Cement and Concrete Research,* vol. 40, pp. 1129-1137, 2010.

[227] G. DE SHUTTER and L. TAERWE, “Specific Heat and Thermal Diffusivity of Hardening Concrete,” *Magazine of Concrete Research,* vol. 47, no. 172, pp. 203-208, 1995.

[228] M. COSTOYA, Effect of Particle Size on the Hydration Kinetics and Microstructural Development of Tricalcium Silicate, PhD Thesis, Ecole Polytechnique Federale de Lausanne, 2008 .

[229] H. LE CHATELIER and J. LATHROP MACK, Experimental Researches on the Constitution of Hydraulic Mortars, New York: McGraw Publishing Company, 1905.

[230] Japan Concrete Institute, “Comittee Report,” in *Autogenous Shrinkage of Concrete*, E. TAZAWA, Ed., London, E and FN Spon, 1999, pp. 1-68.

[231] M. GEIKER, Studies of Portland Cement Hydration by Measurements of Chemical Shrinkage and a Systematic Evalution of Hydration Curves by Means of the Dispersion Model, PhD thesis, Technical University of Denmark, 1983.

[232] G. SANT, P. LURA and J. WEISS, “Measurement of Volume Change in Cementitious Materials at Early Ages – Review of Testing Protocols and Interpretation of Results,” *Journal of the Transportation Research Board,* pp. 21-29, 2006.

[233] V. S. RAMACHANDRAN, “Thermal Analysis,” in *Handbook of Analytical Techniques in Concrete Science Technology – Principles, Techniques and Applications*, V. S. RAMACHANDRAN and J. J. BEAUDOIN, Eds., William Andrew Publishing, 2001, pp. 127-173.

[234] W. W. WENDLANDT, Thermal Methods of Analysis, 2nd, Ed., New York: Wiley-Interscience, 1974.

[235] A. K. CHATTERJI, “X-Ray Diffraction,” in *Handbook of Analytical Techniques in Concrete Science Technology – Principles, Techniques and Applications*, V. S. RAMACHANDRAN and J. J. BEAUDOIN, Eds., William Andrew Publishing, 2001, pp. 275-332.

[236] I. U. o. Crystallography, The Rietveld Method, R. A. YOUNG, Ed., Oxford: Oxford University Press, 2002.

[237] M. A. G. ARANDA, A. G. DE LA TORRE and L. LEON-REINA, “Rietveld Quantitative Phase Analysis of OPC Clinkers, Cements and Hydration Products,” *Reviews in Mineralogy and Geochemistry,* vol. 74, pp. 169-209, 2012.

[238] G. LE SAOUT, V. KOCABA and K. L. SCRIVENER, “Application of the Rietveld Method to the Analysis of Anhydrous Cement,” *Cement and concrete Research,* vol. 41, pp. 133-148, 2011.

[239] G. CAGLIOTI, A. PAOLETTI and F. P. RICCI, “Choice of Collimators for a Crystal Spectrometer for Neutron Diffraction,” *Nuclear Instruments,* vol. 3, pp. 223-228, 1958.

[240] L. B. McCUSKER, R. B. VON DREELE, D. E. COX, D. LOUER and P. SCARDI, “Rietveld Refinement Guidelines,” *Journal of Applied Crystallography,* vol. 32, pp. 36-50, 1999.

[241] W. A. DOLLASE, “Correction of Intensities for Preferred Orientation in Powder Diffractometry: Application of the March Model,” *Journal of Applied Crystallography,* vol. 19, pp. 262-272 , 1986.

[242] E. J. SONNEVELD and J. W. VISSER, "Automatic Collection of Powder Data from Photographs," *Journal of Applied Crystallography,* vol. 8, no. 1, pp. 1-7, 1975.

[243] N. V. Y. SCARLETT and I. C. MADSEN, "Quantification of Phases with Partial or No Known Crystal Stucture," *Powder Diffraction,* vol. 21, pp. 278-284, 2006.

[244] S. T. BERGOLD, F. GOETZ-NEUNHOEFFER and J. NEUBAUER, "Quantitative Analysis of C-S-H in Hydrating Alite Pastes by in-situ XRD," *Cement and Concrete Research,* vol. 53, pp. 119-126, 2013.

[245] R. SNELLINGS, A. SALZE and K. L. SCRIVENER, "Use of X-Ray Diffraction to Quantify Amorphous Supplementary Cementitious Materials in Anhydrous and Hydrated Blended Cements," *Cement and Concrete Research,* vol. 64, pp. 89-98, 2014.

[246] W. A. KLEMM and J. SKALNY, "Selective Dissolution of Clinker Minerals and Its Applications," *Martin Marietta Technical Report, 77-32,* 1997.

[247] P. STUTZMAN, "Guide for X-Ray Powder Diffraction Analysis of Portland Cement Clinker," *National Institute of Standards and Technology, NISTIR 5755,* 1996.

[248] F. NISHI, Y. TAKEUCHI and I. MAKI, "Tricalcium silicate Ca3O [SiO4]: the monoclinic superstructure," *Zeitschrift für Kristallographie-Crystalline Materials ,* Vols. 172.1-4, pp. 297-314, 1985.

[249] T. TSURUMI, Y. HIRANO, H. KATO, T. KAMIYA and M. DAIMON, "Crystal Structure and Hydration of Belite," *Ceramic Transactions,* vol. 13, no. 40, pp. 19-25, 1994.

[250] P. MONDAL and J. W. JEFFERY, "The crystal structure of tricalcium aluminate, Ca3Al2O6," *Acta Crystallographica, Section B,* vol. 31, pp. 689 - 697, 1975.

[251] F. NISHI and Y. TAKEUCHI, "The Al6 O18 rings of tetrahedra in the structure of Ca8.5 Na Al6 O18," *Acta Crystallographica, Section B,* vol. 31, pp. 1169-1173, 1975.

[252] J. MALVEIRO, T. RAMOS, L. P. FERREIRA, J. C. M. R. WAERENBORGH, M. GODINHO and M. D. CARVALHO, "Magnesium doping on brownmillerite Ca2FeAlO5," *Journal of Solid State Chemistry,* vol. 180, no. 6, pp. 1863-1874, 2007.

[253] A. KIRFEL and G. WILL, "Charge density in anhydrite, CaSO4, from X-ray and neutron diffraction measurements," *Acta Crystallographica, Section B,* vol. 36, pp. 2881-2890, 1980.

[254] H. WEISS and M. F. BRAEU, "How much water does calcined gypsum contain?," *Angewandte Chemie, International Edition,* vol. 48, pp. 3520-3524, 2009.

[255] K. OJIMA, Y. NISHIHATA and A. SAWADA, "Structure of Potassium Sulfate at Temperatures from 296 K down to a5 K," *Acta Crystallographica, Section B,* vol. 51, pp. 287-293, 1995.

[256] S. ONO, J. P. BRODHOLT and G. D. PRICE, "First-Principles Simulation of High-Pressure Polymorphs in MgAl2O4," *Physics and Chemistry of Minerals,* vol. 35, pp. 381-386, 2008 .

[257] H. SITEPU, "Texture and Structural Refinement Using Neutron Diffraction Data From Molybdite (MoO3) and Calcite (CaCO3) Powders and in a Ni-rich Ni50.7Ti49.30 Alloy," *Powder Diffraction Journal,* vol. 24, pp. 315-326, 2009.

[258] Q. HUANG, O. CHMAISSEM, J. J. CAPONI, C. CHAILLOUT, M. MAREZIO, J. L. THOLENCE and A. SANTORO, "Neutron Powder Diffraction Study of the Crystal Structure of HgBa2Ca4Cu5O12+d at Room Temperature and at 10K," *Physica, C:Superconductivity,* vol. 227, pp. 1-9, 1994.

[259] H. E. PETCH, "The Hydrogen Position in Portlandite, Ca(OH)2, as Indicated by the Electron Distribution," *Acta Crystallographica,* vol. 14, pp. 950-957, 1961.

[260] F. GOETZ NEUNHOEFFER and J. NEUBAUER, "Refined Ettringite (Ca6Al2(SO4)3(OH)12.26H2O) Structure for Quantitative X-ray Diffraction Analysis," *Powder Diffraction,* vol. 21, pp. 4-11, 2006.

[261] T. RUNCEVSKI, R. E. DINNEBIER, O. V. MAGDYSYUK and H. POELLMANN, "Crystal Structures of Calcium Hemicarboaluminate and Carbonated Calcium Hemicarboaluminate from Synchrotron Powder Diffraction Data," *Acta Crystallographica, Section B,* vol. 68, pp. 493-500, 2012.

[262] M. FRANCOIS, G. RENAUDIN and O. EVRARD, "A Cementitious Compound with Composition 3CaO.Al2O3.CaCO3.11H2O," *Acta Crystallographica, Section C,* vol. 54, pp. 1214-1217, 1998.

[263] R. ALLMANN, "Refinement of the Hybrid Layer Structure (Ca2Al(OH)6)+(0.5SO4.3H2O)+," *Neues Jahrbuch Fuer Mineralogie,* pp. 136-144, 1977.

[264] M. BELLOTTO, B. REBOURS, O. CLAUSE, J. LYNCH, D. BAZIN and E. ELKAIM, "A Reexamination of hydrotalcite Crystal Chemistry," *Journal of Physical Chemistry,* vol. 100, pp. 8527-8534 , 1996.

[265] B. O'CONNOR and M. D. RAVEN, "Application of the Rietveld Refinement Procedure in Assaying Powdered Mixtures," *Powder Diffraction Journal,* vol. 3, pp. 2-6, 1988.

[266] M. SCHREYER, L. GUO, M. TJAHJONO and M. GARLAND, "Three Approaches to Total Quantitative Phase Analysis of Organic Mixtures Using an External Standard," *Journal of Applied Crystallography,* vol. 44, pp. 17-24, 2011.

[267] D. JANSEN, F. GOETZ-NEUNHOEFFER, C. STABLER and J. NEUBAUER, "A Remastered External Standard Method Applied to the Quantification of Early OPC hydration," *Cement and Concrete Research,* vol. 41, pp. 602-608, 2011.

[268] D. JANSEN, C. STABLER, F. GOETZ-NEUNHOEFFER, S. DITTRICH and J. NEUBAUER, "Does Ordinary Portland Cement Contain Amorphous Phase? A Quantitative Study Using an External Standard Method," *Powder Diffraction Journal,* vol. 26, pp. 31-38, 2011.

[269] D. JANSEN, F. GOETZ-NEUNHOEFFER, B. LOTHENBACH and J. NEUBAUER, "The Early Hydration of Portland Cement (OPC): An Approach Comparing Measured Heat Flow With Calculated Heat Flow Measured from QXRD," *Cement and Concrete Research,* vol. 42, pp. 134-138, 2012.

[270] E. PRINCE, International Tables for Crystallography, Volume C, 2004.

[271] D. JANSEN, S. T. BERGOLD, F. GOETZ-NEUNHOEFFER, B. LOTHENBACH and J. NEUBAUER, "The Hydration of Alite: a Time-Resolved Quantitative X-ray Diffraction Approach Using the G –Factor Method Compared With Heat Release," *Journal of Applied Crystallography,* vol. 44, pp. 895-901, 2011.

[272] K. L. SCRIVERNER, "Backscattered Electron Imaging of Cementitious Microstructures: Understanding and Quantification," *Cement and Concrete Composites,* vol. 26, pp. 935-945, 2004.

[273] JEOL, A Guide to Scanning Electron Microscope Obsevation, http://www.jeolusa.com/RESOURCES/ElectronOptics/DocumentsDownloads/tabid/320/Default.aspx?EntryId=1, accessed July 2014.

[274] E. GALLUCCI, X. ZHANG and K. L. SCRIVENER, "Effect of Temperature on the Microsctructure of Calcium Silicate Hydrate (C-S-H)," *Cement and Concrete Research,* vol. 53, pp. 185-195, 2013.

[275] C. FAMY, K. L. SCRIVENER and A. K. CRUMBIE, "What causes differences of C-S-H gel grey levels in backscattered electron images?," *Cement and Concrete Research,* vol. 32, no. 9, pp. 1465-1471, 2002.

[276] K. L. SCRIVENER, H. H. PATEL, P. L. PRATT and L. J. PARROTT, "Analysis of Phases in Cement Paste Using Backscattered Electron Images, Methanol Adsorption and Thermogravimetric Analysis," *Materials Research Society Symposium Proceedings,* vol. 85, pp. 67-76, 1987.

[277] X. BRUNETAUD, M. R. KHELIFA and M. AL-MUKHTAR, "Size Effect of Concrete Samples on the Kinetics of External Sulfate attack," *Cement and Concrete Composites,* vol. 32, pp. 370-376, 2012.

[278] A. BENTUR, "Effect of gypsum on the hydration and strength of C3S pastes," *Journal of the American Ceramic Society,* vol. 59, no. 5-6, pp. 210-213, 1976.

[279] I. JELENIC, A. PANOVIC, R. HALLE and T. GACESA, "Effect of Gypsum on the Hydration and Strength Development of Commercial Portland Cements Containing Alkali Sulfates," *Cement and Concrete Research,* vol. 7, pp. 239-246, 1977.

[280] B. K. MARSH and R. L. DAY, "Pozzolanic and cementitious reactions of fly ash in blended cement pastes," *Cement and Concrete Research,* vol. 18, pp. 301-310, 1988.

[281] M. ZAJAC, A. ROSSBERG, G. LE SAOUT and B. LOTHENBACH, "Influence of limestone and anhydrite on the hydration Portland cements," *Cement and Concrete Composites,* vol. 46, pp. 99-108, 2014.

[282] C. LABBEZ, I. POCHARD, A. NONAT and B. JONSSON, "Colloidal behavior of C-S-H nanohydrates in cement paste," *Proceedings of the CONMOD; Lausanne, Switzerland,* 2010.

[283] C. SHI and R. L. DAY, "A Calorimetric Study of Early Hydration of Alkali-Slag Cements," *Cement and Concrete Research,* vol. 25, pp. 1333-1346, 1995.

[284] B. LOTHENBACH, "Thermodynamic Equilibrium Calculations in Cementitious Systems," *Materials and Structures,* vol. 43, pp. 1413-1433, 2010.

[285] P. LAWRENCE, M. C Y R and E. RINGOT, "Mineral Admixtures in Mortars – Effect of Inert Materials on Short Term Hydration," *Cement and Concrete Research,* vol. 33, pp. 853-861, 2003.

[286] H. MINARD, S. GARRAULT, L. REGNAUD and A. NONAT, "Mechanisms and Parameters Controlling the Tricalcium Aluminate Reactivity in the Presence of Gypsum," *Cement and Concrete Research,* vol. 37, pp. 1418-1426.

[287] D. DUTTA and P. C. BORTHAKUR, "Activation of Low Lime High Alumina Granulated Blast Furnace Slag by Anhydrite," *Cement and Concrete Research,* vol. 20, pp. 711-722, 1990.

[288] P. TERMKHAJORNKIT and T. NAWA, "Composition of C-S-H in the hydration products of fly ash—cement system," in *Proceedings CANMET, ninth international conference fly ash, silica fume, slag and natural Pozzolan in concrete*, Warssaw, Poland, 2007.

[289] T. ISHIDA, Y. LUAN, T. SAGAWA and T. NAWA, "Modelling of Early Age Behaviour of Blast Furnace Slag Concrete Based on Micro-Physical Properties," *Cement and Concrete Research,* vol. 41, pp. 1357-1367, 2011.

[290] I. G. RICHARDSON and G. W. GROVES, "The structure of the calcium silicate hydrate phases present in hardened pastes of white Portland cement blast-furnace slag blends," *Journal of Materials Science,* vol. 32, no. 18, p. 4793–4802, 1997.

[291] L. E. COPELAND and D. L. KANTRO, "Hydration of Portland cement," *5th International Congress on the Chemistry of Cement, Tokyo,* vol. 2, pp. 387-420, 1968.

[292] R. BARBARULO, H. PEYCELON and S. LECLERCQ, "Chemical equilibria between C–S–H and ettringite, at 20 and 85 °C," *Cement and Concrete Research,* vol. 37, pp. 1176-1181, 2007.

[293] G. KALALI, S. TSIVILIS, E. AGGELI and M. BATI, "Hydration products of C3A, C3S and Portland cement in the presence of CaCO3," *Cement and Concrete Research,* vol. 30, pp. 1073-1077, 2000.

[294] H. J. KUZEL and H. POLLMAN, "Hydration of C3A in the Presence of Ca(OH)2, CaSO4.2H2O and CaCO3," *Cement and Concrete Research,* vol. 21, pp. 885-895, 1991.

[295] S. D. WANG and K. L. SCRIVENER, "Hydration Products of Alkali Activated Sag Cement," *Cement and Concrete Research,* vol. 25, pp. 561-571, 1994.

[296] M. REGOURD, "Cements Made from Blastfurnace Slag," in *Lea's Chemistry of Cement*, London, Butterworth-Heinemann, 1998, pp. 637-678.

[297] G. W. BRINDLEY and S. KIKKAWA, "A crystal-chemical study of Mg,Al and Ni,N hydroxy-perchlorates and hydroxycarbonates," *American Mineralogist,* vol. 64, no. 7-8, pp. 836-843, 1979.

[298] S. IGARASHI, M. KAWAMURA and A. WATANABE, "Analysis of cement pastes and mortars by a combination of backscatter-based SEM image analysis and calculations based on the Powers model," *Cement and Concrete Composites,* vol. 26, p. 977–985, 2004.

[299] M. ZAJAC and M. BEN HAHA, "Experimental investigation and modeling of hydration and performance evolution of fly ash cement," *Materials and Structures,* vol. 47, pp. 1259-1269 , 2013.

[300] H. M. JENNINGS, "Refinements to colloid model of C-S-H in cement: CM-II," *Cement and Concrete Research,* vol. 38, p. 275–289, 2008.

[301] J. J. THOMAS, J. J. CHEN and H. M. JENNINGS, "Ca-OH Bonding in the C-S-H Gel Phase of Tricalcium Silicate and White Portland Cement Pastes Measured by Inelastic Neutron Scattering," *Chemistry of Materials,* p. 15, 3813-3817.

[302] E. GALLUCCI, E. COSTOYA, A. QUENNOZ and K. SCRIVENER, "In-Situ C-S-H Density Measured with Continous Analytical Methods - Influence of Particle Size and Hydration Conditions," in *11th International Congress on the Chemistry of Cement*, Madrid, 2011.

[303] P. TERMKHAJORNKIT, Q. H. VU, R. BARBARULO, S. DARONNAT and G. CHANVILLARD, "Dependence of Compressive Strength on Phase Assemblage in Cement Pastes: Beyond Gel-Space Ratio – Experimental Evidence and Micromechanical Modelling," *Cement and Concrete Research.*

[304] S. GUNAY, G. S, A. NONAT and P. TERMKHAJORNKIT, "Influence of Calcium Sulphate on Hydration and Mechanical Strength of Tricalcium silicate," *Proceedings of the 13th ICCC, Madrid,* 2011.

[305] M. MEDALA, Etudes des Interactions entre les phases minérales constituant le ciment Portland et des solutions salinesées, PhD Thesis, Dijon, 2005.

[306] R. SERSALE, R. CIOFFI, G. FRIGIONE and F. ZENONE, "Relationship Between Gypsum Content, Porosity and Strength in Cement," *Cement and Concrete Research,* vol. 21, pp. 120-126, 1991.

[307] P. FAUCON, A. DELAGRAVE, J. C. PETIT, C. RICHET, J. M. MARCHAND and H. ZANNI, "Aluminium Incorporation in Calcium Silicate Hydrates (C-S-H) Depending on their Ca/Si Ratio," *Journal of Physical Chemistry B,* vol. 103, no. 37, pp. 7796-7802, 1999.

[308] A. NEVILLE, "The Confused World of Sulfate Attack on Concrete," *Cement and Concrete Research ,* vol. 34, pp. 1275-1296, 2004.

[309] M. SANTHANAM, M. D. COHEN and J. OLEJK, "Sulphate Attack Research - Whither Now?," *Cement and Concrete Research,* vol. 31, pp. 845-851, 2001.

[310] D. HEINZ, W. MULLAUER and R. E. BEDDOE, “Mechanismen des Sulfatangriffs auf Beton - Aspekte des Chemischen und Physikalischen Widerstands,” in *Ibausil*, Weirmar, 2012.

[311] W. KUNTHER, B. LOTHENBACH and J. SKIBSTED, “Influence of the Ca/Si ratio of the C-S-H Phase on the Interaction with Sulfate Ions and its Impact on the Ettringite Crystallisation Pressure,” *Cement and Concrete Research,* vol. 69, pp. 37-49, 2015.

Appendices

A.1. Observations of Mortar Prisms Exposed to External Sulfates

Appendix A offers the visual observations of the mortar prisms exposed to sulfate solution by the end of the testing period, e.g. ~100 weeks. Of all the investigated systems, only the neat system showed appreciable damage (Figure A.1 through Figure A.5). In this sample, cracking occurred at the corners of the specimen.

Figure A.1 – Visual Observation of Mortar Prism C_1 After Exposure to Sulfates

Figure A.2 – Visual Observation of Mortar Prism C_140S_b After Exposure to Sulfates

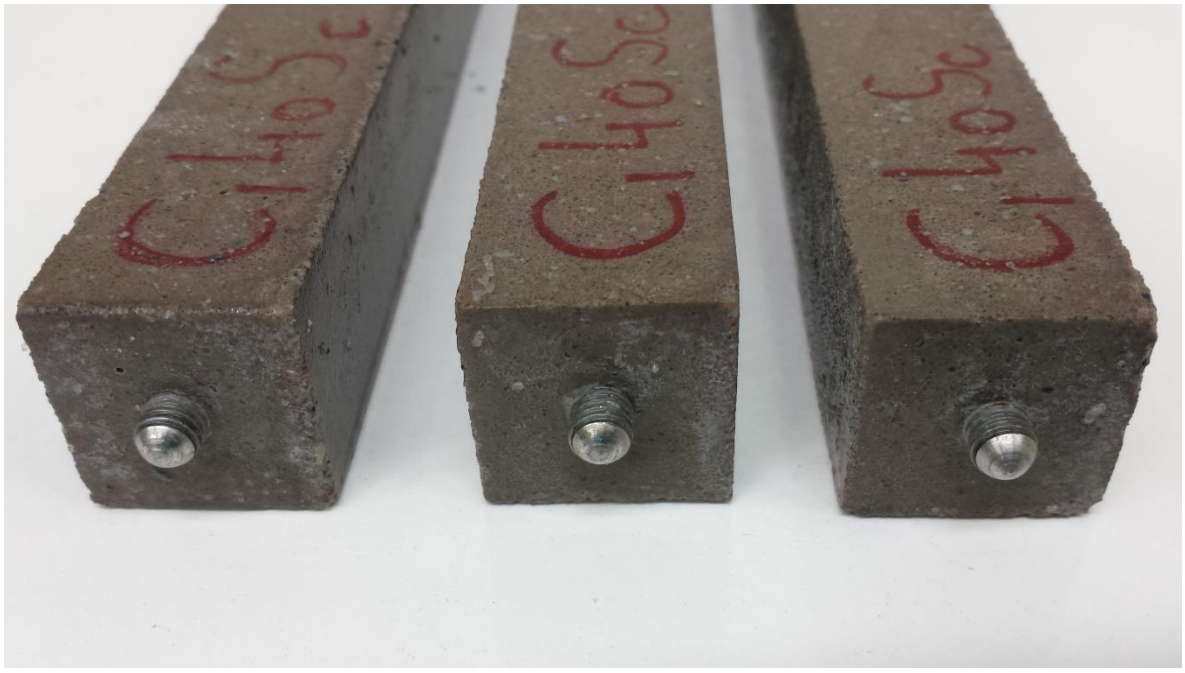

Figure A.3 – Visual Observation of Mortar Prism C_140S_c After Exposure to Sulfates

Figure A.4 – Visual Observation of Mortar Prism $C_1 40 S_c \$$ After Exposure to Sulfates

Figure A.5 – Visual Observation of Mortar Prism $C_1 70 S_c$ After Exposure to Sulfates

A.2. **Pastes Sample Exposed to a Sulfate Solution**

Only the neat system had shown macroscopic damage after just 56 days of curing in a sulfate solution (Figure A.6). Cracking had formed at both along the length of the sample and the near the faces of the cylinders. All the slag blends showed no damage after such a short exposure time.

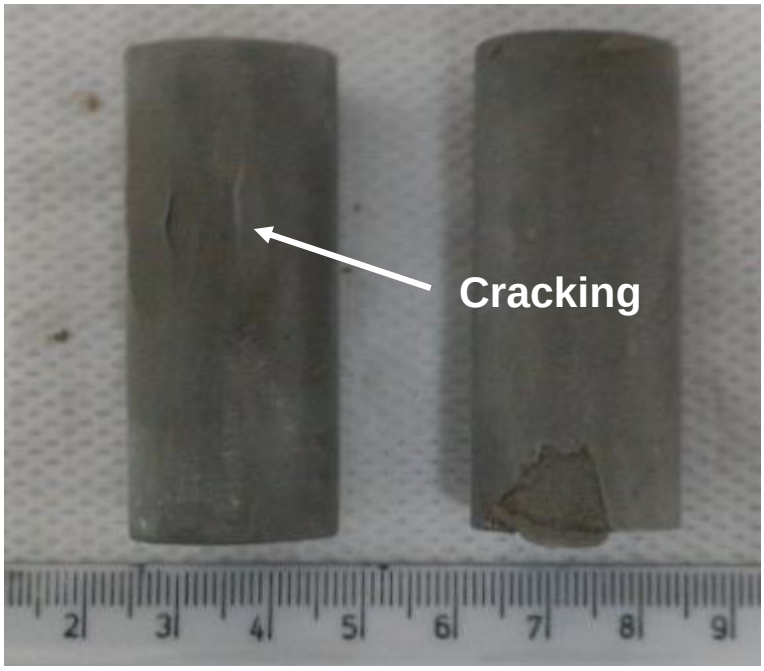

Figure A.6 – Visual Observation of Paste C_1 Exposed to Sulfates for 56 Days

After 180 days of curing in a sulfate solution, the neat system C_1 was heavily damaged (Figure A.7). Of all the slag composite cements, only C_140S_c started showing signs of fatigue (Figure A.8); the faces of the sample was marked with cracking along its edge. Gradually, the first 1 mm of the sample was effectively spalling off the core.

Figure A.7 – Visual Observation of Paste C_1 Exposed to Sulfates for 180 Days

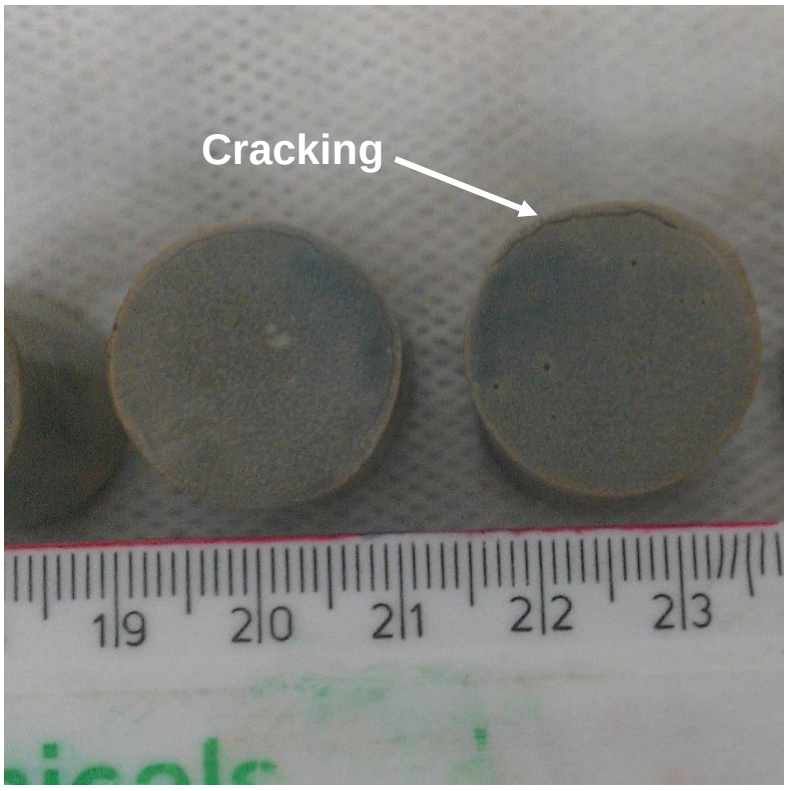

Figure A.8 – Visual Observation of Paste C_140S_c Exposed to Sulfates for 180 Days

After 360 days of curing in a sulfate solution, all samples showed some form of damage (Figure A.9 through Figure A.13). By then, All the slag blended systems had shown some sign of damage, with cracks appearing near the faces of the sample. Between all the blends prepared with 40 % slag, blend C_140S_c had shown the largest amount of cracking. Subsituting slag C for B, the latter being the poorest in aluminium, or adding sulfates in the mix design, had significantly improved resistance. The same effect was observed by increasing the slag content.

Figure A.9 – Visual Observation of Paste C_1 Exposed to Sulfates for 360 Days

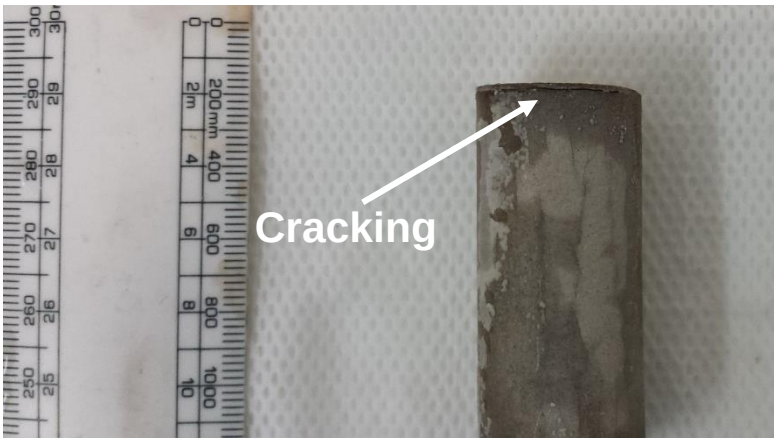

Figure A.10 – Visual Observation of Paste C_140S_b Exposed to Sulfates for 360 Days

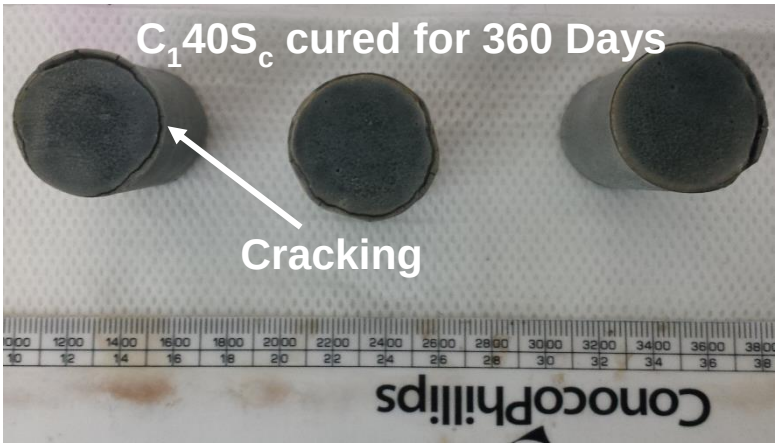

Figure A.11 – Visual Observation of Paste $C_1 40 S_c$ Exposed to Sulfates for 360 Days

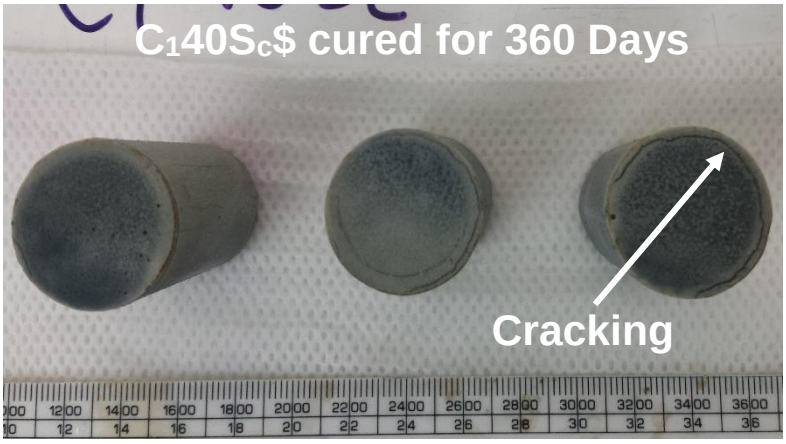

Figure A.12 – Visual Observation of Paste $C_1 40 S_c$\$ Exposed to Sulfates for 360 Days

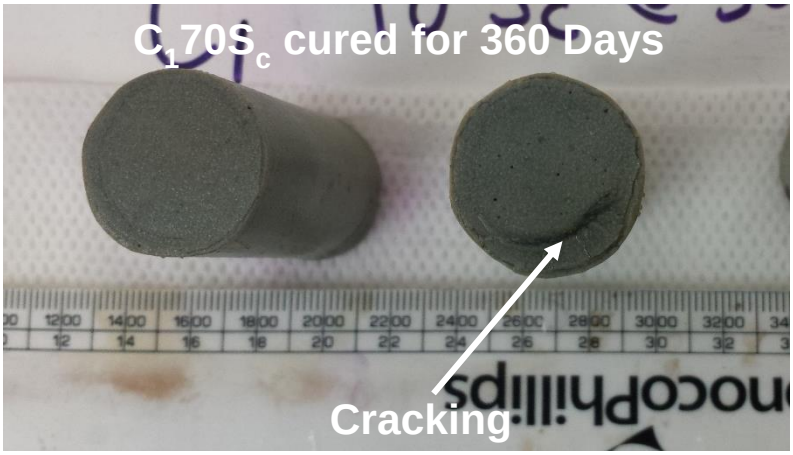

Figure A.13 – Visual Observation of Paste $C_1 70 S_c$ Exposed to Sulfates for 360 Days

A.3. **Expansion of all 28 Mortar Prisms Exposed to External Sulfates**

The following plots detail the expansion of all 28 mixes prepared with time (Figure A.14 through Figure A.16). The plots have been grouped to best separate the impact of cement type, slag content, and sulfate content. However, the sulfate resistance of all slag blends proved excellent, making any comparing between slag blends difficult.

From the expansion plots of the neat systems, it can however be seen that the neat cement had expanded the most, when comparing C_1 with C_2. The benefit of additional sulfate into the mix design also proved beneficial, and blend C_1\$ had expanded less than the sulfate free analogue. The impact of slag loading can also guessed in blends using cement C_1; the blends richest in slag had expanded less than all blends containing 40% slag.

Impact of Cement Type

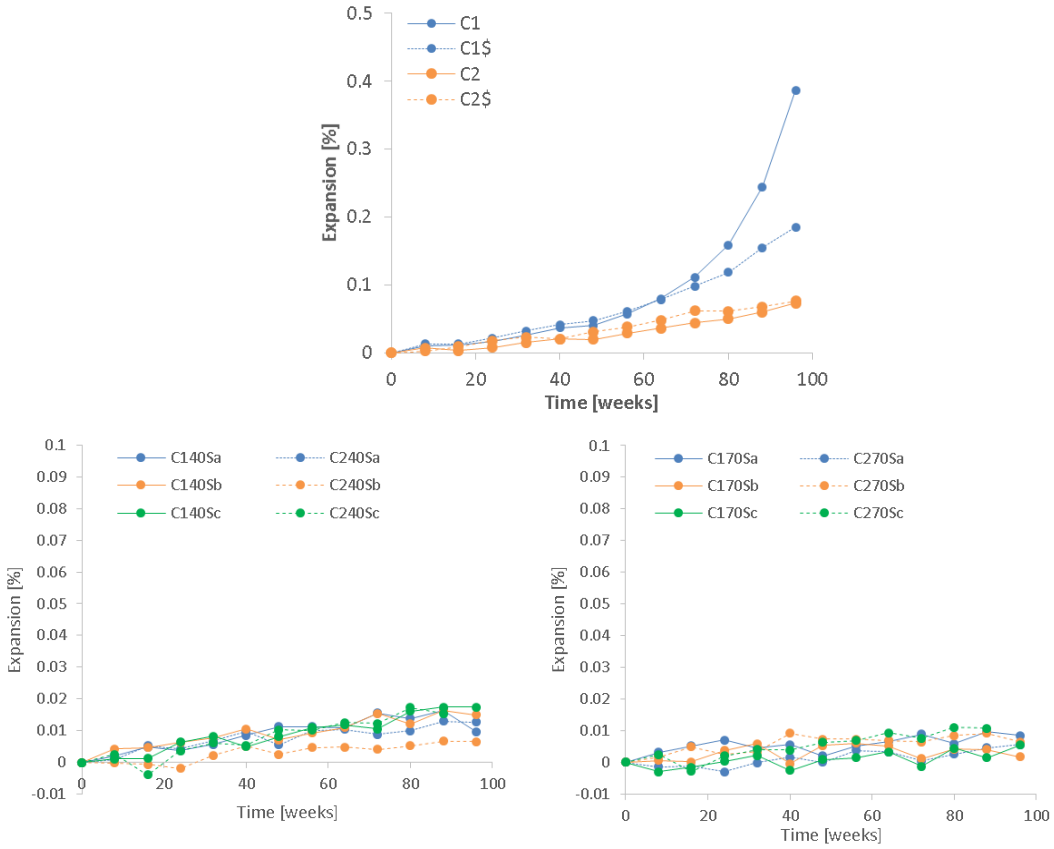

Figure A.14 – Impact of Cement Type on Expansion of Mortar Prisms

Impact of Slag Content

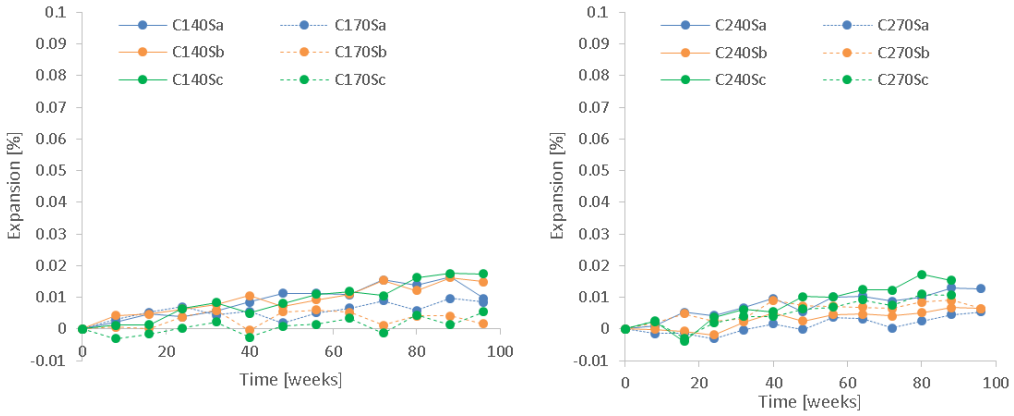

Figure A.15 – Impact of Slag Content on Expansion of Mortar Prisms

Impact of Additional Sulfate

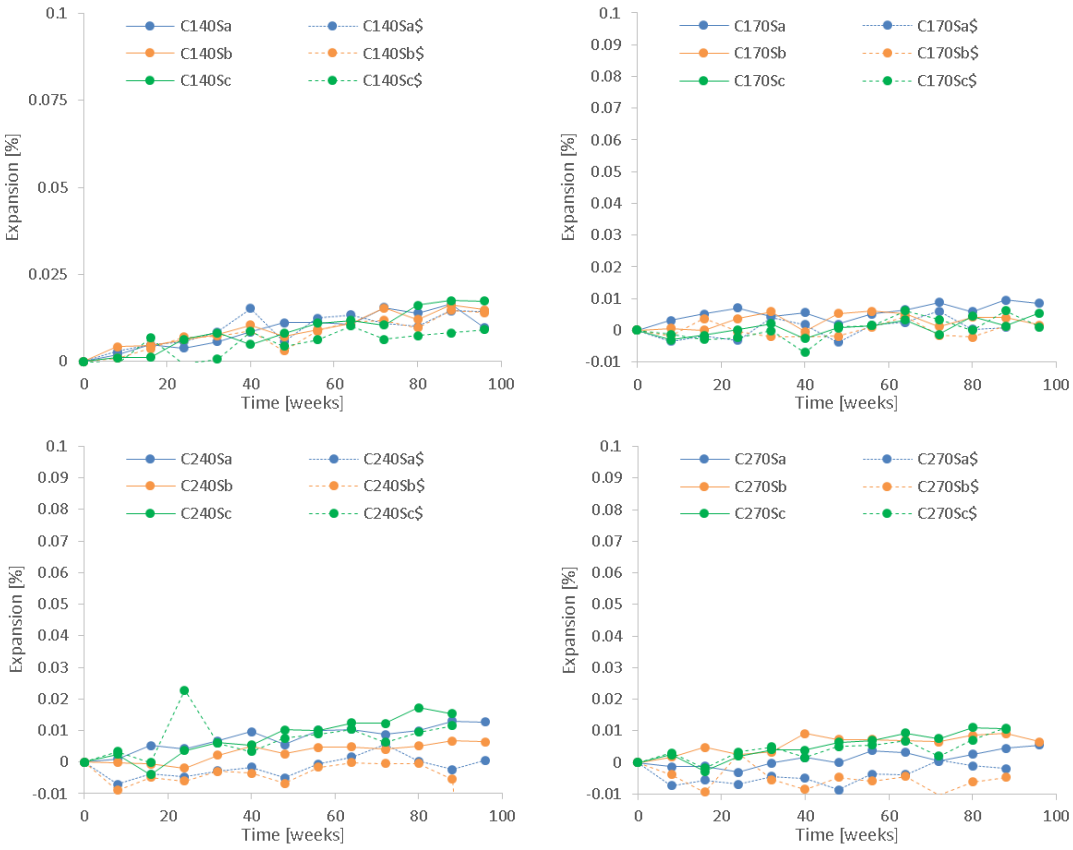

Figure A.16 – Impact of Additional Sulfate on Expansion of Mortar Prisms

A.4. Changes in Ca/Si and Al/Si of the C-S-H phase Measured on Pastes Exposed to Sulfates

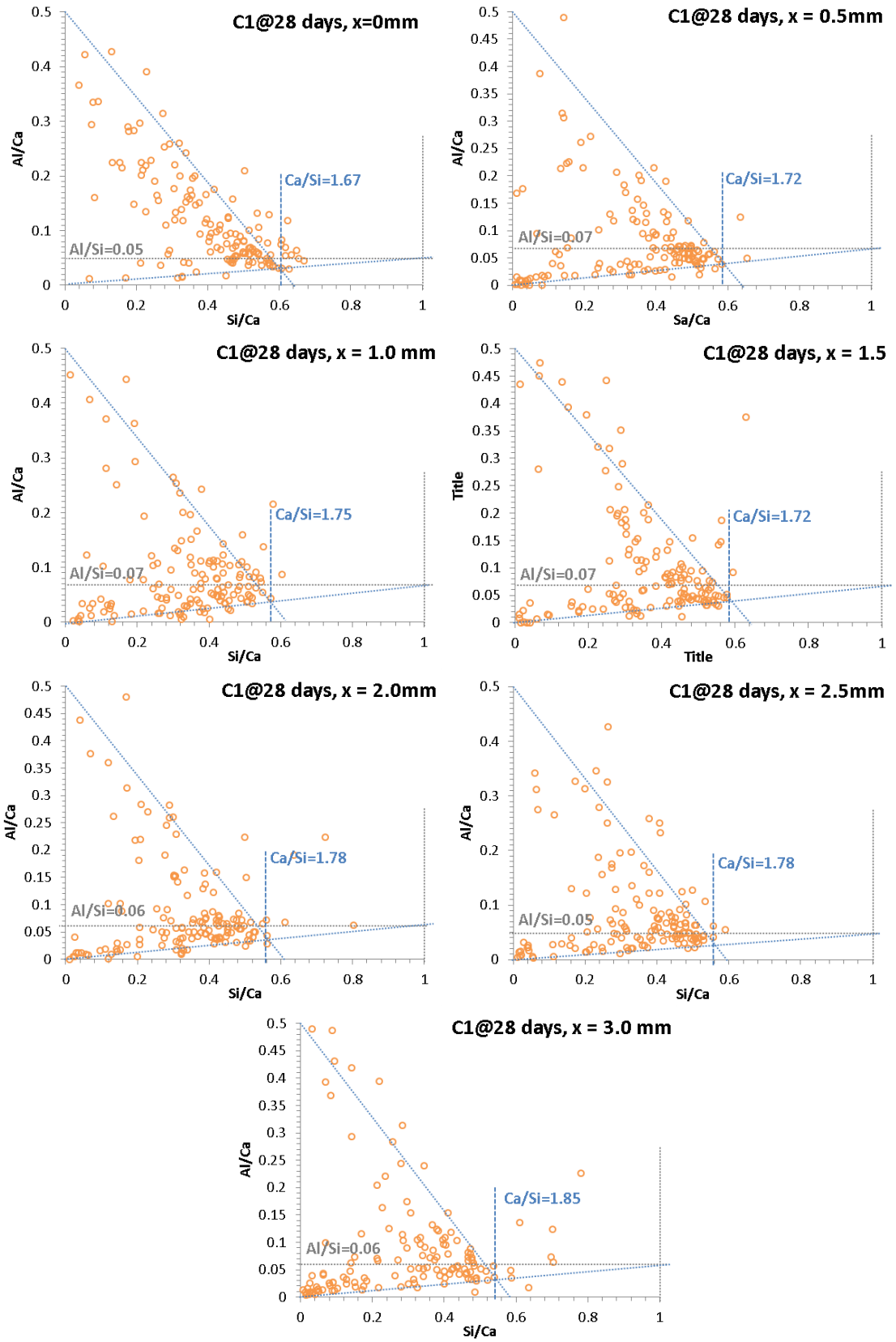

Figure A.17 – Changes in C-S-H Composition in C_1 Cured for 28 days in a 3 $g.L^{-1}$ Na_2SO_4 Solution

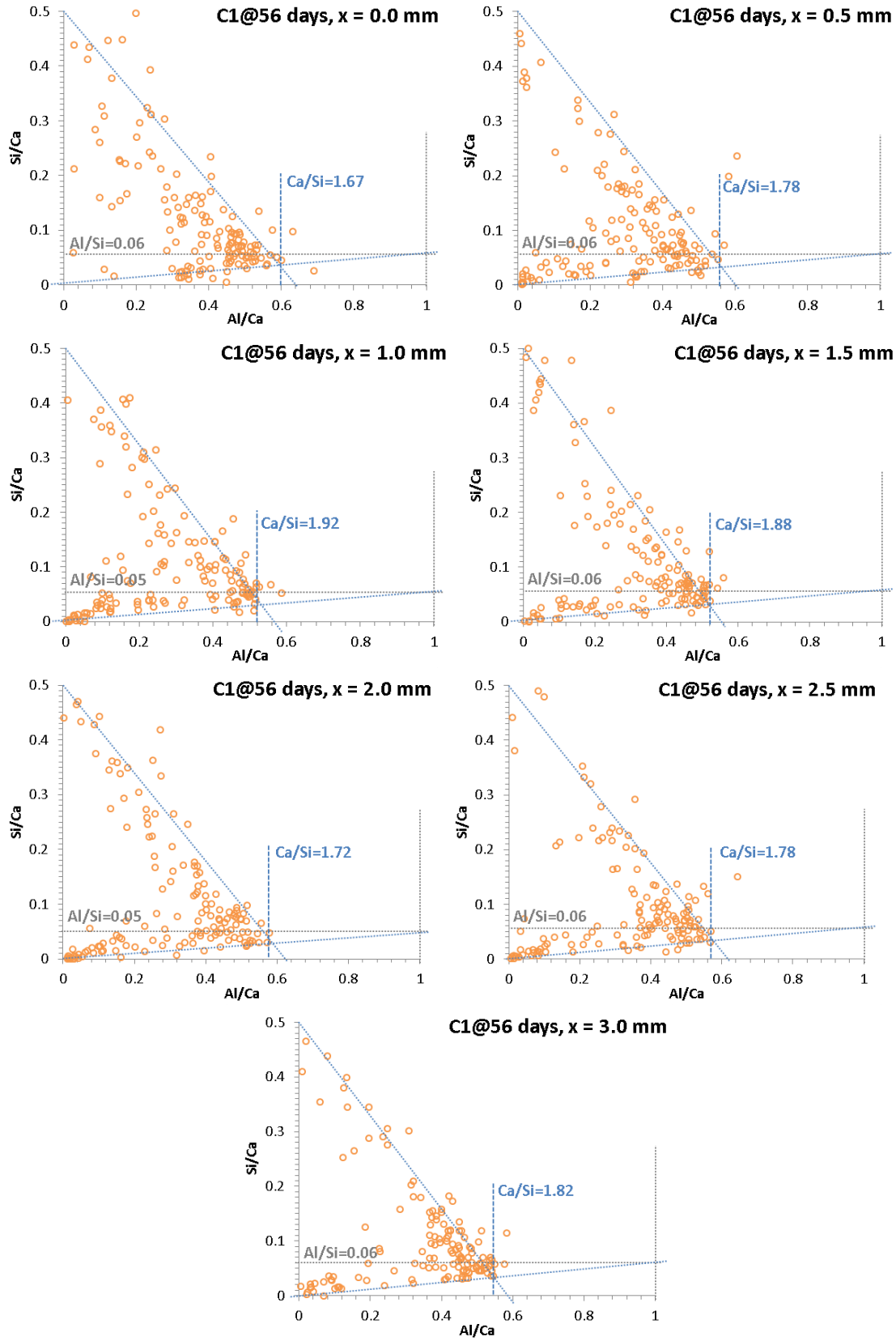

Figure A.18 – Changes in C-S-H Composition in C_1 Cured for 56 days in a 3 g.L^{-1} Na_2SO_4 Solution

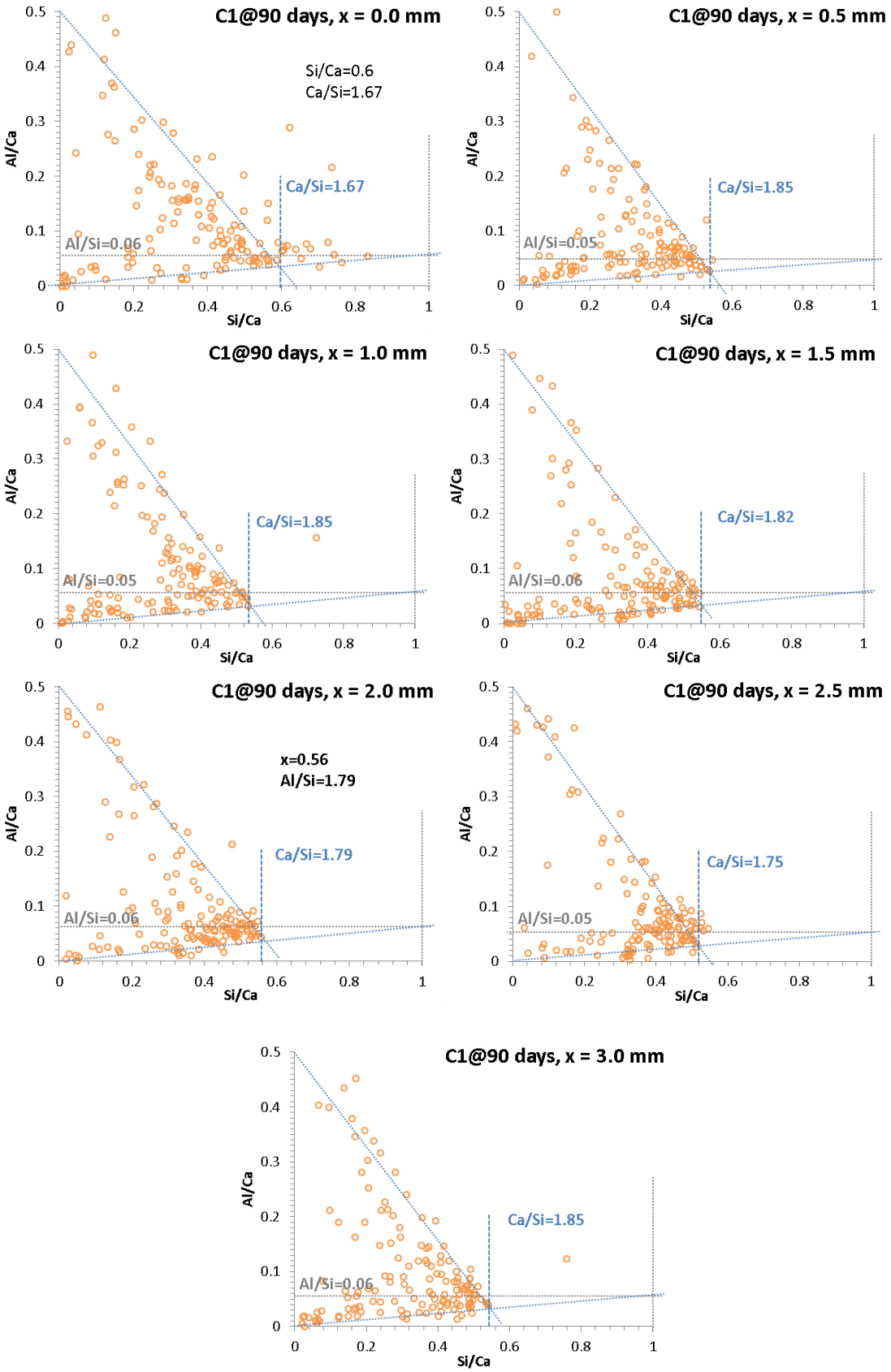

Figure A.19 – Changes in C-S-H Composition in C_1 Cured for 90 days in a 3 g.L^{-1} Na_2SO_4 Solution

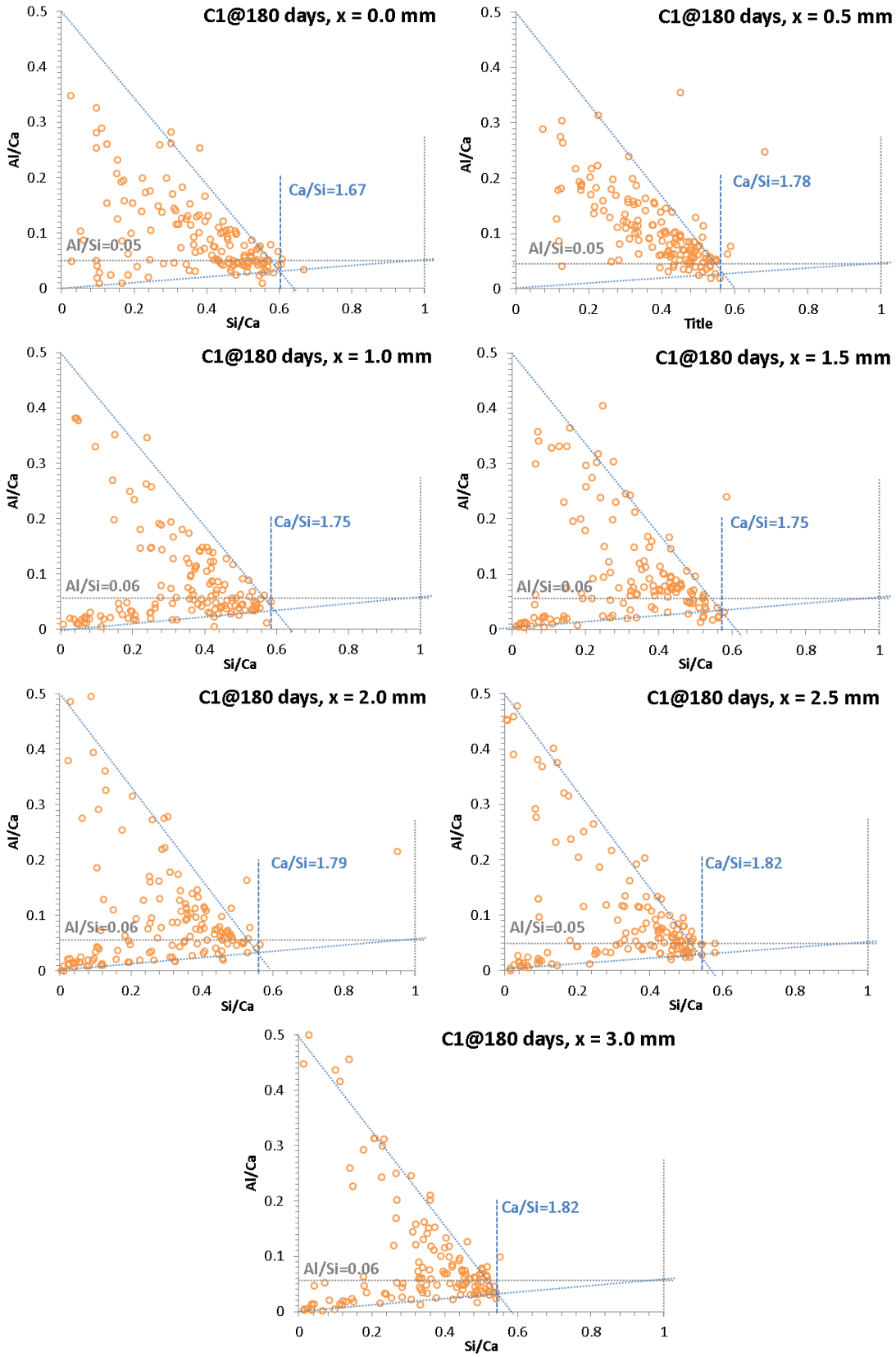

Figure A.20 – Changes in C-S-H Composition in C_1 Cured for 180 days in a 3 g.L^{-1} Na_2SO_4 Solution

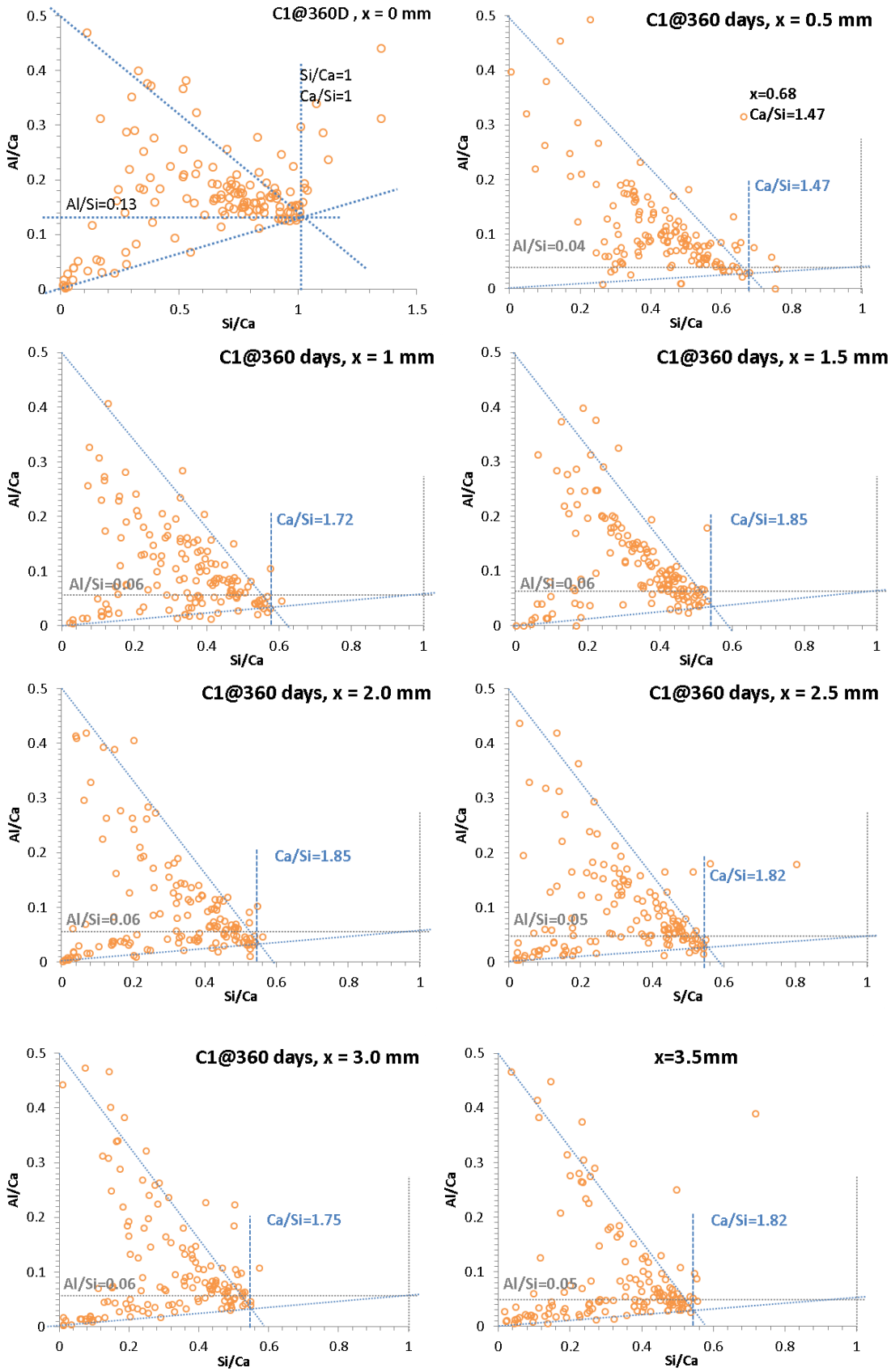

Figure A.21 – Changes in C-S-H Composition in C_1 Cured for 360 days in a 3 g.L^{-1} Na_2SO_4 Solution

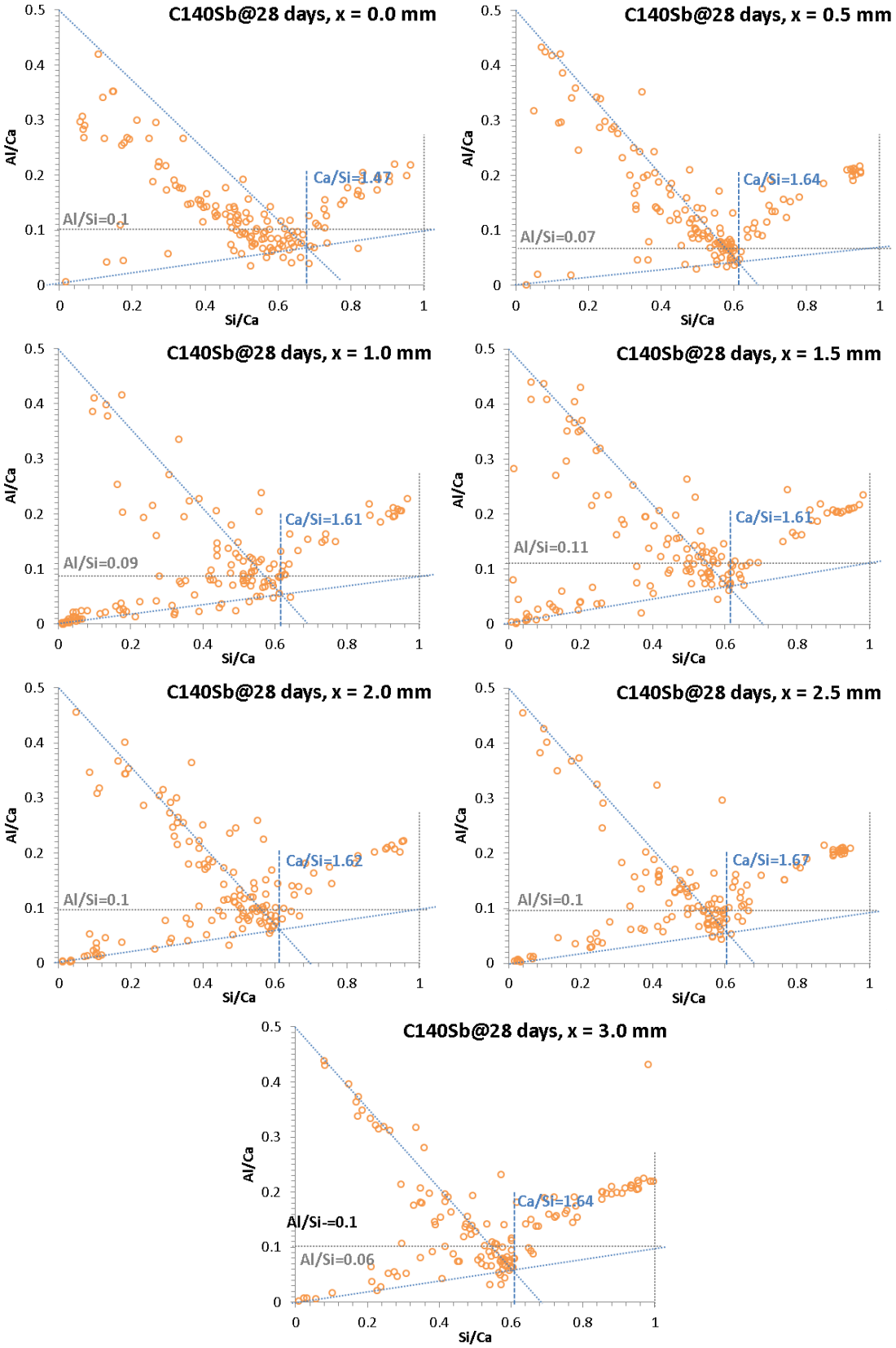

Figure A.22 – Changes in C-S-H Composition in C_140S_b Cured for 28 days in a 3 g.L^{-1} Na_2SO_4 Solution

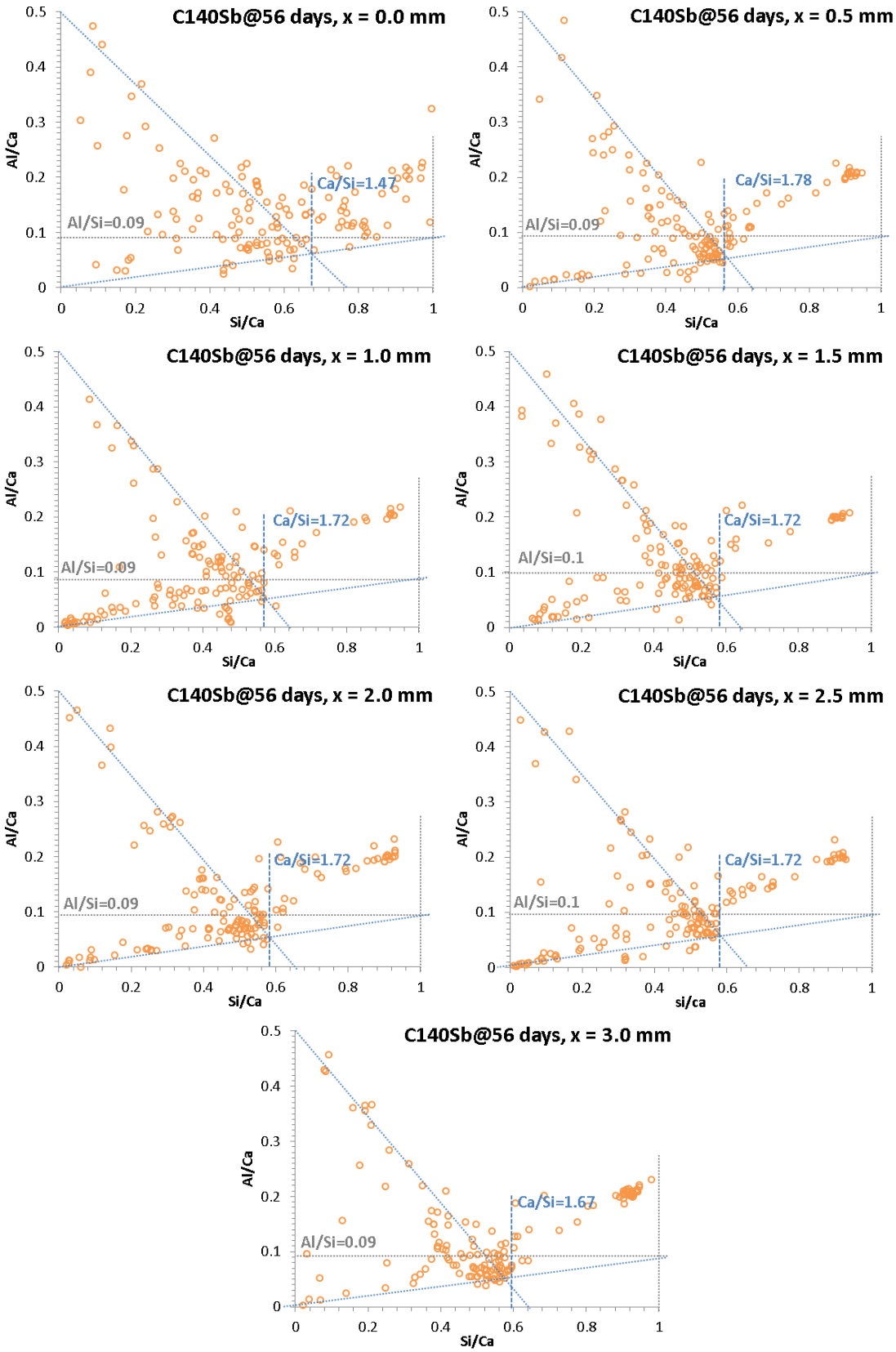

Figure A.23 – Changes in C-S-H Composition in C_140S_b Cured for 56 days in a 3 g.L^{-1} Na_2SO_4 Solution

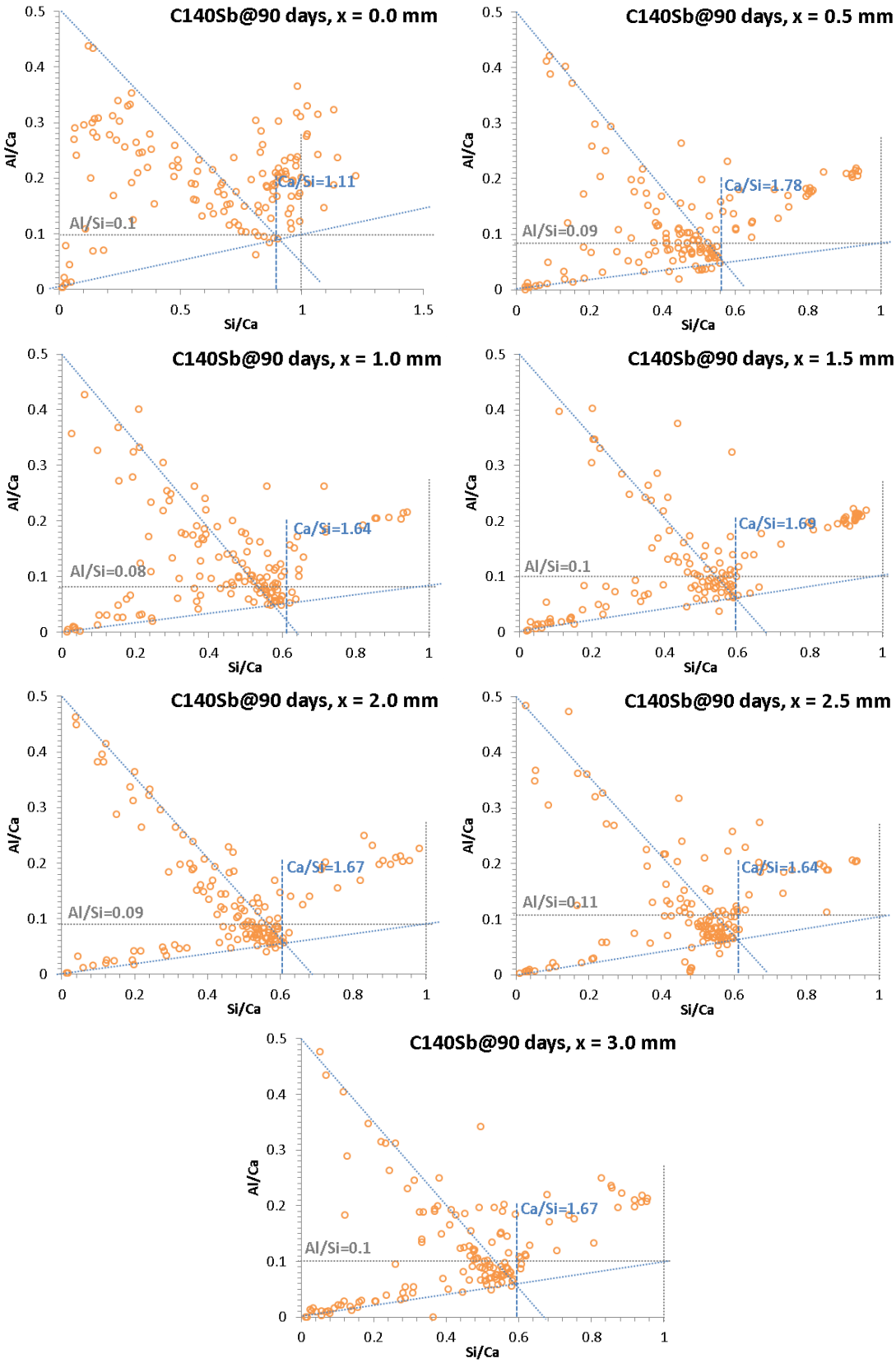

Figure A.24 – Changes in C-S-H Composition in $C_1 40S_b$ Cured for 90 days in a 3 g.L^{-1} Na_2SO_4 Solution

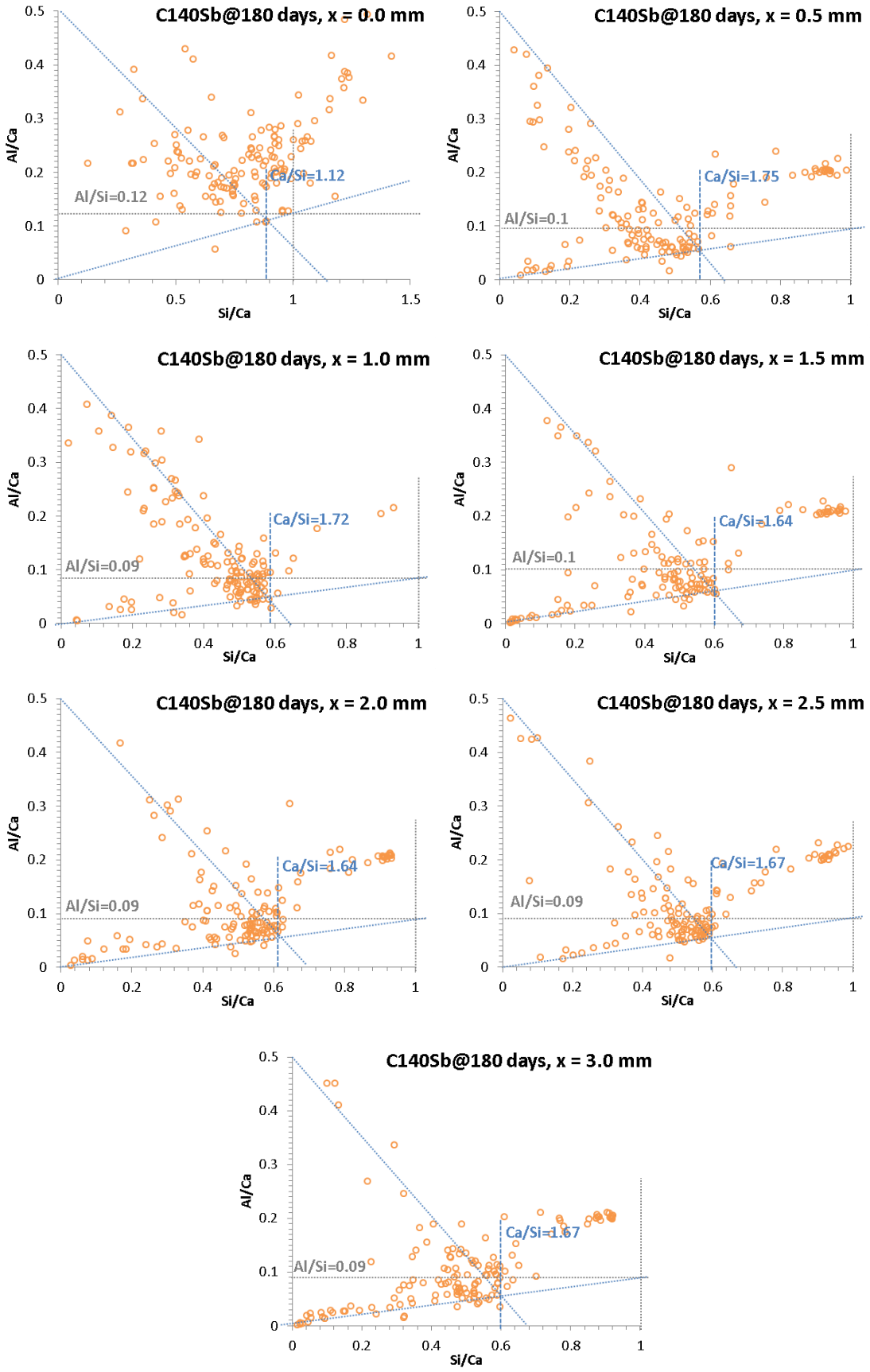

Figure A.25 – Changes in C-S-H Composition in C_140S_b Cured for 180 days in a 3 $g.L^{-1}$ Na_2SO_4 Solution

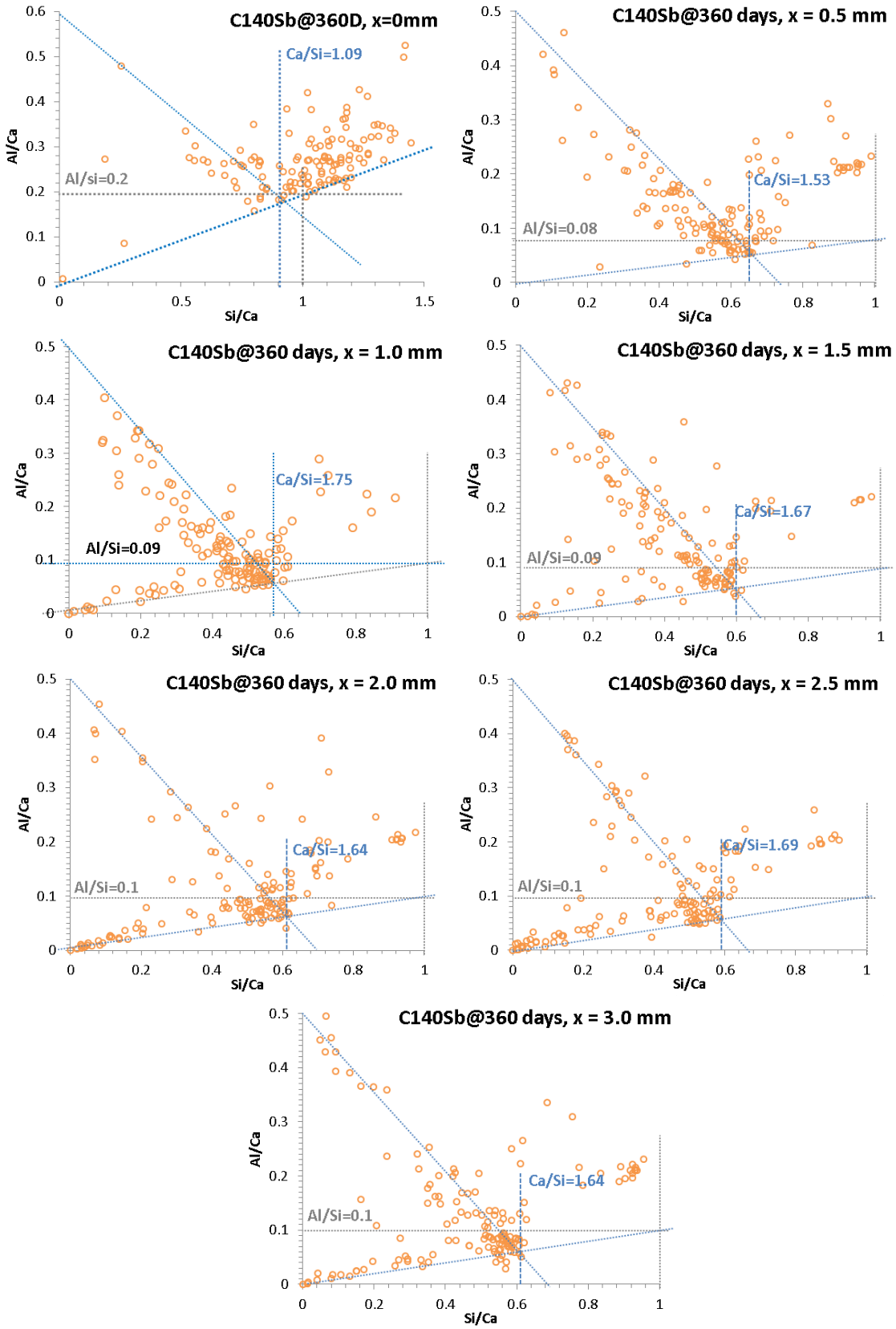

Figure A.26 – Changes in C-S-H Composition in C_140S_b Cured for 360 days in a 3 g.L^{-1} Na_2SO_4 Solution

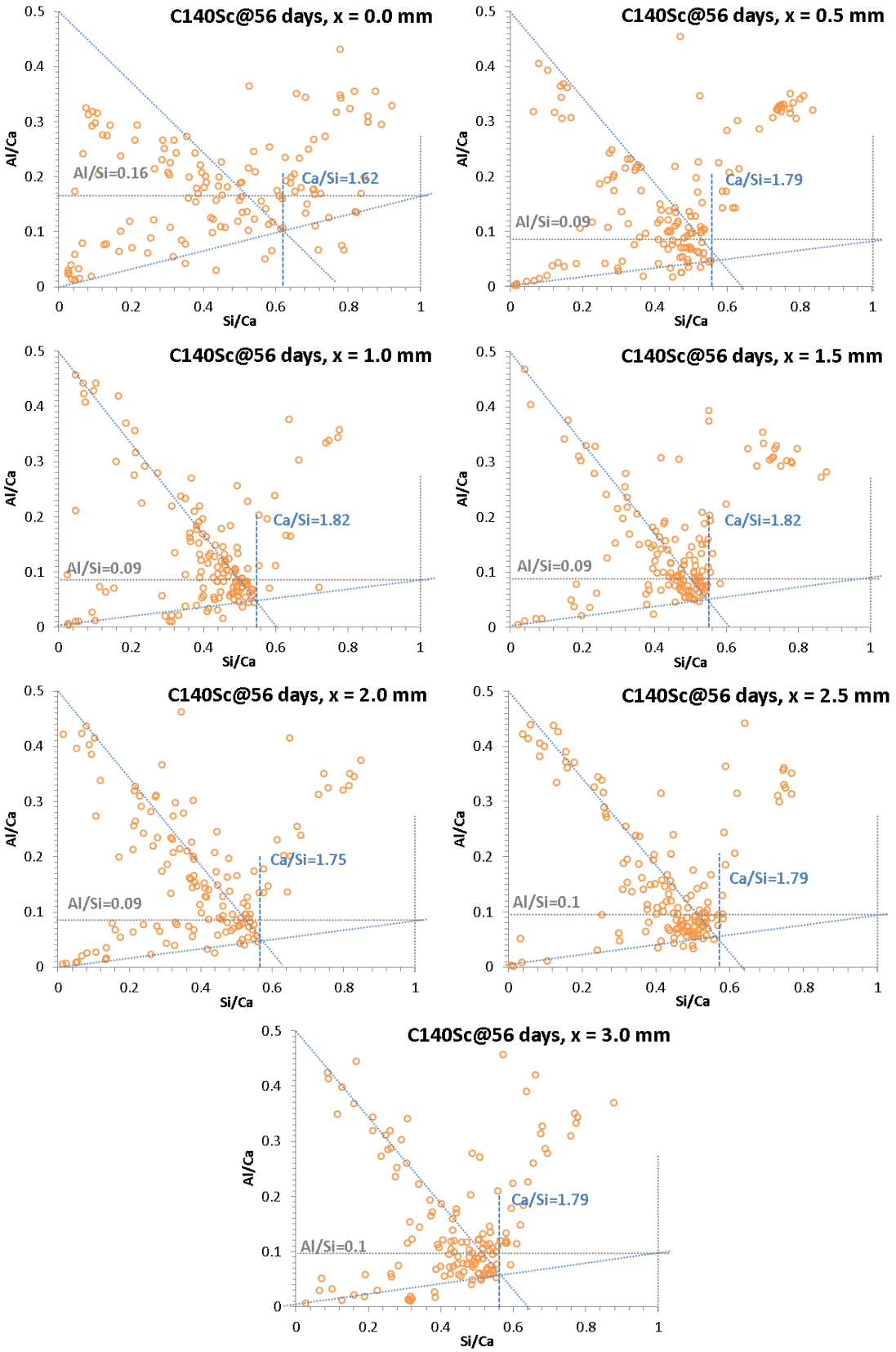

Figure A.27 – Changes in C-S-H Composition in C_140S_c Cured for 56 days in a 3 $g.L^{-1}$ Na_2SO_4 Solution

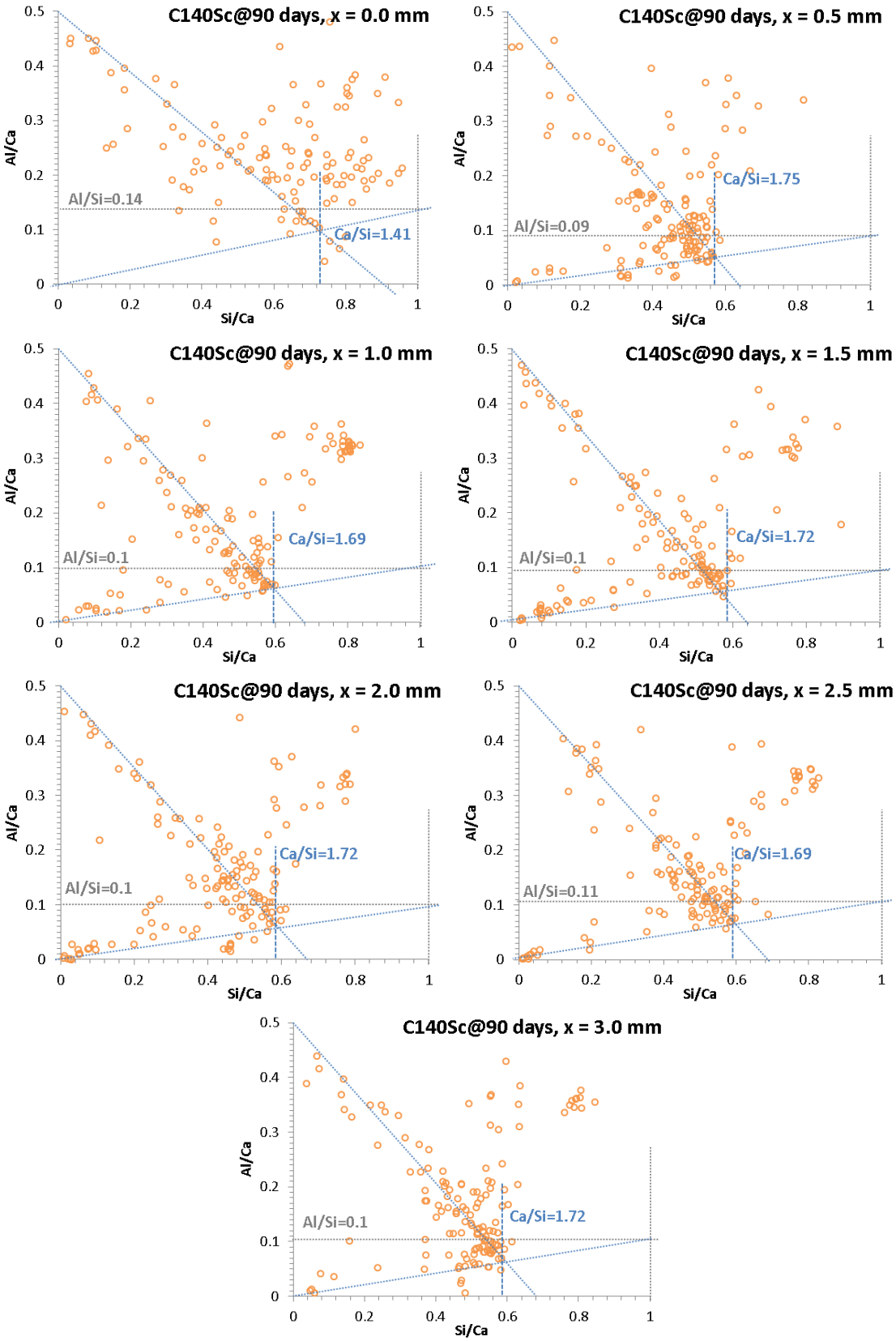

Figure A.28 – Changes in C-S-H Composition in C_140S_c Cured for 90 days in a 3 g.L^{-1} Na_2SO_4 Solution

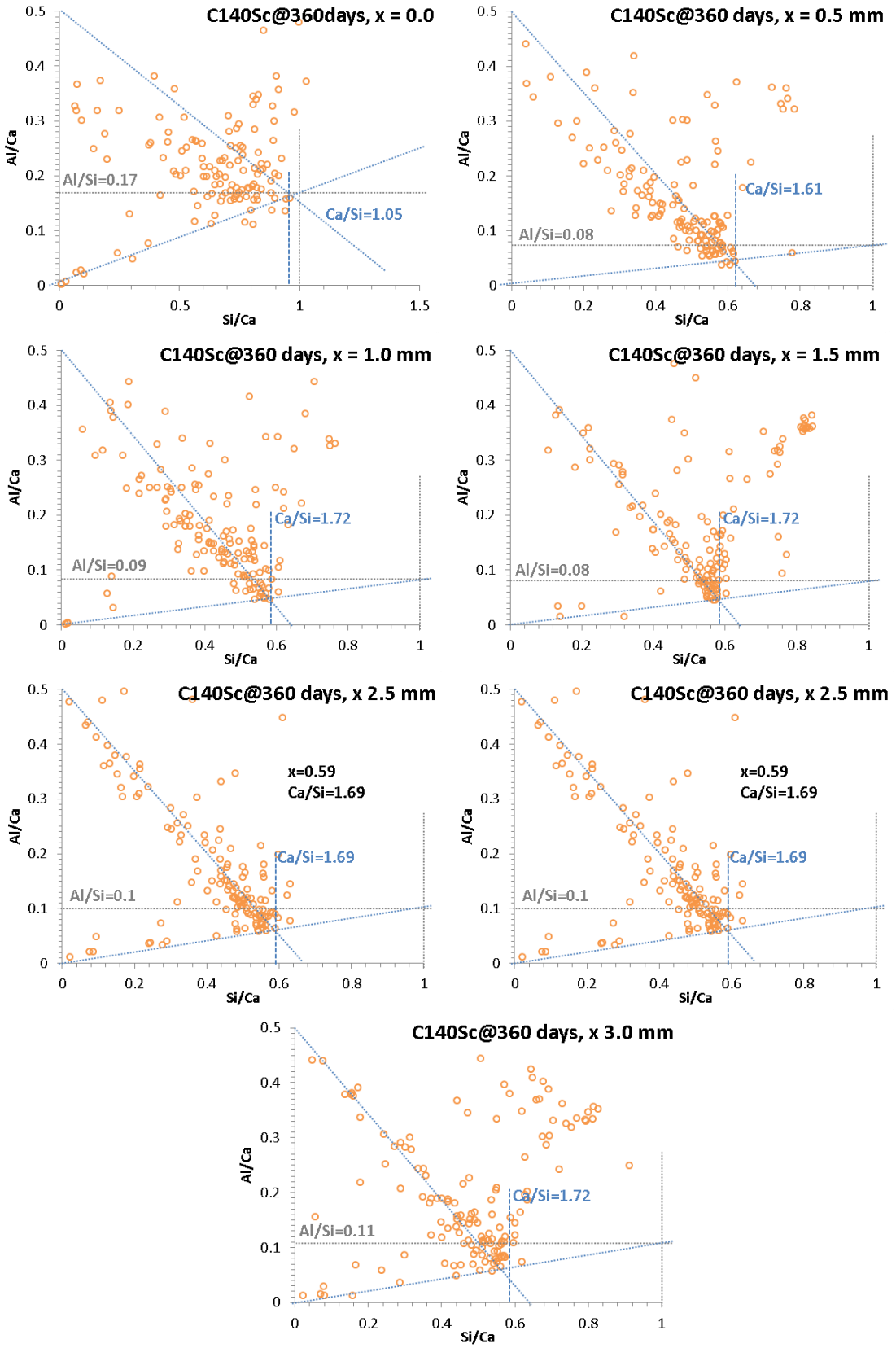

Figure A.29 – Changes in C-S-H Composition in C_140S_c Cured for 360 days in a 3 g.L^{-1} Na_2SO_4 Solution

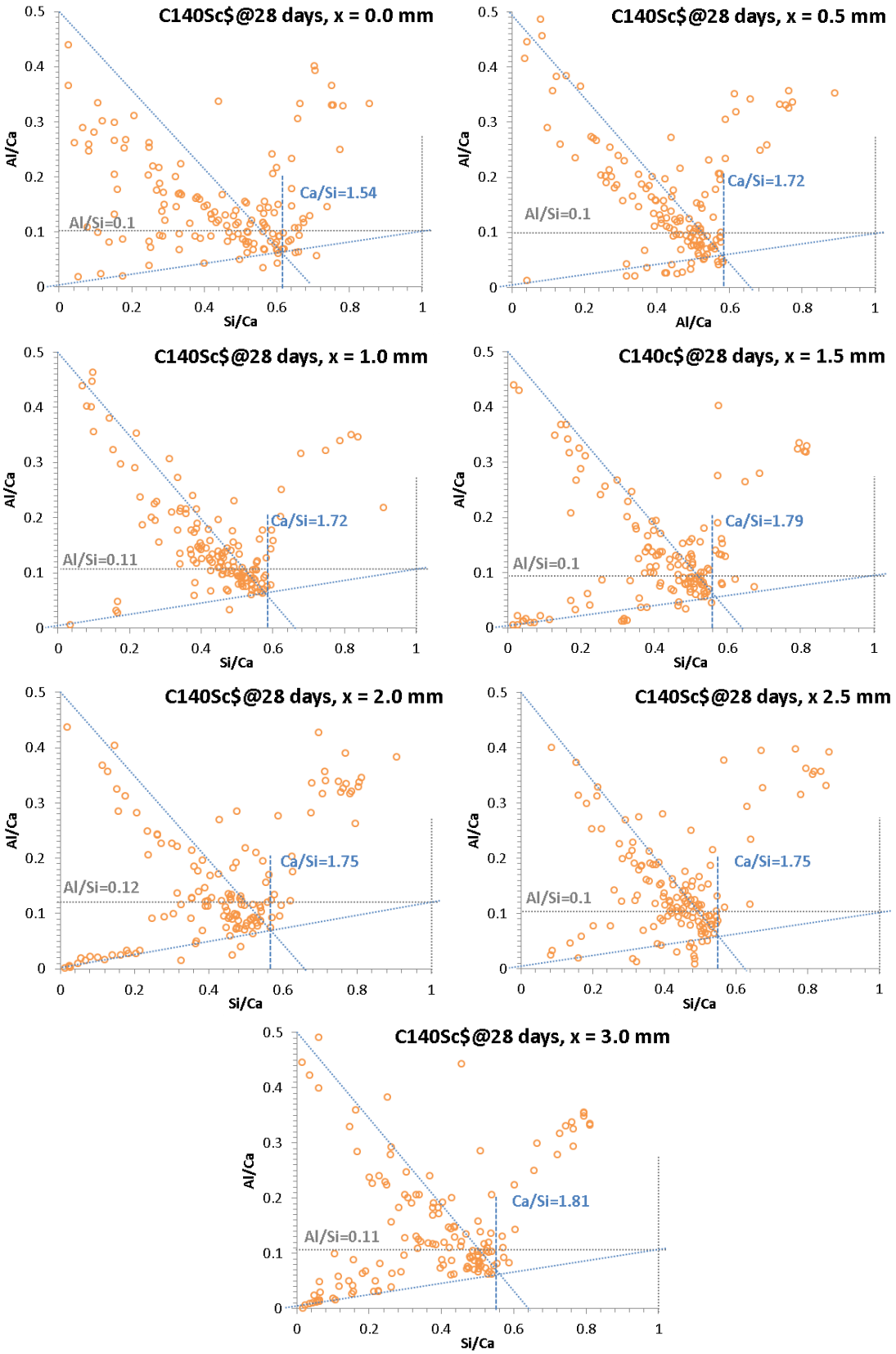

Figure A.30 – Changes in C-S-H Composition in $C_1 40 S_c$\$ Cured for 28 days in a 3 $g.L^{-1}$ Na_2SO_4 Solution

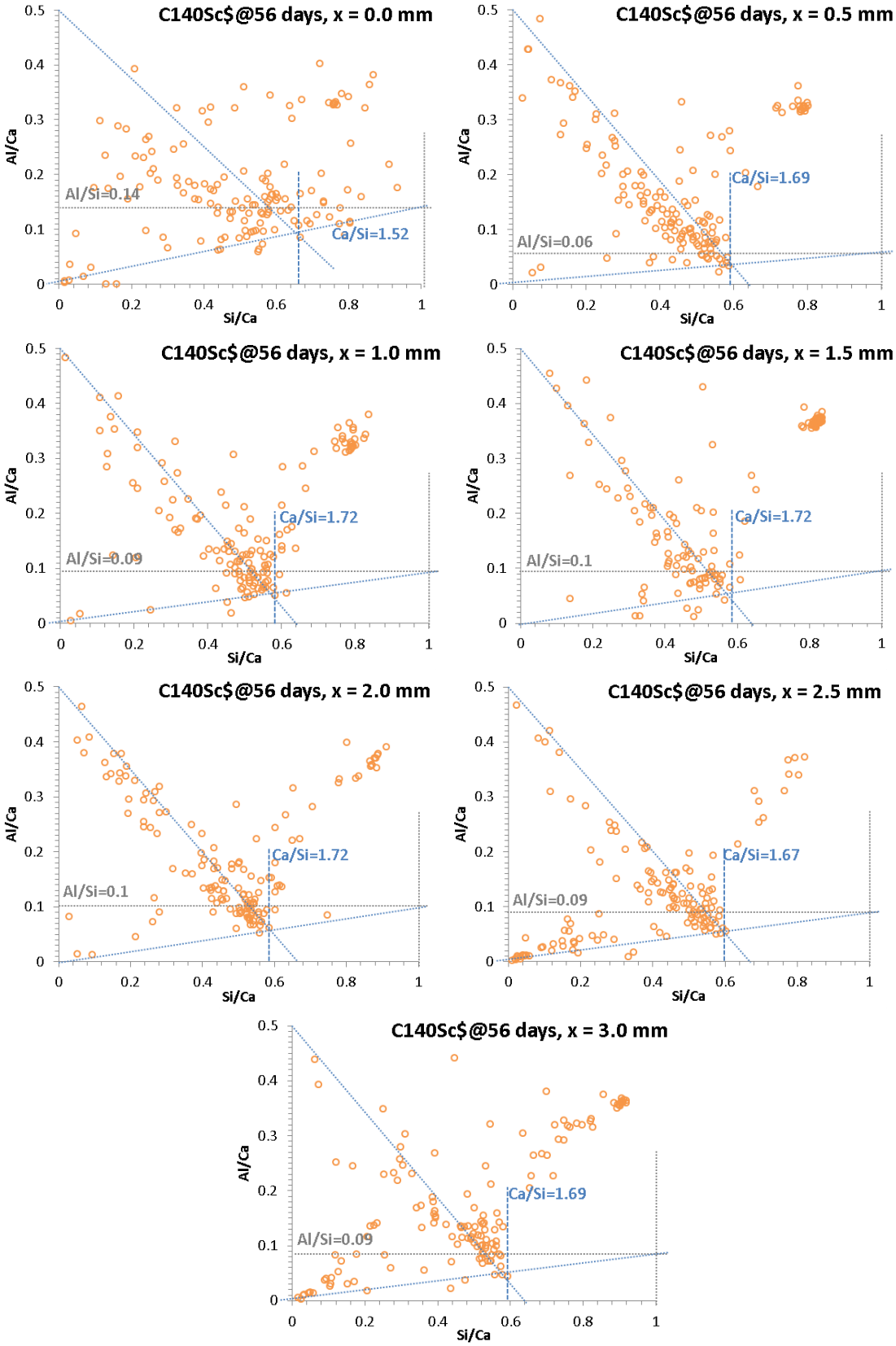

Figure A.31 – Changes in C-S-H Composition in C_140S_c Cured for 56 days in a 3 g.L^{-1} Na_2SO_4 Solution

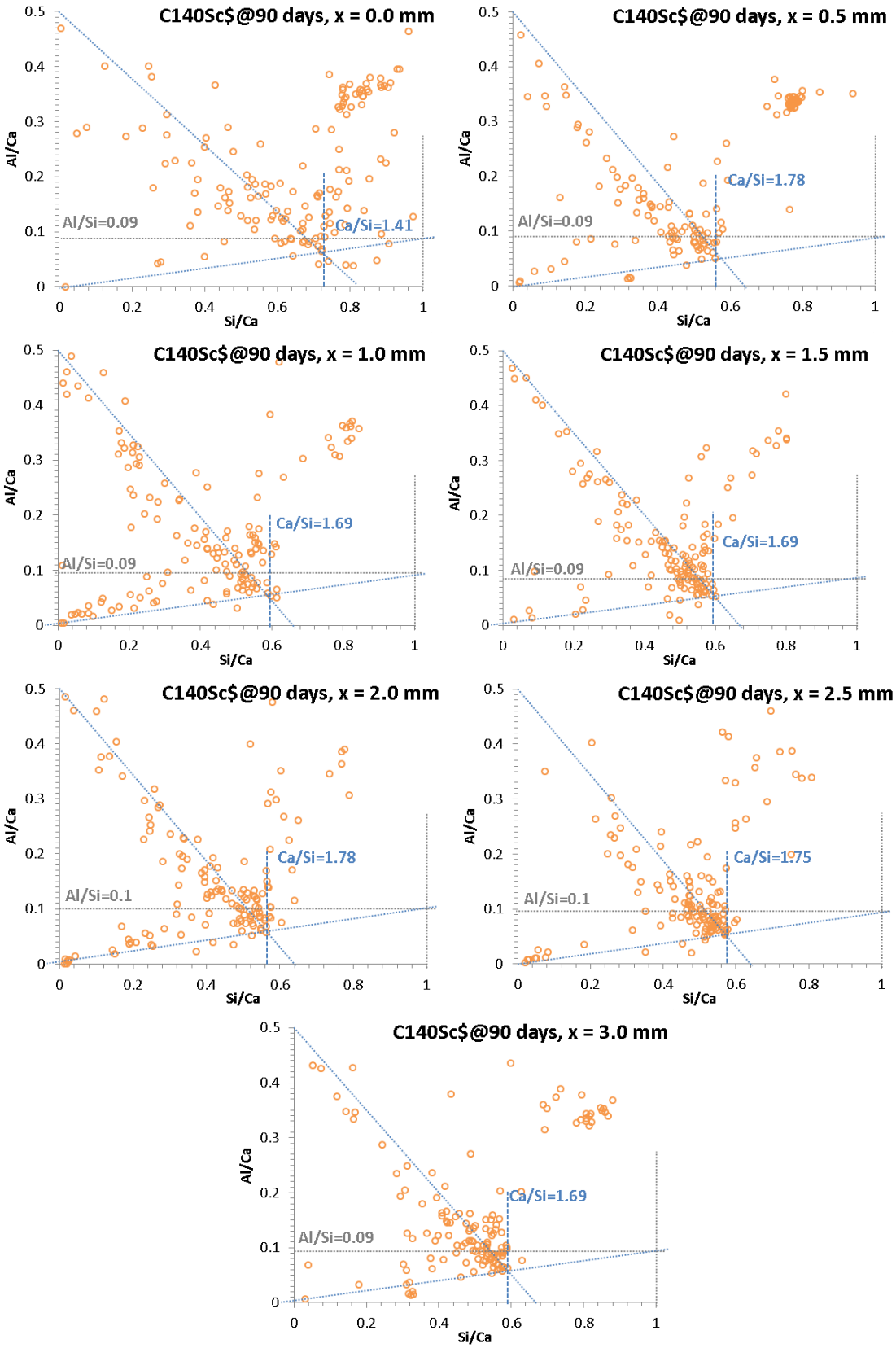

Figure A.32 – Changes in C-S-H Composition in C_140S_c Cured for 90 days in a 3 $g.L^{-1}$ Na_2SO_4 Solution

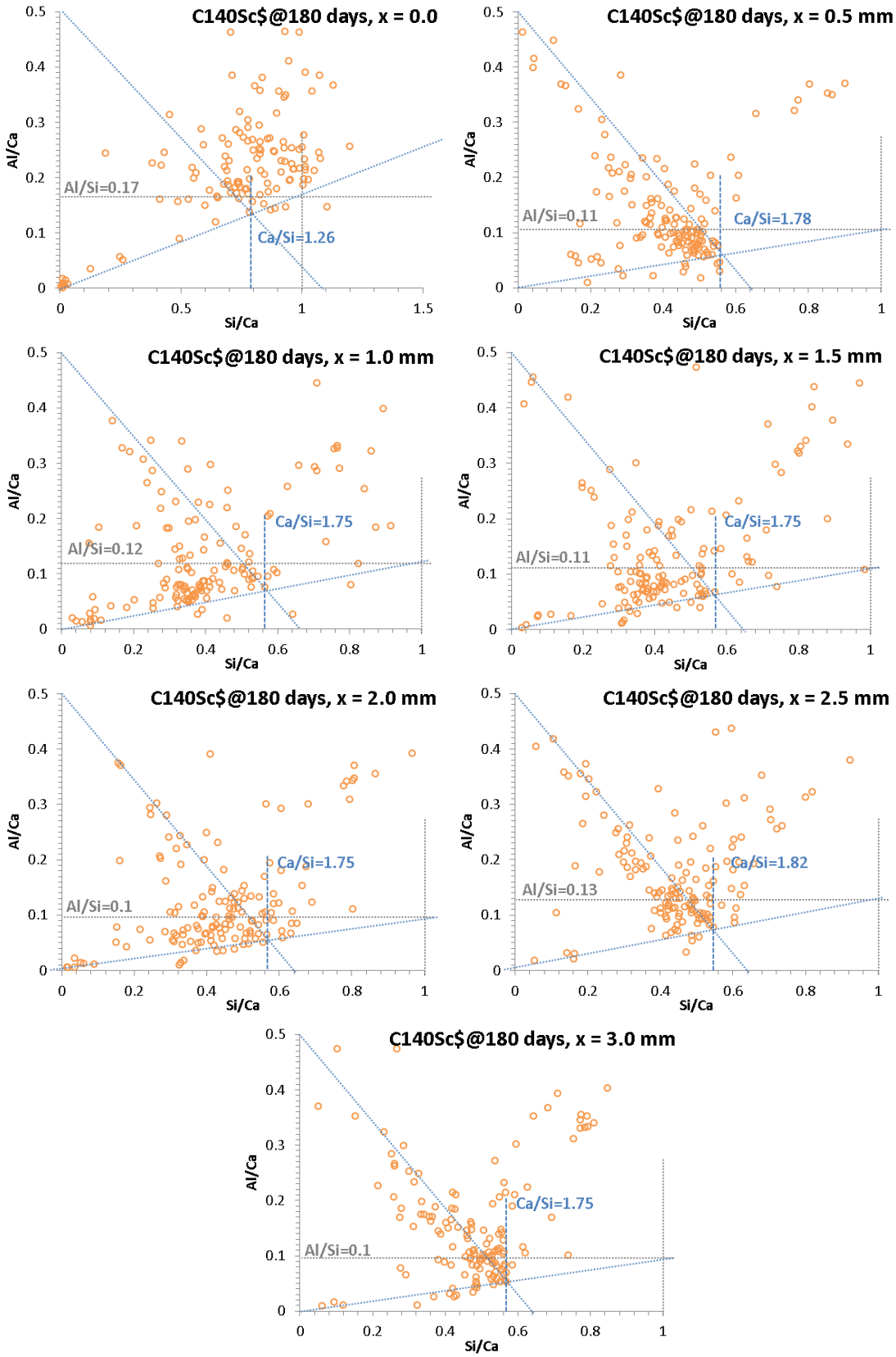

Figure A.33 – Changes in C-S-H Composition in $C_1 40 S_c$ Cured for 180 days in a 3 $g.L^{-1}$ Na_2SO_4 Solution

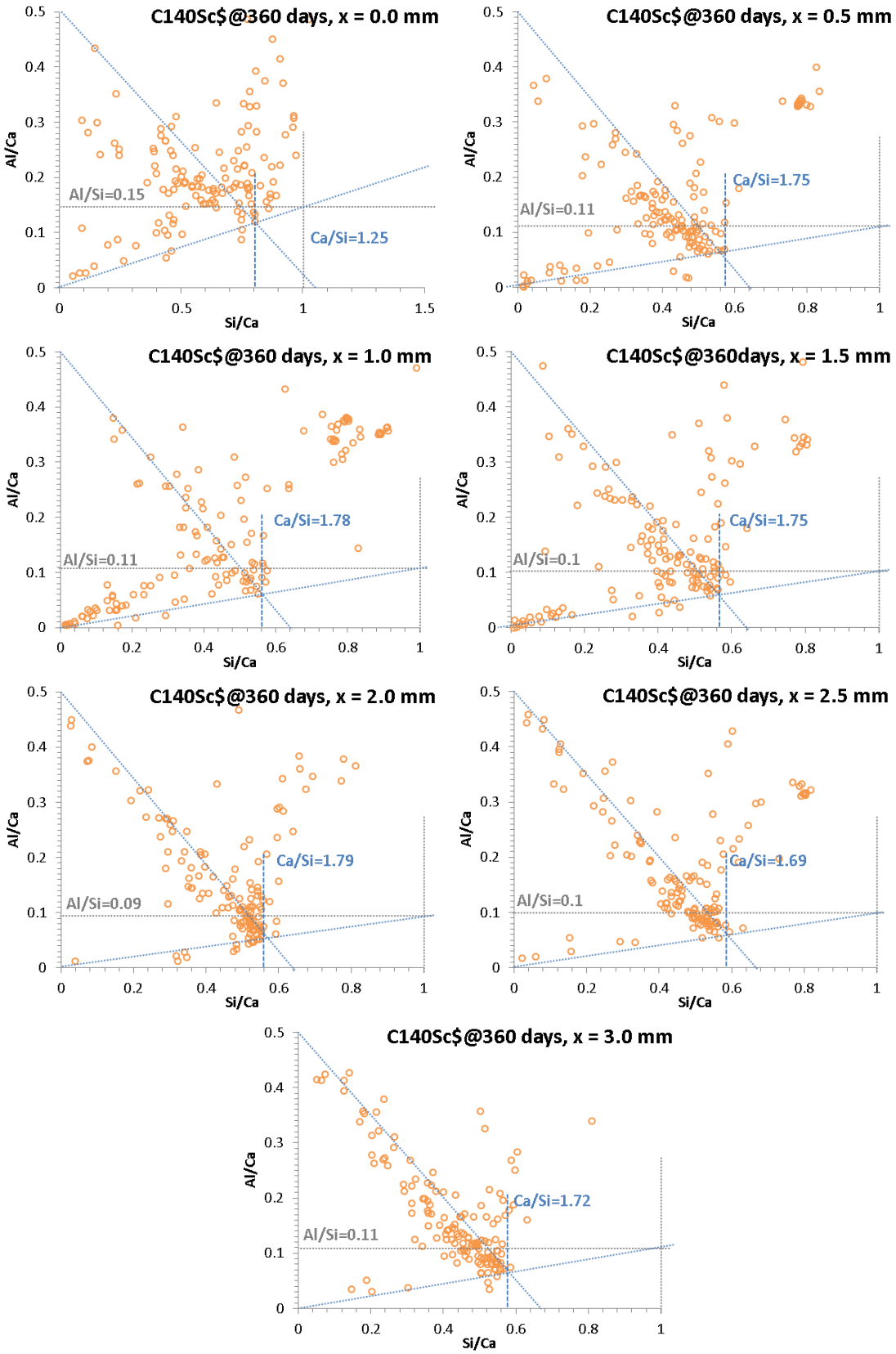

Figure A.34 – Changes in C-S-H Composition in C_140S_c Cured for 360 days in a 3 g.L^{-1} Na_2SO_4 Solution

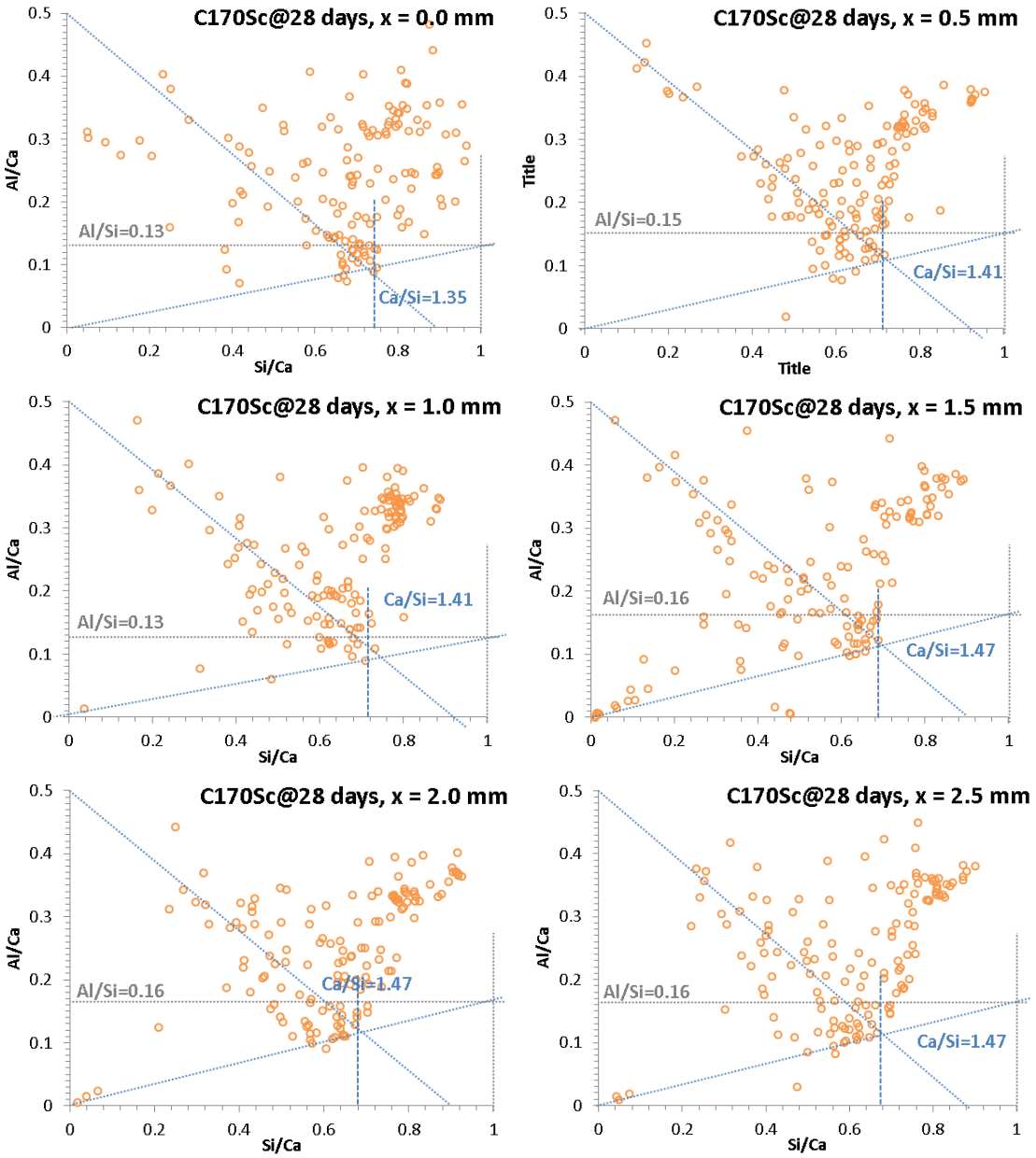

Figure A.35 – Changes in C-S-H Composition in C_170S_c Cured for 28 days in a 3 g.L^{-1} Na_2SO_4 Solution

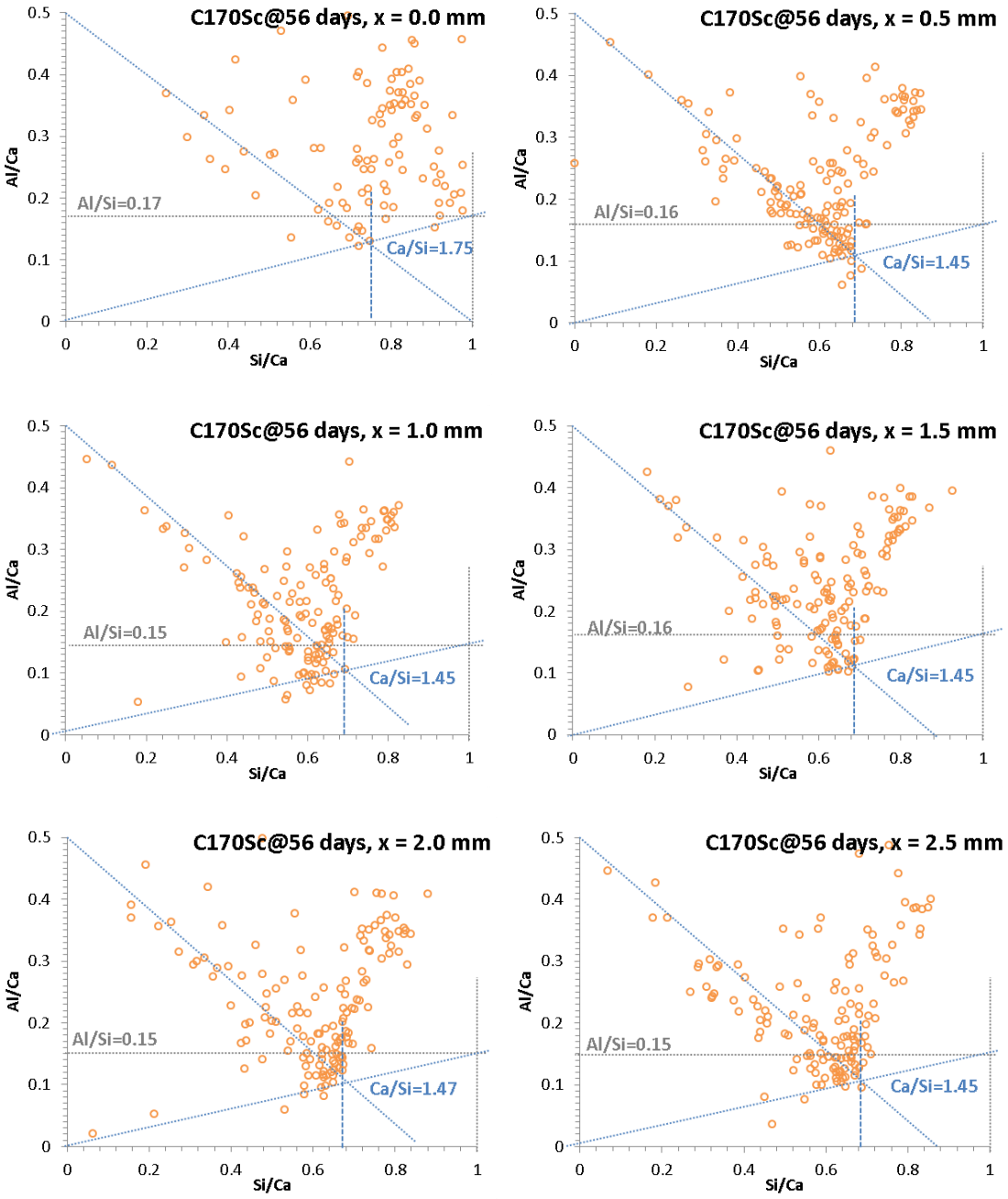

Figure A.36 – Changes in C-S-H Composition in $C_1 70S_c$ Cured for 56 days in a 3 $g.L^{-1}$ Na_2SO_4 Solution

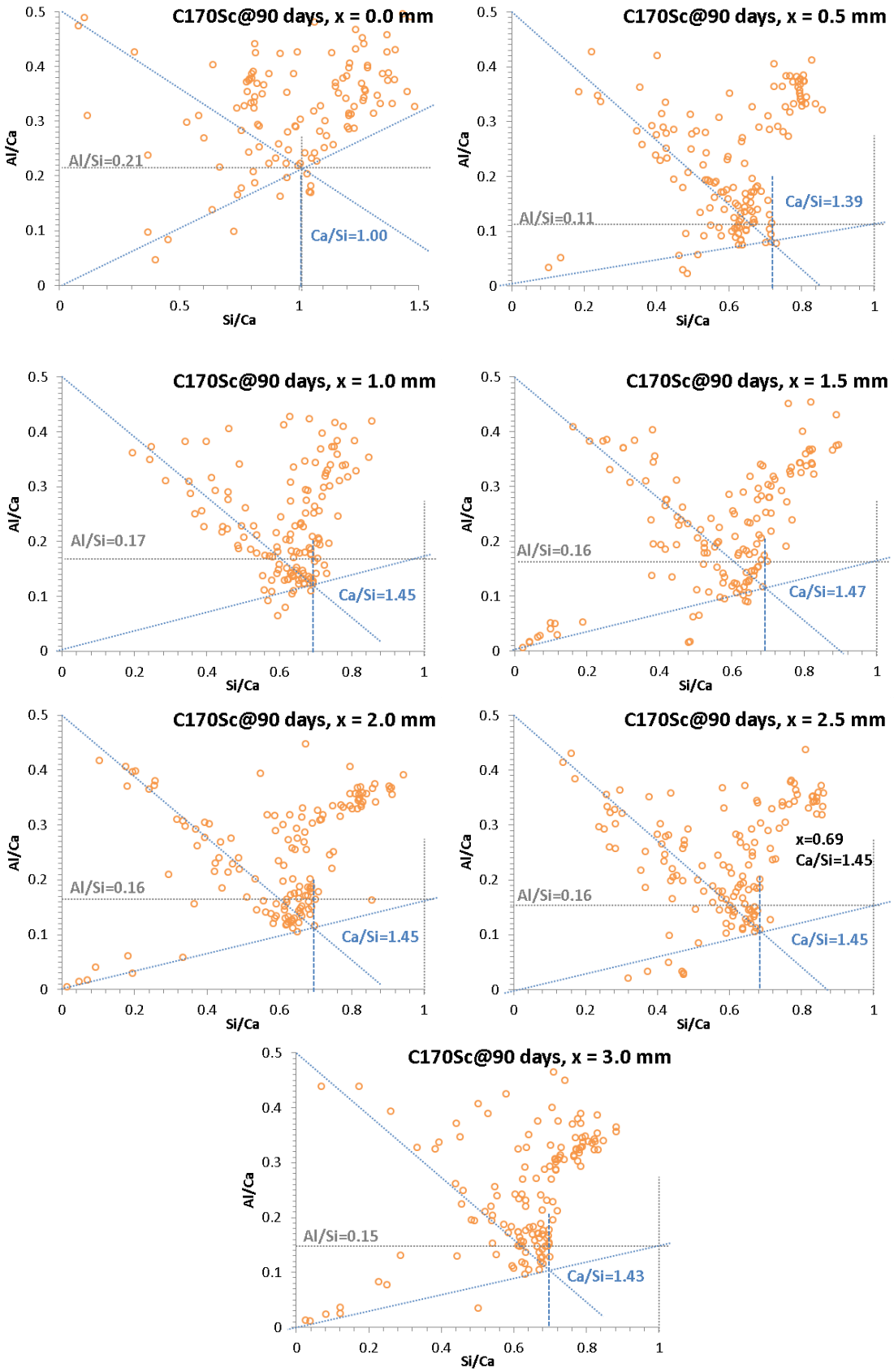

Figure A.37 – Changes in C-S-H Composition in $C_1 70S_c$ Cured for 90 days in a 3 g.L^{-1} Na_2SO_4 Solution

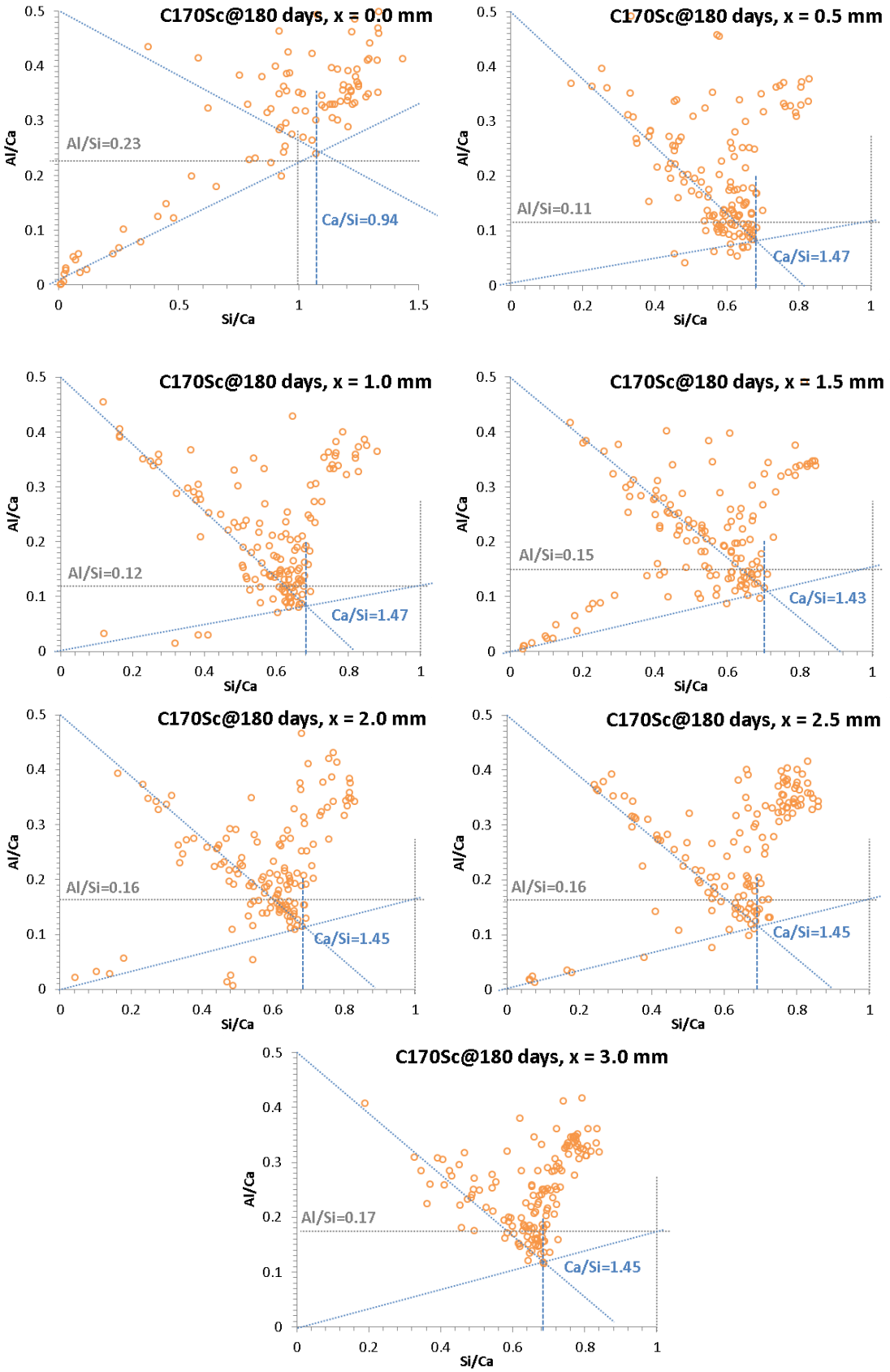

Figure A.38 – Changes in C-S-H Composition in $C_{1}70S_{c}$ Cured for 180 days in a 3 $g.L^{-1}$ Na_2SO_4 Solution

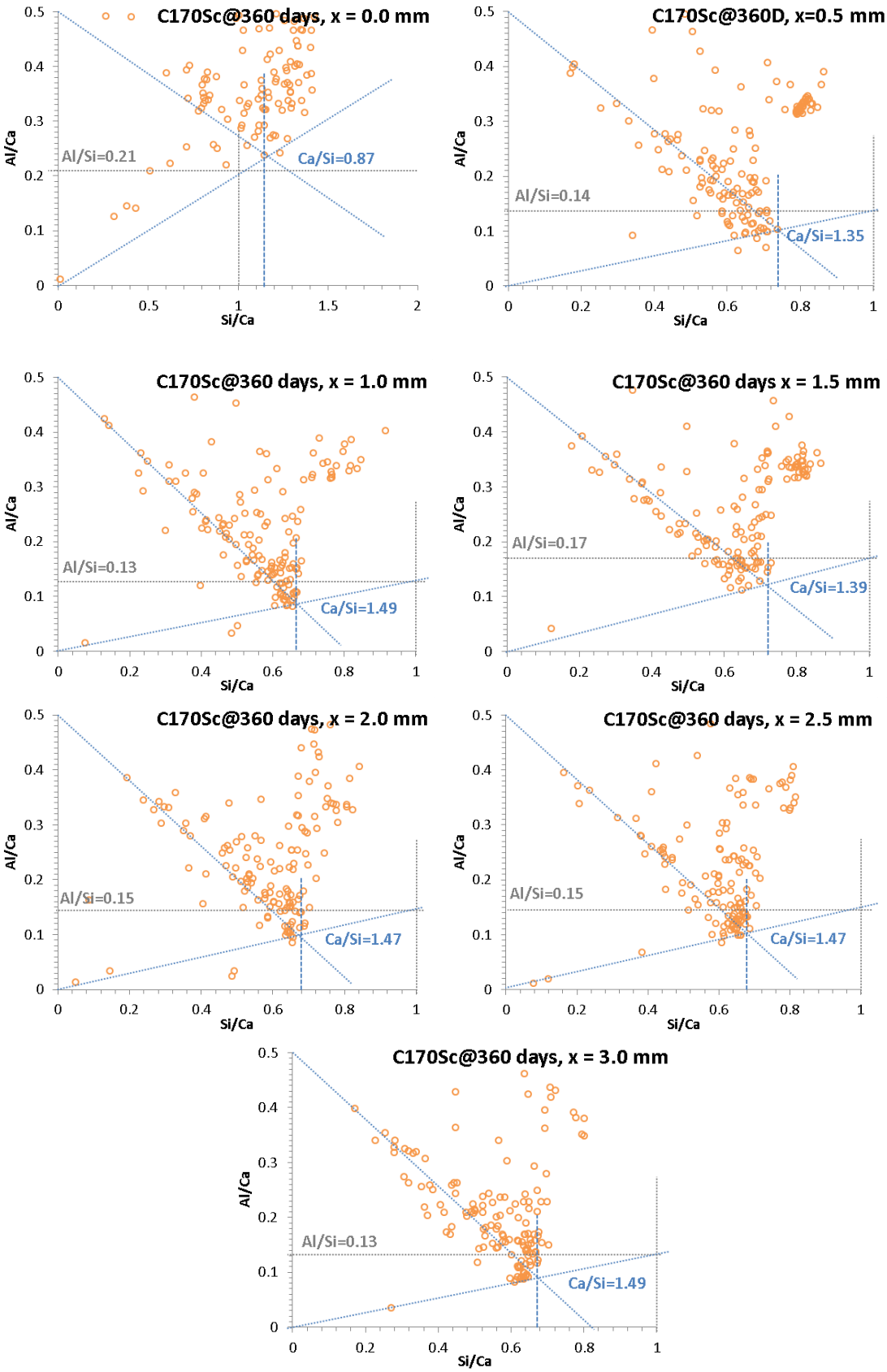

Figure A.39 – Changes in C-S-H Composition in $C_1 70S_c$ Cured for 360 days in a 3 g.L^{-1} Na_2SO_4 Solution

A.5. Changes in the Aluminate Hydrates Measured on Pastes Exposed to Sulfates

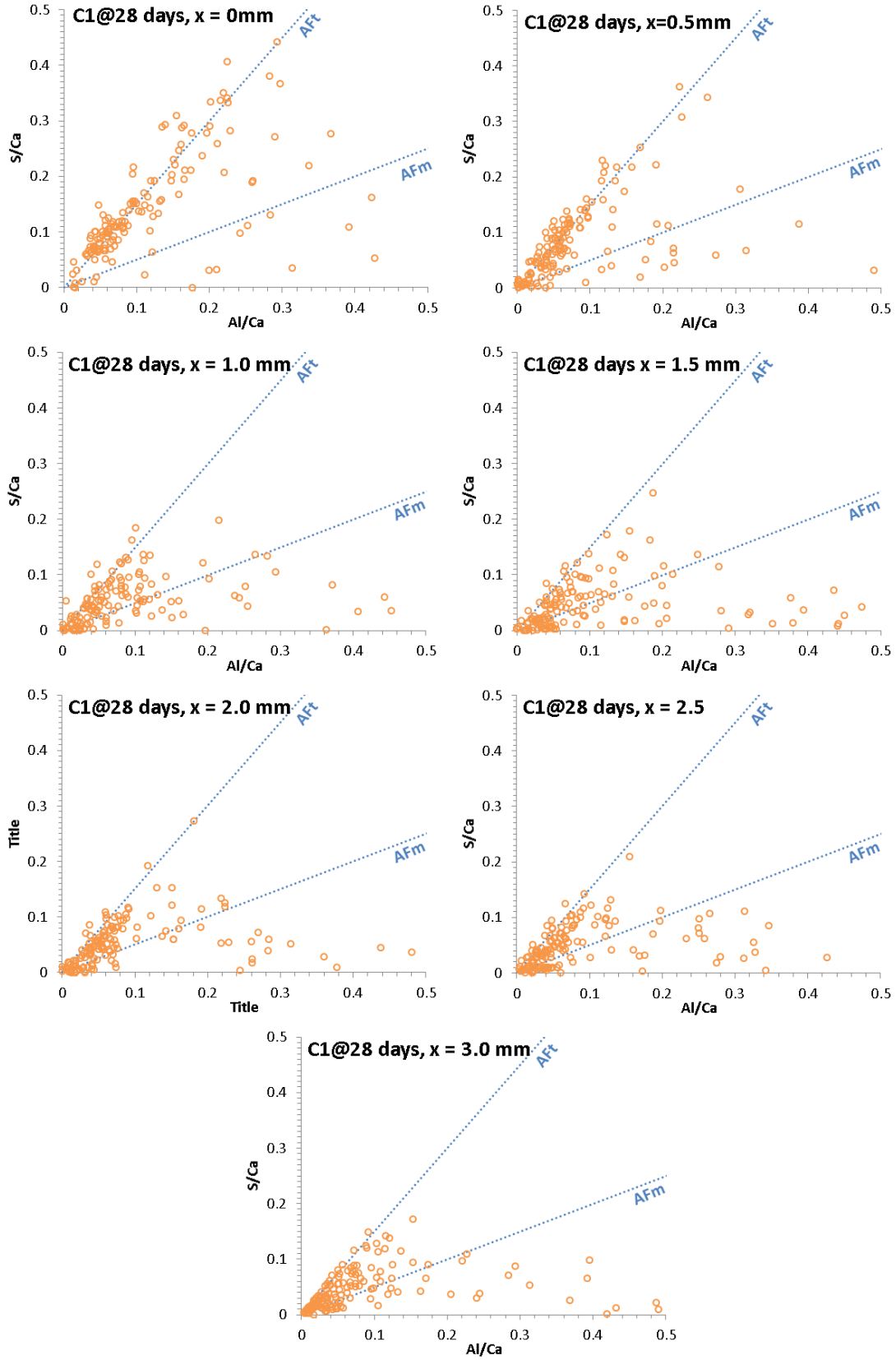

Figure A.40 – Changes in the AFm-AFt distribution in C_1 Cured for 28 days in a 3 $g.L^{-1}$ Na_2SO_4 Solution

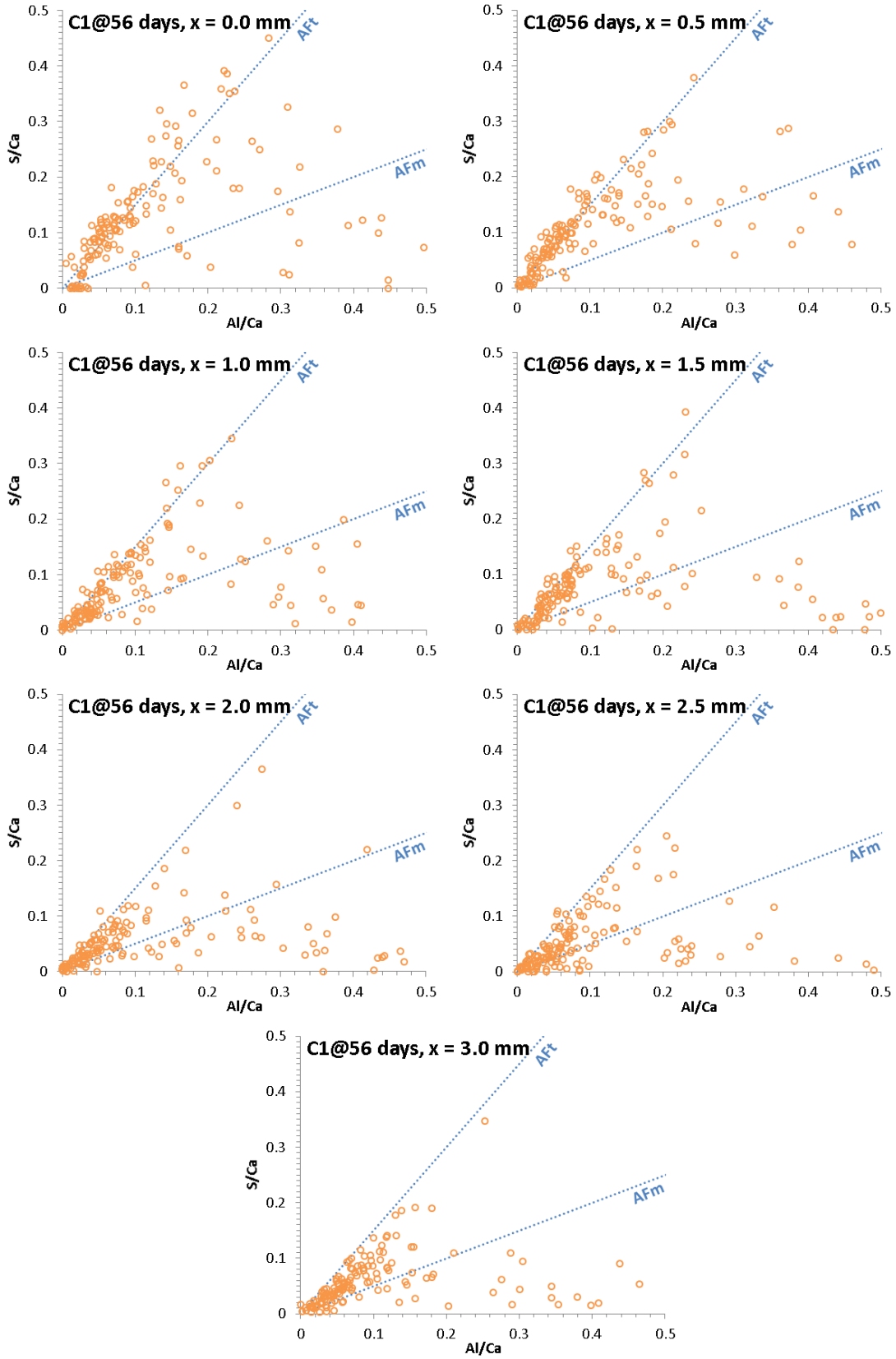

Figure A.41 – Changes in the AFm-AFt distribution in C_1 Cured for 56 days in a 3 g.L^{-1} Na_2SO_4 Solution

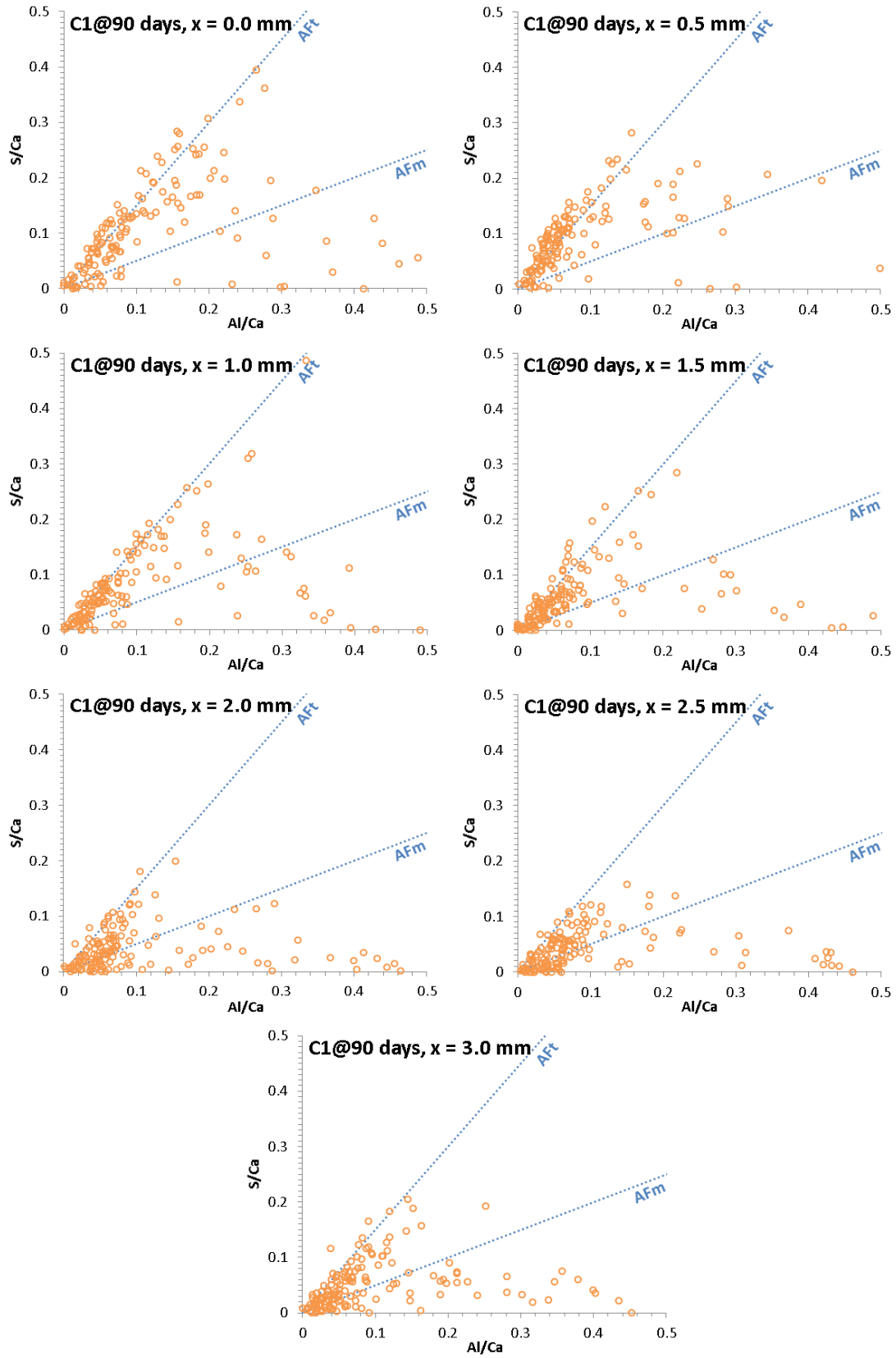

Figure A.42 – Changes in the AFm-AFt distribution in C_1 Cured for 90 days in a 3 $g.L^{-1}$ Na_2SO_4 Solution

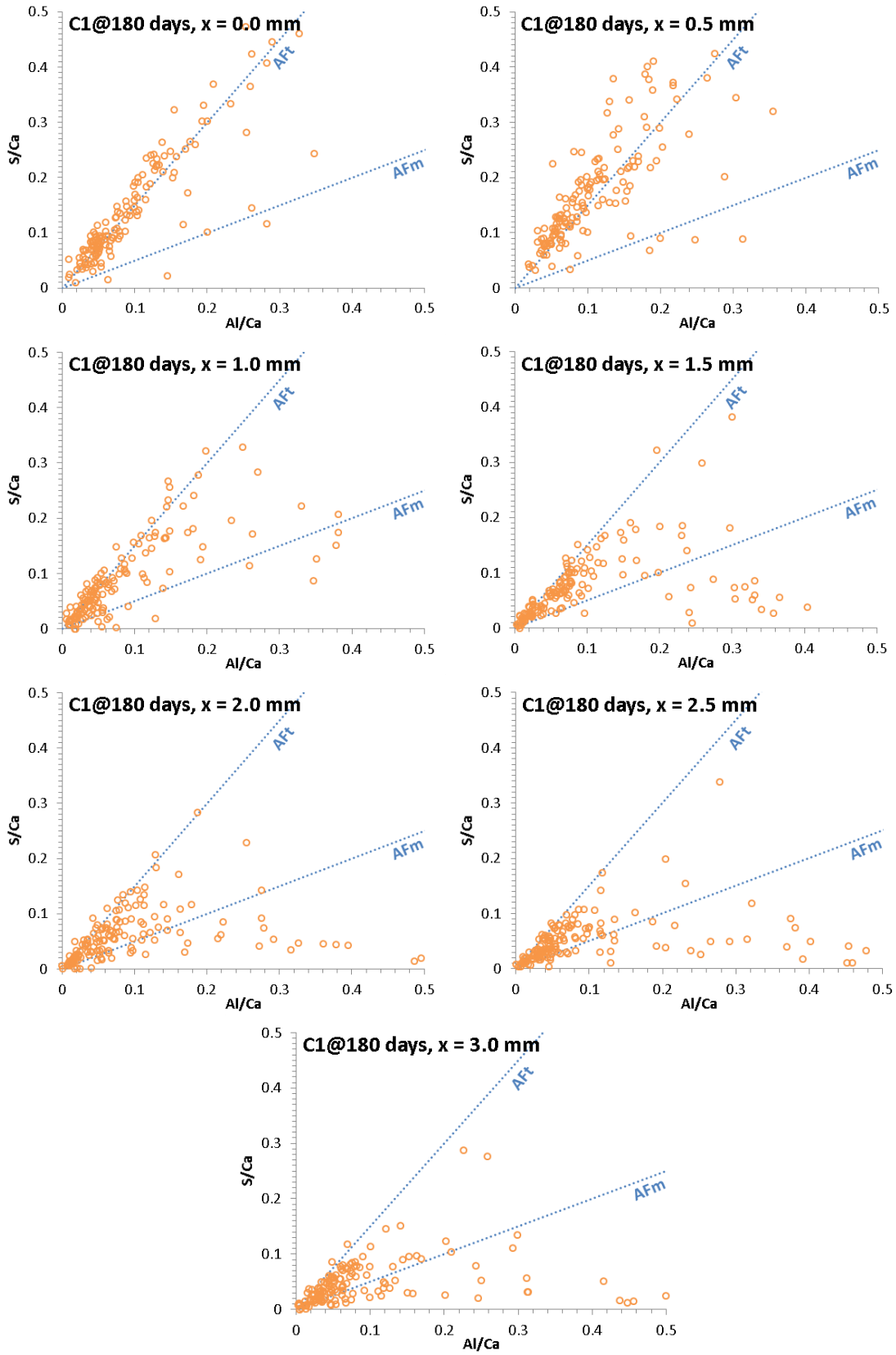

Figure A.43 – Changes in the AFm-AFt distribution in C_1 Cured for 180 days in a 3 g.L^{-1} Na_2SO_4 Solution

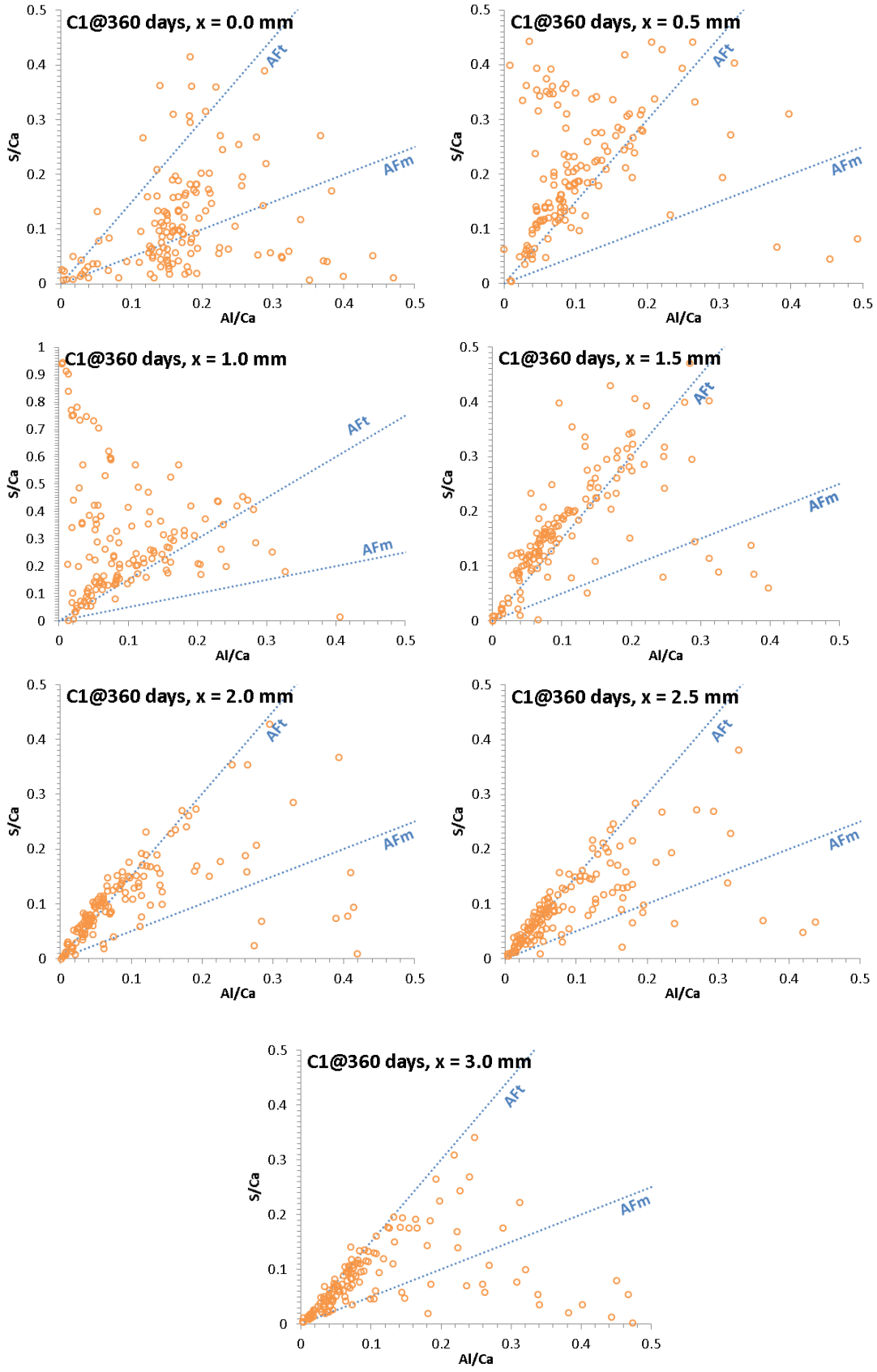

Figure A.44 – Changes in the AFm-AFt distribution in C_1 Cured for 360 days in a 3 g.L^{-1} Na_2SO_4 Solution

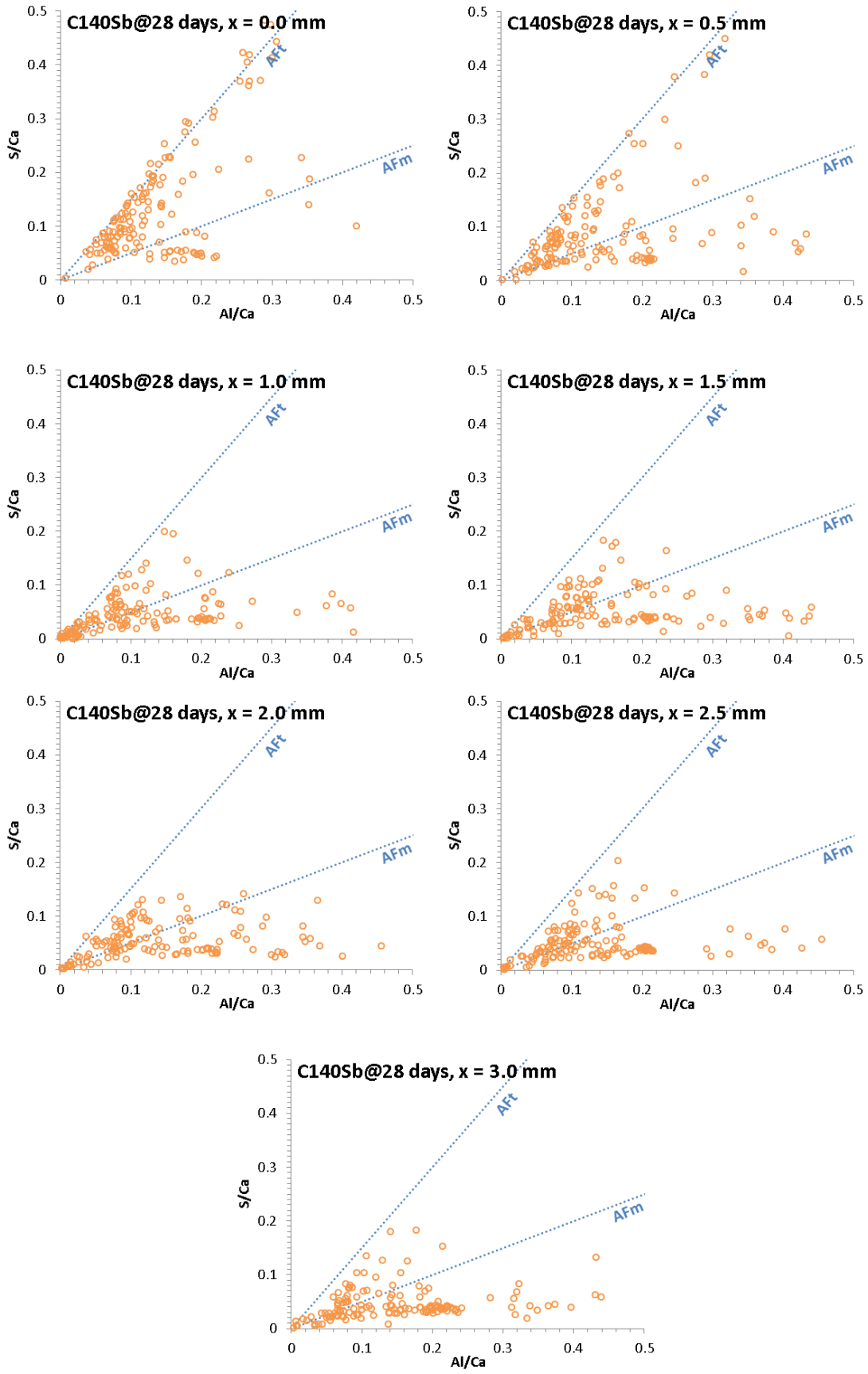

Figure A.45 – Changes in the AFm-AFt distribution in $C_1 40S_b$ Cured for 28 days in a 3 g.L^{-1} Na_2SO_4 Solution

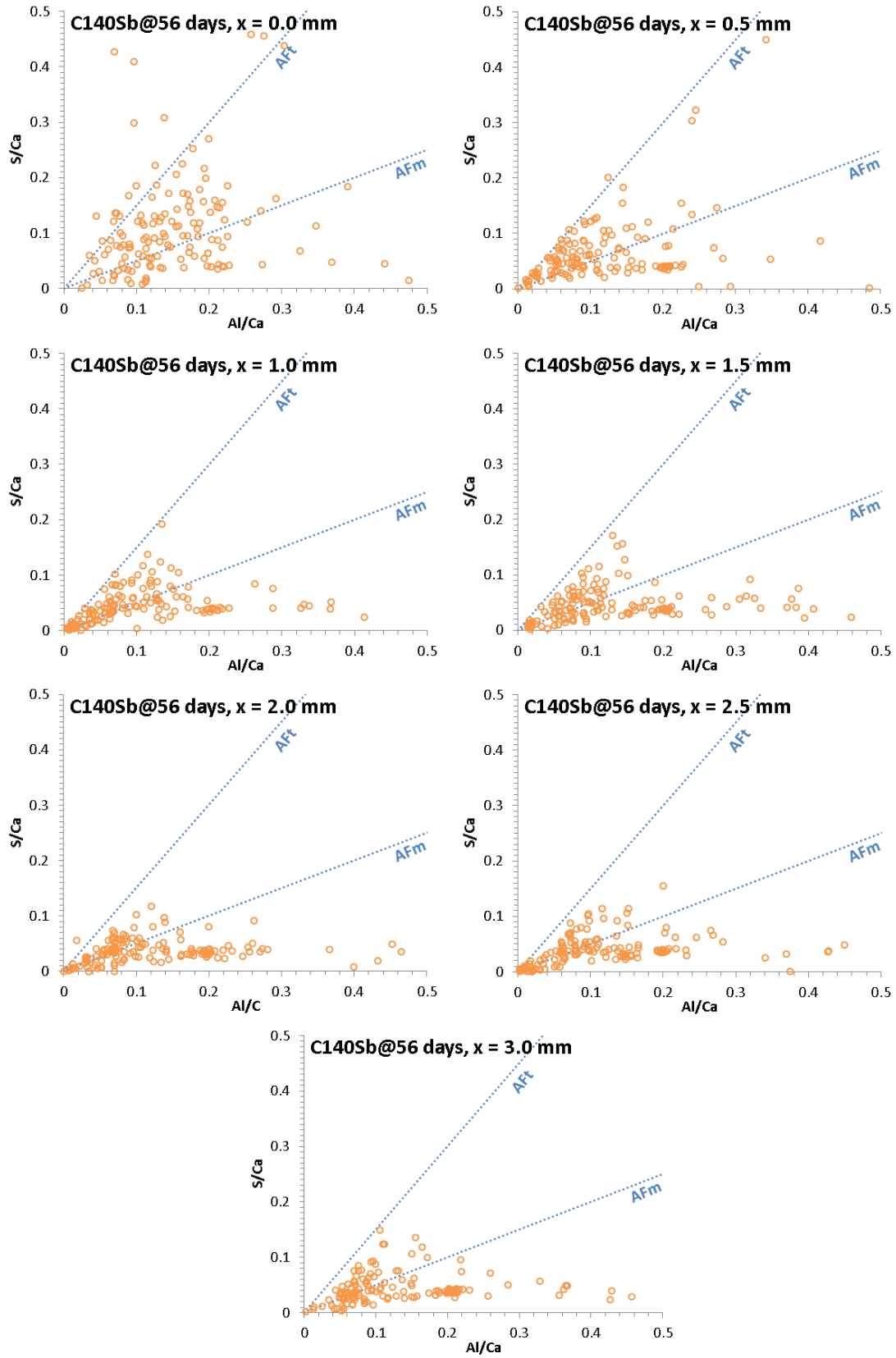

Figure A.46 – Changes in the AFm-AFt distribution in C_140S_b Cured for 56 days in a 3 g.L^{-1} Na_2SO_4 Solution

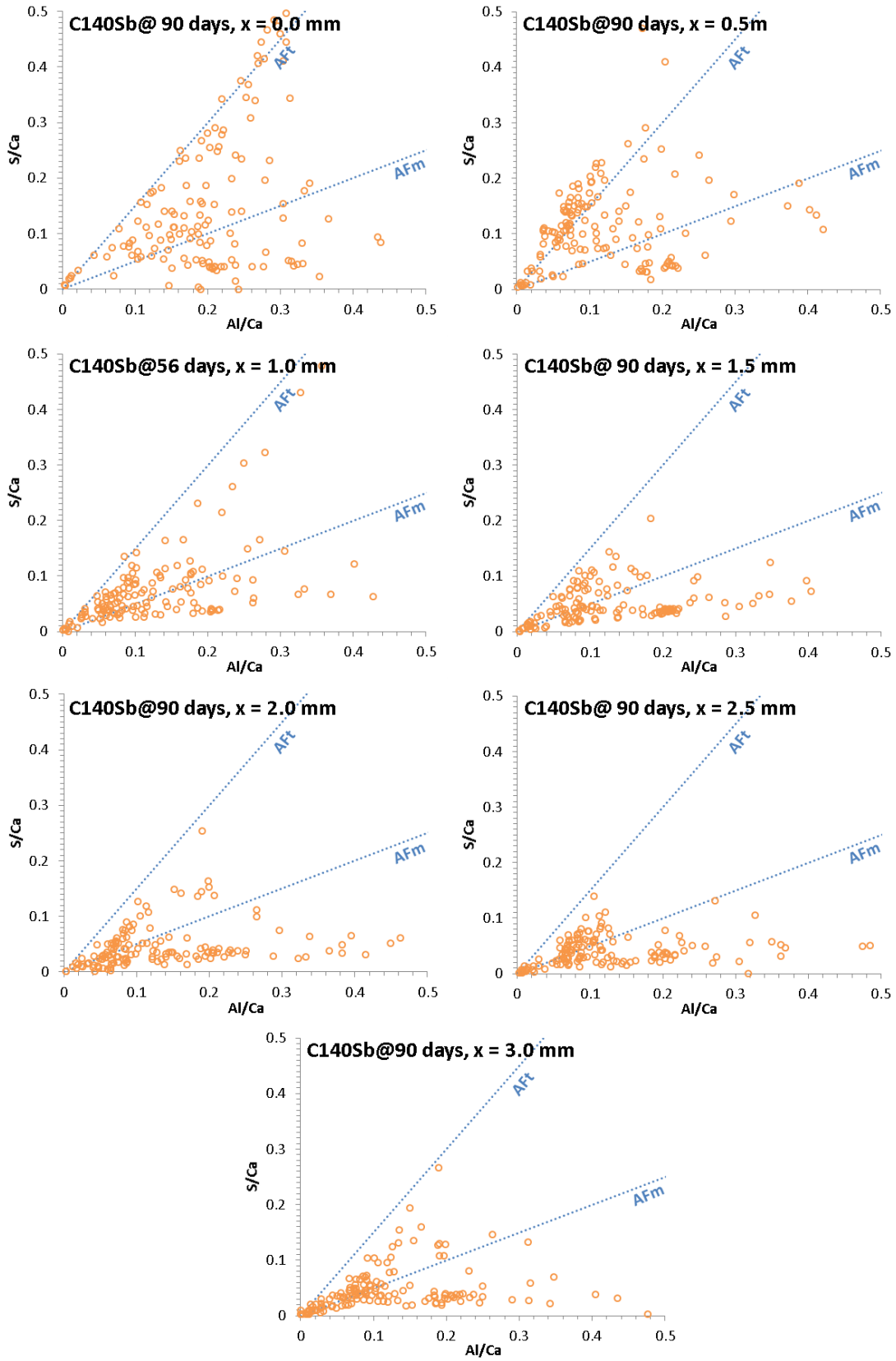

Figure A.47 – Changes in the AFm-AFt distribution in C_140S_b Cured for 90 days in a 3 $g.L^{-1}$ Na_2SO_4 Solution

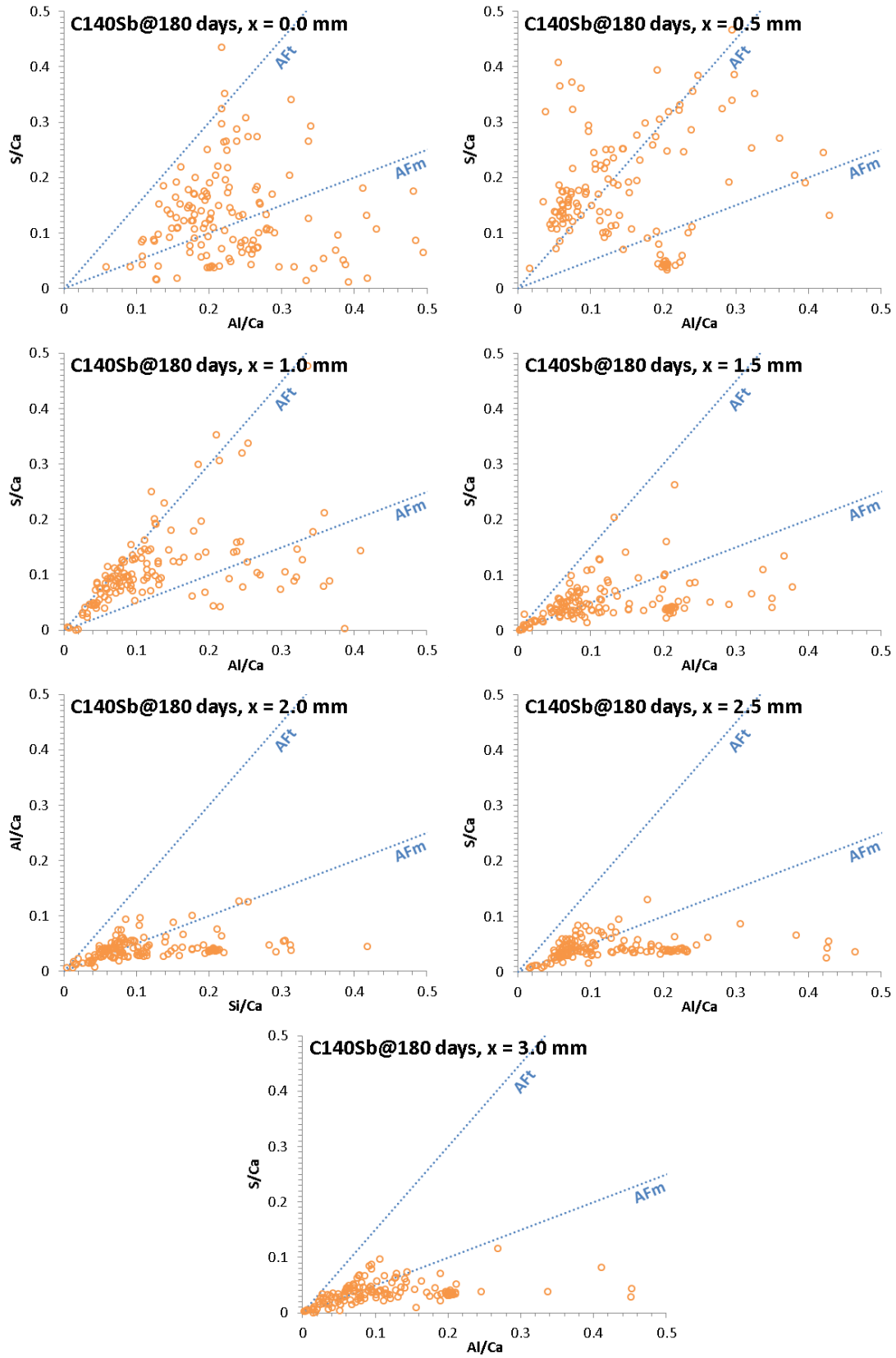

Figure A.48 – Changes in the AFm-AFt distribution in C_140S_b Cured for 180 days in a 3 g.L^{-1} Na_2SO_4 Solution

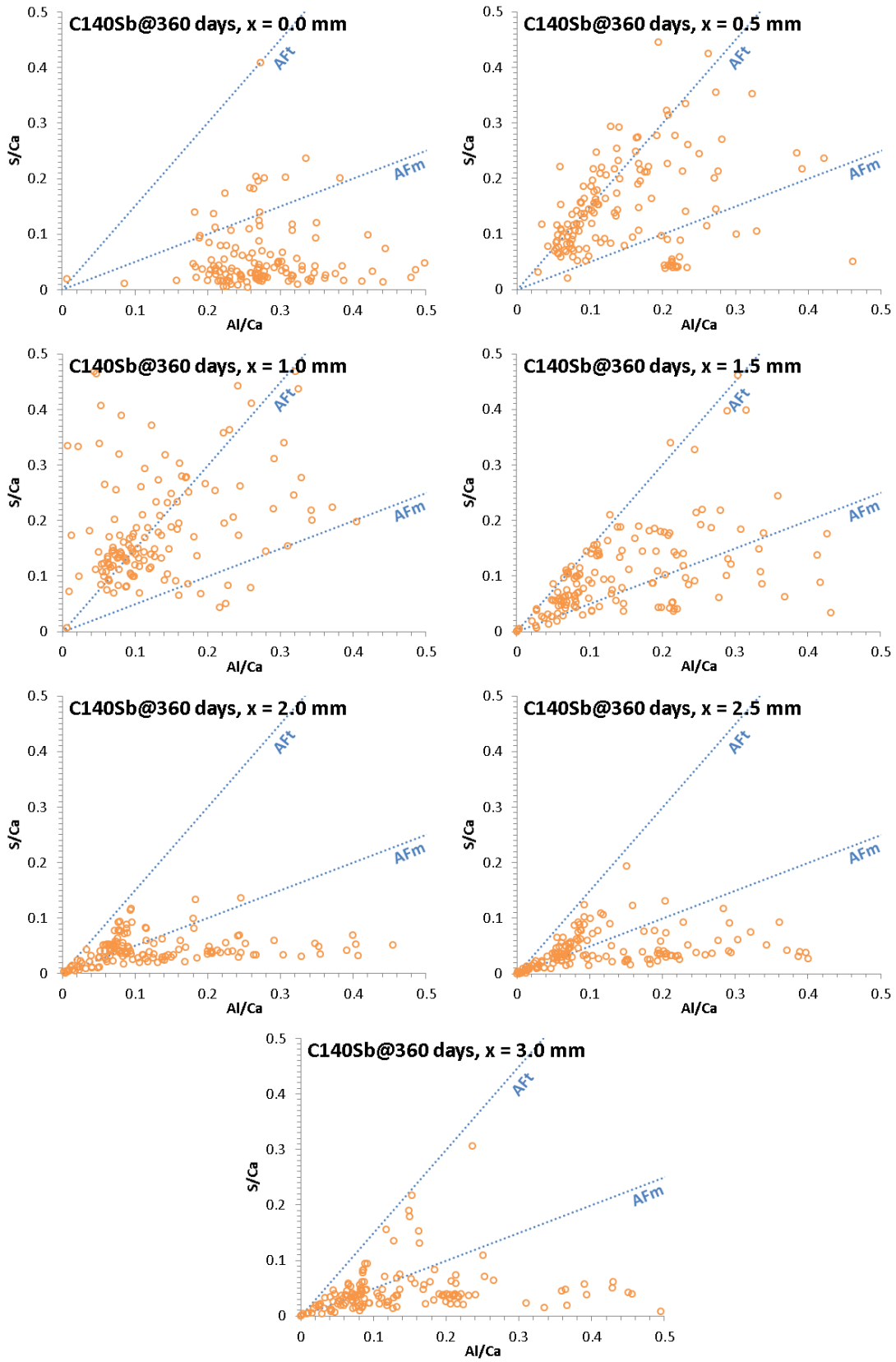

Figure A.49 – Changes in the AFm-AFt distribution in C_140S_b Cured for 360 days in a 3 $g.L^{-1}$ Na_2SO_4 Solution

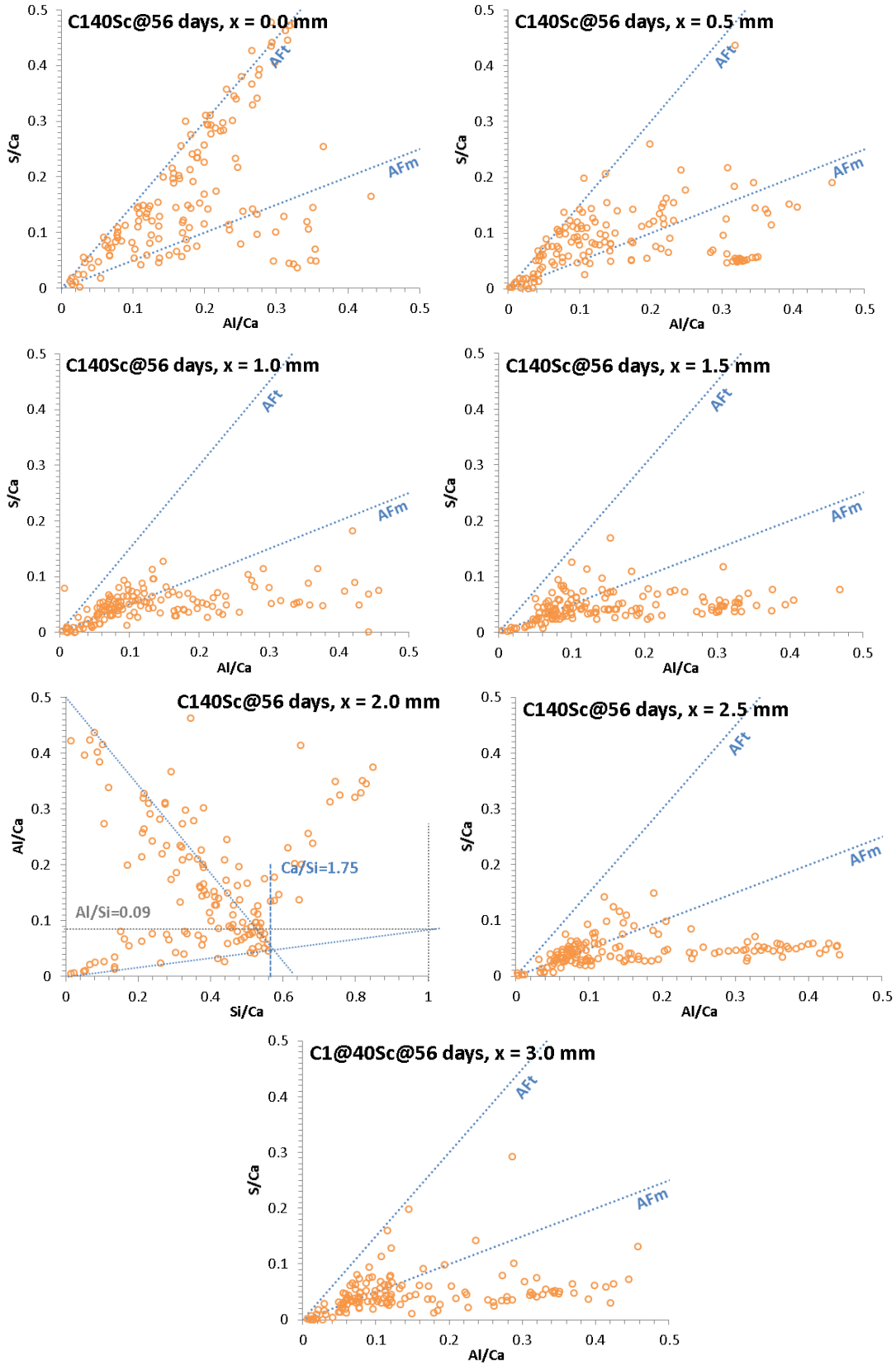

Figure A.50 – Changes in the AFm-AFt distribution in $C_1 40S_c$ Cured for 56 days in a 3 g.L^{-1} Na_2SO_4 Solution

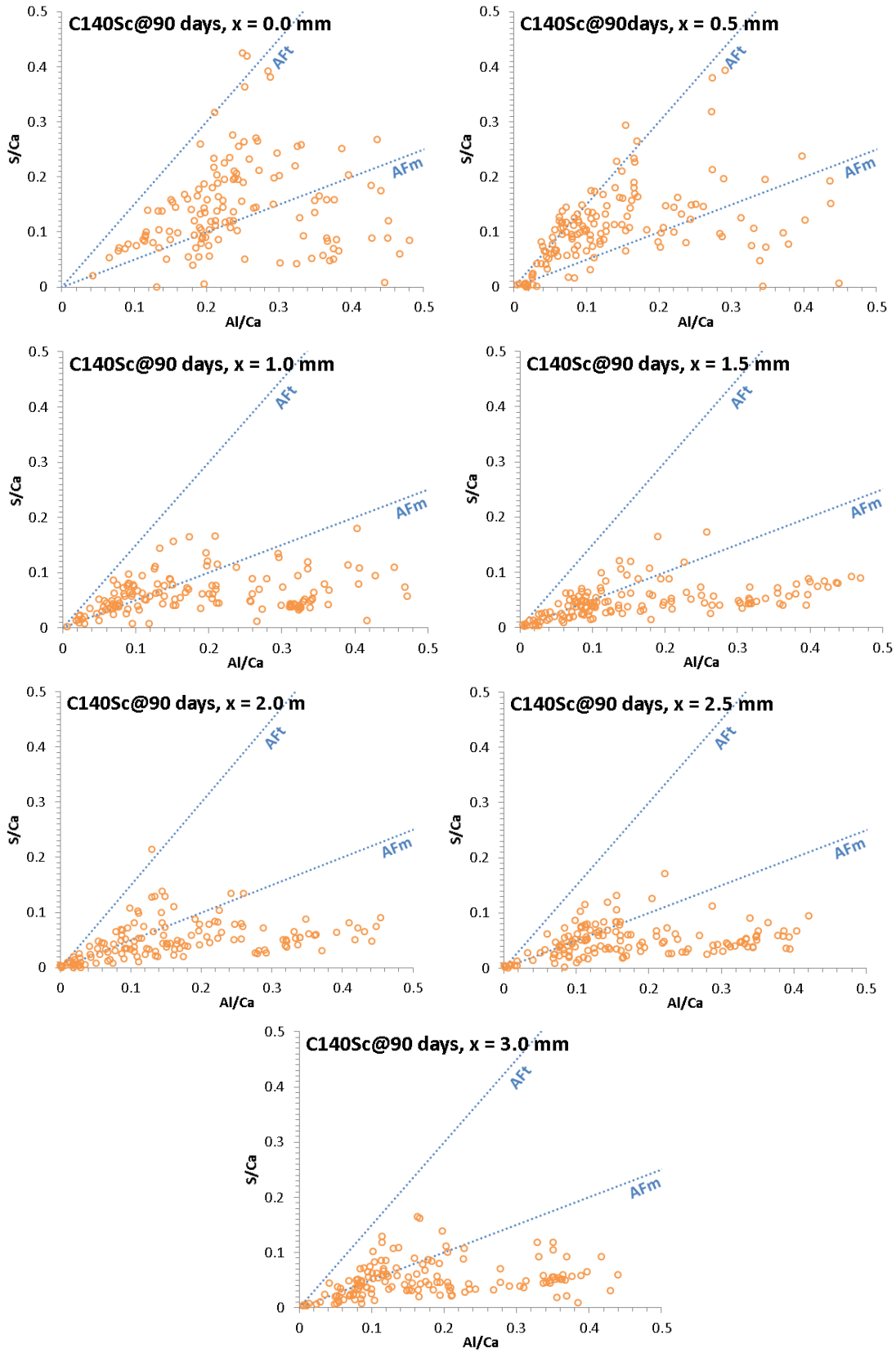

Figure A.51 – Changes in the AFm-AFt distribution in $C_1 40S_c$ Cured for 90 days in a 3 $g.L^{-1}$ Na_2SO_4 Solution

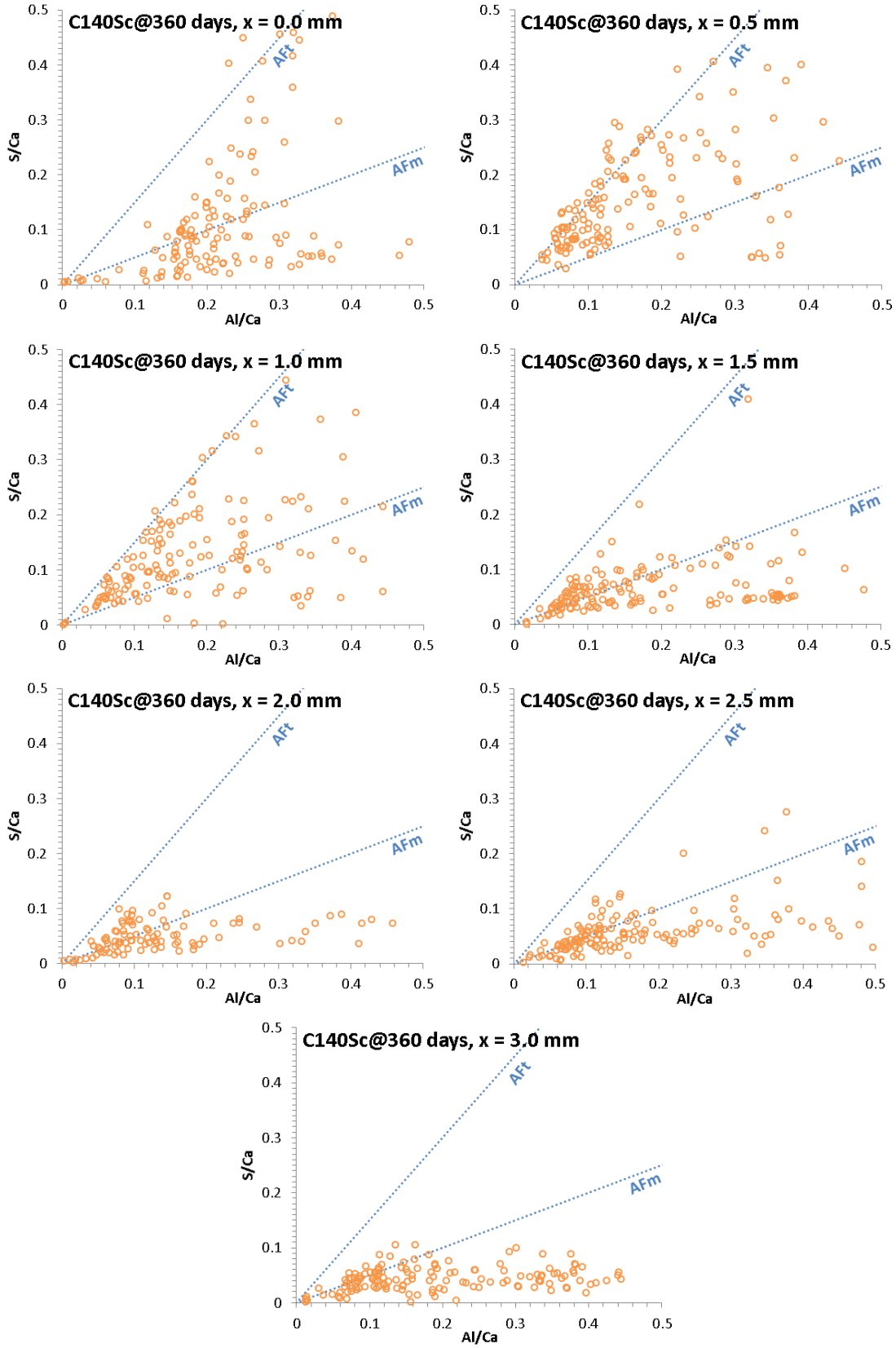

Figure A.52 – Changes in the AFm-AFt distribution in C_140S_c Cured for 360 days in a 3 g.L^{-1} Na_2SO_4 Solution

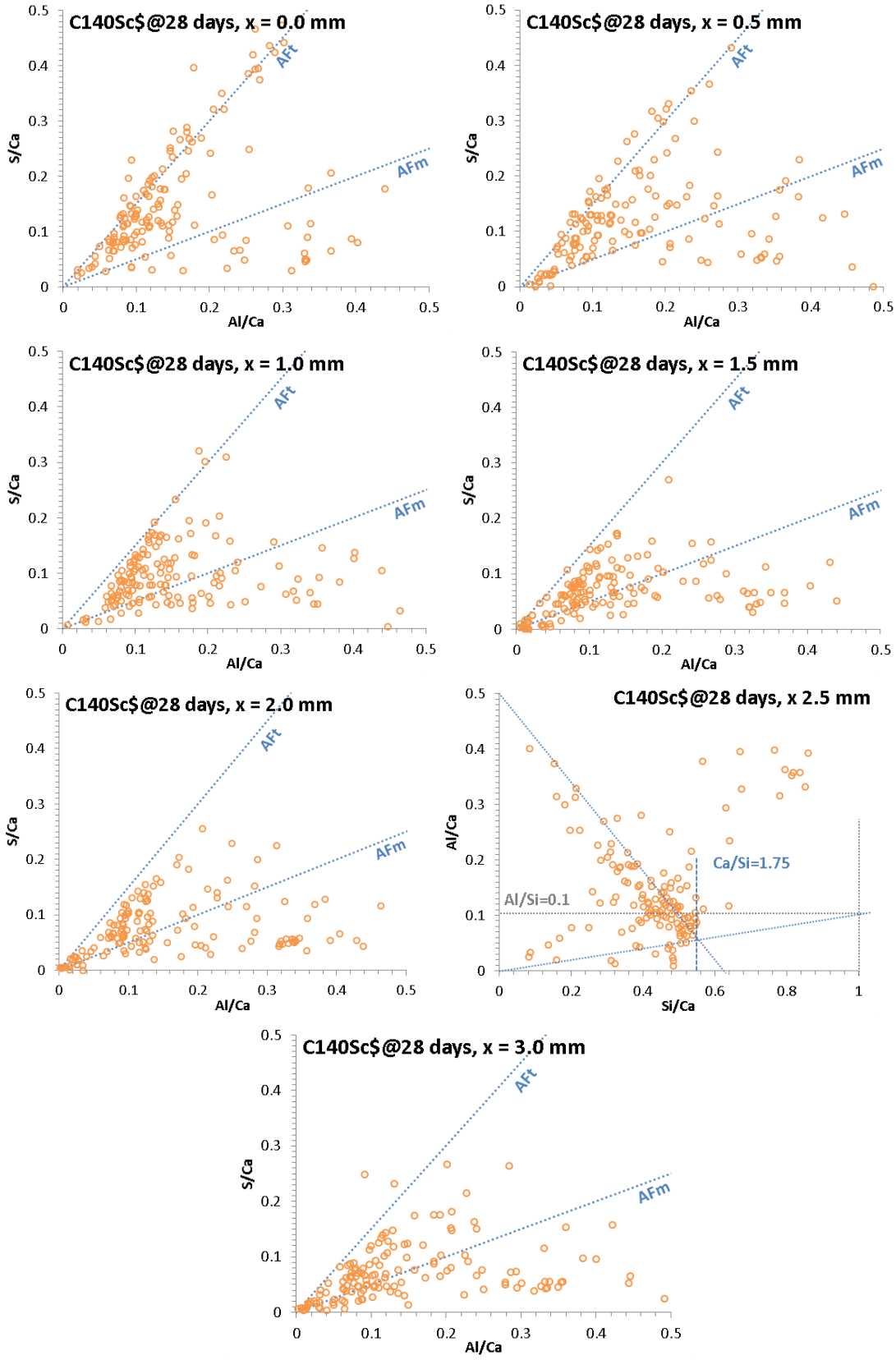

Figure A.53 – Changes in the AFm-AFt distribution in $C_1 40 S_c$ Cured for 28 days in a 3 $g.L^{-1}$ Na_2SO_4 Solution

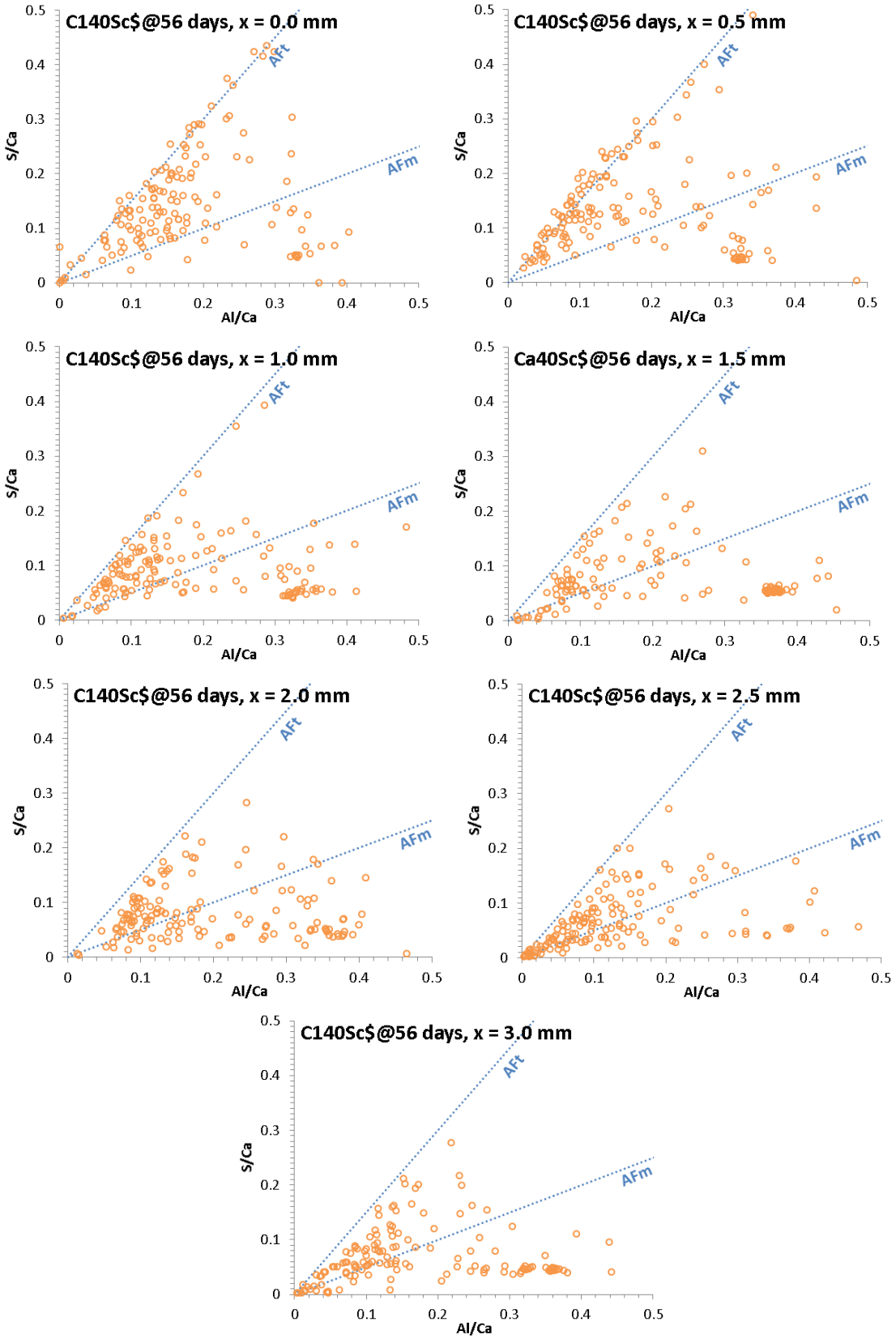

Figure A.54 – Changes in the AFm-AFt distribution in C_140S_c Cured for 56 days in a 3 g.L^{-1} Na_2SO_4 Solution

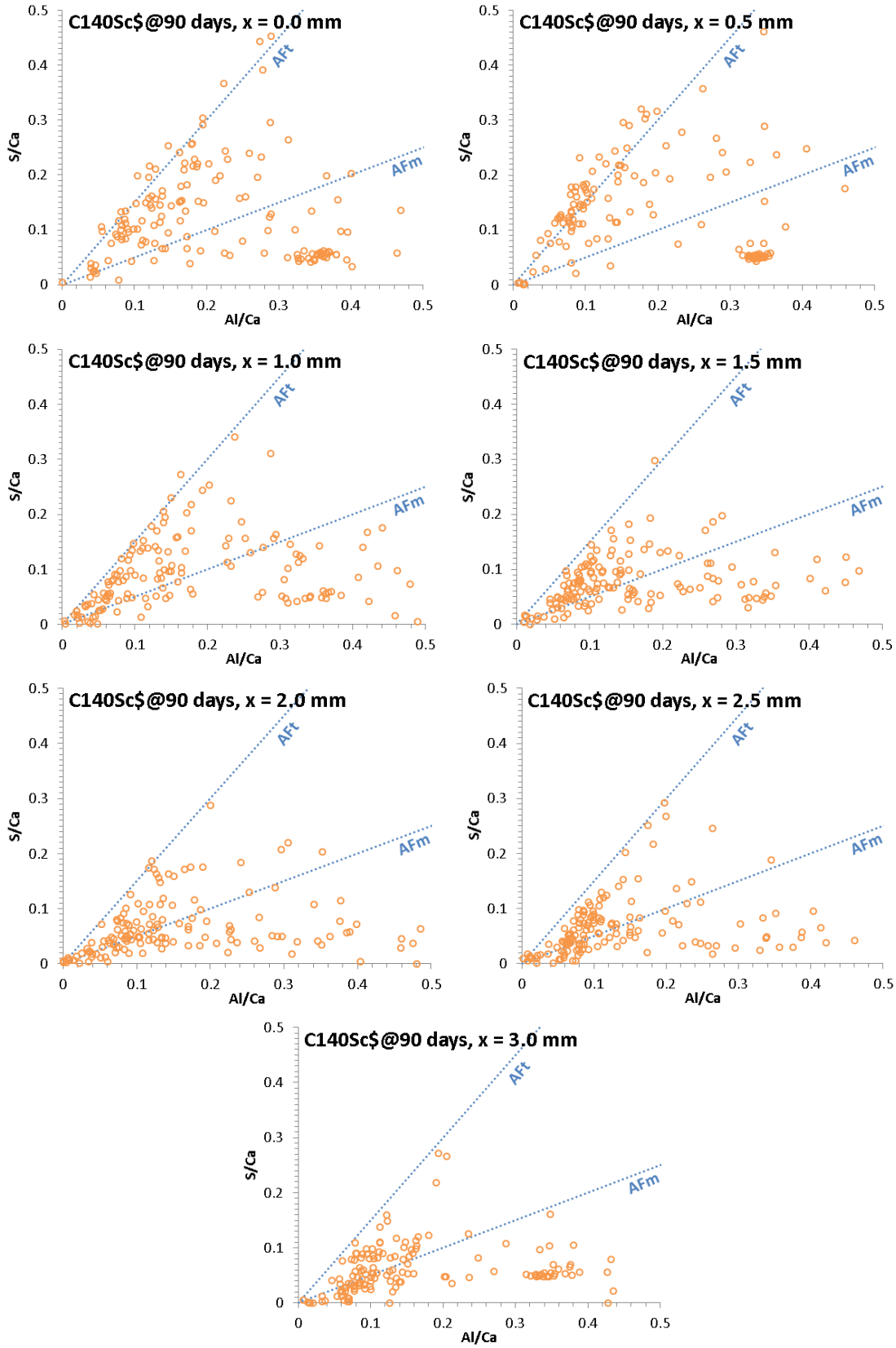

Figure A.55 – Changes in the AFm-AFt distribution in $C_1 40 S_c$ Cured for 90 days in a 3 $g.L^{-1}$ Na_2SO_4 Solution

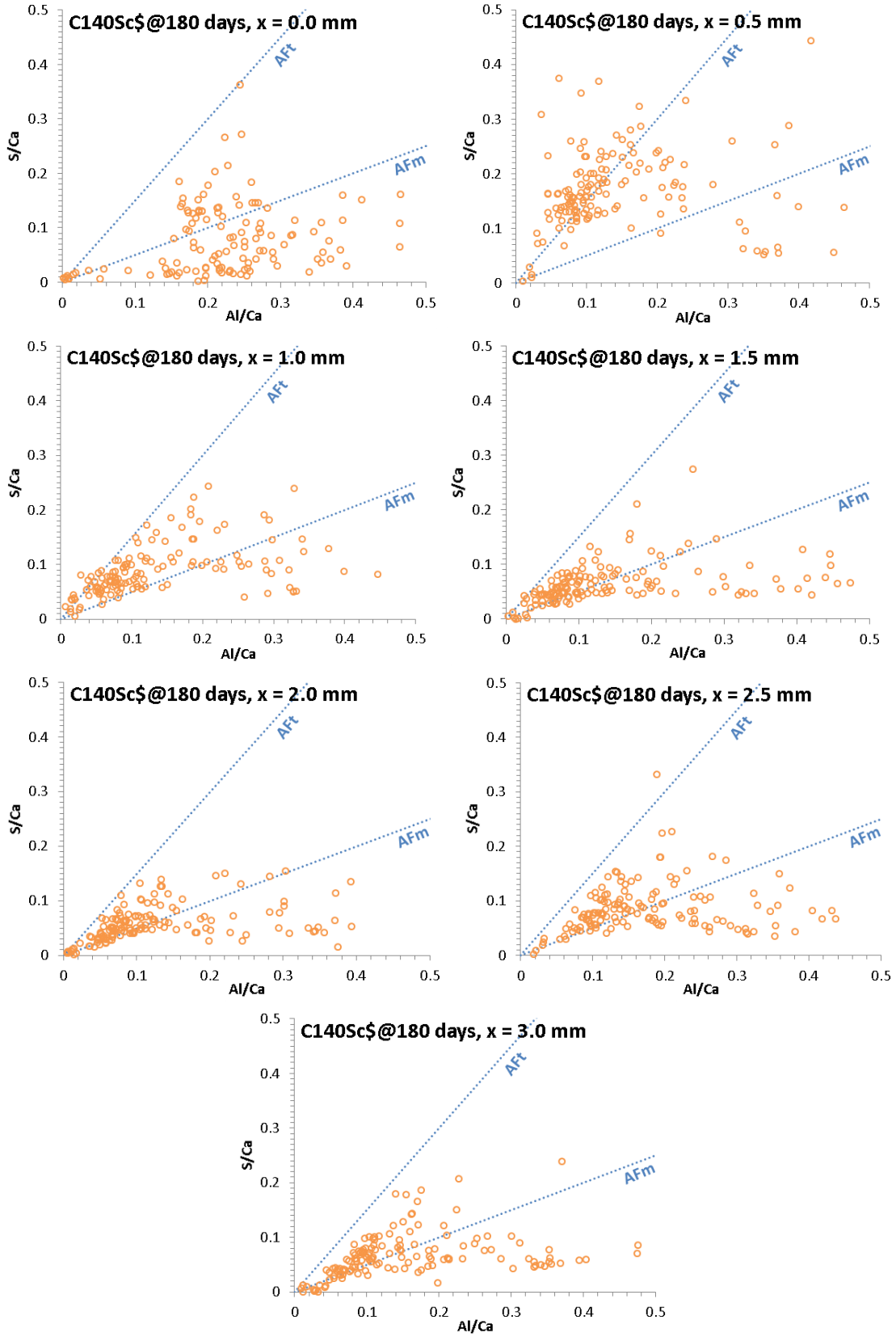

Figure A.56 – Changes in the AFm-AFt distribution in $C_1 40 S_c$ Cured for 180 days in a 3 g.L^{-1} Na_2SO_4 Solution

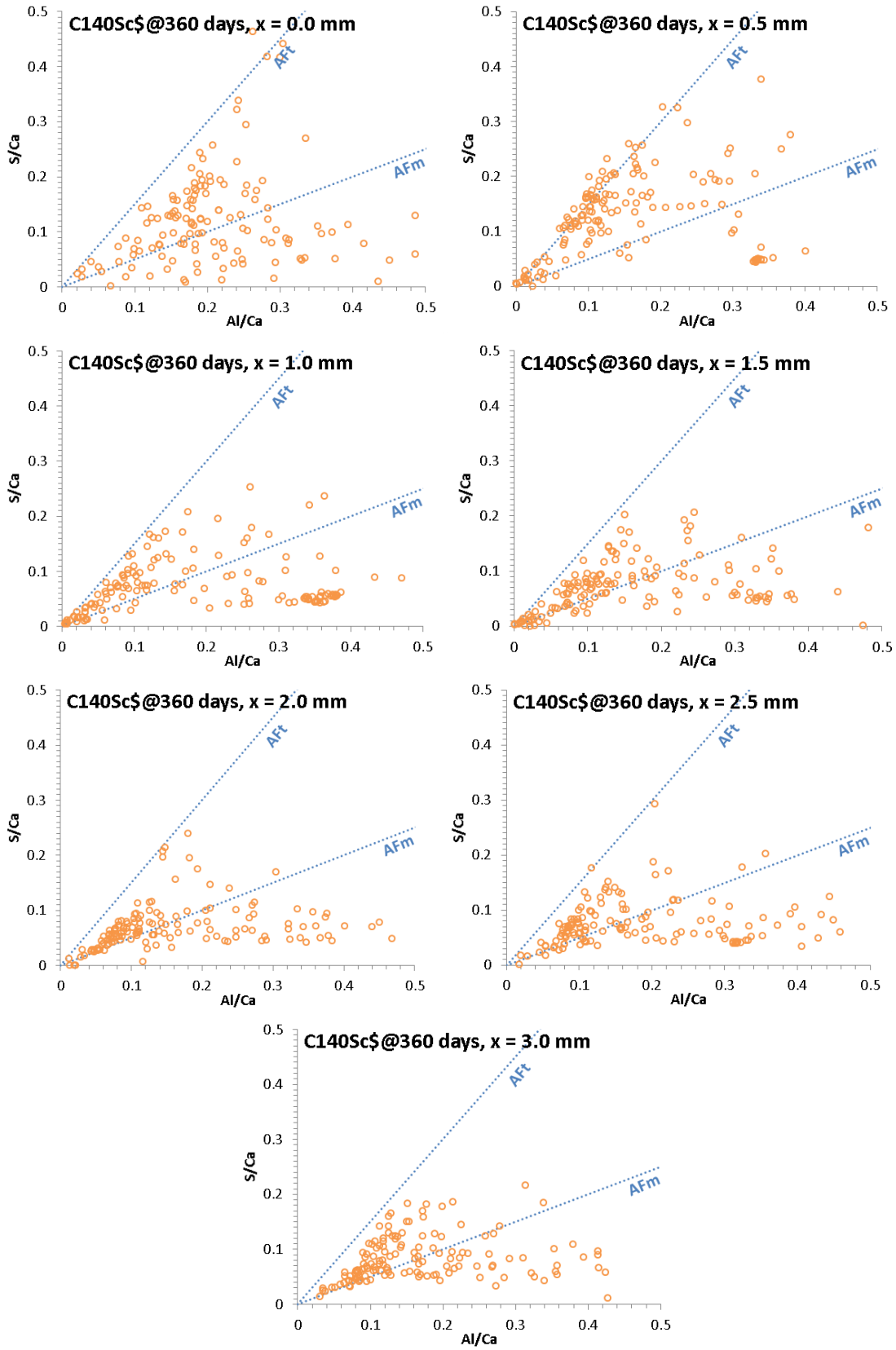

Figure A.57 – Changes in the AFm-AFt distribution in $C_1 40 S_c$ Cured for 360 days in a 3 g.L^{-1} Na_2SO_4 Solution

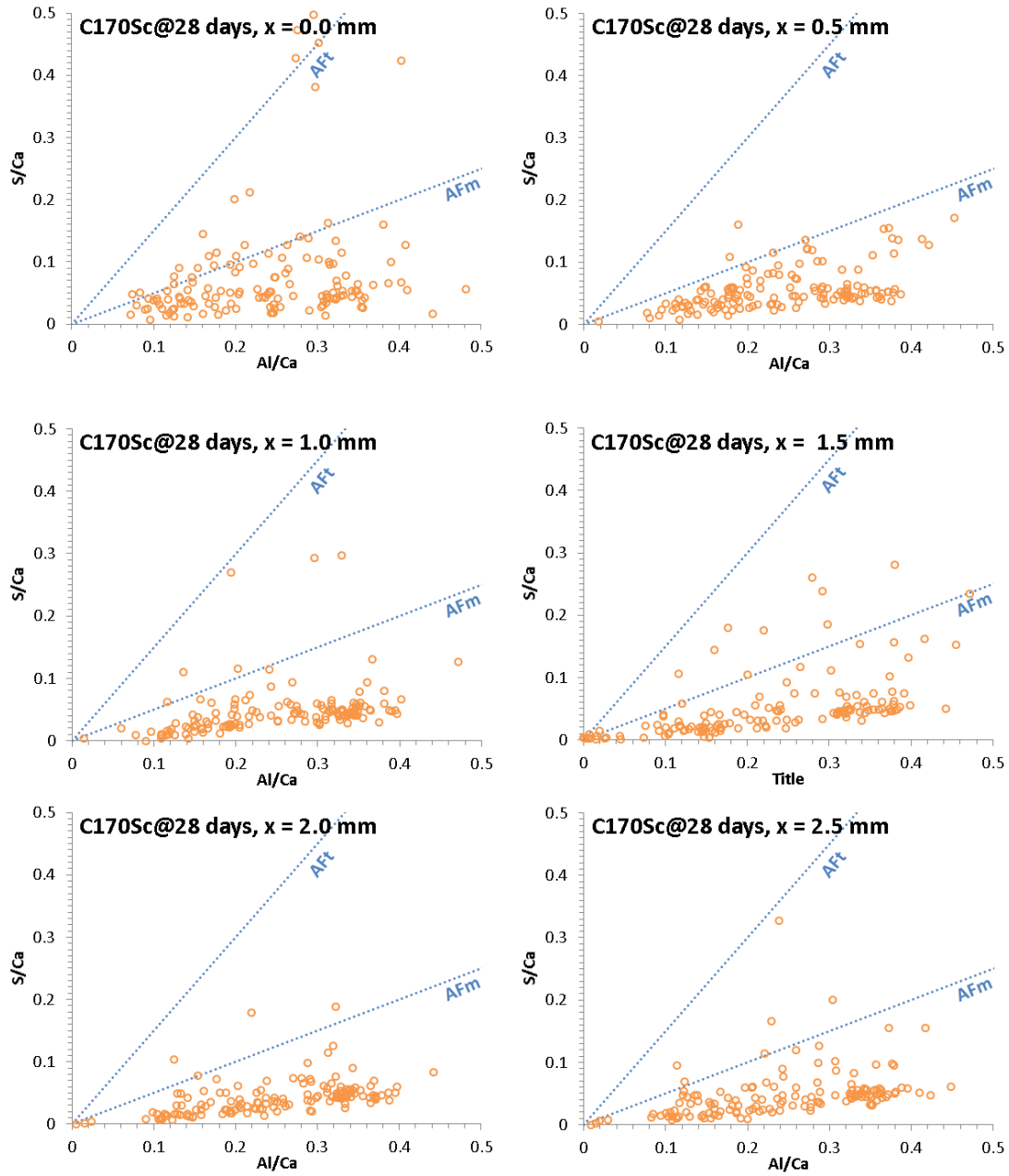

Figure A.58 – Changes in the AFm-AFt distribution in C_170S_c Cured for 28 days in a 3 g.L^{-1} Na_2SO_4 Solution

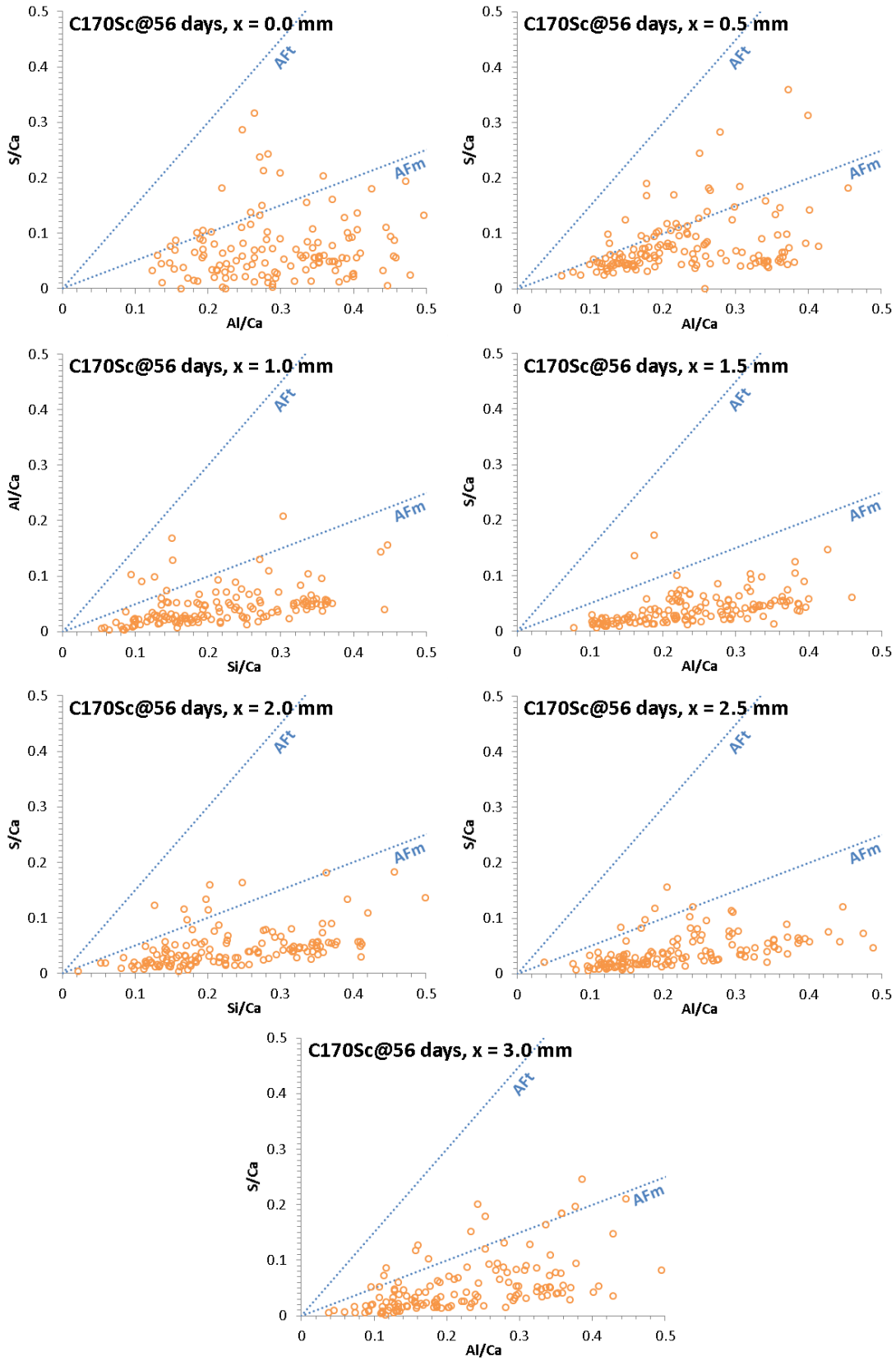

Figure A.59 – Changes in the AFm-AFt distribution in $C_1 70S_c$ Cured for 56 days in a 3 g.L^{-1} Na_2SO_4 Solution

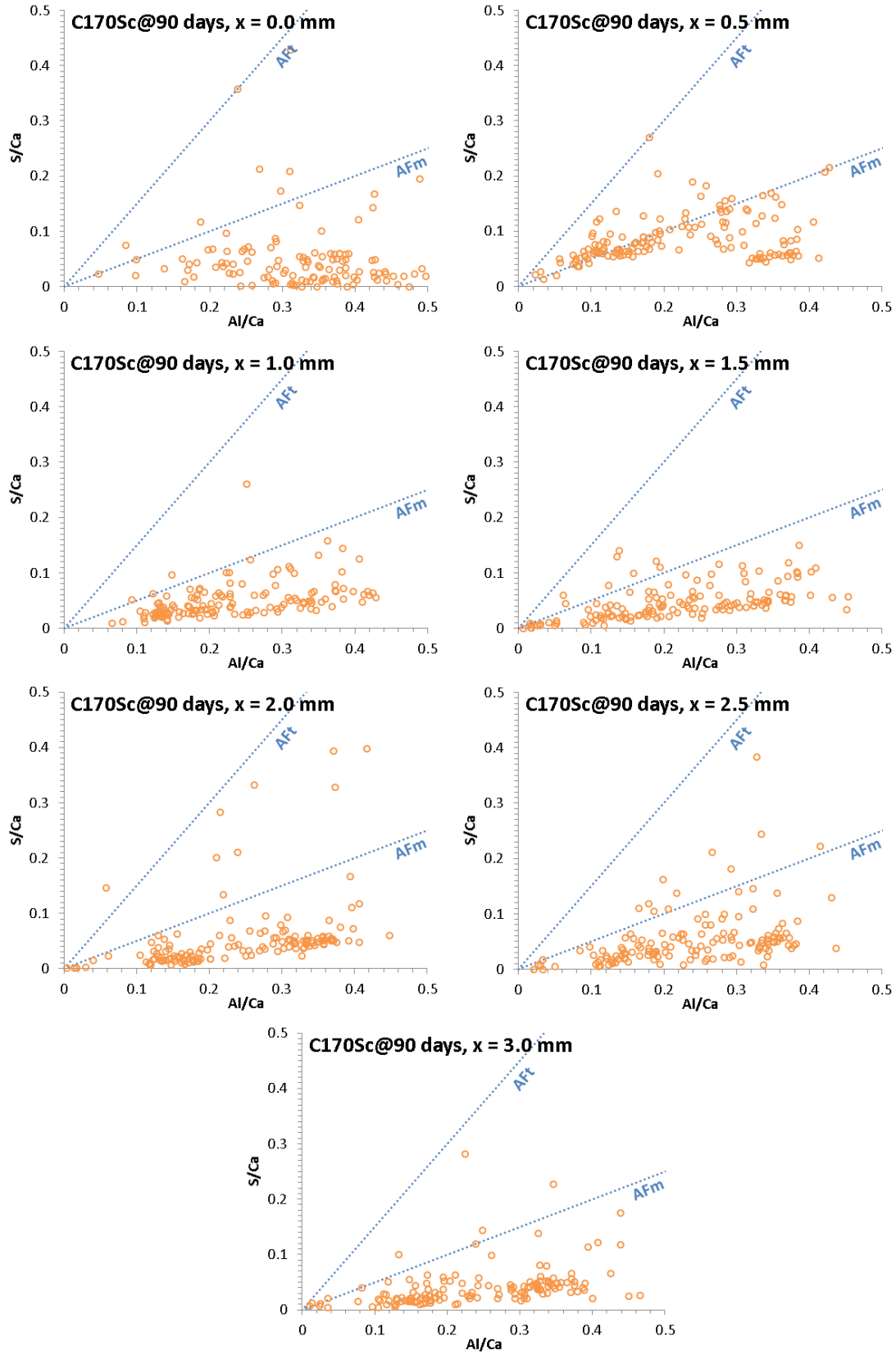

Figure A.60 – Changes in the AFm-AFt distribution in C_170S_c Cured for 90 days in a 3 $g.L^{-1}$ Na_2SO_4 Solution

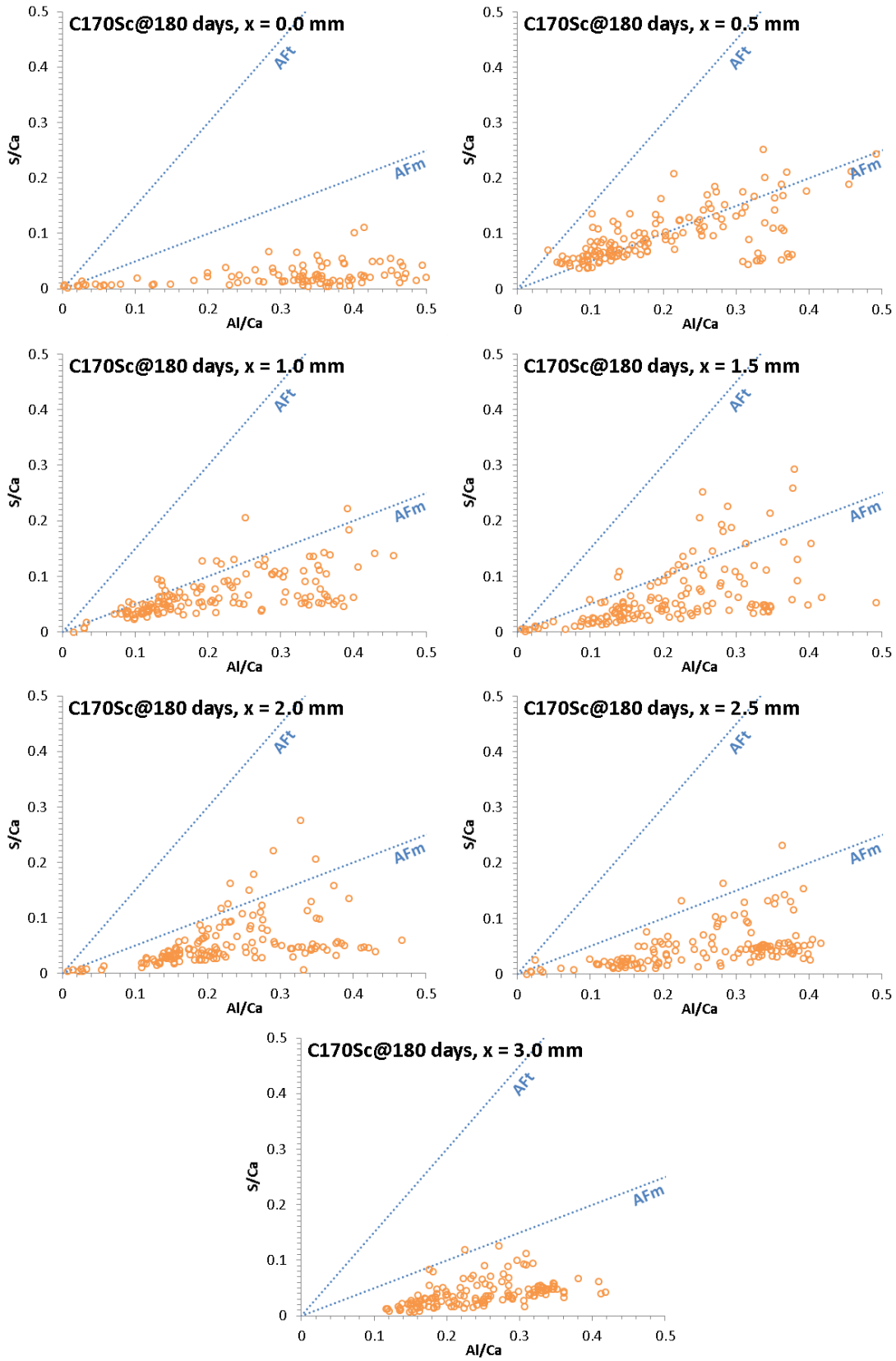

Figure A.61 – Changes in the AFm-AFt distribution in $C_1 70S_c$ Cured for 180 days in a 3 $g.L^{-1}$ Na_2SO_4 Solution

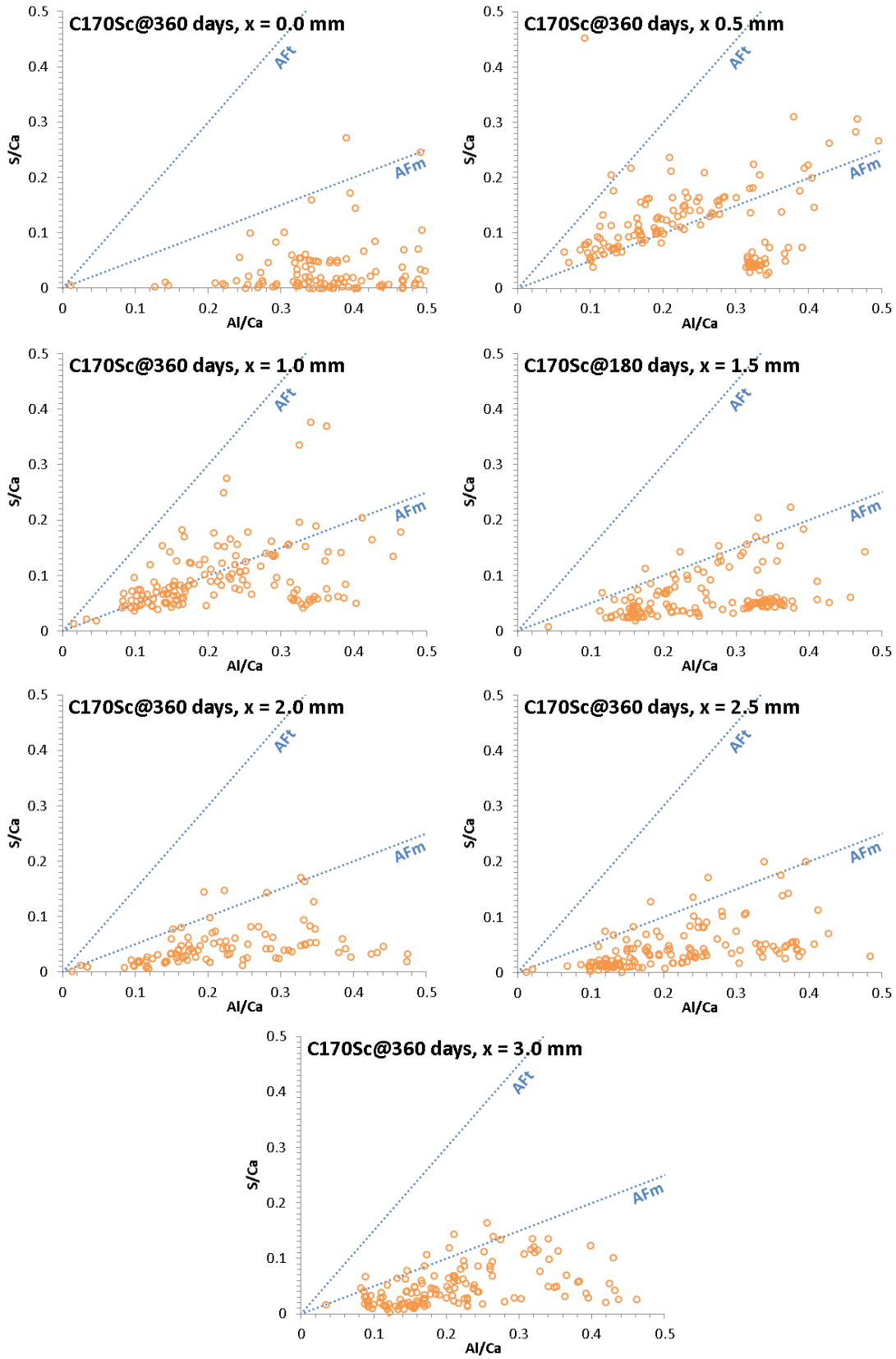

Figure A.62 – Changes in the AFm-AFt distribution in C_170S_c Cured for 360 days in a 3 g.L^{-1} Na_2SO_4 Solution